DESIGN AND EXPERIMENTAL TESTING OF AN ADSORBENT BED FOR A THERMAL WAVE ADSORPTION COOLING CYCLE

A THESIS SUBMITTED TO
THE GRADUATE SCHOOL OF NATURAL AND APPLIED SCIENCES
OF
MIDDLE EAST TECHNICAL UNIVERSITY

BY

AHMET ÇAĞLAR

IN PARTIAL FULFILLMENT OF THE REQUIREMENTS
FOR
THE DEGREE OF DOCTOR OF PHILOSOPHY
IN
MECHANICAL ENGINEERING

SEPTEMBER 2012

Approval of the thesis:

DESIGN AND EXPERIMENTAL TESTING OF AN ADSORBENT BED FOR A THERMAL WAVE ADSORPTION COOLING CYCLE

submitted by **AHMET ÇAĞLAR** in partial fulfillment of the requirements for the degree of **Doctor of Philosophy in Mechanical Engineering Department, Middle East Technical University** by,

Prof. Dr. Canan Özgen
Dean, Graduate School of **Natural and Applied Sciences** _________________

Prof. Dr. Süha Oral
Head of Department, **Mechanical Engineering** _________________

Assoc. Prof. Dr. Cemil Yamalı
Supervisor, **Mechanical Engineering Dept., METU** _________________

Assoc. Prof. Dr. Derek K. Baker
Co-supervisor, **Mechanical Engineering Dept., METU** _________________

Examining Committee Members:

Prof. Dr. Kahraman Albayrak
Mechanical Engineering Dept., METU _________________

Assoc. Prof. Dr. Cemil Yamalı
Mechanical Engineering Dept., METU _________________

Asst. Prof. Dr. Ahmet Yozgatlıgil
Mechanical Engineering Dept., METU _________________

Prof. Dr. Bilgin Kaftanoğlu
Manufacturing Engineering Dept., Atılım University _________________

Asst. Prof. Dr. Hüseyin Topal
Mechanical Engineering Dept., Gazi University _________________

Date: _________________

I hereby declare that all information in this document has been obtained and presented in accordance with academic rules and ethical conduct. I also declare that, as required by these rules and conduct, I have fully cited and referenced all material and results that are not original to this work.

Name, Last name: Ahmet ÇAĞLAR

Signature :

ABSTRACT

DESIGN AND EXPERIMENTAL TESTING OF AN ADSORBENT BED FOR A THERMAL WAVE ADSORPTION COOLING CYCLE

Çağlar, Ahmet
Ph.D., Department of Mechanical Engineering
Supervisor : Assoc. Prof. Dr. Cemil Yamalı
Co-Supervisor: Assoc. Prof. Dr. Derek K. Baker

September 2012, 187 pages

Poor heat and mass transfer inside the adsorbent bed of thermal wave adsorption cooling cycles cause low system performance and is an important problem in the adsorbent bed design. In this thesis, a new adsorbent bed is designed, constructed and tested to increase the heat and mass transfer in the adsorbent bed. The adsorbent bed is constructed from a finned tube in order to enhance the heat transfer. Additionally, the finned bed geometry is theoretically modeled and the model is solved time dependently by using Comsol Multiphysics software program. The distributions of dependent variables, i.e. temperature, pressure and amount adsorbed, are simulated and plotted in Comsol Multiphysics. In the model, the dependent variables are computed by solving the energy, mass and momentum transfer equations in a coupled way and their variations are investigated two-dimensionally. The results are presented with multicolored plots in a 2-D domain. Furthermore, a parametric study is carried out for determining factors that enhance the heat and mass transfer inside the adsorbent bed. In this parametric study, the effects of several design and operational parameters on the dependent variables are investigated. In the experimental study, the finned tube is tested using natural zeolite-water and silica gel-water working pairs. Temperature, pressure and amount adsorbed variations inside the adsorbent bed at various operating conditions are investigated. After that, a second adsorbent bed with a larger size is constructed and tested. The effect of the particle diameter of the adsorbent is also investigated. The experimental and theoretical results are compared.

Keywords: Thermal Wave Adsorption Cooling Cycle, Adsorbent Bed, Heat and Mass Transfer, Modeling, Comsol Multiphysics

ÖZ

BİR ISIL DALGA ADSORPSİYONLU SOĞUTMA ÇEVRİMİNİN ADSORBAN YATAĞININ TASARIMI VE DENEYSEL OLARAK TEST EDİLMESİ

Çağlar, Ahmet
Doktora, Makina Mühendisliği Bölümü
Tez Yöneticisi : Doç. Dr. Cemil Yamalı
Ortak Tez Yöneticisi: Doç. Dr. Derek K. Baker

Eylül 2012, 187 sayfa

Isıl dalga adsorpsiyonlu soğutma sistemlerinin adsorban yatağı içerisindeki zayıf ısı ve kütle transferi, düşük sistem perfomansına neden olmakta ve adsorban yatak tasarımında önemli bir problem teşkil etmektedir. Bu tezde, adsorban yatak içerisindeki ısı ve kütle transferini artırmak için yeni bir adsorban yatak tasarlanmış ve bu yatak imal edilerek bir deney düzeneğinde test edilmiştir. Adsorban yatağı, ısı transferinin geliştirilmesi açısından radyal kanatçıklı bir borudan imal edilmiştir. Diğer taraftan, belirtilen kanatçıklı boru yatak geometrisi teorik olarak modellenmiş ve bu model Comsol Multiphysics programı kullanılarak zamana bağlı çözdürülmüştür. Bağımlı değişkenler olan sıcaklık, basınç ve adsorbe edilen miktarın zamanla değişimleri Comsol Multiphysics programında simüle ettirilmiş ve çizdirilmiştir. Bu modelde bağımlı değişkenler, enerji, kütle ve momentum transfer denklemleri birbirine bağlı olarak çözdürülerek hesaplanmış ve bunların değişimleri iki boyutlu olarak incelenmiştir. Sonuçlar 2-boyutlu bir alanda çokrenkli çizimlerle gösterilmiştir. Ayrıca, adsorban yatakta ısı ve kütle transferini artıran faktörleri belirlemek için parametrik bir çalışma yapılmıştır. Bu parametrik çalışmada, birkaç tasarım ve işletim parametresinin bağımlı değişkenler üzerindeki etkileri incelenmiştir. Deneysel çalışmada, kanatçıklı boru zeolit-su ve silika jel-su çalışma çiftleri kullanılarak test edilmiştir. Farklı çalışma koşullarında adsorban yatak içerisindeki sıcaklık, basınç ve adsorbe edilen miktarın değişimleri incelenmiştir. Daha sonra çapı daha büyük ikinci bir yatak daha imal edilmiş ve testleri yapılmıştır. Farklı parçacık çaplarında aynı adsorban malzeme test edilerek adsorban malzemenin parçacık çapının yatak performansına etkisi de ayrıca incelenmiştir. Deneysel ve teorik çalışmalardan elde edilen sonuçlar karşılaştırılmış ve yorumlanmıştır.

Keywords: Isıl Dalga Adsorpsiyonlu Soğutma Çevrimi, Adsorban Yatak, Isı ve Kütle Transferi, Modelleme, Comsol Multiphysics

To My Family

ACKNOWLEDGMENTS

I am deeply grateful to my supervisor, Assoc. Prof. Dr. Cemil YAMALI, for his guidance, inspiration, and invaluable help all throughout the study.

I also wish to express my gratitude to Assoc. Prof. Dr. Derek K. BAKER, my co-supervisor, for his helpful comments and suggestions for developing my thesis and his guidance throughout completing my thesis work.

I would like to thank to Prof. Dr. Bilgin KAFTANOĞLU for his precious advices, encouragement and support.

I also would like to thank to Prof. Dr. Kahraman ALBAYRAK and to Asst. Prof. Dr. Hüseyin TOPAL for their precious advices and comments in my thesis progression.

I gratefully acknowledge Mustafa YALÇIN, for his technical assistance in manufacturing and operating the experimental setup.

I would like to appreciate my parents, Ömer and Fidan ÇAĞLAR for their patience, love, encouragement and helpful support during my thesis work, and especially, would like to thank my wife for her invaluable support, kindness, and for being in my life with her endless love, forever.

Finaly, I would like to dedicate all my work to my beloved son.

This work is supported by The Scientific & Technological Research Council of Turkey (TÜBİTAK) project 110M378. This study is also supported by the State Planning Organization (DPT) Grant No: BAP-08-11-DPT2002K120510.

TABLE OF CONTENTS

CHAPTERS

APPENDICES

LIST OF TABLES

TABLES

LIST OF FIGURES

FIGURES

LIST OF SYMBOLS

SYMBOLS

A	area, m^2
c	specific heat of incompressible subtance, Jkg^{-1}K^{-1}
c_p	ideal gas specific heat at constant pressure, Jkg^{-1}K^{-1}
COP	coefficient of performance
D_o	reference diffusivity, m^{2}s^{-1}
D_m	mass diffusion coefficient, m^{2}s^{-1}
$\dot{E}$	energy, kJ
E_a	activation energy of surface diffusion, Jmol^{-1}
$\mathbf{f}$	total mass flux, kgm^{-2}s
h	specific enthalpy, kJkg^{-1}
h_i	convective heat transfer coefficient between tube and fluid, Wm^{-2} K^{-1}
h_c	interfacial conductance between tube and adsorbent, Wm^{-2} K^{-1}
HTF	heat transfer fluid
HTT	heat transfer tube
ΔH	heat of adsorption, kJkg^{-1}
k	thermal conductivity, Wm^{-1}K^{-1}
k_m	internal mass transfer coefficient, s^{-1}
P	pressure, Pa
q	heat transfer, W
q''	heat flux, Wm^{-2}
r	radius, m
R	universal gas constant, Jmol^{-1}K^{-1}

R_v	ideal gas constant for water vapor, $\mathrm{Jkg^{-1}K^{-1}}$
t	time, s
T	temperature, K
u	specific internal energy, $\mathrm{kJkg^{-1}}$
$\mathbf{u}$	vapor velocity vector, $\mathrm{ms^{-1}}$
X	amount of water vapor adsorbed by adsorbent per unit mass of adsorbent, $\mathrm{kg_w kg_s^{-1}}$
v_{ave}	HTF mean velocity, $\mathrm{ms^{-1}}$
v_f	HTF velocity, $\mathrm{ms^{-1}}$
$\mathbf{V}$	velocity, $\mathrm{ms^{-1}}$
V	volume, $\mathrm{m^3}$

Greek Symbols

ε	porosity
κ	permeability, $\mathrm{m^2}$
κ_E	Forchheimer coefficient, m
μ	dynamic viscosity, $\mathrm{kgm^{-1}s^{-1}}$
ρ	density, $\mathrm{kgm^{-3}}$
Γ	open fraction of porous media

Subscripts

ad	adsorbate adsorbed by the adsorbent
adv	advected
b	bed
c	condenser
cond	conduction
cont	thermal contact
conv	convection

e	equilibrium, effective
f	fluid
i	inlet, inner
l	liquid, lateral
o	outlet, outer
p	particle
s	(solid) adsorbent, stored
sat	saturation
t	tube
T	total
v	vapor

CHAPTER 1

INTRODUCTION

Cooling and heating demands constitute almost half of the total energy demands all over the world. These demands include many applications from simple space cooling/heating to food preservation and heat treatments. They are basic needs for human being and indispensable for a healthy life. There are several ways to meet cooling and heating demands. Firing a fuel, using electricity directly or indirectly and installation of solar collectors on the roof are some of them. Technological developments have made the use of cyclic devices possible in obtaining cooling and heating effects. These systems can be categorized into two major groups: electrically driven and thermally driven systems. Vapor compression and thermoelectric systems are electrically driven while absorption, desiccant, ejector and adsorption systems are thermally driven.

CO_2 emissions and other greenhouse gases have increased environmental considerations. Intensive consumption of fossil fuels and the use of hazardous gases have resulted in fatal outcomes such as ozone layer depletion, climate change, global warming, air pollution and so on. Oil reserves are getting smaller and smaller and the decrease in the supplies of oil and gas as well as the increase in energy demands causes energy crisis. Nowadays, governments are trying to get out of fossil fuel dependency for energy production. The governments support the investments and investigations of renewable energy sources such as solar, wind, biomass and geothermal. Adsorption cooling cycle is one of the alternative cooling systems which use renewable energy sources and sustainable technologies since it makes use of environmentally benign materials, zeolite-water pair for example, and may be driven by solar or waste energy.

Appropriate technologies should be used in order to keep the balance between technology development and protection of main components of the environment. The majority of chemical compounds affect the environmental media (air, water and soil). Therefore, they also affect human health harmfully. The rising levels of nutrients such as nitrates and phosphates, for example, have caused a serious deterioration in the water quality of many rivers, lakes and reservoirs. Therefore, the removal of nutrients originating from sewages and fertilizers can be achieved by adsorption technologies. The pollution of the air is caused by the use of contaminated raw materials without purifying in order to decrease the cost of manufacturing goods. Coal is used for residential heating without a preliminary desulfurization and this also causes environmental pollution. Dust and smog are other air contaminants. Adsorption technologies are the most important techniques to control and remove natural, anthropogenic, municipal, agricultural and other pollutants. The adsorption technologies play a significant role in overcoming the degradation of environmental quality and in human health control. They can be used in the transportation sectors for automobile air conditioning or for food preservation in trucks. Local environmental issues that are caused by flue gasses like SO_x and NO_x may be solved by advanced adsorption techniques. These are a few examples showing the contributions of these systems to a clean environment [1].

Vapor compression refrigeration cycles are the most common cooling cycles and have advantages of having high performance (i.e. COP, coefficient of performance) and the feasibility for industrial applications. However, they operate using the electricity produced by primary energy resources such as oil, coal, natural gas and hence extensive use of vapor compression cycles causes a rapid decrease in these energy resources due to low energy conversion efficiencies. Therefore in last decades, the interest in thermally driven systems which can use alternative energy sources and waste heat has increased. These systems can eliminate the disadvantages of electrically driven systems in two ways. Firstly, they use directly the thermal energy produced by combustion to provide cooling and heating and this eliminates the inefficiencies associated with the conversion of thermal energy to electricity. Secondly, they can provide cooling and heating by direct use of heat sources such solar, geothermal or waste heat without using any fuel. The ability to use thermal energy directly also enables making the recovery of waste heat [2].

Thermally driven systems can be divided into four main categories: absorption, ejector, adsorption and desiccant cooling cycles. The former two are appropriate for utilization of low temperature applications (45-95 ^{o}C) while the other two are operated at high temperatures (100-350 ^{o}C) [3]. Absorption and adsorption cooling cycles are briefly compared as follows. Although adsorption cooling cycles show similarities to absorption cycles in the type of heat sources and in the physical events performed during the cycle, there are distinct differences between two. In absorption process, gas or liquid penetrates (diffuses) into a liquid or solid material producing a solution and resulting in a chemical reaction or phase change while in adsorption process, gas or liquid is accumulated at the surface of solid or liquid substance by the utilization of unbalanced surface forces. Absorption is a bulk phenomenon and the concentration is uniform throughout the bulk of absorbent. However, the adsorption is a surface phenomenon and the concentration of adsorbate on the surface of adsorbent is higher than that in the bulk of adsorbent. Adsorption cooling cycles are discussed in detail in the next section. For more information on absorption cooling cycles, readers can be referred to references [4,5].

1.1 Adsorption Cooling Cycles

Adsorption is a surface phenomenon and is generally considered to occur between gas and solid phases in cooling applications. Therefore, adsorption is also called *solid sorption* in the literature on cooling. Some solids have an affinity to adsorb vapor onto or into their surface structure. The solids that adsorb gas molecules are termed as adsorbent and the gas molecules adsorbed by adsorbent are termed as adsorbate. The adsorbate is accumulated on the surface of the adsorbent in adsorption. Adsorption has a great technological importance. Some adsorbents are used as desiccants, catalysts or catalyst supports while the others are used for the separation of gases, the purification of liquids, pollution control or for respiratory protection. Additionally, adsorption phenomena play a significant role in many solid state reactions and biological mechanisms [6].

To obtain a specific cooling capacity, adsorbents are generally packed in a bed. This packed bed is called an adsorbent bed and constitutes an adsorption cycle together with three main components of conventional cooling cycles; evaporator, condenser and expansion valve. Adsorption refrigeration attracted a significant attention when it first came out in 1920s. However, the attention decreased because of the developments in the performance of mechanical compression refrigeration cycles. Nowadays, the researches on adsorption cooling have increased again with the increasing interest in porous media. A number of studies have been performed to get the performance of adsorption cycles to a level that can compete with that of other cycles. Adsorption cooling cycles have some advantages and disadvantages when compared to other cooling cycles [7,8,9]:

Advantages

- Usage of environmentally benign materials
- Utilization of renewable (solar, geothermal) or waste heat sources
- Heat&mass recoverability
- Lower or no emissions
- Low maintenance cost
- No corrosion
- Wide operating temperature ranges (50-350 ^{o}C)
- No noise and vibration
- Long life time

Disadvantages

- Low COP values
- Low specific cooling power (SCP)
- Long cycle times
- Difficulty in obtaining vacuum tightness
- High initial cost
- Having greater volume and weight than conventional types

There are two types of adsorption processes: physical adsorption and chemical adsorption. Physical adsorption occurs when adsorbed molecules (gas or vapor) are weakly bound to adsorbent’s surface, often by van der Waals and/or dispersion forces due to induced dipole-dipole interactions [10,11]. The energy barrier which molecules have to overcome in order that adsorption may occur is usually very small. Desorption is the reverse of adsorption and occurs when the adsorbed particle gains energy enough to break the binding with the surface [12]. In physical adsorption, the heat of liquefaction of the adsorbate gas is approximately equal to the heat of desorption and this quantity is close to heat of adsorption which is the energy when adsorption process occurs. Thus, adsorption and desorption processes are reversible and non-activated. Reversible means that adsorbent can readsorb after a desorption process. However, the process is not reversible when capillary condensation occurs in adsorbents containing fine pores. This usually leads to hysteresis in the adsorption isotherm [13]. In chemical adsorption which is also called chemisorption, strong chemical bonds are formed and molecules have to have sufficient energy (the activation energy) to surmount the energy barrier and fall into the lower potential well of the chemisorbed state [10]. Chemical adsorption is out of the scope of this study.

Adsorption cooling cycles are categorized into three main systems: basic, heat recovery and heat & mass recovery adsorption cooling systems. The following are the definitions of these systems. Thermal wave cycle is then introduced in detail separately.

1.1.1 Basic Adsorption Cycle

The schematic of basic adsorption refrigeration system is shown in Figure 1.1. The basic cycle consists of adsorbent bed (adsorber), evaporator, condenser and throttling valve. The adsorbent bed is filled by an adsorbent material and it adsorbs/desorbs a working fluid (refrigerant) that flows by a pressure difference. The adsorbent bed is heated or cooled according to the process performed.

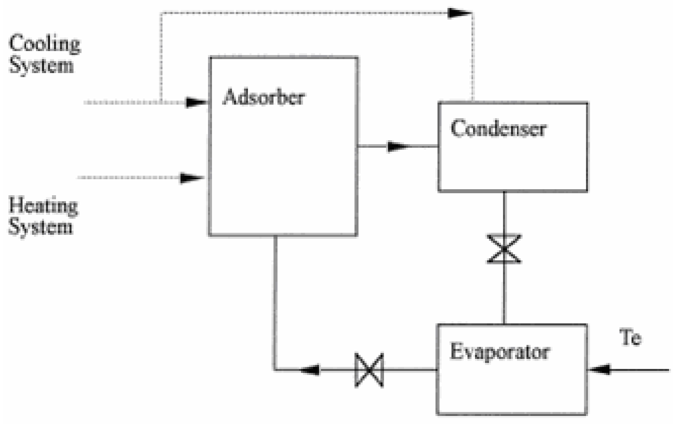

Figure 1.1 Schematic of basic adsorption cycle [14].

Basic adsorption refrigeration cycle is represented by the Clapeyron diagram (lnP vs. -1/T) in Figure 1.2. The cycle consists of four processes. The cycle begins at point 1 where the adsorbent is at low temperature (T_1) and low pressure (evaporation pressure, $P_{sat}(T_e)$). Adsorption capacity is at maximum level at this point. In process 1-2, the adsorbent bed receives heat from high-temperature heat source and the adsorbate is desorbed isosterically (at constant adsorption level). The adsorbent bed is pressurized since there exists no flow of refrigerant to the condenser. Therefore, this process is called pressurization process. Progressive heating causes the vapor desorbed to move to the condenser when the pressure inside the adsorbent bed reaches the condenser pressure. Desorption process takes place at constant pressure (isobaric process) and the refrigerant vapor leaving the bed is condensed during 2-3 process. Desorption ceases when the temperature of the bed is at the cycle maximum temperature T_3. The condensed liquid is expanded to the evaporator pressure and transferred into the evaporator by passing through the expansion device (throttling valve). The hot adsorbent bed is cooled and depressurized during 3-4 process. The process is called depressurization since the pressure decreases due to isosteric cooling. The adsorbent bed has the minimum adsorption capacity during this process. Adsorption process (process 4-1) begins when the pressure inside the bed decreases to evaporator pressure. The refrigerant is vaporized in the evaporator producing the cooling effect and then moves to the adsorbent bed. The adsorbent adsorbs the refrigerant vapor isobarically during the adsorption process. The process continues until the bed reaches the maximum adsorption capacity. The bed temperature decreases to cycle minimum temperature (T_1) at the end of the adsorption process. At this point, the cycle is completed and can be repeated. The cycle can be summarized as follows [15]:

- **1-2 Isosteric heating process:** The temperature of the adsorbent bed is increased from T_1 to T_2 by outside heating (solar, electrical or waste heat). The bed is pressurized to the condenser pressure without performing desorption.
- **2-3 Isobaric desorption:** The adsorbent bed continues to be heated and desorption process occurs at constant pressure. The refrigerant is condensed in the condenser and goes to the evaporator by passing through the throttling valve.
- **3-4 Isosteric cooling process:** Desorption ceases and the absorbent bed is cooled from T_3 to T_4 temperature without performing adsorption. The pressure inside the bed decreases to evaporation pressure due to the isosteric cooling.

- **4-1 Isobaric adsorption:** The bed continues to be cooled and adsorption process occurs at constant pressure. The cycle is completed when the temperature of the bed decreases to T_1.

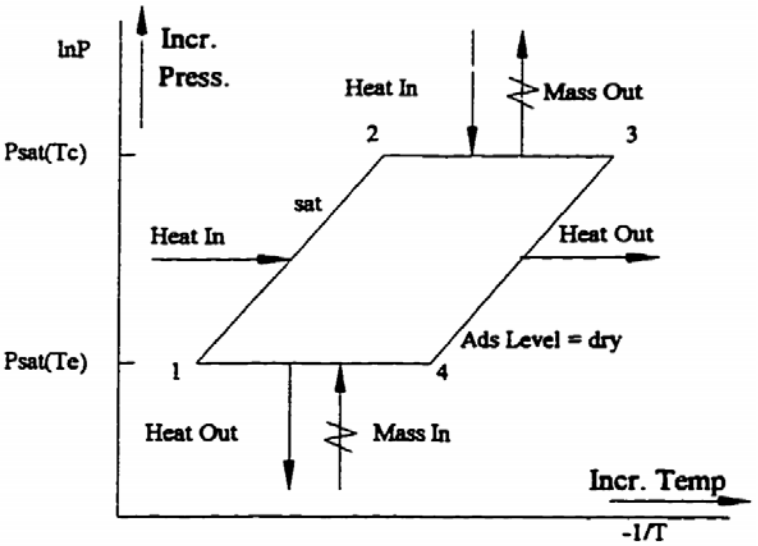

Figure 1.2 Basic adsorption refrigeration cycle [2].

The coefficient of performance (COP) for the basic adsorption refrigeration cycle can be expressed as:

$$COP = \frac{Q_{evap}}{Q_{1-2} + Q_{2-3}} \tag{1.1}$$

1.1.2 Heat Recovery Systems

The basic adsorption cycle is intermittent and needs to be modified in order to be a continuous cycle. The adsorbent bed is first charged with adsorbate and adsorption (cooling effect) stops when the adsorbate starts to be desorbed from the bed. The cycle waits for the desorption process to be able to create cooling effect again. There is an idle time for the regeneration of the adsorbent bed. Additionally, single bed does not permit the use of heat rejected by the adsorbent bed. Both the sensible heat and heat of adsorption cannot be used for heat regeneration and there is a significant waste heat [16]. Two beds at least are needed to obtain a continuous and heat regenerative cycle. Heat recovery can be achieved by adding only a pump and heat recovery loop. In a simple heat recovery system two beds are operated out of phase: one bed is heated (regenerated) while the other is cooled [3]. The bed to be cooled transfers its heat to the bed to be heated. This recovery process leads to a higher COP than that of basic cycle. The greater the amount of heat regenerated, the higher COP can be obtainable. An adsorption refrigeration cycle with heat recovery is shown in Figure 1.3.

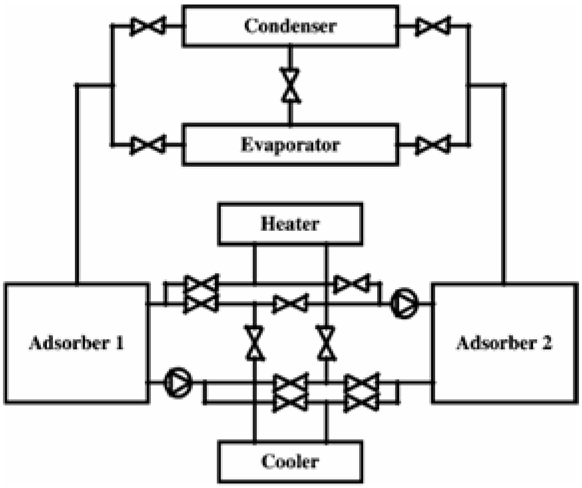

Figure 1.3 Schematic of two-bed adsorption refrigeration cycle with heat recovery [9].

Multi-beds can be adopted to get more heat recovery and hence to achieve higher COP, but the operation of a practical system is complicated [17]. Further, using multi-beds can increase the capacity of the system and the flexibility in building the system [9]. The recovered thermal energy can reach about 30% of the total necessary heat input of the basic cycle [14]. More details for working principles of the heat recovery cycles can be found in Wang et al. [18] and Saha et al. [19]. Various applications of heat recovery systems can be seen in references [20-24].

The COP of the heat recovery system can be written as [25,26]:

$$COP = \frac{Q_{evap}}{Q_{1-2} + Q_{2-3} - Q_{reg}} \tag{1.2}$$

where Q_{reg} is the heat recovered. Q_{1-2} and Q_{2-3} are heats supplied to the bed during 1-2 and 2-3 processes in Figure 1.2, respectively.

1.1.3 Heat & Mass Recovery Systems

In addition to heat recovery, it is possible to employ refrigerant mass recovery between the adsorbent beds to enhance both the SCP and COP [27]. In a mass recovery process, a certain part of pressurization/depressurization process can be done by transferring refrigerant vapor between the beds. The mass recovery process can be simply made by the connection of two beds with piping and valve [28]. Upon connecting the two beds directly, before switching between adsorption and desorption, refrigerant vapor flows from the high pressure desorber (high-temperature bed) to the low pressure adsorber (low-temperature bed) [29]. The desorber further desorbs and the adsorber further adsorbs hence the refrigerant mass circulation is increased inside the beds [30]. The process continues until an equilibrium pressure (approximately the average of evaporator and condenser pressures) is obtained. Mass recovery increases the cyclic adsorption capacity and hence the SCP and also increases the ability of an adsorption cycle to utilize low temperature heat source [31]. A series of investigations of mass recovery systems has been made by two research groups in Tokyo University of A&T [32-37] and in Shanghai Jiao Tong University [38-43].

The advantages of both heat and mass recovery concepts can be integrated in multi-bed adsorption cycles. Figure 1.4 shows a heat and mass recovery cycle in the Clapeyron diagram (lnP vs 1-/T). Desorber which is at the regeneration temperature T_{g2} and condensing pressure P_c is to be cooled to serve as adsorber (temperature from T_{g2} to T_{a2}, pressure from P_c to P_e) while adsorber which is at T_{a2} and evaporating pressure P_e is to be heated to serve as desorber (temperature from T_{a2} to T_{g1}, pressure from P_e to P_c). Pressure changes inside the beds are accelerated by the connection between the beds and the beds reach an equilibrium at the average pressure $P_m=(P_e+P_c)/2$. This process causes more desorption in the desorber and more adsorption in the adsorber. Heat recovery is represented by e-e’ line while mass recovery is represented a_3-g_3 line [44]. The heat recovery recovers thermal energy from the temperature difference between the beds while the mass recovery increases the cycled refrigerant mass [45]. As a result, SCP and COP of the adsorption cycle can be effectively improved. Working principle of heat and mass recovery cycle is well described in [46-50].

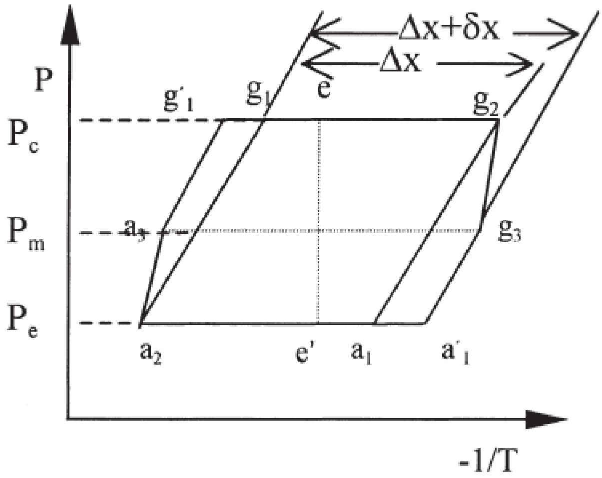

Figure 1.4 Diagram of heat and mass recovery cycle [44].

The effect of mass recovery on the cycle performance strongly depends on the system operating conditions [51]. Therefore, the best improvement in both SCP and COP can be achieved by proper selections of the operating conditions and recovery times for the specific demands of the system [31,52]. The influence of mass recovery also depends on the sorption characteristics of the pair [53]. The SCP and COP can be improved by 20% in a properly designed heat and mass recovery cycle [54] and can be further improved with the intensification of heat transfer inside the beds, for example by the utilization of heat pipe technology [55-59]. Mass recovery can be carried out before or after heat recovery, but gives higher performances when carried out before heat recovery [60]. Heat and mass recovery cycle not only can improve SCP and COP, but also can shorten the cycle time [61].

1.2 Thermal Wave Cycle

Thermal wave cycle was first proposed by Shelton [62]. Thermal wave cycle is the simplest way of heat regeneration. There should be at least two adsorbent beds to obtain a heat recovery cycle as mentioned before. Thermal wave cycle has two adsorbent beds and a reversible heat transfer fluid (HTF) loop. There are two heat exchangers (heater and cooling heat exchanger) and one (or two) circulating pump connected in series in the loop. To achieve higher COP values heat is recovered so that HTF (high temperature oil) in the loop receives heat from the hot bed and transfers this heat to the cold bed. There are additional heating and cooling in the heat exchangers.

The cycle is illustrated in Figure 1.5. Evaporator (18) and condenser (15) are connected to both adsorbent beds (bed 1 and bed 2) in parallel through check valves. The check valves connected between the condenser and the beds allow refrigerant vapor to flow only from the beds to the condenser. The check valves connected between the evaporator and the beds allow refrigerant vapor to flow only from the evaporator into the beds. An expansion valve is connected between the evaporator and the condenser and allows refrigerant flow from the condenser to the evaporator. The refrigerant vapor desorbed from the bed being heated flows to the condenser while refrigerant vapor coming from the evaporator flows to the bed being cooled to be adsorbed therein [62].

The HTF may be operated in two different ways. One way is to circulate part of the HTF heated by the heater through the bed to be heated and then directly back to the heater for reheating while circulating another part of the HTF cooled by the cooling heat exchanger through the bed to be cooled and then directly back to the cooling heat exchanger. Another way is to circulate the heated HTF from the heater through the bed being heated, then through the cooling heat exchanger for further cooling, then through the bed being cooled, and finally back to the heater for further heating of the HTF [62]. The second type of circulating loop is considered here.

The temperature profiles for the beds during the four steps of the thermal wave cycle are shown in Figure 1.6. The four steps of the cycle are performed in the following manner. In step 1, HTF is circulated in a clockwise direction and hot fluid at T_h flows from the

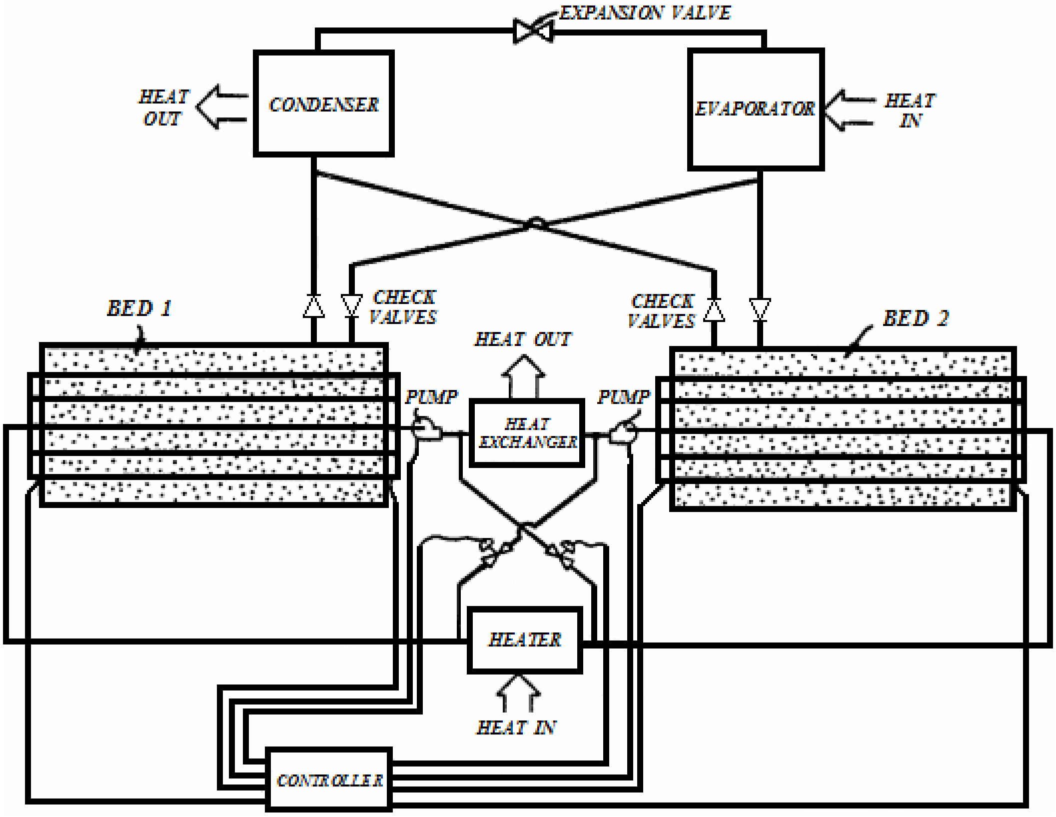

Figure 1.5 A schematic drawing of the thermal wave cycle [62].

heater through the bed 1. The heat transfer fluid then passes through the cooling heat exchanger and then through the bed 2. The fluid finally comes back to the heater. So, the bed 1 is heated for desorption while the bed 2 is cooled for adsorption. The heater always heats the fluid to upper operating temperature T_h. Temperature profiles of both beds at the first step are illustrated in Figure 1.6. The temperature profile is illustrated at the beginning of the step in a solid line and at the end of the step in a dashed line. The temperature of the fluid in bed 1 decreases by generating a thermal wave front (or temperature front) and in bed 2 temperature of the fluid increases by generating an opposite shaped thermal wave front. The thermal wave fronts move along the beds (from the left to the right in step 1) until they come to the other ends of the beds. On the other hand, the temperature of bed 1 increases to T_h while the temperature of the fluid decreases to T_{l+}. The fluid at temperature T_{l+} enters the cooling heat exchanger and cools to the lower operating temperature T_l. The HTF then is heated to temperature T_{h-} passing through the bed 2 while the bed 2 is cooled to temperature T_l [62].

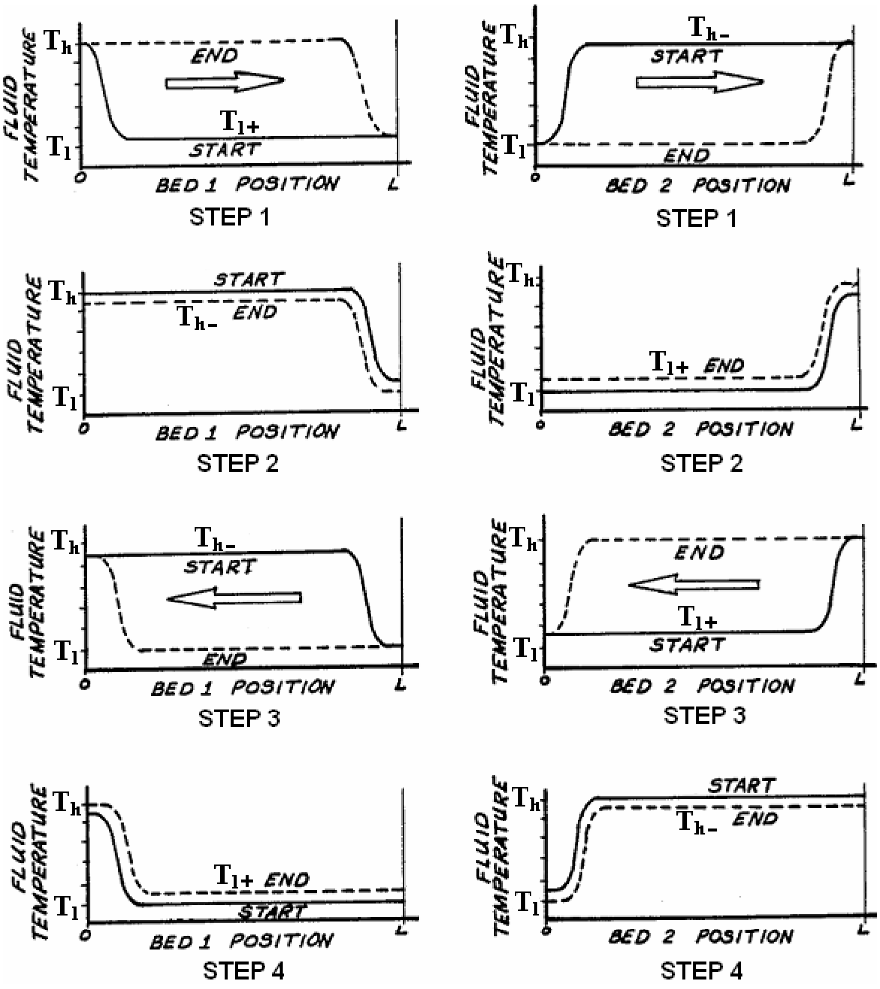

Figure 1.6 The temperature profiles during operation steps [62].

The flow direction of the heat transfer fluid is reversed and step 2 starts when the fluid temperature at the right end of the bed 1 raises a prescribed amount above the initial bed temperature T_{l+}. The HTF is circulated in a counter-clockwise direction in step 2. However, the purposes of the heater and cooling heat exchanger do not change such that the heater always heats the fluid while the cooling heat exchanger always cools the fluid. The hot HTF leaving the heater now enters bed 2 from the right end of the bed and heats the bed desorbing water vapor from the adsorbent at that end of the bed. The desorbed refrigerant vapor causes an increase in the pressure of bed 2 since there is no vapor flow from the bed to the evaporator due to the check valve or to the condenser due to pressure difference (isosteric process). On the other side, the cold fluid leaving the bed 2 first passes through the cooling heat exchanger for further cooling and enters bed 1 from the right end. The cold HTF causes adsorption of the refrigerant vapor. This adsorption decreases the pressure of the bed 1 since there is no vapor flow from the evaporator due to the pressure difference and from the condenser due to the check valve. Therefore this step is termed *pressurization* for the bed 2 and *depressurization* for the bed 1. As the pressure in the bed 2 increases, the adsorbent material in the bed 2 tends to adsorb more refrigerant vapor and this adsorption releases the *heat of adsorption* resulting in an increase in the temperature of the bed 2 from T_l to T_{l+} as seen in Figure 1.6. In a similar manner, as the pressure in the bed 1 decreases, the adsorbent material tends to desorb some of adsorbate and this desorption receives the *heat of desorption* resulting in a decrease in the temperature of the bed 1 from T_h to T_{h-}.

The fluid continues to flow in counter-clockwise direction in step 3. The heater heats the fluid leaving the bed 1 at T_{h-} exit temperature to temperature T_h. The hot fluid then enters the bed 2 and causes to desorb refrigerant vapor at condenser pressure. The thermal wave moves to the left in bed 2 and the refrigerant vapor desorbed moves to the condenser. The desorption process continues until the fluid temperature at the left end of bed 2 rises a prescribed amount above the initial bed temperature of T_{l+}. On the other hand, the HTF leaving the bed at temperature T_{l+} passes through the cooling heat exchanger and then enters bed 1 at temperature T_l. Refrigerant vapor coming from the evaporator is adsorbed by the adsorbent in the bed 1 since the pressure inside the bed is at evaporator pressure. The adsorption progresses to the left side of the bed together with the thermal wave. The adsorption is at the maximum level when the temperature of the HTF at the exit of the bed drops a prescribed amount below the temperature T_{h-} (see Figure 1.6).

The HTF flow is again reversed in the last step (step 4). The bed 1 is heated for desorption while bed 2 is cooled for adsorption. This step is a pressurization process for the bed 1 and depressurization process for the bed 2. Temperature profiles at the start and the end of the processes are shown in Figure 1.6 for step 4. Heat of adsorption causes an increase in the temperature of bed 1 while heat of desorption causes a decrease in the temperature of bed 2 due to the reasons mentioned before.

The controller monitors the temperature of the HTF at both ends of both beds and reverses the HTF flow when the temperature of the fluid at the exit of the bed reaches a prescribed amount above the initial bed temperature. The exit temperature of the HTF from either bed may be used by the controller to reverse the HTF flow.

There are other ways for obtaining a continuous and heat recovery cycle. Thermal wave cycles are applicable to only a single stage cycle. The single stage cycles have some restrictions, that is, they do not perform well at very low temperatures and cannot effectively use high-temperature heat source. *Multi-stage* and *cascade* cycles can be used to improve the system performance under such situations [17]. However, the construction of these cycles is rather complicated. In these cycles, adsorption and/or desorption processes are performed at different temperature and/or pressure levels for heat recovery. Cascade cycles are especially used if the operating temperature range of the cycle is large [63]. Multi-stage cycles use the same working pair and can show a significant performance improvement by the internal re-use of heat of condensation or adsorption while cascade cycles use different working pairs and can make good use of high temperature heat source by performing evaporation process in stages. COP of a cascade cycle may be much (about 62%) higher than that of a heat and mass recovery cycle [64].

1.3 Enhancement of Heat and Mass Transfer in the Adsorbent Bed

Main factors limiting the performance of adsorption cooling cycles are poor heat and mass transfer in the adsorbent bed. The poor heat and mass transfer prevent adsorption machines from commercialization and widespread utilization [31]. The reason for poor heat transfer is high thermal resistances caused by low thermal contact between the metal and the adsorbent at the interface and by low thermal conductivity of the adsorbent. Poor heat and mass transfer result in slower reaction rates, long cycle times, and low SCP and COP. These drawbacks also lead to bulky and costly systems. The size and cost of the adsorption systems must be reduced to become more attractive [27]. It is also essential to control limiting factors of heat and mass transfer in order to optimize the adsorbent bed [8]. Considerable efforts have been done by different research groups to enhance heat and mass transfer in the adsorbent bed. Two techniques are generally applied for this purpose: adsorbent bed design and adsorbent material improvement.

1.3.1 Improvement of Adsorbent Bed Design

Adsorbent bed of the adsorption cooling cycle is designed differently from conventional heat exchangers in geometry and shape to enhance heat transfer. Mass transfer that depends on both interparticle flow and intraparticle diffusion of the refrigerant should also be considered in the bed design [7]. Heat capacity of metal used between adsorbent and HTF should also be minimized [31]. Studies on the bed design can be classified in three categories:

1.3.1.1 Extended Surfaces

Different types of heat exchangers (HXs) with and without fins can be used for the adsorbent bed. HXs can be designed with extended surfaces to increase the heat transfer area. A flat-plate type HX with fins [65], a serpentine flat-pipe HX, a spiral plate HX [66], plate-finned tubes (aluminum plate), and a capillary tube bundle HX [67] have been investigated. The HXs can be seen in Figure 1.7. The drawback of the extended-surface HX is the increase in the thermal capacity of the adsorbent bed [8,27]. On the other hand, mass transfer is enhanced by creating voids in the bed. Using materials with high surface area and adsorption capacity like activated carbon fiber [68] and creating gas paths through the bed [69] are some of enhanced mass transfer applications. However, extended surfaces will not be a suitable solution for both the beds having low wall heat transfer coefficient and the adsorbents having swelling and shrinking effect [27].

1.3.1.1.1 Constructal (tree-network) theory

Constructal theory is a new theory that aims to enhance flow (heat, fluid, mass) characteristics. There are imperfections in flow against resistances. The constructal design method is about the *optimal distribution of imperfection*. The constructal law calls for configurations with successively smaller global flow resistances in time. Resistances cannot be eliminated. They can be matched neighbor to neighbor, distributed (vascularized) so that their global effect is minimal and the whole system is the least imperfect that it can be [70].

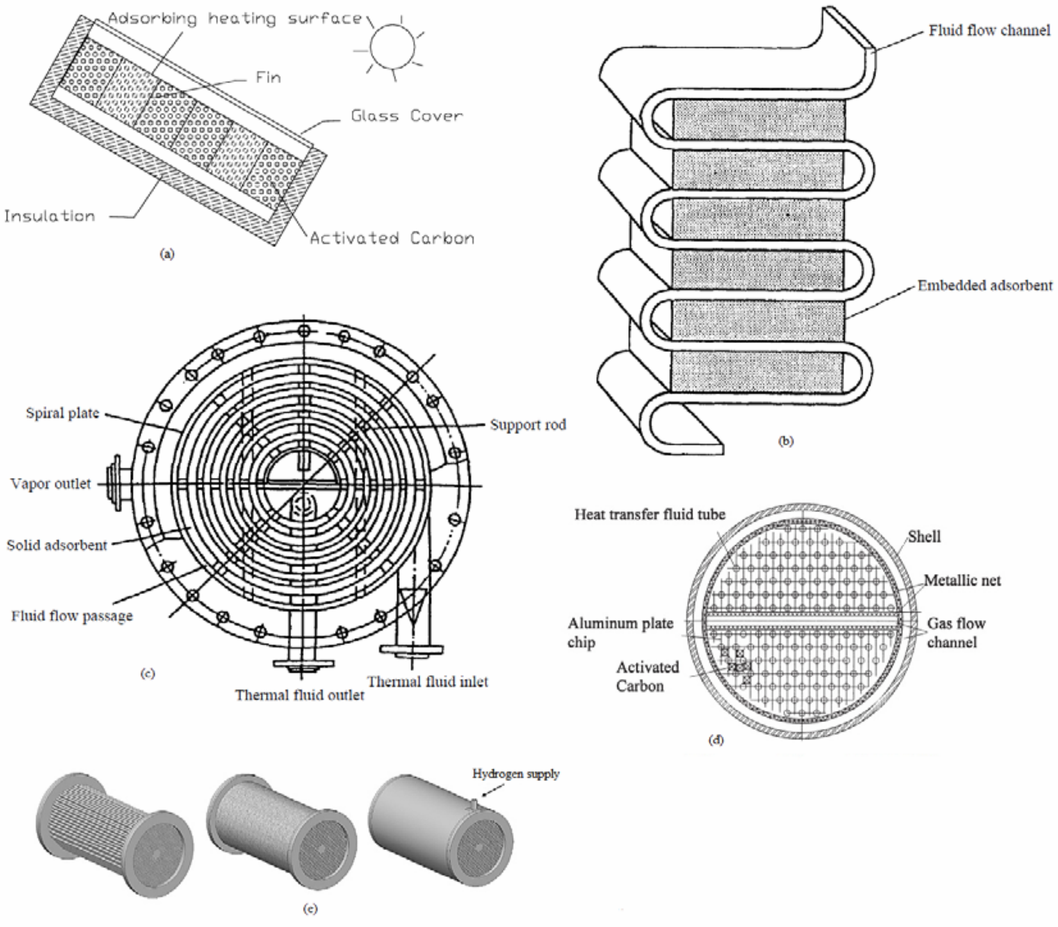

Figure 1.7 Various adsorbent beds with extended surface: (a) Flat-plate HX with fins; (b) Serpentine flat-pipe HX; (c) Spiral plate HX; (d) Plate-finned tubes; (e) Capillary tube bundle.

The configuration that the constructal law suggests is a tree-shaped flow which is the theoretical way of providing effective flow access between one point (source, sink) and an infinity of points (area, volume). The tree is a complex flow structure, which has multiple-length scales that are distributed non-uniformly over the available area or volume. Thinking of the vascularized tissues, city traffic or trees in electronics makes one to get a sense of universality of the principle that was used to generate and discover the tree configuration [70]. For detailed information about constructal theory, see [70,71].

In this study, the constructal theory is planned to use in optimum design and construction of the bed. Thus, the shape and dimensions of the finned tube are determined by the constructal theory. However, the optimum design of the adsorbent bed determined is not used due to the difficulty in the manufacturing. Instead, a simple geometry easy to manufacture is used.

1.3.1.2 Coated Beds

This method is based on the adhesion of the adsorbent to the wall of HX tube or plate to increase the wall heat transfer coefficient by decreasing the contact resistance. Various coating techniques can be applied to obtain a uniform surface: spray coating; curtain coating; coil coating and electrically assisted coating [9]. To improve the wetting of the metal surface and to promote physical and chemical interactions between metal surface and growing crystals, the metal surface should be pre-treated before coating [72]. If a homogenous coating and stabilization of the adsorbent can be obtained, a strong rise of the metal/adsorbent wall heat transfer coefficient and, consequently, a significant improvement in the SCP of the system can be achieved [73]. There is an optimum value of adsorbent layer thickness for each wall thicknesses of the tubes employed [74]. The pressure applied in coating should also be optimized to decrease contact resistance avoiding problems caused by high mass transfer resistances [75]. Several experimental activities were performed with different adsorbent materials [76-78]. Figure 1.8 shows examples from coated adsorbent beds in the literature.

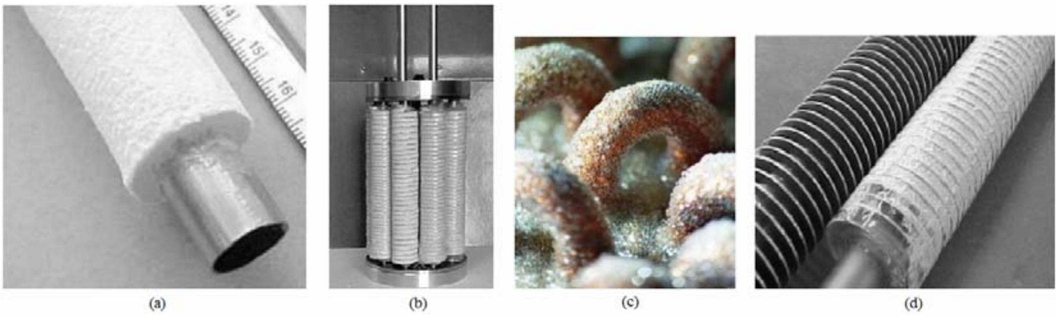

Figure 1.8 Coated adsorbent beds: (a) Metal-bound zeolite layer [73]; (b) Finned tubes HX coated with zeolite [76]; (c) Silica gel coated tube HX [78]; (d) Finned tube coated with silica gel [7].

1.3.1.3 Heat Pipe Technology

In adsorbent bed design, a heat pipe can be used to reduce the thermal resistance between the HTF and the adsorbent bed wall. Heat pipes can transfer a considerable amount of heat using a small area since high heat transfer coefficient (10^3-10^5 W/m^2K^{-1}) in the evaporator and condenser zones of heat pipes can be obtained [79]. The evaporation of the working fluid of the heat pipe can absorb both the sensible heat and heat of adsorption during adsorption phase while the condensation of the fluid can release the necessary heat to regenerate the adsorbent bed during desorption phase. The use of heat pipe could also help to reduce the high initial costs of adsorption machines due to the lack of moving parts to drive the HTF [27]. Several applications of heat pipe can be seen in [80-83]. The components of different heat pipe adsorbent beds are shown in Figure 1.9.

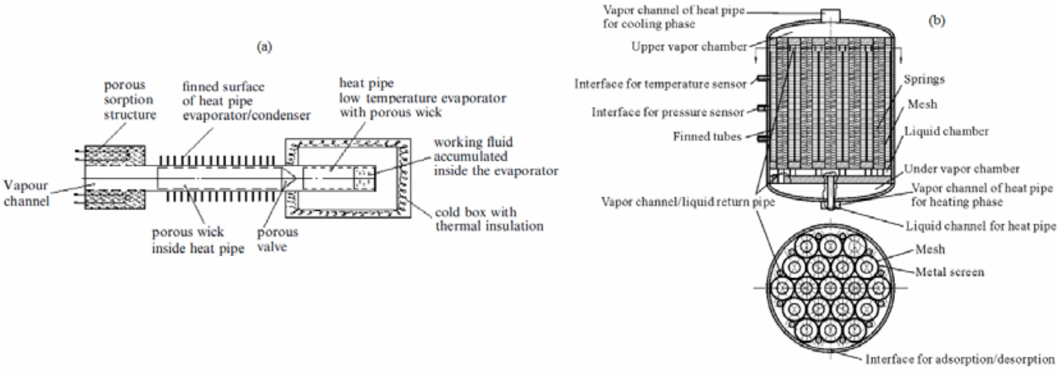

Figure 1.9 Heat pipe adsorbent beds: (a) Sorption heat pipe [79]; (b) Split heat pipe [80].

1.3.2 Improvement of Adsorbent Material

Granular adsorbents have low effective thermal conductivity due to the high porosity and discontinuity of the adsorbent material. The enhancement of thermal conductivity of the adsorbent is one of the most effective methods to enhance the heat transfer since the conduction is the dominant heat transfer mechanism in the bed. However, the improvement in the heat transfer performance of the adsorbent usually results in a reduction in the mass transfer performance. The mass transfer must be enhanced as well as heat transfer if the effect of the mass transfer on the adsorption system is significant. Reducing the thickness of the adsorbent layer may be a solution to poor mass transfer, but at the expense of lower effective capacity of the bed due to less amount of adsorbent [31].

New adsorbent materials and consolidated adsorbents are being developed to achieve both heat and mass transfer enhancement and compact size [84]. The most common methods to increase thermal conductivity in the adsorbent bed are the use of additive materials with high thermal conductivity by mixing with the adsorbent and the use of consolidated adsorbents.

1.3.2.1 Additives

Materials with high thermal conductivity such as metallic pieces, metal powders, expanded graphite, activated carbon, carbon fibers, polyaniline and vermiculite have been used as additives to granular adsorbents in order to enhance heat transfer, mass transfer or both in the bed. Mixing the different size adsorbent granules together can also improve the heat transfer [31]. Expanded graphite, carbon fibers and vermiculite improve the mass transfer increasing the permeability significantly. Metallic foams can also be used as an additive mixing with granules to increase thermal conductivity but these lead to high thermal contact resistance between the foams and granules [84]. Also, additional costs due to additives can reach about ten times the conventional material cost [85]. Some of the additives such as metallic pieces do not play a role in adsorption process, and therefore creates a dead mass in the bed. Thus, the effect of the dead mass on SCP and COP is to be considered [86].

Expanded graphite originates from the exfoliation of graphite intercalation compounds submitted to a brutal thermal shock and it provides a support matrix for reactive materials [87]. Activated carbon is produced from a wide variety of carbonaceous materials activated by physical or chemical means to increase the porosity. Carbon fibers can have axial thermal conductivities as high as 1100 W/mK^{-1} depending on the fiber type and quality [88].

Several studies have been performed to investigate the effect of the additives on heat transfer rate, SCP and COP [89, 90]. Metal pieces used in the former study [89] are shown in Figure 1.10.

Figure 1.10 Metal pieces used to enhance thermal conductivity: (a) copper; (b) aluminum; (c) stainless steel; and (d) brass [89].

1.3.2.2 Consolidated Adsorbent Beds

Another way of heat transfer enhancement in the bed is to use consolidated adsorbents with high thermal conductivity. Consolidated adsorbent beds are obtained from adsorbent powders combined with a binder or other materials with high thermal conductivity. Consolidation can provide heat conduction paths by producing continuous adsorbent blocks with reduced void spaces. Thus, a dramatic increase in the thermal conductivity and wall heat transfer coefficient can be obtained [91]. However, consolidated adsorbents have generally lower mass transfer than granular adsorbents and this causes low reaction rates especially in vacuum systems. Therefore, permeability should also be taken into account as well as thermal conductivity and wall heat transfer coefficient. Heat and mass transfer properties can be controlled by controlling the compression pressure and the mass ratio between the adsorbent and inert material during the consolidation process. Metallic foam used in the compound has significant effect on the thermal conductivity. Carbon fibers are used to increase the thermal conductivity and permeability in the bed.

The length and position of the carbon fibers used are also important parameters that affect the heat transfer process [27].

Thermal conductivity obtained from a consolidated adsorbent varies by the consolidation method used. The thermal conductivity can reach 40 W/mK^{-1} in consolidated activated carbon [92], 32 W/mK^{-1} in consolidated activated carbon with expanded graphite [93], 49 W/mK^{-1} in consolidated expanded graphite-metallic salt complex [94], 20 W/mK^{-1} in consolidated composites of expanded graphite and silica gel [95] and 8 W/mK^{-1} in consolidated compound made from a mixture of zeolite and copper foam [96].

Sinterized metal foams that have high adsorbent to metal mass ratio are also used for thermal applications due to their relatively higher adsorption capacities [97].

1.4 Adsorbents, Refrigerants and Pairs

1.4.1 Adsorbents

The suitable adsorbents are porous materials that should adsorb large amounts of refrigerant fluids in vapor phase [98]. In adsorption refrigeration systems, the adsorbents have the following characteristics [1,91]:

- High adsorption capacity in a small temperature range
- Desorption of most of the refrigerant when exposed to thermal energy
- Low cost and wide availability
- Good thermal conductivity
- High latent heat of adsorption compared to sensible heat
- Non-toxic and non-corrosive
- No deterioration with use or age

The adsorbents commonly used in adsorption refrigeration systems are zeolite, silica gel, activated carbon and alumina [84,99]. There are different types of each four having different characteristics. The smaller the pore size, the higher the adsorption energy and the regeneration temperature generally. Adsorbents may be classified by the degree of temperature-lift (adsorber-evaporating temperature or desorber-condensing temperature). The degree of temperature-lift is a function of the size of adsorbent micropore and smaller micropores lead to higher temperature-lifts [84].

Zeolites are porous crystalline aluminosilicates [100]. There are about 40 types of natural zeolites and about 150 types of synthetic zeolites [101]. The adsorption capacity of zeolite depends on the temperature and the adsorbate vapor pressure. Although for silica gel and active carbon, adsorption level is very low at low concentrations of the adsorbate, zeolites can adsorb large quantities of adsorbate even at very low concentrations. The shape of the adsorption isosteres, describing the adsorption equilibrium characteristics, makes the zeolite favorable in adsorption cycles. Zeolite has particular advantages at high temperatures (higher than 100 ^{o}C) although it may be in competition with the other adsorbents for low temperatures (below 100 ^{o}C) [102]. On the other hand, natural zeolites such as clinoptilolites are widely available in Turkey and can be activated to increase their adsorption capacity.

The binding energy of silica gels is lower than most carbons and zeolites. Therefore, the regeneration temperature of silica gels is comparatively lower (70-100 ^{o}C). For a non-regenerative cycle this leads to higher COPs since the adsorbent itself and container vessel does not need to be heated to high temperatures. In regenerative cycles, higher temperatures or temperature-lifts are required to achieve higher COPs and zeolites and carbons are used for such a high temperatures [84].

Carbons can be used with most refrigerants except for water and are available in the forms of granular, fibre, felt, cloth, extruded, and consolidated. Activated carbon is made of materials such as wood, coal, peat, fossil oil, chark, bone, coconut shell and nut stone [101]. Most of carbons used in adsorption refrigeration systems can adsorb ammonia or methanol up to 30% of its own mass while super-activated carbons can adsorb up to twice its mass having lower temperature-lifts. The adsorption process within active carbon is a function of active sites and pore size distribution [84].

1.4.2 Refrigerants

Refrigerant is one of the most important elements of any refrigeration system including adsorption cycles since the working conditions and the system compatibility with the environment principally depend on it. Requirements expected from the refrigerants used in adsorption refrigeration systems are listed as follows [1,91,101]:

- High latent heat of vaporization per unit volume (for high SCPs)
- Good thermal stability with the adsorbent at the cycle operating temperatures
- Non-toxic, non-polluting, non-flammable, non-corrosive
- Evaporation temperature below 0 ^{o}C
- Small molecular size to enable it to be adsorbed into the adsorbent
- Low saturation pressures (slightly above atmospheric) at normal operating temperature
- Low specific volume

Vapor pressure of the refrigerant must be near atmospheric pressure level in the temperature range between 263-353 K for technical and safety aspects.

The refrigerants commonly used in adsorption refrigeration systems are water, methanol and ammonia [99]. They have high latent heat, but, however different working pressures. There is no refrigerant that satisfies all the requirements listed above since each refrigerant has advantages and disadvantages. The characteristics of these common refrigerants are reported in Table 1.1.

The latent heat of the refrigerant should be high as compared with the specific heats of the adsorbent and metal container for energy efficiency. This is because the thermal energy added to or removed from the adsorbent and metal container does not directly contribute to the cooling or heating effect and is wasted. The utilization of refrigerants with comparatively low latent heat such as butane and R134a leads to very low COPs [84].

Table 1.1 Refrigerant characteristics [3].

Ammonia	**Methanol**	**Water**
Toxic	Toxic	Non-Toxic
Flammable in some concentrations	Flammable	Non-Flammable
Not compatible with copper	Not compatible with copper at high temperatures	Compatible with copper
High operating pressure	Low pressure	Extremely low operating pressures
Good latent heat	Good latent heat	High latent heat
Thermally stable	Unstable beyond 393K	Thermally stable
Non polluting	Polluting	Polluting

In some ways water is the ideal refrigerant since it has the highest latent heat of vaporization among common refrigerants and is non-toxic. It is used with zeolites and silica gels. However, the adsorption refrigeration systems using water as refrigerant may have vacuum leak and poor mass transfer problems due to the sub-atmospheric vapor pressure of the water. Moreover, the applications are limited to air conditioning and chilling since the minimum evaporation temperature of water is a few degrees Celsius [84].

The vapor pressure of methanol is also sub-atmospheric but higher than that of water. Methanol is suitable for ice-making and can be used with silica gels, active carbons and certain zeolites. However it is unstable at temperatures higher than 120 ^{o}C [84].

There is no mass transfer limitations in ammonia based systems since ammonia has higher vapor pressures (a few bars). Ammonia is environmentally friendly and stable with the adsorbent until at least 200 ^{o}C. It can be used for cooling down to about -40 ^{o}C. However, the disadvantages of ammonia are being toxic and noncompatible with copper and copper alloys, and having less than half the latent heat of water [84].

1.4.3 Adsorbent/Refrigerant Pairs

The selection of any adsorbent/refrigerant pair depends on certain desirable characteristics of its constituents ranging from their thermodynamic and chemical properties to their physical properties and to their costs or availability [91].

Current adsorbent/refrigerant pairs are summarized in Table 1.2 in light of studies in the literature [17]. The table includes technology and heat source used and performances (both COP and cooling power) as well as the pair used in the study.

Zeolite/water, silica gel/water, activated carbon/methanol and activated carbon/ammonia appear to be the most suitable pairs. In selection of the pair, some other considerations such as environmental conditions and cost as well as design and operating parameters should be taken into account. Zeolite/water pair, for example, reaches the highest COP values in mild climate conditions [1].

Three of the adsorbent/refrigerant pairs mentioned above have usually been used in adsorption refrigeration systems. The first is molecular sieve (zeolite) 13X-water pair which is very suitable to be used in adsorption cycles because of the extremely non-linear pressure dependence of its adsorption isotherm. Molecular sieve can adsorb large quantities of water vapor at ambient temperature even for low partial pressures. Since water has a convenient boiling point and high latent heat of vaporization, the molecular sieve 13X-water pair is one of the most preferred working pair. The pair of molecular sieve 13X-water has both high adsorptive capacity and high heat of adsorption. The only disadvantage of this pair is high regenerating temperature for desorption and low operating pressure. The second pair is silica gel-water. The adsorption refrigeration system with silica gel-water pair can operate at a lower temperature (70-100 ^{o}C) and is more suitable for using a low temperature heat source or solar energy. However, the refrigeration capacity of silica gel is lower than that of molecular sieve 13X, so a larger adsorbent bed is required. The third is activated carbon-methanol pair. Since methanol has a relatively lower solidifying point (-98 ^{o}C) and a higher boiling point (64.7 ^{o}C), the adsorption system using activated carbon-methanol pair can produce a temperature below 0 ^{o}C. The disadvantages of this pair are that the latent heat of evaporation of methanol is only half that of water and methanol is harmful to the environment [103]. Furthermore, the maximum regenerating temperature is limited to 150 ^{o}C due to methanol instability at higher temperatures [91].

Table 1.2 Pairs used in developing technologies [17].

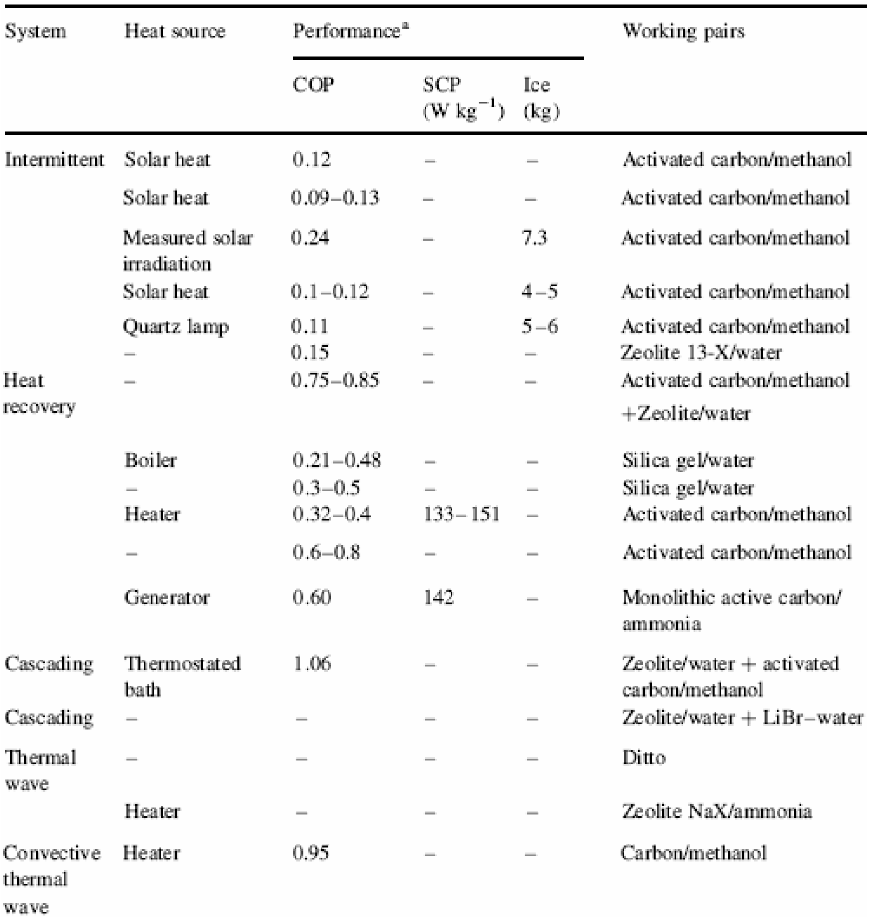

System	Heat source	Performance[a]			Working pairs
		COP	SCP (W kg^{-1})	Ice (kg)	
Intermittent	Solar heat	0.12	–	–	Activated carbon/methanol
	Solar heat	0.09–0.13	–	–	Activated carbon/methanol
	Measured solar irradiation	0.24	–	7.3	Activated carbon/methanol
	Solar heat	0.1–0.12	–	4–5	Activated carbon/methanol
	Quartz lamp	0.11	–	5–6	Activated carbon/methanol
	–	0.15	–	–	Zeolite 13-X/water
Heat recovery	–	0.75–0.85	–	–	Activated carbon/methanol +Zeolite/water
	Boiler	0.21–0.48	–	–	Silica gel/water
	–	0.3–0.5	–	–	Silica gel/water
	Heater	0.32–0.4	133–151	–	Activated carbon/methanol
	–	0.6–0.8	–	–	Activated carbon/methanol
	Generator	0.60	142	–	Monolithic active carbon/ ammonia
Cascading	Thermostated bath	1.06	–	–	Zeolite/water + activated carbon/methanol
Cascading	–	–	–	–	Zeolite/water + LiBr–water
Thermal wave	–	–	–	–	Ditto
	Heater	–	–	–	Zeolite NaX/ammonia
Convective thermal wave	Heater	0.95	–	–	Carbon/methanol

1.5 Objectives of the Thesis

It is stated before that major disadvantages of adsorption cooling cycles are low COP and SCP values and long cycle times. In recent researches, studies to solve these problems are focused on three main aspects: i) to develop new cycles which can recover more heat; ii) to enhance the heat and mass transfer in the adsorbent bed; iii) to develop new adsorbent materials or new adsorbent/refrigerant pairs.

From the thermodynamic point of view, the maximum thermal regeneration can be achieved by dividing the adsorbent equally among an infinite number of beds distributed evenly throughout the cycle, and then allowing these beds to interact thermally to minimize the heat transfer from the high-temperature source [104]. On the other hand, an another study by Baker [105] has shown that the thermodynamic limits to the performance of the thermal wave cycle are predicted to be higher than that for a system with an infinite number of beds following the basic adsorption cycle and utilizing maximum thermal regeneration between the beds. These results show that the improvements in the thermal wave cycles would be more effective than that in the basic cycles.

The basic problem in the design of adsorption cooling cycles is the design of the adsorbent bed. This is because the adsorbent bed is the major component of the cycle. From mechanical engineering point of view, the enhancement of heat and mass transfer in the adsorbent bed is focused on rather than to develop a new adsorbent. This dissertation aims to enhance the heat transfer in the adsorbent bed. Low thermal conductivity of the bed reduces the rate of heat transfer and causes long cycle times. Moreover, long thermal wavelengths cause less effective heat recovery. Thermal wavelength should be minimized in order to enhance the effectiveness of the heat recovery. A typical thermal wave front is shown in Figure 1.11.

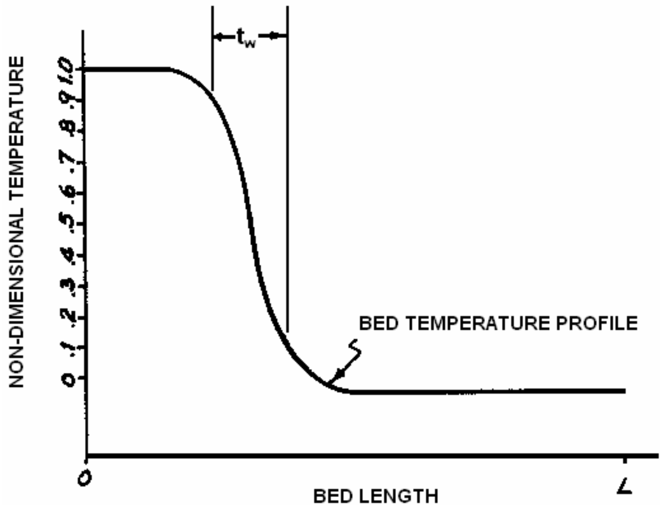

Figure 1.11 The shape of thermal wave in the bed [62].

The shorter the thermal wavelength, the greater volume of the bed can be cycled between the upper and lower temperatures and the less dead volume is obtained at the ends of the bed which is not completely cycled through the temperatures. On the other hand, a thermal wave is generated both in the heat transfer fluid passing through the bed and in the adsorbent bed itself and it is desirable that the two wavelengths coincide as much as possible and move in together axially along the length of the bed [62].

The main objective of this study is to investigate the improvement in the heat transfer inside the adsorbent bed of a thermal wave adsorption cooling cycle by using a new model finned tube adsorbent bed. The study is performed both theoretically and experimentally. The theoretical modeling and simulations are made with Comsol Multiphysics software package. An experimental setup that was established in a previous scientific project is used for the experimental study. The adsorbent bed of the experimental setup that was designed for the basic adsorption cycle is changed with the new model adsorbent bed. The results from the experimental study are compared with those of the theoretical study. In addition to the main objective, the most suitable adsorbent/refrigerant pair for the thermal wave cycle examined is investigated by using zeolite-water and silica gel-water pairs.

CHAPTER 2

LITERATURE SURVEY

This chapter is a review of previous studies performed on thermal wave cycles. The literature survey covers convective thermal wave cycles as well as the basic thermal wave cycles. The studies performed on the basic and other types of adsorption cooling cycles are not referred to here since they were well defined and cited in Chapter 1.

2.1 Basic Thermal Wave Cycles

Coupled heat and mass transfers in an adsorbent bed being heated with external fluid were studied numerically by Sun et al. [106]. Heat transfer and Ergun flow of the adsorbate inside the adsorbent bed were incorporated in their one-dimensional model. Their study showed that uniform pressure condition assumption inside the bed could not be accepted since the dynamics of the bed were significantly limited by poor mass transfer inside the bed. Poor heat transfer resulted from low gas density at low operating pressures of zeolite 13X/water pair. The poor mass transfer can lead to very large pressure variations and hence pressure cannot be assumed to be uniform at low operating pressures and long adsorbent beds whereas the uniform pressure assumption is acceptable for pairs operating at much higher pressures (several bars).

Shelton et al. made a thermodynamic analysis of the thermal wave cycle assuming a square thermal wave temperature profile. The effects of several design and operating parameters on the cycle performance (COP) were also investigated. Results showed that increasing the temperature of high-temperature heat source up to 316 ^{o}C increased the cycle COPH (heating COP), with further increases having a small detrimental effect on the performance for selected ammonia/zeolite pair. The COPH decreased with decreasing temperature of low-temperature heat source, i.e. evaporation temperature. But this decrease was half of the decrease in an electrically driven heat pump performance over the same temperature ranges. Results also showed that wavelengths greater than 0.7 (for dimensionless bed length) resulted in severe drops in the performance due to lower heat regeneration. The researchers concluded that negative effect of thermal mass of a heat exchanger embedded in the adsorbent bed could be minimized by heat recovery [107]. Same researchers made another thermodynamic analysis using ramp wave model rather than a square wave model to simulate the thermal wave front [108]. They used a more physically realistic ramp wave model to overcome the shortcomings of the square wave model. In this model, temperature wave was assumed to be linear while adsorption profile was obtained as a segmented ramp based on the temperature at the midpoint of the ramp. Both models can be seen in Figure 2.1. They investigated the effects of the same parameters with the previous study on the performance and found similar results in trends but smaller COPs in magnitude.

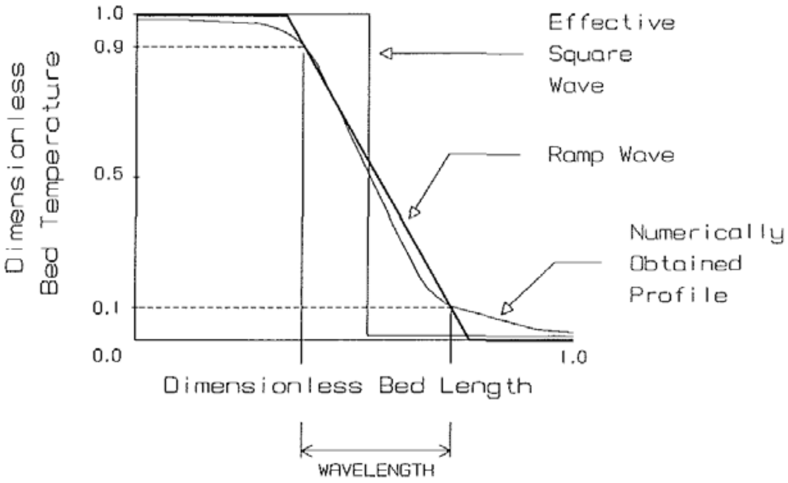

Figure 2.1 Ramp and square wave approximations [108].

Sun et al. [109] performed a numerical analysis of an adsorptive heat pump system with thermal wave heat regeneration. The analysis was based on a two-dimensional model which considered axial heat transfer in the fluid and radial heat conduction in the adsorbent bed. The two-dimensional model was solved in a one-dimensional way by neglecting the axial heat conduction in the adsorbent bed. Uniform pressure in the bed was assumed since ammonia that works at high pressures was used as adsorbate. The effects of the thermal conductivity and cycle time on the performance were also presented. Both the COP and PCP (power of cold production per unit mass of adsorbent) increased with thermal conductivity as expected. However the effect lessened at thermal conductivities higher than 10 W/(mK). There was an optimum value of cycle time based on the intersection of the COP and PCP curves.

Thermodynamic and heat transfer models were integrated in [110]. By integrating the bed and fluid heat transfer equations into the thermodynamic model, the need for assuming a wave shape to calculate performance was eliminated. The effects of several major dimensionless groups such as DR (diffusivity ratio), Pe (Peclet number), Bi (Biot number) and KA_r (radial conductivity ratio) on the performance and capacity of the system were investigated. A stack of tube spirals located within a cylindrical shell was used to circulate the heat transfer fluid through the shells. The adsorption pair, heat transfer fluid tube, and the outer shell (collectively known as the bed) at a given radius and time were at the same temperature while the heat transfer fluid was at a different temperature and therefore the model was called two-temperature model. Results showed that COPH and capacity increased with increasing DR, Bi and KA_r and with decreasing Pe number. The decrease in performance and capacity with increased Pe number was caused due to longer wavelengths.

Another numerical analysis was made by Amar et al. using a two-dimensional model taking into account both heat and mass transfer in the adsorbent bed [111]. The study was performed on two different adsorption systems corresponding to quite different operating pressures: an activated carbon/ammonia pair and a zeolite/water pair. The effect of the bed permeability on COP and power of cold production (PCP) was investigated for two different gas flow configurations: axial and radial gas flow configurations. It was seen that in case of the axial gas flow configuration, the resistances to mass transfer were very important, even for a large permeability. This led to small cycled adsorbate masses and poor process performance. The performance for the radial gas flow configuration was always greater than that for axial configuration.

Local equilibrium theory was utilized to provide the asymptotic maximum performance obtainable from a thermal wave cycle by ignoring the effects of resistances to heat and mass transfer within the system [112]. Reducing the temperature of the heat source and raising the condenser temperature were found to reduce performance as expected. The cycle time and the slope of the temperature front increased by the movement of refrigerant inlet and outlet valves to the center of the bed. On the other hand, the division of the adsorbent bed into sections to restrict flow was found to have little effect on performance. Furthermore, it was an unexpected result of the study that each section of the sectioned bed could not reach the operating pressure simultaneously. Instead, the bed was first pressurized in the section where the temperature wave was located.

The second law analysis of the adsorption cycles with thermal regeneration was developed with the help of the concepts of “entropic mean temperature” and “equivalent Carnot cycles” [113]. The effects of the cycle time and flow rate of heat transfer fluid were analyzed. A reduction in the heat transfer fluid flow was seen to reduce the irreversibilities in the heat transfer between the fluid and the adsorbent bed significantly. This reduction yielded a reduction in the quantity of heat required from the heating source and hence a significant increase in the COP. However the reduction in fluid flow rate induced a quasi-proportional reduction in cooling power. The analysis gave an opportunity of determining the optimal cycle time considering different effects of the cycle time on COP and cooling power.

Pons et al. [114] stated that *global NTU* (number of transfer units) and Θ_0 (dimensionless outlet fluid temperature at the end of the cooling period) are two of the main parameters of adsorption cycles with thermal regeneration in the design and analysis of the cycles. The results of the model solving nonlinear differential equations with partial derivatives showed that these two were the basic parameters of the cycle although they did not appear directly in the equations. It was concluded that these parameters could be effectively used for optimization of the system and for comparison to other systems. The dependence of the COP on the *global NTU* was quasi-logarithmic until an asymptotic value of COP 1.6. Operational optimal value of Θ_0 was dependent on the *global NTU* value for the bed designed [115].

A novel refrigeration system whose adsorbent bed was a specially designed finned plate heat exchanger was proposed by Waszkiewicz et al. [116]. The finned heat exchanger was coated with a new type of zeolite, CBV 901, and tested with zeolite-methanol pair in both a single bed and twin bed (thermal wave) adsorption cycle. A mathematical code based on the Dubinin-Astakhov equation and thermodynamic analyses was developed to calculate the effects of operating conditions on COP. Real data was used in simulations to investigate heat transfer coefficients and temperature distribution in the heat exchanger. The results showed that the COP was obtained as 0.535 for the single bed and as 0.925 for the twin bed. The adsorbent bed design can be seen in Figure 2.2.

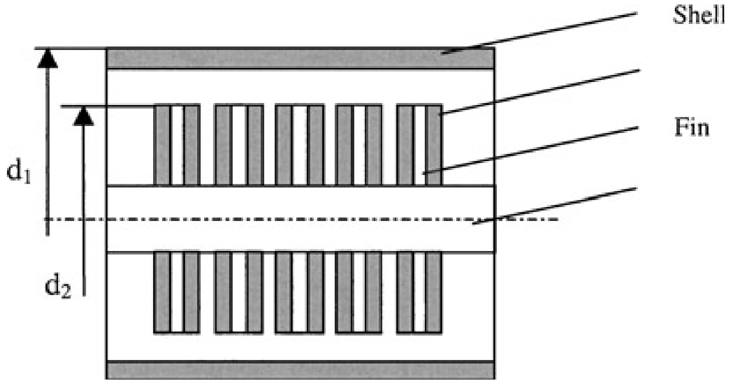

Figure 2.2 Shell-and-tube heat exchanger with coated fins, where d_1=100 mm is the outside diameter of the shell and d_2=76 mm is the diameter of the coated plate [116].

Zheng et al. [117] investigated the effects of two operating parameters, the regeneration temperature and the ambient temperature, on the performance and cooling capacity of a thermal wave adsorption heat pump with activated carbon-ammonia working pair. The ambient temperature was very important parameter since both the condenser and heat transfer fluid were cooled by the ambient air. The results showed that increasing the regeneration temperature increased both cooling capacity and COP. However, the improvement in the cooling capacity was more significant than that in COP with increasing regeneration temperature. The cooling capacity and COP increased by 50% and 20%, respectively, as the regeneration temperature was increased from 180 ^{o}C to 260 ^{o}C. The cooling capacity and COP increased significantly with decreasing ambient temperature. The cooling capacity and COP increased by 40% and 50%, respectively, when the ambient temperature was reduced from 35 ^{o}C to 25 ^{o}C. On the other hand, both increase in regeneration temperature and decrease in ambient temperature require the system to be operated at a higher bed cycling speeds (regeneration time). Results also showed that optimum bed cycling speeds were linearly related to the regeneration and ambient temperatures.

A numerical *3T* model of a solid sorption heat pump system working with thermal wave regeneration concept was developed and presented by Miles et al. [118] for analysis and design. It was referred to as *3T* model since the model calculated the time- and position-dependent temperatures of three different media in the adsorbent bed: heat transfer fluid, tube and sorbent. In this study, a variable input gas-fired (natural gas) heat exchanger was used to heat the beds for regeneration and electricity was used for pumps, fans and controls. In this way, the waste energy resulting from conversion of thermal energy to electricity was significantly decreased and the COP was therefore increased. A COP of 0.76 for cooling and a COP of 1.21 for heating were calculated based on the higher heating value of natural gas. Several bed designs using carbon-ammonia pair were built and tested on a laboratory test stand. The model also included an optimization methodology that could identify the combination of bed geometry and heat exchangers that provided the desired trade-off between equipment cost and annual operating cost.

Jet Propulsion Laboratory (JPL) in USA built and tested a series of cryogenic sorption refrigeration systems for spacecraft sensor cooling [119]. A JPL Shuttle flight experiment was planned to test a -263 ^{o}C (10 K) hydride sorption refrigerator for tracking missiles for Strategic Defense Initiative Office (SDIO) “Star Wars” program. JPL then applied this technology to domestic heat pumps using actual sorption isotherm data and detailed analytic thermal computer models. The analysis with the new regenerative system predicted reasonable values such as cooling COPs of at least 1.0 and heating COPs of at least 2.0 using carbon/ammonia pair.

Meunier et al. [120] focused on thermal irreversibilities caused by the cycle design to analyze the effect of the heat transfer fluid management and more specifically of the thermal coupling irreversibilities on the COP of two different regenerative adsorption refrigeration cycles: one was uniform temperature n-adsorber cycle and the other was thermal wave cycle. The analysis was performed using thermal entropy production concept as a direct measure of the efficiency degradation. Internal and external components of the thermal entropy production were discussed separately. The internal entropy production was due to heat recovery between adsorbers and the external entropy production was due to the thermal coupling between the adsorbers and heat reservoirs. The COP of the two regenerative cycles was also compared with the COP of Carnot cycle. The results showed that using regenerative cycles was the key issue to reduce the irreversibilities and increase the COP of a one-adsorber cycle. For uniform temperature n-adsorber cycle, the external thermal entropy production was reduced at the expense of an increase in the internal thermal entropy production due to the heat recovery phases and this yielded a COP value equal to 54% of the Carnot COP for an 11-adsorber cycle. On the other hand, for thermal wave cycle, the thermal entropy production and COP were highly dependent on the cycle time. For short cycle times, the external thermal entropy production was very small while the internal thermal entropy production was significant. For long cycle times, the external thermal entropy production was very large while the internal thermal entropy production in the adsorbers did not increase. The maximum COP for thermal wave cycle was obtained as 54% of the Carnot COP for optimum cycle time.

A ‘three-temperature’ model was used to investigate the effect of different parameters on the performance of a heat regenerative adsorption cycle [121]. The effect of the heat source temperature on the thermodynamic efficiency was investigated. Different internal vapor transports for pressurization and depressurization of the adsorber were examined for the pair zeolite NaX-water in order to reduce internal irreversibilities. The types of vapor transport were direct pressurization/depressurization, internal vapor mass recovery between the adsorbers (partial pressurization/depressurization) and separation of the adsorber into compartments (internal vapor redistribution). Results showed that the first transport method significantly reduced the COP, while second one enhanced the cooling power, and third one did not change the COP. The authors concluded that a heat regenerative adsorption cycle should be operated with vapor mass recovery and with only one vapor compartment in the adsorber.

A combination of a multi-effect desalination system with an open cycle adsorption heat pump with zeolite 13X-water pair using heat recovery implemented based on the thermal wave concept was studied by Zejli et al. [122]. A solar parabolic trough collector was used to heat the heat transfer fluid which flowed through the tubes in the adsorbent beds.

The water production, heat recovery and energy consumption of the system were calculated by a theoretical model developed based on equations in thermodynamic balance. This study was an innovative thermally driven distillation technique that offered promising possibilities for future developments.

Chahbani et al. [123] made an analysis of intraparticle mass transfer limitations on the performance of adsorption cooling cycle with thermal wave heat regeneration taking both heat and mass transfer into account. Linear Driving Force (LDF) model was used to obtain the mean adsorbed concentration within the particle. Effects of intraparticle mass transfer limitations on COP, SCP, the coefficient of regeneration, the refrigerant flow rate and the pressurization/depressurization times were investigated. Simulation results showed that the COP and the SCP were remarkably reduced due to the fact that the quantity of refrigerant cycled decreased. The authors concluded that the slow adsorption rate would require long cycle times which were not recommended from an economic point of view. Thus rapid diffusing refrigerant would be preferred to obtain higher performances. However, if cold production (the SCP) was the key issue for a specific application, the effect of using a slow diffusing refrigerant would not be very significant and could be easily compensated by increasing the cycle time. A schematic representation of the adsorber of the cycle analyzed is shown in Figure 2.3.

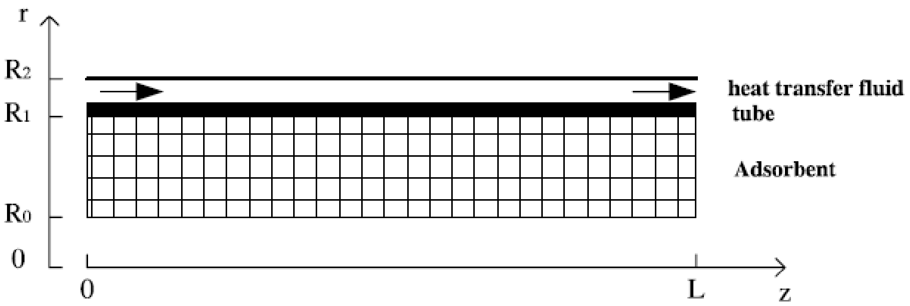

Figure 2.3 Schematic representation of the adsorber for [123].

A generative adsorption cycle based on the utilization of low-cost tubular modules arranged in a multirow bed was introduced by Critoph [124]. It was a kind of thermal wave cycle, capable of a high COP. The study was focused on the development of a small-scale combined heat, cold, and power (trigeneration) system using engine waste heat. Simulation of a specific module configuration showed that it was possible to obtain COPs in excess of 1.1 at the expense of very low SCP depending on a suitable choice of heating fluid flow rate and time between flow reversals. A range of COP and SCP combinations could be achieved by operating the same machine with a control strategy. It was concluded that there was a design compromise between COP (related to operation costs) and SCP (related to capital costs) and the compromise could be decided only by an appropriate economic optimization.

A new design solar powered adsorption heat pump and ice thermal reservoir were modeled and presented by Lambert [125]. The new design adsorber combined the robust shell-and-tube configuration and other reliable heat exchanger components (multi-lumen tubes, annular finned tubes). Metal wool was loosely packed between the annular fins in order to further augment the metal surfaces of the heat exchanger. The view of the adsorber is given in Figure 2.4. The principal innovation of the design was the activation of the heat exchanger of the adsorber by using metallic fins soldered on the HTF tubes to increase the surface area to volume ratio. The new configuration greatly magnified the contact area between the granular or powdered activated carbon with $CaCl_2$ coating and the heat exchanger to increase the junction conductance, and simultaneously reduced the thickness of the adsorbent bed. COP for cooling was predicted as 1.60 for this new design.

Taylan et al. [126] presented three different models for ideal thermal wave adsorption cooling cycles without mass recovery, with adiabatic mass recovery and with isothermal mass recovery. A square wave model in which the thermal wavelength goes to zero was used for the ideal thermal wave cycle to investigate the theoretical limits to COP. The researchers investigated these ideal thermal wave models to provide making relative comparisons and directions for the future studies. The effects of several operating and design parameters on COP were observed by using TRNSYS simulations. Results were also compared with the results of a reversible cycle, which was the thermodynamically limiting cycle, and that of previous models developed for simple and heat recovery cycles. Results showed that in all three cases investigated, COP’s of the thermal wave cycles were significantly larger than those of the simple and heat recovery cycles and were approximately 40-75% that of the reversible cycle. The condensation and

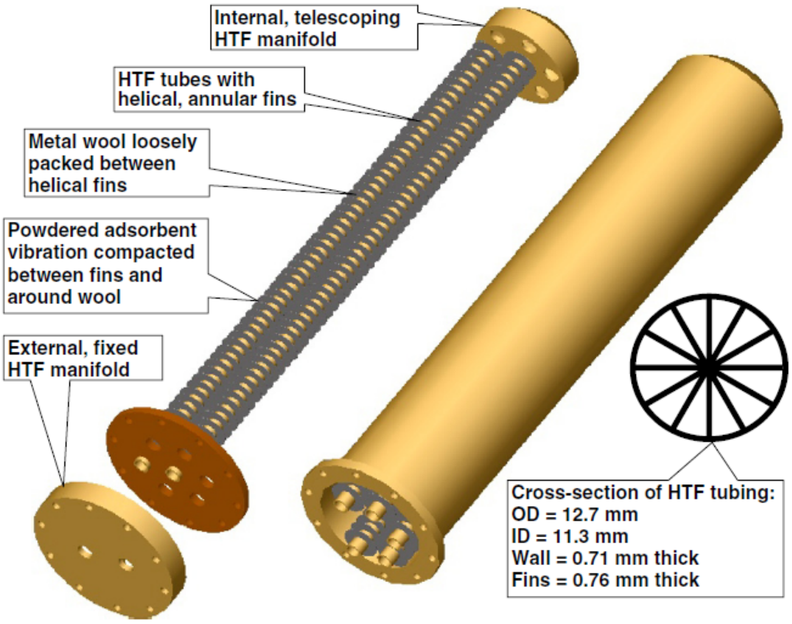

Figure 2.4 View of the adsorber with a regular hexagonal array of 7 HTF tubes with 12 lumens and helical annular fins [125].

evaporation temperatures were found to be parameters having the biggest impact on COP as a result of the parametric study. Furthermore, variations in the heat capacity ratio were found to have little impact on COP of the thermal wave cycle unlike in case of the simple and heat recovery cycles. This result suggested that a high COP thermal wave bed might be possible with a large dead mass.

A computational modeling of thermal wave and multiple-bed adsorption cycles was carried out by Metcalf et al. [127] in order to determine whether the power output per unit mass or volume of machine provides the optimal trade-off between COP and power density. The modeling was performed with a plate heat exchanger type generator shown in Figure 2.5 for the activated carbon-ammonia working pair. Mass recovery was also incorporated in the modeling of the two-bed, four-bed and thermal wave cycles. It was concluded that the multiple-bed cycles gave a superior trade-off between COP and power density and were therefore recommended over thermal wave cycles. The heating COP of the four-bed, two-bed and thermal wave cycles were predicted as 1.53, 1.45 and 1.35, respectively, for a specific heating power of 2 kW/kg and under typical heat pump conditions. However, in cases where the purpose is to maximize the COP at the expense of high capital cost, thermal wave cycles can achieve higher COP. Results also showed that if the adsorption technology was integrated to a gas fired heat pump in such a way that the system were driven by heat from a gas burner with a gross efficiency of 85%, then the overall COP would be 1.3, 1.23 and 1.15 for the four-bed, two-bed and thermal wave cycles, respectively.

Figure 2.5 Plate heat exchanger adsorption generator [127].

2.2 Convective Thermal Wave Cycles

The convective (or forced convection) thermal wave cycle was proposed by Critoph [128]. The convective thermal cycles are based on the concept of thermal wave cycle. Thermal wave cycle has low power density because of poor heat transfer through the adsorbent bed. It is possible to heat the refrigerant gas outside the bed and to circulate it through the bed in order to heat the sorbent rather than attempting to heat the bed directly. In other words, the refrigerant was used as the heating/cooling medium, thus convective heat and mass transfer exists in the adsorbent bed. The high surface area of grains leads to very effective heat transfer with only parasitic power at low levels needed for pumping. A schematic of the proposed system is shown in Figure 2.6. Two *active* beds are packed with adsorbent material (activated carbon in this study) and two *inert* beds are packed with non-reactive particles such as steel balls. Figure 2.6 shows the half-cycle during which Active bed 1 is heated for desorption while Active bed 2 is cooled for adsorption of the refrigerant (ammonia). On the left, a low power pump circulates the refrigerant vapor through inert bed 1 which is initially hot. The vapor is heated by the bed and a cold wave passes through the bed from right to left. Thus, the vapor is preheated by the inert bed and heated further to maximum cycle temperature in a heat exchanger. The refrigerant vapor then passes through the active bed 1 heating the adsorbent and a hot thermal wave passes through the active bed from left to right. Pressurization occurs and vapor condenses in the condenser rejecting heat to the environment [17]. The condensed refrigerant passes through a throttle and an evaporator and useful cooling is obtained at the evaporator. The refrigerant vaporized at the evaporator is adsorbed in active bed 2 at low pressure. Heat removal from the bed is achieved by cold vapor coming from both the evaporator and the loop at the right hand side. A cold wave occurs through the bed from left to right. Hot refrigerant leaving the active bed 2 is precooled in inert bed 2 generating a hot thermal wave from the right to left and then further cooled in a heat exchanger which rejects heat to the environment. Initial simulations of the cycle implied that with careful choice of carbon, grain size, bed size and flow rates it would be possible to obtain a satisfactory combination of COP and power density [129].

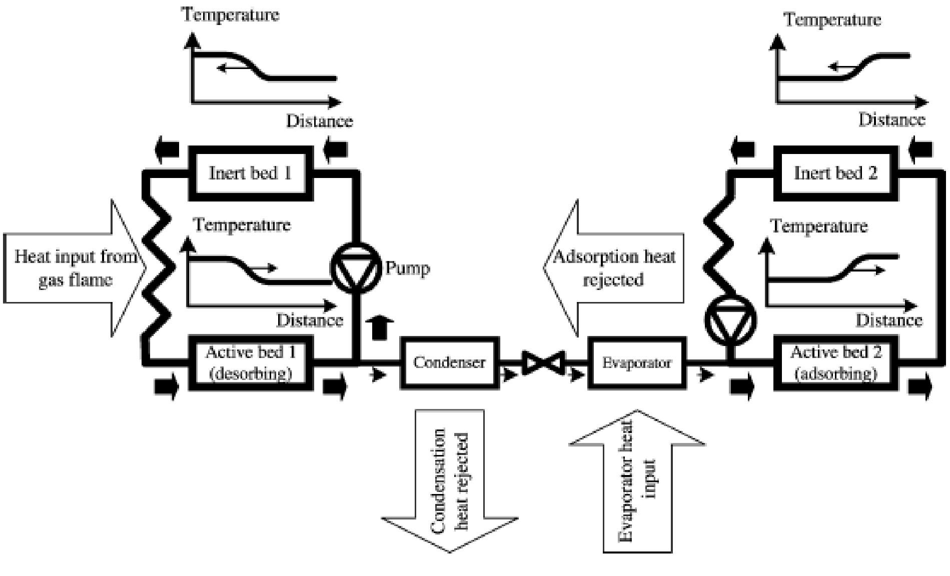

Figure 2.6 Convective thermal wave adsorption refrigeration cycle [128].

A different configuration was proposed by Lai [130] based on the combination of convective thermal wave cycle proposed by Critoph [128] and periodic flow reversal cycle introduced by Lai et al. [131] terming it as ‘Periodic Reversal Forced Convective Cycle’. A schematic of the proposed cycle is shown in Figure 2.7. The main objective of the study was to evaluate the practical feasibility of the proposed system using a mathematical model taking zeolite 13X-water as a working pair. The effects of several operating modes of flow reversal on the heat regeneration and COP were investigated. Results obtained from the proposed cycle were compared with that from convective thermal wave cycle and from non-flow reversal cycle. It was concluded that the periodic reversal forced convective cycle might have the following advantages: good heat regeneration between two adsorbers, more favorable conditions for adsorption/desorption processes and their combination with thermal recovery, enhanced heat transfer rate and hence shorter cycle time and high efficiency.

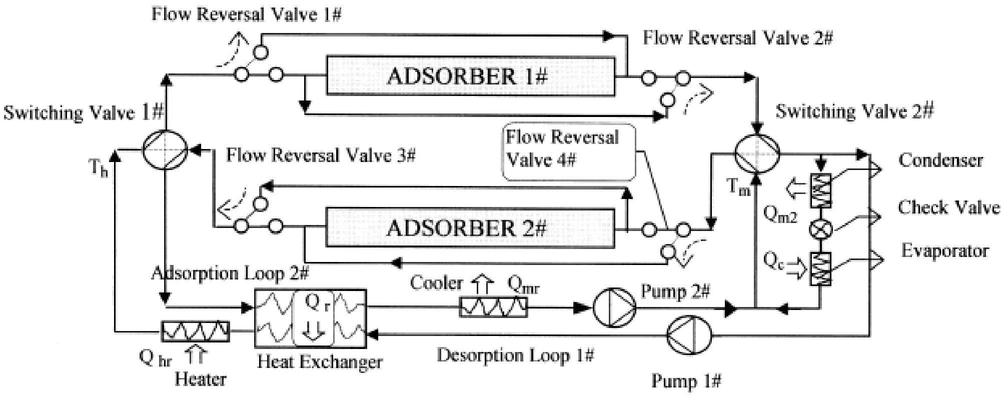

Figure 2.7 The proposed periodic reversal forced convective cycle [130].

A convective thermal wave adsorption chiller employing activated carbon-methanol pair was investigated theoretically by Tierney [132]. Axial temperature and concentration profiles and pumping power were predicted. Results showed that if the parasitic pumping power was neglected, good COPs and cooling powers could be obtained. However, pumping power predictions were not realistic for both COPs higher than 0.27 and SCPs higher than 1 W/kg.

In brief, most of the solutions in the literature are 1-D and include either heat or mass transfer analysis in the adsorbent bed. Only a few studies on 2-D coupled analysis were performed. Finite difference methods were generally used for the solution. Consolidated and coated adsorbent beds were studied experimentally in thermal wave cycles, but metal additives are generally used in basic adsorption cycles. This thesis makes a significant contribution to the literature in several aspects. The novelties of this thesis can be listed as follows:

- A two dimensional model that analyses transient coupled heat and mass transfer in the adsorbent bed has been made and the results have been presented in 2-D multicolored plots.

- Comsol Multiphysics that uses finite element method has been used for the solution.

- A metal additive (the mixture of natural zeolite clinoptilolite and copper pieces) has been tested experimentally with a finned tube adsorbent bed.

- Different adsorbent materials (zeolite, white and orange silica gels) have been tested in a thermal wave cycle. Silica gels with different particle diameters have also been tested.

CHAPTER 3

GOVERNING EQUATIONS

The objective of this thesis is to increase the performance of a thermal wave adsorption cooling cycle by enhancing the heat and mass transfer inside the adsorbent bed of the cycle. The enhancement or improvement in the heat and mass transfer inside the bed can be evaluated in terms of temperature, pressure and amount adsorbed distributions. In order to determine these distributions, a mathematical model is developed. The mathematical model and governing equations are obtained by applying the conservation of mass, momentum and energy. This chapter describes the development of the mathematical model based on the principles of these conservation equations.

3.1 Model Definition

The elemental representation of the adsorbent bed is given in Figure 3.1. The bed consists of a cylindrical heat transfer tube (HTT) surrounded by an adsorbent material. A heat transfer fluid (HTF) passes through the HTT to heat or cool the adsorbent material. The HTT are usually made of copper, aluminum or stainless steel pipe. The HTF is a fluid that has a high boiling temperature. The adsorbent material is a microporous material that has high porosity and large surface areas per mass of adsorbent. The adsorbents can adsorb a certain amount of refrigerant vapor as mentioned in Chapter 1. The adsorbent particles are commonly packed in a bed or column to obtain a significant cooling effect and this column is called packed bed adsorbent. The mathematical model includes energy equations for the HTF, HTT and adsorbent material, mass equation for the adsorbent material and momentum equation for the adsorbent material.

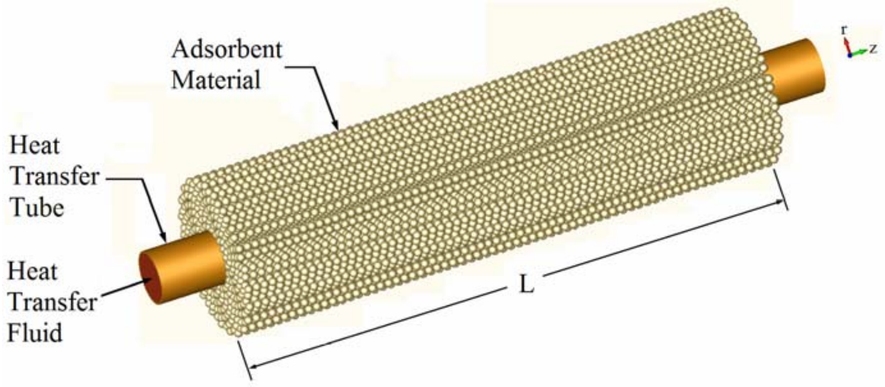

Figure 3.1 Elements of the adsorbent bed.

3.1.1 Porous Media and Packing Structure

To derive the governing equations for the porous media, i.e. packed bed adsorbent, the porous media should be defined with a representative elementary volume given in Figure 3.2. The representative volume is much smaller than the overall system dimensions but much larger than the individual adsorbent particles. Three phases are contained in the representative volume. The first is solid adsorbent particles. The second is adsorbate which is the refrigerant adsorbed by the adsorbent. The third one is refrigerant vapor that exists in gas phase and is free to move within the void space surrounding the adsorbent particles [2]. The three phases are termed hereafter adsorbent, adsorbate and vapor, respectively, for brevity.

The permeability and porosity are generally used to specify a porous media. The permeability is a measure of mass transfer resistance for the refrigerant vapor flow through the void space. The porosity or void fraction of a porous media can be defined as the fraction of the total volume of the porous media that is occupied by void spaces [133]. However, this definition of the porosity is limited to bed porosity or interparticle porosity which is the void fraction occupied between the adsorbent particles. There are also void spaces within the particles due to the nature of the porous structure and the fraction of the total volume of an adsorbent particle that is occupied by the voids within the particle is called particle porosity or intraparticle porosity. In general, adsorbent particles have different sizes and shapes. However, they will have an average interparticle porosity after being packed in a column [134]. For a packed bed, the bed porosity ε_b and the particle porosity ε_p can be calculated by Wankat [135], respectively, as follows

$$\varepsilon_b = \frac{void\ volume\ between\ particles}{total\ volume\ of\ packed\ bed} \tag{3.1}$$

$$\varepsilon_p = \frac{void\ volume\ inside\ all\ particles}{total\ volume\ of\ all\ particles} \tag{3.2}$$

The total porosity, ε_T, of the bed is then can be calculated by the following equation

$$\varepsilon_T = \varepsilon_b + (1-\varepsilon_b)\varepsilon_p \tag{3.3}$$

considering that the adsorbent particles are just occupied in the volume fraction of (1- ε_b) [135]. The particle porosity of adsorbent materials can be characterized in many different ways. For industrial purposes, the most important characterization methods of adsorbent materials are [11]:

1. Mercury penetration porosimetry
2. Helium density measurements by pycnometers
3. Gas adsorption (N_2, Ar, CO_2)
4. Calorimetric measurements

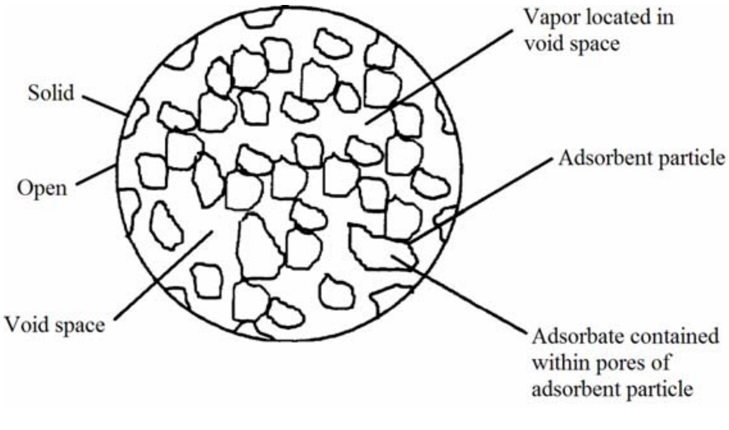

Figure 3.2 Representative volume of the porous media [2].

3.2 The Governing Equations

Adsorption cooling cycles are governed by three different physical mechanisms inside the adsorbent bed. These are the conduction and convection associated with heat transfer, the convection and diffusion associated with mass transfer and Darcy or Forchheimer flow associated with momentum transfer. The modeling of the bed, therefore, requires a coupled analysis of these three mechanisms. The solution of each physical mechanism requires the solution obtained from some of the other mechanisms. If the physical mechanisms are only one-way coupled with each other, i.e. if physical mechanism (1) does not depend on the other two mechanisms and physical mechanism (2) depends on (1) only and physical mechanism (3) depends on the other two, then this requires a sequential form of solution.

Momentum equation, for example, can be solved independently when the required boundary conditions corresponding to dependent variables (pressure and velocity) are known. The energy transport can then be solved using the results of the momentum equation. Finally, the mass transport can be solved using the solutions of the momentum and energy equations. This solution approach is presented in Figure 3.3.

However, the physical mechanisms do not have regularly encountered equations in the case of porous media. When the medium is porous and reactive, there is a reaction term that involves the rate of adsorption or desorption in the mass balance equation. There is also a source term that involves the heat transfer by refrigerant vapor flowing inside the bed and the heat of adsorption or desorption in the energy balance equation. The source term may have positive or negative values depending on whether the process involves an adsorption or desorption process in the bed. The reaction and source terms are functions of dependent variables in the momentum equation, pressure and velocity. Therefore the solution procedure in a porous media requires a fully coupled modeling seeking a simultaneous solution. This approach can also be presented in Figure 3.3. The fully coupled model is solved by using the simultaneous solution approach in this study.

In this study, adsorbent and adsorbate that is accumulated on the surface of the adsorbent are considered as a single solid phase and hence volume fraction of the adsorbate is neglected. On the other hand, the temperature difference between the solid (adsorbent +

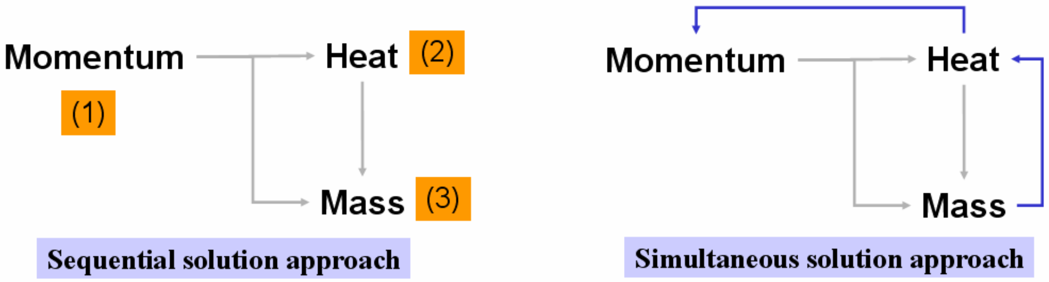

Figure 3.3 Solution approaches to the mathematical model.

adsorbate) and vapor phases is generally insignificant and temperature gradients between the two phases can be neglected [133]. Except for a short time at the beginning of desorption process at the wall where the vaporization takes place, the maximum difference between the local values of temperature of the solid and vapor is very small [136]. Therefore, local thermal equilibrium assumption in which the three phases, i.e. adsorbent, adsorbate and vapor, are assumed to be at the same temperature is used in this study. For the local thermal equilibrium, the following equality can be written

$$T_s = T_{ad} = T_v \tag{3.4}$$

where T_s, T_{ad} and T_v are the temperatures of the adsorbent, adsorbate and vapor phases, respectively. The assumptions and simplifications employed in the development of the conservation equations are as follows:

- thermal conductivities for all materials are constant
- specific heats for all materials are constant
- densities for solids and liquids are constant
- adsorbent and adsorbate phase are stationary
- vapor phase behaves as an ideal gas
- HTF flows at constant velocity within the HTT
- there is local thermal equilibrium between adsorbent, adsorbate and vapor phases
- specific heat of the adsorbate is considered to be of liquid phase

- viscous dissipation, radiative effects and the work done by pressure changes are negligible
- adsorbent bed is considered as a continuous media and hence conduction heat transfer in the porous media can be characterized by an equivalent thermal conductivity
- adsorbent particles have identical properties and are uniformly distributed in the bed, i.e. the porous media is homogeneous and isotropic
- heat of adsorption, total porosity, permeability, dynamic viscosity, mass diffusivity are all constant

The five governing conservation equations, conservation of energy for the HTF, conservation of energy for the HTF, conservation of mass for the adsorbent bed (porous media), conservation of momentum for the adsorbent bed and conservation of energy for the adsorbent bed are derived in the following section.

3.2.1 Conservation of Energy for the HTF

The conservation of energy for the HTF can be developed by choosing a control volume (CV) with an infinitesimal moving element of HTF as in Figure 3.4. The conservation of energy equation defines the flow of energy through a CV and can be written in general form by the following equation

$$\dot{E}_{in} - \dot{E}_{out} + \dot{E}_{generated} = \dot{E}_{stored} \tag{3.5}$$

where $\dot{E}_{in}$ is the rate of energy transfer into the CV, $\dot{E}_{out}$ is the rate of energy transfer out of the CV, $\dot{E}_{generated}$ is the rate of change of energy generated within the CV, and $\dot{E}_{stored}$ is the rate of change of energy stored within the CV [137]. Energy is transferred into the CV by conduction heat transfer and heat transfer through the moving fluid. Energy is transferred out of the CV by conduction heat transfer, convection heat transfer at the fluid/tube interface and heat transfer through the moving fluid. There is no energy generation in the CV. As a result, the conservation of energy at any point in the CV can be stated as follows

$$\begin{bmatrix}\text{Net rate of}\\ \text{heat transfer}\\ \text{into the CV}\\ \text{by conduction}\end{bmatrix}+\begin{bmatrix}\text{Net rate of}\\ \text{energy transfer}\\ \text{into the CV due}\\ \text{to moving fluid}\end{bmatrix}-\begin{bmatrix}\text{Rate of heat transfer}\\ \text{out of the CV by}\\ \text{convection at}\\ \text{fluid/tube interface}\end{bmatrix}=\begin{bmatrix}\text{Rate of}\\ \text{change of}\\ \text{energy in}\\ \text{the CV}\end{bmatrix} \tag{3.6}$$

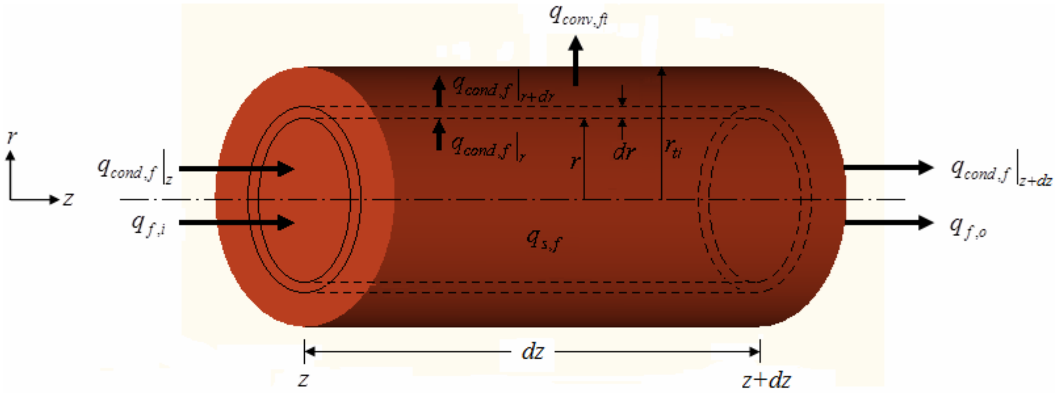

Figure 3.4 The control volume for the HTF.

Equation (3.6) can be rearranged by using the notations represented in Figure 3.4 as follows

$$\left(q_{cond,f}\big|_{r}-q_{cond,f}\big|_{r+dr}\right)+\left(q_{cond,f}\big|_{z}-q_{cond,f}\big|_{z+dz}\right)+\left(q_{f,i}-q_{f,o}\right)-q_{conv,ft}=q_{s,f} \tag{3.7}$$

where the first parenthesis denotes the net rate of conduction heat transfer in r (radial) direction, the second parenthesis denotes the net rate of conduction heat transfer in z (axial) direction, the third parenthesis denotes the rate of energy transfer due to the fluid flow, the last term on the LHS denotes the rate of convection heat transfer from the HTF to the HTT, and the term at RHS denotes energy stored within the CV, respectively. Each term in Equation (3.7) is addressed in detail below.

Conduction heat transfer is described by Fourier's Law

$$q_{cond}=-kA\nabla T \tag{3.8}$$

where k is the thermal conductivity of the material, A is the cross-sectional area normal to the direction of heat flow, and ∇T is del operator for the temperature gradient. In cylindrical coordinates, heat transfer by conduction in the HTF in the radial (r) and axial (z) directions can be written as follows, respectively

$$q_{cond,f,r} = -k_f A_{f,r} \frac{\partial T_f}{\partial r} \tag{3.9}$$

$$q_{cond,f,z} = -k_f A_{f,z} \frac{\partial T_f}{\partial z} \tag{3.10}$$

where k_f and T_f are the thermal conductivity and temperature of the HTF, respectively. $A_{f,r}$ and $A_{f,z}$ are the cross-sectional areas for the radial and axial directions in the HTF, respectively, and can be expressed by using the coordinate system shown in Figure 3.5.

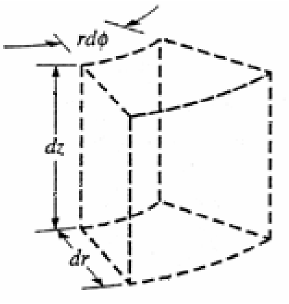

Figure 3.5 Cylindrical coordinate system.

$$A_{f,r} = rd\phi dz \tag{3.11}$$

$$A_{f,z} = rd\phi dr \tag{3.12}$$

Rate of heat transfers by conduction at ($r+dr$) and ($z+dz$) can be expressed by using Taylor expansion as follows

$$q_{cond,f}\Big|_{r+dr}=q_{cond,f,r}+\frac{\partial q_{cond,f,r}}{\partial r}dr \tag{3.13}$$

$$q_{cond,f}\Big|_{z+dz}=q_{cond,f,z}+\frac{\partial q_{cond,f,z}}{\partial z}dz \tag{3.14}$$

Using Equations (3.9), (3.11) and (3.13) for the radial direction and Equations (3.10), (3.12) and (3.14) for the axial direction and making the necessary simplifications, net rate of heat transfer by conduction can be written as follows

$$q_{cond,f}\Big|_{r}-q_{cond,f}\Big|_{r+dr}=-\frac{\partial q_{cond,f,r}}{\partial r}dr=\frac{\partial}{\partial r}\left(k_f r\frac{\partial T}{\partial r}\right)d\phi dzdr \tag{3.15}$$

$$q_{cond,f}\Big|_{z}-q_{cond,f}\Big|_{z+dz}=-\frac{\partial q_{cond,f,z}}{\partial z}dz=\frac{\partial}{\partial z}\left(k_f\frac{\partial T}{\partial z}\right)rd\phi drdz \tag{3.16}$$

Neglecting changes in potential energy, the energy transfer due to moving fluid is the sum of thermal internal energy (e) and kinetic energy ($V^2/2$) advected with the bulk fluid motion across the CV [138]. Writing only in z direction since the radial velocity of the HTF is zero, i.e. v_r=0, and using Taylor expansion, the net rate at which this energy enters the CV is

$$\begin{aligned}\dot{E}_{adv}\Big|_{z}-\dot{E}_{adv}\Big|_{z+dz}=q_{f,i}-q_{f,o}&=\rho_f v_f\left(e+\frac{{v_f}^2}{2}\right)A_{f,z}-\left\{\rho_f v_f\left(e+\frac{{v_f}^2}{2}\right)\right.\\&\left.+\frac{\partial}{\partial z}\left[\rho_f v_f\left(e+\frac{{v_f}^2}{2}\right)\right]dz\right\}A_{f,z}\\&=-\frac{\partial}{\partial z}\left[\rho_f v_f\left(e+\frac{{v_f}^2}{2}\right)\right]A_{f,z}dz\end{aligned} \tag{3.17}$$

where ρ_f, and v_f denote density and velocity of the HTF. The kinetic energy is rarely used in heat transfer problems and can be neglected. The change in the internal energy assuming no phase change can be written as follows defining a single specific heat c_f for an incompressible fluid with constant specific heat, i.e. $c_v=c_p=c_f$,

$$de = c_f dT \tag{3.18}$$

Rearranging Equation (3.17) for the HTF with constant density and velocity and substituting $A_{f,z}$ given in Equation (3.12) into Equation (3.17) yields

$$q_{f,i} - q_{f,o} = -\rho_f v_f c_f \frac{\partial T_f}{\partial z} r d\phi dr dz \tag{3.19}$$

The rate of heat transfer by convection from the HTF to the HTT at the interface between the HTF and HTT is determined by Newton’s law of cooling as

$$q_{conv,ft} = h_i 2\pi r_{ti} dz (T_f - T_t) \tag{3.20}$$

where h_i is the convective heat transfer coefficient between the HTF and HTT, r_{ti} is the HTT inner radius and T_t is the HTT temperature.

Finally, energy stored within the CV can be expressed by

$$q_{s,f} = \rho_f c_f \frac{\partial T_f}{\partial t} r d\phi dr dz \tag{3.21}$$

Equations (3.15), (3.16), (3.19), (3.20) and (3.21) can now be substituted into Equation (3.7). Thus, Equations (3.7) can be rewritten as follows

$$\begin{gathered}\frac{\partial}{\partial r}\left(k_f r \frac{\partial T_f}{\partial r} \right) d\phi dz dr + \frac{\partial}{\partial z}\left(k_f \frac{\partial T_f}{\partial z} \right) r d\phi dr dz - \rho_f v_f c_f \frac{\partial T_f}{\partial z} r d\phi dr dz \\ -h_i 2\pi r_{ti} dz (T_f - T_t) = \rho_f c_f \frac{\partial T_f}{\partial t} r d\phi dr dz\end{gathered} \tag{3.22}$$

Equation (3.22) can be simplified by dividing both sides by the volume of the infinitesimal volume element shown in Figure 3.5, i.e. $dV=rd\phi drdz$. However, the last term on the LHS of Equation (3.22) which is the heat transfer by convection at the interface occurs at a certain radius ($r=r_{ti}$) and the volume for this term can be taken as $\pi r_{ti}^2 dz$. The last form of the conservation of energy equation for the HTF then becomes

$$\frac{1}{r}\frac{\partial}{\partial r}\left(k_f r\frac{\partial T_f}{\partial r}\right)+\frac{\partial}{\partial z}\left(k_f\frac{\partial T_f}{\partial z}\right)-\rho_f v_f c_f\frac{\partial T_f}{\partial z}-\frac{2}{r_{ti}}h_i(T_f-T_t)=\rho_f c_f\frac{\partial T_f}{\partial t} \quad (3.23)$$

3.2.2 Conservation of Energy for the HTT

The conservation of energy equation for the HTT can be developed starting from a CV selection and driving an energy balance for the CV as in the derivation of conservation equation for the HTF. The CV selected for the HTT is shown in Figure 3.6.

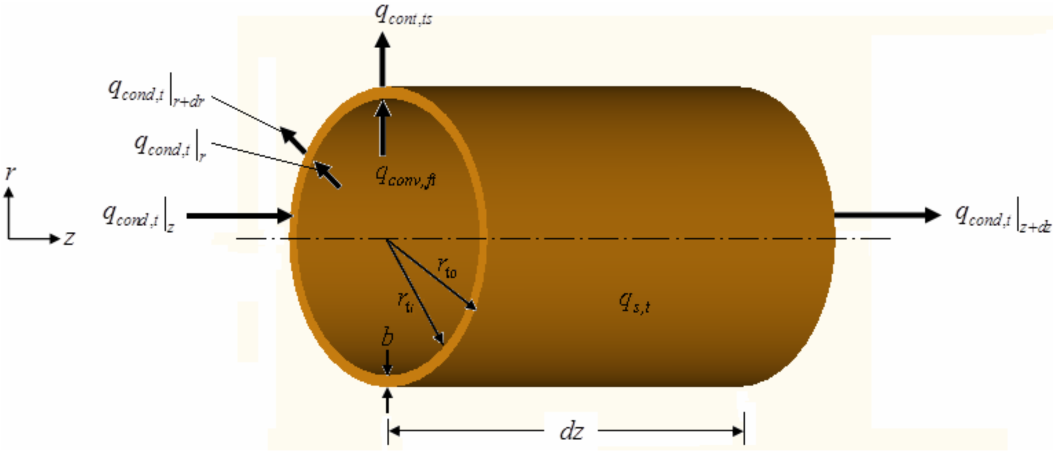

Figure 3.6 The control volume for the HTT.

Energy is transferred into the CV by conduction heat transfer and convection heat transfer from the HTF. Energy is transferred out of the CV by conduction heat transfer through the HTT itself and conduction heat transfer through the thermal contact of the HTT and adsorbent. Thus, the conservation of energy for the CV can be stated as

$$\begin{bmatrix}\text{Net rate of}\\ \text{heat transfer}\\ \text{into the CV}\\ \text{by}\\ \text{conduction}\end{bmatrix} + \begin{bmatrix}\text{Rate of heat}\\ \text{transfer into the}\\ \text{CV by convection}\\ \text{at the fluid/tube}\\ \text{interface}\end{bmatrix} - \begin{bmatrix}\text{Rate of heat}\\ \text{transfer out of the CV}\\ \text{through the contact}\\ \text{resistance between the}\\ \text{tube and adsorbent}\end{bmatrix} = \begin{bmatrix}\text{Rate of}\\ \text{change}\\ \text{of energy}\\ \text{in the}\\ \text{CV}\end{bmatrix} \quad (3.24)$$

Using the notations for the energy transfers illustrated in Figure 3.6, Equation (3.24) can be written as

$$\left(q_{cond,t}\Big|_{r} - q_{cond,t}\Big|_{r+dr}\right) + \left(q_{cond,t}\Big|_{z} - q_{cond,t}\Big|_{z+dz}\right) + q_{conv,ft} - q_{cont,ts} = q_{s,t} \quad (3.25)$$

where the first two parentheses denote the net rate of conduction heat transfer through the HTT in r and z directions, respectively. $q_{conv,ft}$ and $q_{cont,ts}$ denote the convection heat transfer from the HTF and the conduction heat transfer through the thermal contact between HTF/HTT surfaces (interstitial heat transfer), respectively. $q_{s,t}$ denotes the energy stored within the HTT. Expressions for each term are given below.

The net rate of conduction heat transfer in r and z directions can be obtained in a similar manner as in the HTF, similar to Equations (3.15) and (3.16) as follows

$$\left(q_{cond,t}\Big|_{r} - q_{cond,t}\Big|_{r+dr}\right) = \frac{1}{r}\frac{\partial}{\partial r}\left(k_t r \frac{\partial T_t}{\partial r}\right) A_t dz \quad (3.26)$$

$$\left(q_{cond,t}\Big|_{z} - q_{cond,t}\Big|_{z+dz}\right) = \frac{\partial}{\partial z}\left(k_t \frac{\partial T_t}{\partial z}\right) A_t dz \quad (3.27)$$

where k_t, T_t and A_t are the thermal conductivity, temperature and cross-sectional are of the tube, respectively. The convection heat transfer into the CV at the HTF/HTT interface is already given in Equation (3.20). The conduction heat transfer through the thermal contact at HTT/adsorbent interface can be expressed by [2]

$$q_{cont,ts} = h_c 2\pi r_{to} dz (T_t - T_s) \quad (3.28)$$

where h_c is interfacial conductance [139] in W/(m^{2}K), r_{to} is outer radius of the HTT and T_s is adsorbent temperature. The energy stored within HTT can be written similar to that in HTF, i.e. Equation (3.21), as follows

$$q_{s,t} = \rho_t c_t \frac{\partial T_t}{\partial t} A_t dz \tag{3.29}$$

where ρ_t and c_t are the density and specific heat of the HTT, respectively.

Substituting Equations (3.26)-(3.29) and Equation (3.20) into Equation (3.25) after diving the unit volume $V_t = A_t dz$, the following equation can be obtained

$$\begin{aligned} &\frac{1}{r}\frac{\partial}{\partial r}\left(k_t r \frac{\partial T_t}{\partial r}\right) + \frac{\partial}{\partial z}\left(k_t \frac{\partial T_t}{\partial z}\right) + \frac{h_i 2\pi r_{ti} dz}{V_t}(T_f - T_t) - \frac{h_c 2\pi r_{to} dz}{V_t}(T_t - T_s) \\ &= \rho_t c_t \frac{\partial T_t}{\partial t} \end{aligned} \tag{3.30}$$

If the lateral areas of the HTT at r_{ti} and r_{to} are defined as $A_{l,ti} = 2\pi r_{ti} dz$ and $A_{l,to} = 2\pi r_{to} dz$, respectively, Equation (3.30) can be simplified to its last form as follows

$$\frac{1}{r}\frac{\partial}{\partial r}\left(k_t r \frac{\partial T_t}{\partial r}\right) + \frac{\partial}{\partial z}\left(k_t \frac{\partial T_t}{\partial z}\right) + \frac{h_i A_{l,ti}}{V_t}(T_f - T_t) - \frac{h_c A_{l,to}}{V_t}(T_t - T_s) = \rho_t c_t \frac{\partial T_t}{\partial t} \tag{3.31}$$

3.2.3 Conservation of Mass for the Adsorbent Bed

The conservation of mass or continuity equation inside the adsorbent bed can be derived considering a finite CV bounded by the control surface CS as sketched in Figure 3.7. Applied to this CV, the conservation of mass for the adsorbent bed can be stated as [2]

$$\begin{bmatrix} \text{Time rate of} \\ \text{change of mass} \\ \text{in the CV} \end{bmatrix} + \begin{bmatrix} \text{Net rate of} \\ \text{mass efflux} \\ \text{across the CS} \end{bmatrix} = 0 \tag{3.32}$$

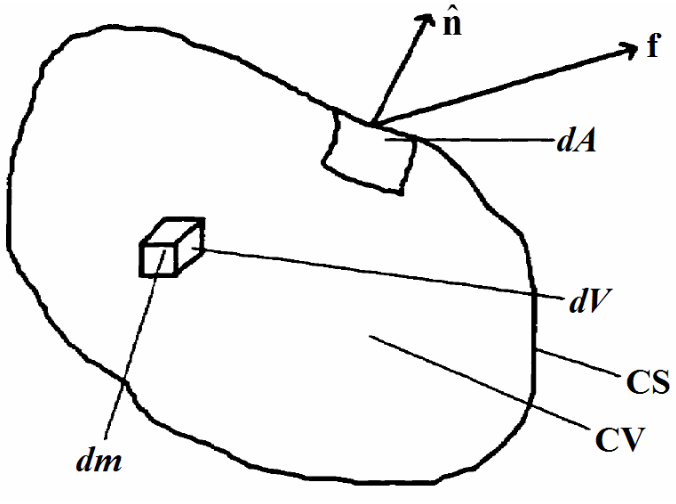

Figure 3.7 The control volume for the derivation of continuity equation in the adsorbent bed [2].

The adsorbent bed includes vapor, solid and adsorbate phases together in the CV. Therefore, the total mass *dm* contained within the elemental volume *dV* can be expressed by the sum of the masses of the three phases as follows

$$dm = (dm)_v + (dm)_s + (dm)_{ad} \tag{3.33}$$

Equation (3.33) can be rearranged by using a volume integral and the relation $dm=\rho dV$

$$\iiint_{CV} dm = \iiint_{CV} [\varepsilon_T \rho_v + (1-\varepsilon_T)\rho_s + (1-\varepsilon_T)\rho_s X] dV \tag{3.34}$$

where ρ_v and ρ_s are the density of refrigerant vapor and the density of solid adsorbent, respectively. X is the amount adsorbed per mass of adsorbent (kg/kg$_s$), and thus the last term in the parenthesis implies the fraction of the mass of adsorbate within the CV. The time rate of change of mass in the CV can be expressed by

$$\frac{\partial}{\partial t}\iiint_{CV} dm = \frac{\partial}{\partial t}\iiint_{CV} (\varepsilon_T \rho_v + (1-\varepsilon_T)\rho_s + (1-\varepsilon_T)\rho_s X) dV \tag{3.35}$$

The total mass flux across the CS is represented by the vector **f** in Figure 3.7. The total mass flux includes both bulk flow and diffusion of vapor [2] and can be written as

$$\mathbf{f} = \rho_v \mathbf{V} - D_m \nabla \rho_v \tag{3.36}$$

where **V** is the velocity vector which is typically called Darcian velocity [2]. D_m is generally defined as mass diffusion coefficient and is also referred to as dispersion coefficient in some references [140,141]. The total mass flux can be averaged over the cross sectional area since the area dA is much larger than the solid grain and individual pore cross sections. The net rate of mass efflux can then be given by

$$\begin{bmatrix}\text{Net rate of}\\ \text{mass efflux}\end{bmatrix} = \iint_{CS} (\mathbf{f} \cdot \hat{\mathbf{n}}) dA \tag{3.37}$$

Substituting Equations (3.35) and (3.37) into Equation (3.32) yields to

$$\frac{\partial}{\partial t} \iiint_{CV} (\varepsilon_T \rho_v + (1-\varepsilon_T)\rho_s + (1-\varepsilon_T)\rho_s X) dV + \iint_{CS} (\mathbf{f} \cdot \hat{\mathbf{n}}) dA = 0 \tag{3.38}$$

The second term of Equation (3.38) can be converted into a volume integral by applying the Gauss Divergence Theorem as

$$\iint_{CS} (\mathbf{f} \cdot \hat{\mathbf{n}}) dA = \iiint_{CV} \nabla \cdot \mathbf{f} \, dV \tag{3.39}$$

On the other hand, the differentiation and integration in the first term of Equation (3.38) can be reversed since the volume does not change with time. Reversing them and substituting Equation (3.39), Equation (3.38) can now be written in a single volume integral as follows

$$\iiint_{CV} \left[\frac{\partial}{\partial t} \left(\varepsilon_T \rho_v + (1-\varepsilon_T)\rho_s + (1-\varepsilon_T)\rho_s X \right) + \nabla \cdot \mathbf{f} \right] dV = 0 \tag{3.40}$$

The time derivative of solid mass, i.e. $\partial[(1-\varepsilon_T)\rho_s]/\partial t$, is zero as the density of the adsorbent and total porosity are constant. Additionally, the above equation is valid for an arbitrary control volume and requires the following equality

$$\frac{\partial}{\partial t}\left(\varepsilon_T \rho_v + (1-\varepsilon_T)\rho_s X\right) + \nabla \cdot \mathbf{f} = 0 \tag{3.41}$$

Substituting the total mass flux in Equation (3.36), the last form of the conservation of mass for the adsorbent bed results in

$$\varepsilon_T \frac{\partial \rho_v}{\partial t} + (1-\varepsilon_T)\rho_s \frac{\partial X}{\partial t} - D_m \nabla^2 \rho_v + \nabla(\rho_v \mathbf{V}) = 0 \tag{3.42}$$

The above equation includes both bulk flow and diffusive mass transfer. Diffusive mass transfer has principally a significant effect for conditions in which the permeability and the pressure driving mass flow are extremely low [2]. If the diffusive term is very small in its order of magnitude, it can be neglected.

3.2.4 Conservation of Momentum for the Adsorbent Bed

The refrigerant vapor is the only component moving in the adsorbent bed. Neglecting the body forces, the conservation of momentum for the vapor can be stated for a CV given in Figure 3.8 as [2]

$$\begin{bmatrix}\text{Rate of}\\ \text{change of}\\ \text{momentum}\\ \text{in the CV}\end{bmatrix} + \begin{bmatrix}\text{Net rate}\\ \text{of efflux}\\ \text{of}\\ \text{momentum}\end{bmatrix} = \begin{bmatrix}\text{Pressure and}\\ \text{viscous forces}\\ \text{exerted by the}\\ \text{surrounding vapor}\end{bmatrix} + \begin{bmatrix}\text{Forces exerted}\\ \text{on the vapor}\\ \text{by the adsorbent}\\ \text{particles}\end{bmatrix} \tag{3.43}$$

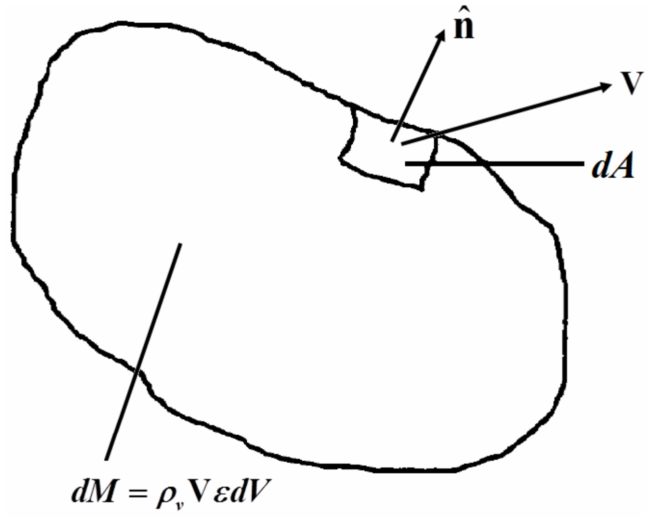

Figure 3.8 Differential element for the conservation of momentum [2].

Each term in Equation (3.43) can be written using the notations in Figure 3.8 as follows [2], respectively

$$\frac{\partial}{\partial t}\iiint_{CV}(\rho_v \mathbf{V})\varepsilon dV + \iint_{CS}(\rho_v \mathbf{V}\mathbf{V})\cdot\hat{\mathbf{n}}\Gamma dA = -\iint_{CS} P\hat{\mathbf{n}}dA + \iint_{CS}\tau\cdot\hat{\mathbf{n}}dA + \iiint_{CV}\mathbf{g}dV \qquad (3.44)$$

where $\mathbf{V}$ is velocity of vapor, εdV is the volume of vapor contained in the differential element, ΓdA is the open area of the control surface through which the vapor can flow (see Figure 3.2), P is pressure, τ is viscous stress tensor and $\mathbf{g}$ is the force exerted on the vapor by the adsorbent per unit volume of the CV. The above equation can be rearranged by applying the Divergence Theorem to the surface integrals and taking the time derivative into the volume integral, yielding

$$\iiint_{CV}\left[\varepsilon\frac{\partial}{\partial t}(\rho_v \mathbf{V}) + \Gamma\nabla\cdot(\rho_v \mathbf{V}\mathbf{V})\right]dV = \iiint_{CV}[-\nabla P + \nabla\cdot\tau + \mathbf{g}]dV \qquad (3.45)$$

The volume integrals in the above equation can be removed for the arbitrary CV and the conservation of momentum can be expressed by [142]

$$\varepsilon \frac{\partial}{\partial t}(\rho_v \mathbf{V}) + \Gamma \nabla \cdot (\rho_v \mathbf{V}\mathbf{V}) + \nabla P - \nabla \cdot \tau - \mathbf{g} = 0 \qquad (3.46)$$

as ε and Γ are constant. Equation (3.46) is also known as the volume averaged Navier-Stokes equation in transport phenomena and can be reduced to two most commonly used equations for steady Newtonian fluid flow in a packed-bed porous media: one is Darcy's equation and the other is Ergun's equation [143]. In fact, in the analysis of order of magnitude, it is proved that all the terms in Equation (3.46) except for the pressure term and **g** term which consists of viscous drag and form drag [143] are negligible [2]. The conservation of momentum equation can therefore be expressed by either Darcy's equation as

$$\mathbf{V} = -\frac{\kappa}{\mu} \nabla P \qquad (3.47)$$

or by Ergun's equation as [133]

$$\mathbf{V} + \frac{\rho_v}{\mu} \kappa_E \mathbf{V} |\mathbf{V}| = -\frac{\kappa}{\mu} \nabla P \qquad (3.48)$$

In Equations (3.47) and (3.48) κ denotes permeability of porous medium and μ denotes dynamic viscosity of the fluid. κ_E is usually called the Forchheimer coefficient. κ and κ_E are also referred as the Darcian and non-Darcian permeability parameters [144], respectively. The former is used to calculate the viscous effect while the latter is used to calculate the inertial effect on the pressure drop. The permeability κ can be expressed by the Carman-Kuzeny equation [133] as

$$\kappa = \frac{d_p^2 \varepsilon_b^3}{150(1-\varepsilon_b)^2} \qquad (3.49)$$

where d_p is diameter of the adsorbent particle. The constant 150 in the denominator of the above equation is given as 180 in some different references [2,142]. The Forchheimer coefficient κ_E can be expressed by the Burke-Plummer equation [133] as

$$\kappa_E = \frac{1.75 d_p}{150(1-\varepsilon_b)} \tag{3.50}$$

Darcy equation is generally valid for laminar flow and low fluid velocities where the inertial effects are negligible and therefore Darcy's equation is used in this study in determining the velocity distribution in the radial and axial directions in the adsorbent bed.

3.2.5 Conservation of Energy for the Adsorbent Bed

The conservation of energy equation in the adsorbent bed can be derived considering a CV represented in Figure 3.9. The conservation of energy for this CV can be stated as follows

$$\begin{aligned}&\begin{bmatrix}\text{Rate of}\\ \text{change of}\\ \text{energy}\\ \text{in the CV}\end{bmatrix}+\begin{bmatrix}\text{Net rate of}\\ \text{energy efflux}\\ \text{due to}\\ \text{mass flow}\end{bmatrix}+\begin{bmatrix}\text{Rate of}\\ \text{flow work}\\ \text{performed}\\ \text{by the CV}\end{bmatrix}\\ &+\begin{bmatrix}\text{Rate of}\\ \text{heat transfer}\\ \text{out of the CV}\\ \text{by conduction}\end{bmatrix}-\begin{bmatrix}\text{Rate of heat transfer}\\ \text{into the CV through the}\\ \text{contact resistance at the}\\ \text{tube/adsorbent interface}\end{bmatrix}=0\end{aligned} \tag{3.51}$$

The change of energy in the CV consists of the sum of change of energy in vapor, adsorbent and adsorbate phases, and can be expressed by the following volume integral

$$\iiint_{CV} dE = \iiint_{CV} [\varepsilon_T \rho_v u_v + (1-\varepsilon_T)\rho_s u_s + (1-\varepsilon_T)\rho_s X u_{ad}] dV \tag{3.52}$$

where u_v, u_s and u_{ad} are internal energy of vapor, adsorbent and adsorbate, respectively. Thus, time rate of change of energy per unit volume of adsorbent bed, let's say $q'''_{s,s}$, can be written by removing the volume integral as follows

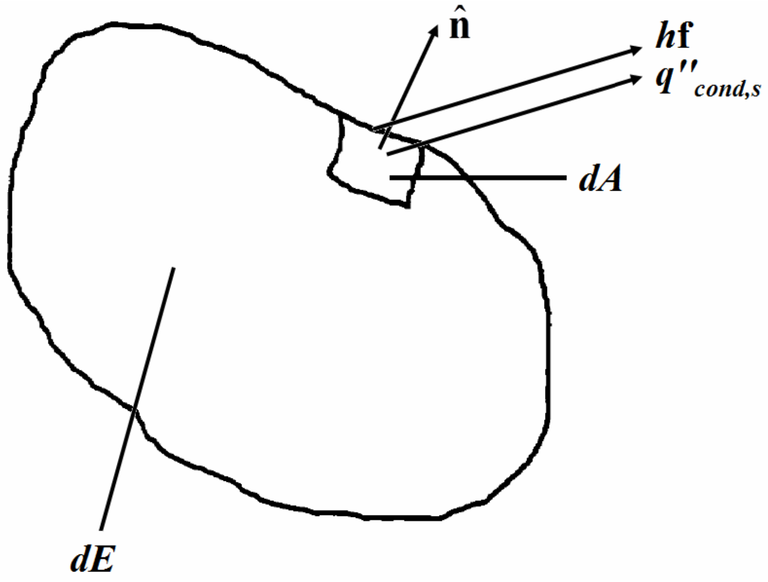

Figure 3.9 Differential element used for the derivation of conservation of energy in the adsorbent bed [2].

$$q'''_{s,s} = \frac{\partial}{\partial t}[\varepsilon_T \rho_v u_v + (1-\varepsilon_T)\rho_s u_s + (1-\varepsilon_T)\rho_s X u_{ad}] \tag{3.53}$$

Second and third terms in Equation (3.51), namely the net rate of energy efflux due to vapor flow and the flow work done by the CV, can be expressed together in a surface integral and then a volume integral using Divergence Theorem as follows

$$\iint_{CS} h_v(\mathbf{f}\cdot\hat{\mathbf{n}})dA = \iiint_{CV} \nabla\cdot(h_v\mathbf{f})dV \tag{3.54}$$

In the above equation, h_v denotes enthalpy of vapor and can also be written as $h_v=u_v+Pv_v$ from thermodynamics. Removing the volume integral and expanding the Del operator, total energy including the flow work and the energy efflux due to mass flow per unit volume of adsorbent bed can be expressed by

$$\nabla\cdot(h_v\mathbf{f}) = h_v\nabla\cdot\mathbf{f} + \mathbf{f}\nabla h_v \tag{3.55}$$

The rate heat transfer by conduction for the CV surrounded by the CS in Figure 3.9 can be expressed by the following equation and can be converted to volume integral as follows

$$\iint_{CS} q''_{cond,s} \cdot \hat{\mathbf{n}} dA = \iiint_{CV} \nabla \cdot q''_{cond,s} \, dV \tag{3.56}$$

where $q''_{cond,s}$ is the total conduction heat flux through all phases (adsorbent, adsorbate and vapor) [2].

The adsorbent bed contains not only solid phase but also gas phase. In other words, the thermal conductivity of the porous media is a combination of the conductivities of these two constituents. Therefore, an effective or overall thermal conductivity for the adsorbent bed can be defined as [142]

$$k_e = (1 - \varepsilon_T) k_s + \varepsilon_T k_v \tag{3.57}$$

where k_s and k_v are the thermal conductivities of solid (adsorbent) and gas (vapor) phases, respectively. However, the solid phase also includes the adsorbate phase and the thermal conductivity of the adsorbate has more significant effect than that of vapor on the effective thermal conductivity when the adsorbate is assumed to be in liquid phase. Therefore, the adsorbate contribution to the effective thermal conductivity should be taken into account as well. Calculating the effective thermal conductivity of the porous media by the following equation will make more sense

$$k_e = (1 - \varepsilon_T) k_s + \varepsilon_T k_v + (1 - \varepsilon_T) X k_l \tag{3.58}$$

where k_l denotes the thermal conductivity of liquid refrigerant. The effective thermal conductivity of common pairs is measured and given in the literature. Thus, it can also be taken directly from the published studies as constant neglecting its dependence on temperature and amount adsorbed. As a result, the heat flux due to the conduction in the adsorbent bed is given by the following equation

$$q''_{cond,s} = -k_e \nabla T_s \tag{3.59}$$

and the conduction heat transfer per unit volume of adsorbent bed can therefore be written as follows substituting the above equation into Equation (3.56) and removing the volume integral

$$q'''_{cond,s} = -k_e \nabla^2 T_s \tag{3.60}$$

The rate of heat transfer by conduction through the thermal contact at HTT/adsorbent interface is found before as in Equation (3.28). It can be written for per unit volume of adsorbent bed V_s as follows

$$q'''_{cont,ts} = \frac{h_c A_{l,to}(T_t - T_s)}{V_s} \tag{3.61}$$

Substituting Equations (3.53), (3.55), (3.60) and (3.61) into Equation (3.51), the conservation of energy equation is obtained as

$$\begin{aligned}&\frac{\partial}{\partial t}[\varepsilon_T \rho_v u_v + (1-\varepsilon_T)\rho_s u_s + (1-\varepsilon_T)\rho_s X u_{ad}] + h_v \nabla \cdot \mathbf{f} + \mathbf{f}\nabla h_v - k_e \nabla^2 T_s \\ &-\frac{h_c A_{l,to}(T_t - T_s)}{V_s} = 0\end{aligned} \tag{3.62}$$

The divergence of the mass flux **f** in the second term of the above equation can be replaced utilizing Equation (3.41) obtained in the derivation of the conservation of mass as follows

$$\begin{aligned}&\frac{\partial}{\partial t}[\varepsilon_T \rho_v u_v + (1-\varepsilon_T)\rho_s u_s + (1-\varepsilon_T)\rho_s X u_{ad}] - h_v \frac{\partial}{\partial t}[\varepsilon_T \rho_v + (1-\varepsilon_T)\rho_s X] \\ &+\mathbf{f}\nabla h_v - k_e \nabla^2 T_s - \frac{h_c A_{l,to}(T_t - T_s)}{V_s} = 0\end{aligned} \tag{3.63}$$

Rearranging the time derivative terms yields [2]

$$\varepsilon_T \frac{\partial(\rho_v u_v)}{\partial t} - \varepsilon_T h_v \frac{\partial \rho_v}{\partial t} + (1-\varepsilon_T)\rho_s \frac{\partial u_s}{\partial t} + (1-\varepsilon_T)\rho_s u_{ad} \frac{\partial X}{\partial t} + (1-\varepsilon_T)\rho_s X \frac{\partial u_{ad}}{\partial t}$$
$$-(1-\varepsilon_T)\rho_s h_v \frac{\partial X}{\partial t} + \mathbf{f}\nabla h_v - k_e \nabla^2 T_s - \frac{h_c A_{l,to}(T_t - T_s)}{V_s} = 0 \tag{3.64}$$

Using the relation $u_v = h_v - P/\rho_v$, the first two terms in the above equation can be simplified to

$$\varepsilon_T \rho_v \frac{\partial h_v}{\partial t} - \varepsilon_T \frac{\partial P}{\partial t} + (1-\varepsilon_T)\rho_s \frac{\partial u_s}{\partial t} + (1-\varepsilon_T)\rho_s u_{ad} \frac{\partial X}{\partial t} + (1-\varepsilon_T)\rho_s X \frac{\partial u_{ad}}{\partial t}$$
$$-(1-\varepsilon_T)\rho_s h_v \frac{\partial X}{\partial t} + \mathbf{f}\nabla h_v - k_e \nabla^2 T_s - \frac{h_c A_{l,to}(T_t - T_s)}{V_s} = 0 \tag{3.65}$$

Assuming the adsorbent, vapor and adsorbate are in local thermal equilibrium at T_s and assuming constant specific heats for the adsorbent and vapor yields

$$\varepsilon_T \rho_v c_{p,v} \frac{\partial T_s}{\partial t} + (1-\varepsilon_T)\rho_s c_s \frac{\partial T_s}{\partial t} + (1-\varepsilon_T)\rho_s X \frac{\partial u_{ad}}{\partial t} - (1-\varepsilon_T)\rho_s (h_v - u_{ad}) \frac{\partial X}{\partial t}$$
$$-\varepsilon_T \frac{\partial P}{\partial t} + \mathbf{f} c_{p,v} \nabla T_s - k_e \nabla^2 T_s + \frac{h_c A_{l,to}(T_s - T_t)}{V_s} = 0 \tag{3.66}$$

The following relation can be written for the internal energy of adsorbate since the specific volume of the adsorbate v_{ad} is very small [2]

$$u_{ad} = h_{ad} - P v_{ad} \approx h_{ad} \tag{3.67}$$

and hence the following equation

$$h_v - u_{ad} \approx h_v - h_{ad} \approx \Delta H \tag{3.68}$$

where ΔH is the heat of adsorption. Heat of adsorption is substituted as absolute value in Equation (3.66) to generalize the conservation of energy equation for adsorption and desorption processes. Furthermore, the adsorbate is assumed to be in liquid phase and the relation $du_{ad}=c_{v,l}dT_s=c_{p,l}dT_s$ can be used for the internal energy of the adsorbate. On the other hand, in Equation (3.66), mass flux can be replaced from Equation (3.36) as $\mathbf{f}=\rho_v\mathbf{V}$ neglecting diffusive mass transfer. Rearranging Equation (3.66) by using these modifications, the last form of the conservation of energy in the adsorbent bed becomes

$$\begin{aligned} &\varepsilon_T\rho_v c_{p,v}\frac{\partial T_s}{\partial t}+(1-\varepsilon_T)\rho_s c_s\frac{\partial T_s}{\partial t}+(1-\varepsilon_T)\rho_s X c_{p,l}\frac{\partial T_s}{\partial t}-(1-\varepsilon_T)\rho_s\left|\Delta H\right|\frac{\partial X}{\partial t} \\ &-\varepsilon_T\frac{\partial P}{\partial t}+\rho_v\mathbf{V}c_{p,v}\nabla T_s-k_e\nabla^2 T_s+\frac{h_c A_{l,to}}{V_s}(T_s-T_t)=0 \end{aligned} \tag{3.69}$$

In summary, five conservation equations have been derived in this chapter. These equations include the conservation of energy equations for the HTF, HTT and adsorbent bed, and the conservation of mass and momentum equations for the adsorbent bed. In the following chapter, a base-case analysis of heat and mass transfer in the adsorbent bed of a thermal wave cycle will be performed by using these equations and defining initial and boundary conditions.

CHAPTER 4

BASE-CASE DESIGN AND ANALYSIS OF HEAT AND MASS TRANSFER IN AN ADSORBENT BED FOR A THERMAL WAVE CYCLE

4.1 Introduction

The researches on adsorption cooling cycles have recently focused on the adsorbent bed since heat and mass transfer inside the bed have significant influence on the system performance. COP can be improved significantly as the mass and especially heat transfer inside the bed are enhanced. Poor heat and mass transfer problem is handled by the models that investigate system parameters affecting the performance. In this chapter, a two dimensional model that analyzes transient coupled heat and mass transfer in the adsorbent bed is presented. The shape of thermal wave formed in a finless tube adsorbent bed is investigated during the desorption process of the cycle.

In the literature, analyses were generally made by one-dimensional models. There is a gap in a two-dimensional solution and representation of heat and mass transfer in the adsorbent bed. The variations of temperature, pressure, amount adsorbed, equilibrium adsorption capacity and mass transfer coefficient are therefore represented two dimensionally by multicolored plots. In the model, temperatures of adsorbent (solid), adsorbate (liquid) and adsorptive (vapor) are taken equal to each other using local temperature equilibrium assumption. Governing equations for energy, mass and momentum transfers are solved by Comsol Multiphysics simultaneously.

4.2 Model Description

There are three subdomains in the model and they have a cylindrical geometry. The three subdomains are heat transfer fluid (HTF) flowing inside a tube, the tube itself, and an adsorbent bed. The adsorbent bed is also called porous media since it is filled with a porous material like zeolite, silica gel or activated carbon. Porous materials have very large volume specific surface area and can adsorb refrigerant vapor into their pores. 3-D and 2-D geometry of the model is represented in Figure 4.1.

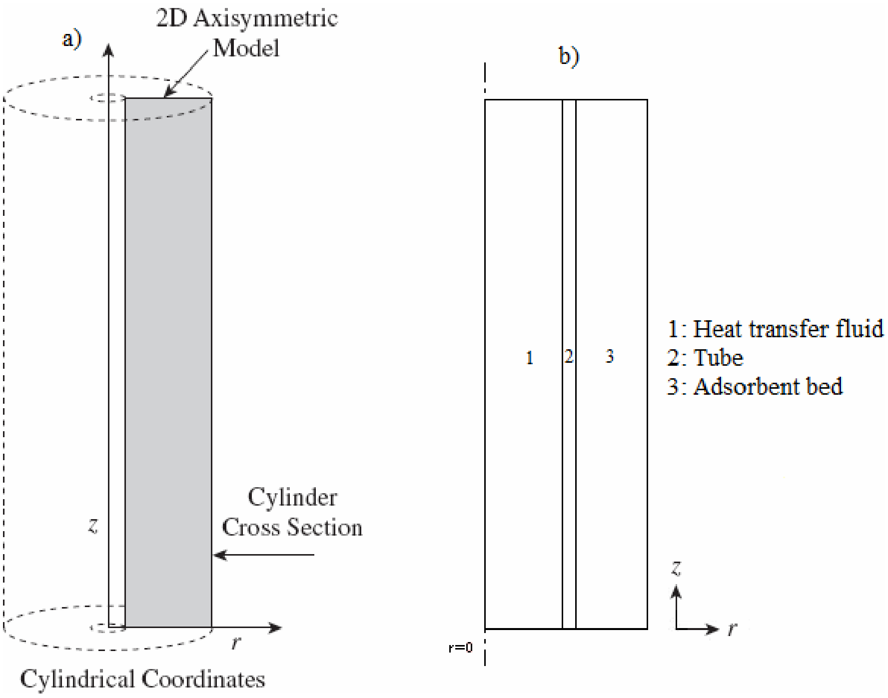

Figure 4.1 a) 3-D, b) 2-D model geometry.

The three subdomains, the HTF, tube and adsorbent bed, are placed in a vacuum chamber. Refrigerant vapor flows into or out of the vacuum chamber during the processes of cycle and the adsorbent bed adsorbs or desorbs the vapor in this vacuum chamber. 3-D model can be reduced to 2-D axisymmetric model by using the symmetry in tangential direction of the cylinder in Figure 4.1 (a). The 2-D model can be simulated faster and more accurately avoiding from the complexity of 3-D model whereas the 3-D model can result in less accurate results because of its limitations on the number of mesh elements. Only one side of the axis line is taken in Fig. 4.1 (b) since there is also an axial symmetry. It should be noted that 3-D simulation is necessary if the model is not symmetrical in tangential direction and cannot be reduced to 2-D like in the case of using a rectangular adsorbent bed instead of the cylindrical geometry.

4.3 Mathematical Model

Energy equation for the HTF and tube, and energy, mass and momentum equations for the adsorbent bed are solved. Energy equation for the HTF including conduction and convection heat transfers can be rearranged using the Del operator in Equation (3.24) as follows:

$$k_f \nabla^2 T_f = \rho_f c_f \frac{\partial T_f}{\partial t} + \rho_f c_f v_f \nabla T_f + \frac{2}{r_{ti}} h_i (T_f - T_t) \tag{4.1}$$

Velocity of HTF can be expressed as following for a fully developed laminar flow:

$$v_f = 2 v_{ave} \left(1 - \frac{r^2}{r_{ti}^{\;2}} \right) \tag{4.2}$$

Energy equation for the HTF tube including the heat conduction in the tube can be rearranged using the Del operator in Equation (3.32) as follows:

$$k_t \nabla^2 T_t + \frac{h_i A_{l,ti}}{V_t} (T_f - T_t) = \rho_t c_t \frac{\partial T_t}{\partial t} + \frac{h_c A_{l,to}}{V_t} (T_t - T_s) \tag{4.3}$$

Energy balance in a porous media has a complex form due to three different phases; solid, gas and adsorbate phases. The energy equation in the adsorbent bed can be written as follows [2]:

$$0=(1-\varepsilon)\rho_s c_s \frac{\partial T_s}{\partial t}+\varepsilon\rho_v c_{p,v}\frac{\partial T_s}{\partial t}+(1-\varepsilon)\rho_s X c_{p,l}\frac{\partial T_s}{\partial t}-(1-\varepsilon)\rho_s\left|\Delta H\right|\frac{\partial X}{\partial t}-\varepsilon\frac{\partial P}{\partial t}$$
$$-k_s\nabla^2 T_s+\rho_v c_{p,v}\mathbf{u}\nabla T_s+\frac{h_c A_{l,to}}{V_s}(T_s-T_t) \tag{4.4}$$

In equation (4.4), temperatures of adsorbent material, refrigerant vapor and adsorbate are taken equal to each other using local thermal equilibrium assumption. ΔH represents heat of adsorption and is taken as constant. The adsorbate that is refrigerant adsorbed by the adsorbent is assumed to be in liquid phase. c_v and c_l represent specific heats of refrigerant in vapor and liquid phases, respectively, and they are taken as constant. The working pair examined in the present study is zeolite-water pair which is operated under vacuum conditions. Water vapor behaves as an ideal gas in low pressure conditions and its density can be calculated by ideal gas relation:

$$P=\rho_v R_v T_s \tag{4.5}$$

The momentum equation for the adsorbent bed can be expressed by Darcy flow that gives a relation between refrigerant gas velocity and pressure:

$$\mathbf{u}=-\frac{\kappa}{\mu}\nabla P \tag{4.6}$$

Conservation of refrigerant mass in the adsorbent bed can be written as follows [2], neglecting diffusive mass transfer:

$$\varepsilon\frac{\partial\rho_v}{\partial t}+(1-\varepsilon)\rho_s\frac{\partial X}{\partial t}+\nabla(\mathbf{u}\rho_v)=0 \tag{4.7}$$

Amount adsorbed, X, can be found by Linear Driving Force (LDF) model that estimates the desorption rate assuming a parabolic concentration profile within the adsorbent particle [145]:

$$\frac{\partial X}{\partial t}=k_m(X_e-X) \tag{4.8}$$

The internal mass transfer coefficient, k_m, can be calculated by the following expression [145]:

$$k_m = \frac{15}{r_p^{\,2}} D_o \exp\left(-\frac{E_a}{RT_s} \right) \tag{4.9}$$

Dubinin–Astakhov equation is used for the equilibrium adsorption capacity, X_e, [146]:

$$X_e = X_o \exp\left[-B\left(\frac{T_s}{T_{sat}} - 1 \right)^n \right] \tag{4.10}$$

Coefficients X_o, B and n can be taken as 0.261, 5.36 and 1.73 respectively for zeolite-water pair [101]. T_{sat} is the saturation temperature of water vapor corresponding to the pressure inside the adsorbent bed and can be calculated as follows

$$T_{sat} = 39.724 + \frac{1730.63}{8.07131 - \log 10(7.500638 \cdot 10^{-3} \cdot P)} \tag{4.11}$$

where P is entered in Pa and T_{sat} is obtained in K.

4.3.1 Initial and Boundary Conditions

Temperature distributions for HTF, tube and adsorbent bed are initially uniform at cycle cooling temperature:

$$T_f(t=0,r,z) = T_t(t=0,r,z) = T_s(t=0,r,z) = T_i \tag{4.12}$$

Pressure and amount adsorbed in the bed are also initially uniform at condenser pressure (P_c) and maximum amount adsorbed (X_o) respectively:

$$P(t=0,r,z) = P_c, \quad X(t=0,r,z) = X_o \tag{4.13}$$

The HTF tube is insulated at the inlet and outlet of the adsorbent bed and this yields no temperature gradient at *z=0* and *z=L*. Furthermore, there is no temperature gradient in HTF in the axial direction at the tube outlet due to the insulation. The adsorbent bed is also insulated on both sides. The presence of adjacent bed elements undergoing the same cycle yields a reflective condition on the lateral surface of the bed, $r=r_{bed}$. These conditions are all represented as follows:

$$\begin{gathered}\frac{\partial T_t}{\partial z}(t,r,z=0)=\frac{\partial T_t}{\partial z}(t,r,z=L)=\frac{\partial T_f}{\partial z}(t,r,z=L)=0,\\ \frac{\partial T_s}{\partial z}(t,r,z=0)=\frac{\partial T_s}{\partial z}(t,r,z=L)=\frac{\partial T_s}{\partial r}(t,r=r_{bed},z)=0\end{gathered} \tag{4.14}$$

Heat conduction into the adsorbent bed is equal to heat transfer from the tube wall, $r=r_t$, yielding:

$$-k_s\frac{\partial T_s}{\partial r}(t,r=r_t,z)=h_c(T_t-T_s) \tag{4.15}$$

HTF enters the tube from the bottom side (*z=0*) at constant heating temperature yielding the following boundary condition:

$$T_f(t,r,z=0)=T_{hot} \tag{4.16}$$

On the other hand, at the other boundaries *z=0*, *z=L* and $r=r_{bed}$, the adsorbent bed is open to the vacuum chamber that enables the refrigerant vapor to flow out at condenser pressure during desorption process. These boundary conditions can be given as follows:

$$P(t,r,z=0)=P(t,r,z=L)=P(t,r=r_{bed},z)=P_c \tag{4.17}$$

The flow of refrigerant vapor is restricted at the boundary $r=r_t$ since the surface at this boundary is enclosed by the tube wall. Therefore the pressure gradient at this boundary in the adsorbent bed is zero:

$$\frac{\partial P}{\partial r}(t, r = r_t, z) = 0 \tag{4.18}$$

Model parameters used in simulations are given in Table 4.1.

Table 4.1 Model parameters [2,101].

Parameter	Value	Unit
c_f	1930	J/kgK
$c_{p,l}$	4180	J/kgK
$c_{p,v}$	1880	J/kgK
c_s	837	J/kgK
c_t	385	J/kgK
D_o	5.8e-9	m^2/s
E_a	1e4	J/mol
h_c	100	W/m^2K
k_f	0.115	W/mK
k_t	400	W/mK
P_c	4.247	kPa
R	8314	J/molK
R_v	461.5	J/kgK
r_p	1e-3	M
T_{hot}	473	K
T_i	313	K
X_o	0.261	kg_w/kg_s
ΔH	3300	kj/kg
ε	0.635	
κ	5e-12	m^2
μ	1e-5	kg/ms
ρ_f	914	kg/m^3
ρ_s	1000	kg/m^3
ρ_t	8700	kg/m^3
b	0.001	m
L	0.25	m
r_t	0.01	m

4.4 Solution to the Model

The complexity and nonlinearity of such coupled heat and mass transfer models make an analytical solution impossible. Numerical methods used include the finite difference method, the finite volume method and the finite element method. Finite difference methods are generally used for solving this set of equations due to its simplicity and ease of varying initial and boundary conditions. In order to simplify the numerical analysis, certain models are used [145]. They can be grouped as:

- Thermodynamic model
- Heat transfer model
- Mass transfer model
- Coupled heat and mass transfer model

In this study, coupled heat and mass transfer model is used to investigate both heat and mass transfer inside the bed. Fully coupled model that includes heat, mass and momentum transfers is simultaneously solved by Comsol Multiphysics software package. In this model, temperature distributions for the HTF, tube and adsorbent bed, and variations of pressure, amount adsorbed, equilibrium adsorption capacity and mass transfer coefficient in the adsorbent bed are investigated for desorption process. Solutions are presented by domain plots that show the results in multi-colored 2D domain. Before presenting the results, an overview of Comsol Multiphysics and its capabilities is given.

4.4.1 Comsol Multiphysics

Comsol Multiphysics is a powerful finite element (FEM) software package modeling and solving all kinds of engineering problems based on partial differential equations (PDEs). It is an integrated environment for solving systems of time-dependent or stationary second order partial differential equations in one, two, and three spatial dimensions. Comsol Multiphysics allows users to model and simulate a wide variety of physical phenomena. The program can tackle technical problems in many fields of science and engineering. Solving the problems with Comsol Multiphysics does not require an in-depth knowledge of mathematics or numerical analysis. Thanks to the built-in physics modes, one can build models by defining the relevant physical quantities such as material properties, loads, constraints, sources, and fluxes rather than by defining the underlying equations. The program can be accessed as a standalone product through a flexible graphical user interface (GUI), or by script programming in the Comsol Script language or in the Matlab language [147].

Traditional finite element method software is offered as a bound package of separate computer programs, each of which is responsible for only a part of the modeling procedure. One program is used to create model geometry, and another program is used to mesh the geometry, apply material properties and specify boundary conditions. A solver is another program that is responsible for solving the problem and saving the solution. At the end, the results are plotted in yet another program that handles postprocessing. Contrary to traditional software packages, Comsol Multiphysics solves this issue by being an all-in-one geometry creator and mesher, solver and postprocessor. In this respect, Comsol Multiphysics is much simpler to use than traditional finite element method software packages.

Comsol Multiphysics enables to perform various types of analysis including:

- Stationary and time-dependent analysis
- Linear and nonlinear analysis
- Eigen-frequency and modal analysis

PDEs are the basis for the laws of science and provide the foundation for modeling a wide range of scientific and engineering phenomena. Comsol Multiphysics can be used in many application areas, from chemical reactions to fluid dynamics and from heat transfer to porous media flow since it can solve a system of PDEs [147]. In its base configuration, Comsol Multiphysics offers modeling and analysis power for many application areas. For several of the key application areas, optional modules are available. These application-specific modules use terminology and solution methods particular to the discipline, which simplifies creating and analyzing models. Comsol Multiphysics software has eight add-on modules: AC/DC, Acoustics, Chemical Engineering, Earth Science, Heat Transfer, MEMS, RF, and Structural Mechanics [148].

The Comsol Multiphysics user interface contains a set of CAD tools for geometry modeling in 1D, 2D, and 3D. CAD data in DXF-file format can be imported. Images and magnetic resonance imaging (MRI) data can also be used to create the geometry in combination with the programming tools [147]. CAD Import Module and its add-ons provide support for all popular types of CAD files.

Comsol Multiphysics automatically meshes geometry when the geometry is completed and various parameters defined. However, the mesh-generation process can be specified by users accessing a set of control parameters [147].

In the solution stage, Comsol Multiphysics uses suitable solvers for stationary, eigenvalue, and time-dependent problems. For solving linear systems, Comsol Multiphysics features both direct and iterative solvers. A range of pre-conditioners are available for the iterative solvers. Comsol Multiphysics sets up application mode-dependent solver defaults appropriate for the chosen application mode and automatically detects linearity and symmetry in the model [147].

Comsol Multiphysics provides the following options for plotting and postprocessing any model quantity or parameter [147]:

- Surface plots
- Slice plots
- Isosurfaces
- Contour plots
- Deformed shape plots and streamline plots
- Particle tracing
- Cross-sectional plots
- Animations
- Data display and interpolation
- Export of solution data to text files and the Comsol Script workspace
- Integration on boundaries and subdomains

For brevity, the adaptation of the model to Comsol Multiphysics is not described in detail in this chapter. Instead, it is given in Appendix A. Moreover, a sample Comsol model report created by the program is given in Appendix B.

4.5 Results and Discussion

The model geometry is meshed by using extremely fine mesh having 15656 triangular elements. To test the mesh goodness, the model was also simulated with the increasing number of mesh elements. Meshing the model with 44560 elements changed the results only ±0.2% at most. Solver parameter has a relative tolerance of 0.01 and an absolute tolerance 0.001 enabling high accuracy and convergence. The model is solved with a time step of one second, but results are presented for only the times t=0s, t=100s, t=1000s and t=5000s for brevity.

Temperature distributions in the HTF, tube and adsorbent bed are presented in Figure 4.2. The adsorbent bed reaches a uniform temperature after about 5000s. A poor heat transfer is seen in radial direction inside the adsorbent bed. A thermal wave or temperature front is formed in the adsorbent bed by heat transfer from HTF. However, the thermal wave length is long due to poor heat transfer in the bed. Thermal wave length is a key factor for a thermal wave adsorption cooling cycle to obtain high heat regeneration between the beds of the cycles [62,107]. High heat regeneration between the beds provides high performance. For this reason, thermal wave length should be shortened by enhancing heat transfer in radial direction inside the bed. Researchers have focused on this problem and have performed several experimental studies [7]. In the present study, a finless tube adsorbent bed with an equivalent thermal conductivity of 0.5 W/mK is examined. By modifying the geometry with a finned tube and increasing the thermal conductivity of the bed, one can enhance the heat transfer in the bed.

Operating conditions also influence the heat transfer in the adsorbent bed. HTF enters the tube and reaches the cycle maximum temperature (423 K) in a short time as seen in Figure 4.2. This is due to high HTF velocity. Average HTF velocity is taken as 0.005 m/s in this study. HTF transfer its energy not in radial direction but axial direction. If lower velocities are used HTF can transfer more heat in radial direction yielding a straighter thermal wave. Thus, heat regeneration and cycle performance can be enhanced. It can be concluded that a parametric study is needed for investigating the effect of design and operating parameters on the heat transfer inside the bed.

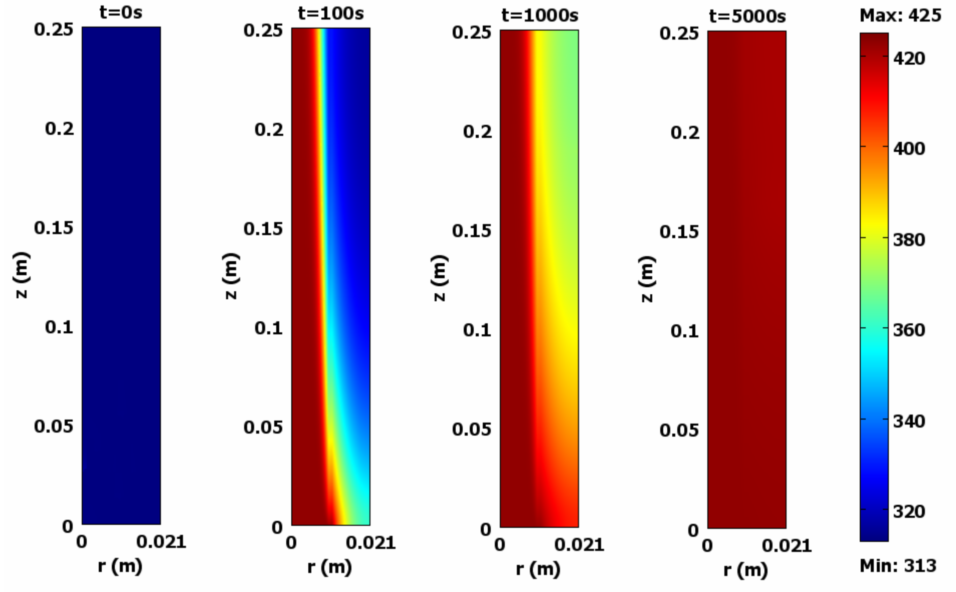

Figure 4.2 Temperature distributions in the HTF, tube and adsorbent bed with time (K).

Pressure distribution in the adsorbent bed is shown in Figure 4.3. Depending on the boundary conditions, pressure starts to increase at the region where temperature increases. The pressure wave expands to upward as temperature increases. The increase in pressure is due to mass transfer resistances as refrigerant vapor is desorbed and removed from the adsorbent material. The permeability of the adsorbent bed has significant effect on the vapor flow through the adsorbent particles. For larger permeability values, the resistance to mass transfer decreases and hence the vapor passes easier through the adsorbent particles yielding smaller pressure gradients in the bed. In Figure 4.3, pressure inside the adsorbent bed returns to its initial value after 5000s since desorption process is completed and the vapor flow is ended. Pressure varies between 4247-4545 Pa during the process. Consequently, the pressure gradient in the bed is not so significant and the pressure may be assumed uniform over the bed.

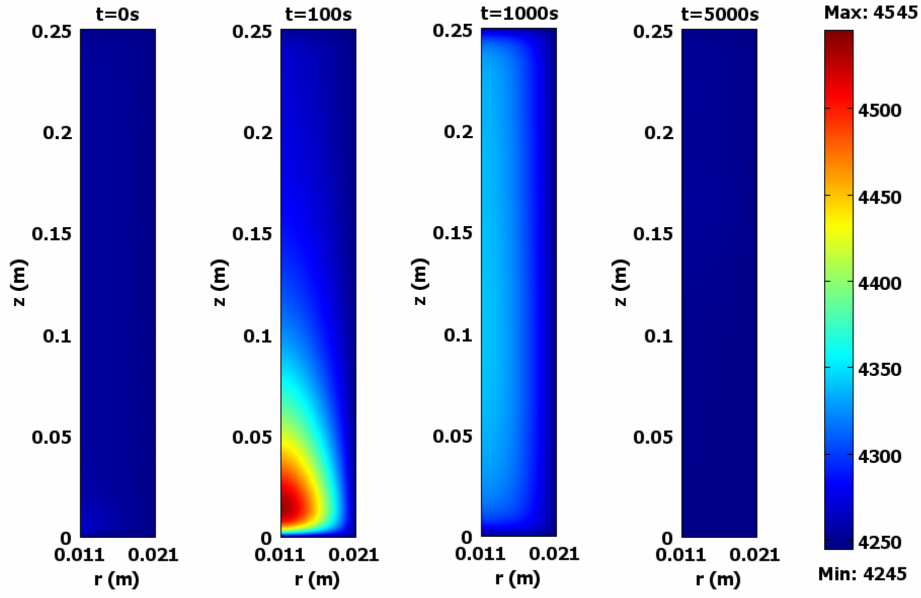

Figure 4.3 Pressure distribution in the adsorbent bed with time (Pa).

Figure 4.4 and Figure 4.5 represent the variations of amount adsorbed and equilibrium adsorption capacity, respectively. As the bed is heated, the amount adsorbed and equilibrium adsorption capacity decrease as expected from desorption process. At the beginning of the desorption process, the amount adsorbed decreases slowly due to the mass transfer resistances as expressed in the discussion of pressure variation. However, equilibrium adsorption capacity shows a similar profile with the temperature. The equilibrium adsorption capacity is theoretical maximum capacity which the adsorbent bed can desorb at given conditions. In practice, it takes a long time to reach the equilibrium state and LDF model can estimate the practical desorption rate taking the adsorption kinetics into account. Amount adsorbed varies between 0.261-0.0889 (26.1%-8.89%) kg water per kg of adsorbent material.

Variation of the mass transfer coefficient in the bed is represented in Figure 4.6. The mass transfer coefficient varies between 0.00186-0.0052 1/s during the process. It increases with time and shows a behavior similar to temperature since it depends only on the adsorbent temperature for a fixed particle size and fixed adsorbent/refrigerant pair as understood from Equation (4.9). The increase in the mass transfer coefficient implies the increase in desorption rate or decrease in amount adsorbed. On the other hand, the mass

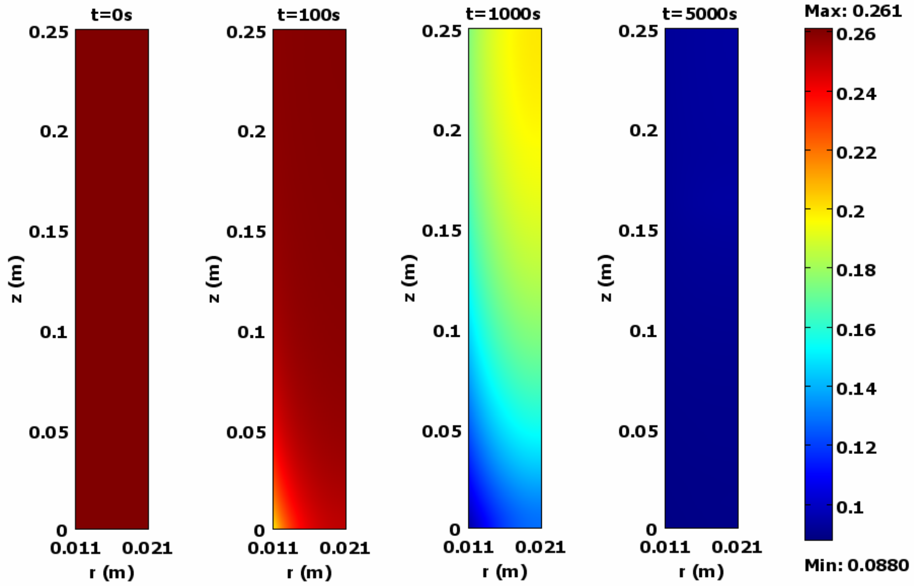

Figure 4.4 Variation of amount adsorbed in the adsorbent bed with time (kg_w/kg_s).

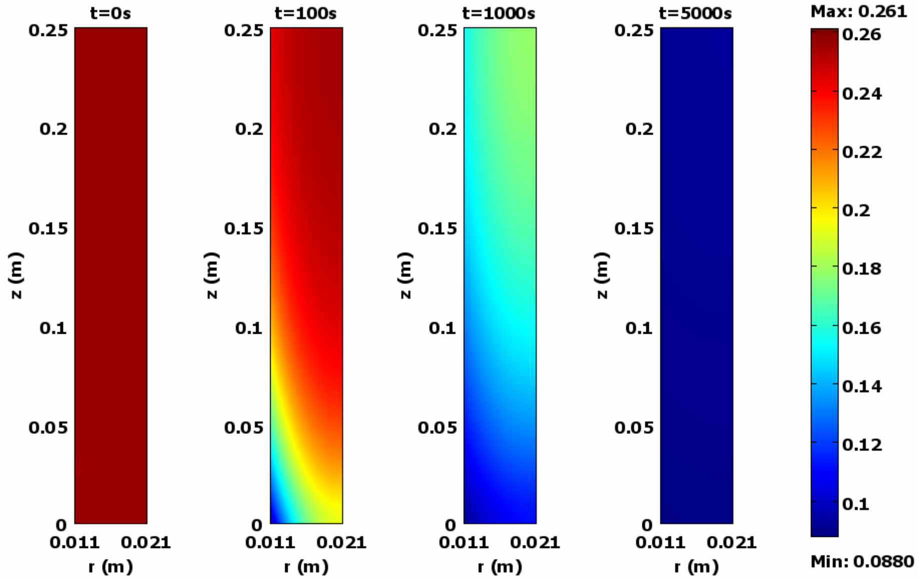

Figure 4.5 Variation of equilibrium adsorption capacity in the adsorbent bed with time (kg_w/kg_s).

transfer coefficient changes for different particle sizes and different pairs. When particle size is increased, for example, a uniform mass transfer coefficient with high value may be expected since mass transfer resistances will decrease. A further study may be performed for investigating the effects of design parameters on the mass transfer coefficient.

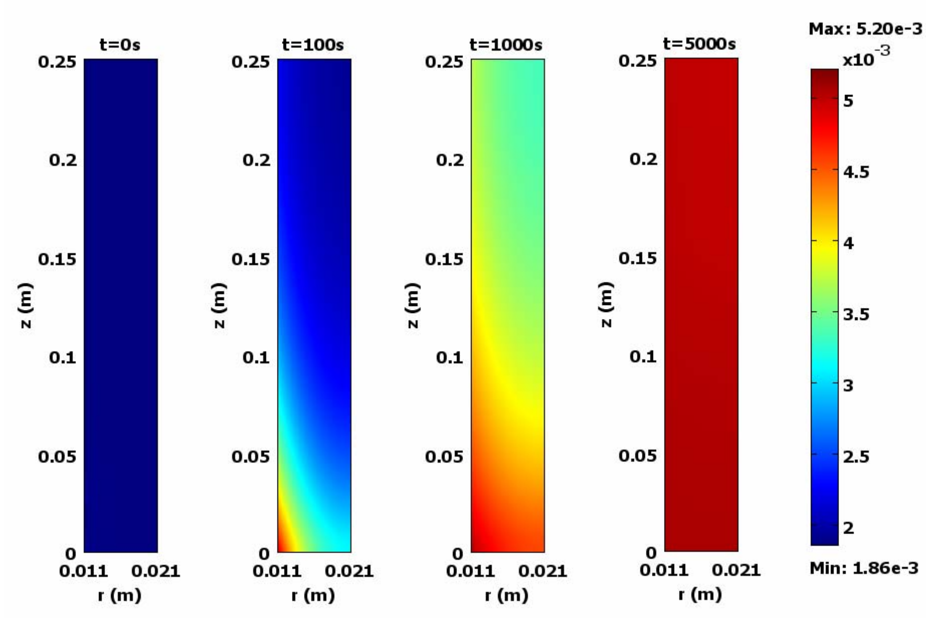

Figure 4.6 Variation of mass transfer coefficient in the adsorbent bed with time (1/s).

A parametric study is required to investigate the effects of design and operational parameters on the dependent variables and thermal wave length. The next chapter covers this parametric study.

CHAPTER 5

PARAMETRIC STUDY OF HEAT AND MASS TRANSFER IN A FINNED TUBE ADSORBENT BED FOR A THERMAL WAVE CYCLE

5.1 Introduction

Poor heat and mass transfer inside the adsorbent bed of adsorption cooling cycles cause low system performance. A parametric study is carried out for determining factors that enhance the heat transfer and mass transfer inside the adsorbent bed. The effects of several design and operating parameters on the transient changes in temperature, pressure and amount adsorbed in the adsorbent bed of a thermal wave adsorption cooling cycle have been investigated two dimensionally.

The shape and length of the thermal wave or temperature front for the HTF is the key factor in thermal wave cycles to obtain high heat regeneration and high performance as described in Shelton's studies [62,108]. In the existing literature, approaches based on one-dimensional models are generally used. However, no studies were identified that present the progression of the thermal wave along the bed in a two dimensional domain. Therefore the objective of the present work is to develop a two dimensional model for coupled heat and mass transfer analysis in a thermal wave bed and apply this model for design purposes. A two dimensional model for coupled heat and mass transfer analysis is presented. Local temperature equilibrium approach that assumes temperatures of adsorbent (solid), adsorbate (liquid) and adsorptive (vapor) to be equal is used. The model is applied to predict the formation and shape of a thermal wave in a finned tube adsorbent bed. The effects of thermal conductivity of the bed, heat transfer fluid (HTF) velocity and bed thickness on temperature, pressure and amount adsorbed profiles are represented two dimensionally using multicolored plots.

5.2 Model Definition

3-D and 2-D drawings of the model can be seen in Fig. 5.1. The shape of the bed is cylindrical and therefore there is symmetry in the tangential direction. The 3-D model can be reduced to a 2-D axisymmetric model by using this symmetry property. Thus, using a 2-D axisymmetric model one can simulate the model faster and more accurately by avoiding the complexity of the 3-D model. There is also axial symmetry and hence only one side of the axis line in Fig. 5.1 (b) is modeled. The model includes three different subdomains all having a cylindrical geometry: 1) the HTF flowing inside a tube; 2) the finned tube that separates the HTF and an adsorbent material; and, 3) the adsorbent material.

The model of the 2-D bed in Fig. 5.1 (b) consists of 3-Subdomains. Subdomain 1 is the HTF, which enters the tube from the bottom end and leaves the tube at the top. Subdomain 2 is the tube and fins. Both the fin and tube are copper, and radial circular fins are used. Negligible thermal contact resistances between the fins and the tube are assumed, which allows the tube and fins to be modeled using a single subdomain. Subdomain 3 is the adsorbent material, also termed the porous media, which fills the gaps between the fins. These three subdomains constitute the extent of the adsorbent bed model. The adsorbent bed is placed into a larger vacuum chamber that is initially evacuated and then filled with refrigerant vapor. This larger vacuum chamber is connected to the condenser and evaporator. During the desorption process, desorbed refrigerant vapor moves from adsorbent material (Subdomain 3) through the vacuum chamber to the condenser. During the adsorption process, refrigerant vapor moves from the evaporator through the vacuum chamber and is adsorbed on the adsorbent material. A simple schematic is presented in Fig. 5.2 to show how the bed fits into the vacuum chamber.

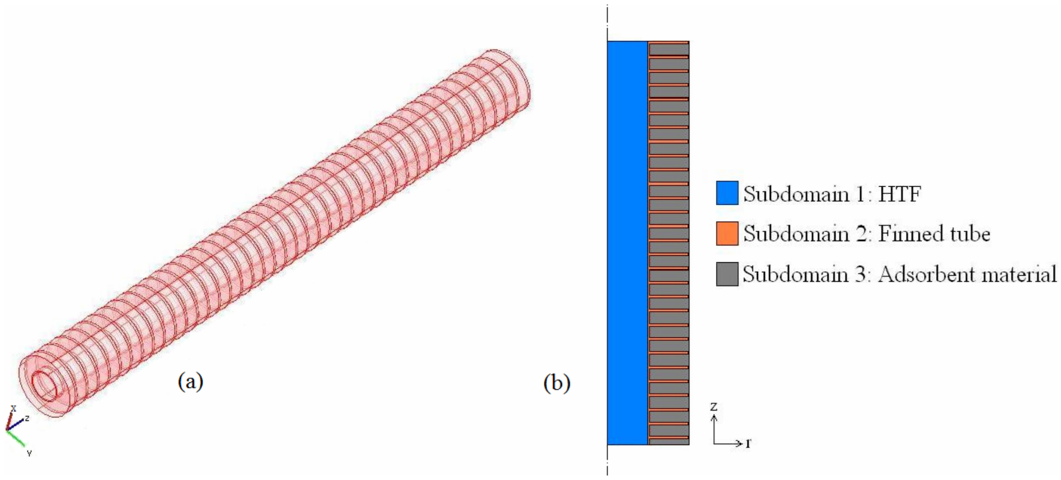

Fig. 5.1 (a) 3-D and (b) 2-D model geometry.

5.3 Mathematical Model

Subdomain 1, i.e. the HTF, includes only energy transport by conduction and convection. The governing equation can be written as follows for a transient analysis [109]:

$$\rho_f c_f \frac{\partial T_f}{\partial t} - k_f \nabla^2 T_f + \rho_f c_f v_f \nabla T_f + \frac{2}{r_{ti}} h_i (T_f - T_t) = 0 \qquad (5.1)$$

For a fully developed laminar flow, the HTF velocity can be expressed as:

$$v_f = 2 v_{ave} \left(1 - \frac{r^2}{r_{ti}^{\ 2}} \right) \qquad (5.2)$$

The energy equation for the HTF tube including the heat conduction in the tube can be given as [109]:

$$\rho_t c_t \frac{\partial T_t}{\partial t} - k_t \nabla^2 T_t + \frac{h_i A_{l,ti}}{V_t} (T_t - T_f) + \frac{h_c A_{l,to}}{V_t} (T_t - T_s) = 0 \qquad (5.3)$$

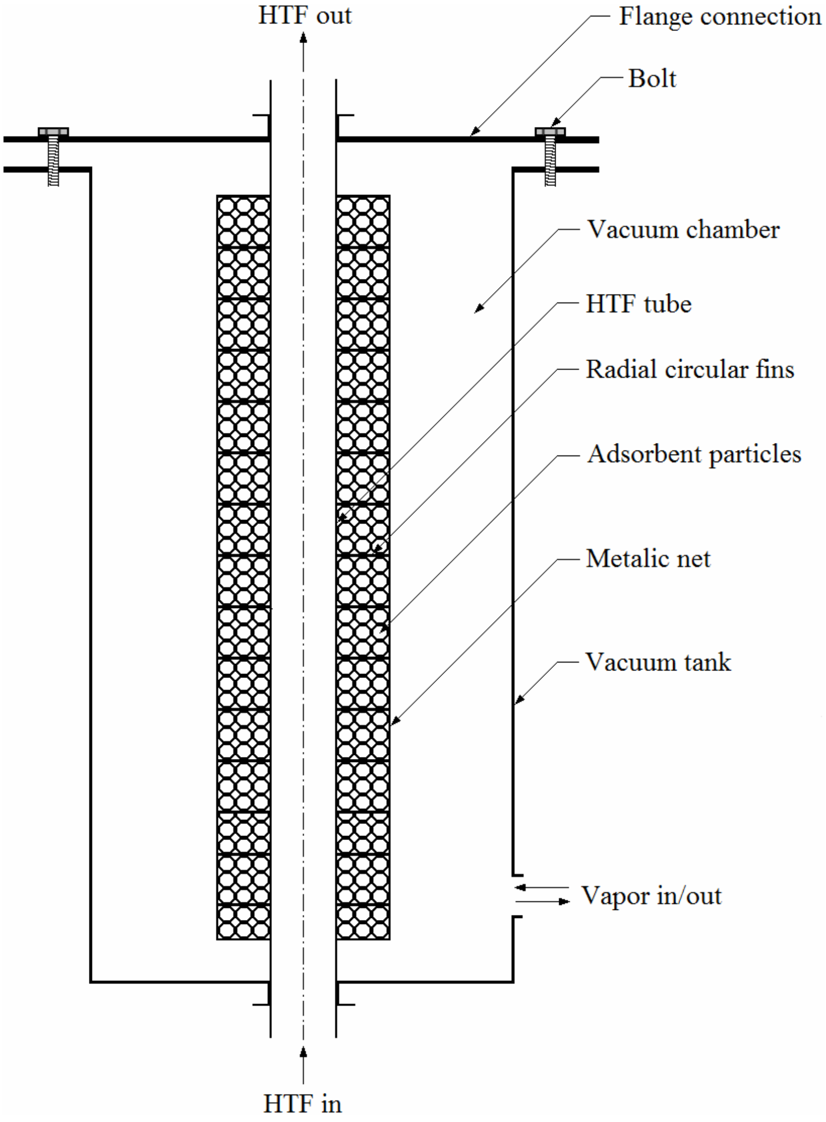

Fig. 5.2 Vacuum chamber.

The energy equation in Subdomain 3, i.e. in the porous media or adsorbent material, is more complex relative to the other subdomains. The energy equation for the porous media can be given as [2,106]:

$$\begin{aligned}&(1-\varepsilon)\rho_s c_s \frac{\partial T_s}{\partial t} + \varepsilon \rho_v c_{p,v} \frac{\partial T_s}{\partial t} + (1-\varepsilon)\rho_s X c_{p,l} \frac{\partial T_s}{\partial t} - (1-\varepsilon)\rho_s \left|\Delta H\right| \frac{\partial X}{\partial t} \\ &-\varepsilon \frac{\partial P}{\partial t} - k_s \nabla^2 T_s + \rho_v c_{p,v} \mathbf{u} \nabla T_s + \frac{h_o A_o}{V_s}(T_s - T_t) = 0\end{aligned} \quad (5.4)$$

In Eq. (5.4), the temperatures of adsorbate and refrigerant vapor are equal to the adsorbent temperature based on the assumption of local thermal equilibrium. Zeolite-water pair is used as the working pair in the simulations. It is noted that zeolite-water pair works at vacuum pressures. It is also noted that herein adsorbate refers to the refrigerant adsorbed by the adsorbent and vapor phase refers to the refrigerant in the vapor phase. The adsorbate is assumed to be in the liquid phase. $c_{p,v}$ and $c_{p,l}$ represent specific heats of refrigerant (water) in vapor and liquid phases, respectively, and they are assumed to be constant. The density of the water vapor is found by the ideal gas relation, $P=\rho_v R_v T_s$, since the water vapor behaves as an ideal gas under these low pressure conditions.

The heat of adsorption, ΔH, is assumed to be constant. Darcy equation is usually valid for the low gas velocities found in porous media such as adsorbent material and is used herein for the vapor velocity in the radial and axial directions:

$$u = -\frac{\kappa}{\mu}\frac{\partial P}{\partial r}, \quad v = -\frac{\kappa}{\mu}\frac{\partial P}{\partial z} \tag{5.5}$$

The mass balance equation for the porous media can be written as follows [2]:

$$\varepsilon \frac{\partial \rho_v}{\partial t} + (1-\varepsilon)\rho_s \frac{\partial X}{\partial t} - D_m \nabla^2 \rho_v + \nabla(\mathbf{u}\rho_v) = 0 \tag{5.6}$$

The second term on the LHS of Eq. (5.6) defines the rate of desorption/adsorption. The third term defines the diffusive mass transfer and is usually neglected.

The Linear Driving Force (LDF) model, which assumes a parabolic concentration profile within the adsorbent particle, can be used for solving for the amount adsorbed, X, by applying the following expression [149]:

$$\frac{\partial X}{\partial t} = k_m (X_e - X) \tag{5.7}$$

The internal mass transfer coefficient, k_m, can be found by the expression [149]:

$$k_m = \frac{15}{{r_p}^2} D_o \exp\left(-\frac{E_a}{RT_s} \right) \tag{5.8}$$

The equilibrium adsorption capacity, X_e, can be found by the Dubinin–Astakhov equation [146]:

$$X_e = X_o \exp\left[-B \left(\frac{T_s}{T_{sat}} - 1 \right)^n \right] \tag{5.9}$$

where the coefficients X_o, B and n are assumed as 0.261, 5.36 and 1.73 respectively for a zeolite-water pair [101].

5.3.1 Initial and Boundary Conditions

Temperature distribution in the whole domain, and pressure and amount adsorbed distributions in the porous media are considered to be initially uniform at the following conditions:

$$\begin{gathered} T_f(t=0,r,z) = T_t(t=0,r,z) = T_s(t=0,r,z) = T_i\,, \\ P(t=0,r,z) = P_c\,, \\ X(t=0,r,z) = X_o \end{gathered} \tag{5.10}$$

The HTF tube is assumed to be adiabatic at the inlet and outlet of the adsorbent bed due to the insulation. Therefore, temperature gradients along the tube at $z=0$ and $z=L$ are zero. Furthermore, once the HTF leaves the tube, its temperature remains constant in the axial direction because of the insulation. This also yields a boundary condition in which the axial temperature gradient of HTF is zero at the outlet. The adsorbent bed is also insulated at both ends in the axial direction. The heat transfer from the outer boundary to the vapor is assumed negligible due to the low pressure of the vapor, and therefore this outer boundary is modeled as being adiabatic. All these conditions can be written as follows:

$$\frac{\partial T_t}{\partial z}(t,r,z=0)=\frac{\partial T_t}{\partial z}(t,r,z=L)=\frac{\partial T_f}{\partial z}(t,r,z=L)=0,$$

$$\frac{\partial T_s}{\partial z}(t,r,z=0)=\frac{\partial T_s}{\partial z}(t,r,z=L)=\frac{\partial T_s}{\partial r}(t,r=r_{bed},z)=0 \tag{5.11}$$

At the inner radial boundary where $r = r_t$, the conduction into the adsorbent must be equal to the heat transfer by convection via HTF motion:

$$-k_s\frac{\partial T_s}{\partial r}(t,r=r_t,z)=h_c(T_t-T_s) \tag{5.12}$$

Hot HTF enters the tube from the bottom side where $z = 0$ yielding the boundary condition:

$$T_f(t,r,z=0)=T_{hot} \tag{5.13}$$

The refrigerant vapor flow inside the adsorbent is restricted at the boundaries $r = r_t$ and $z = L$ since the boundaries here are enclosed by the tube and the fin respectively. Thus the pressure gradient on these boundaries is zero:

$$\frac{\partial P}{\partial z}(t,r,z=L)=\frac{\partial P}{\partial r}(t,r=r_t,z)=0 \tag{5.14}$$

On the other hand, the other boundaries of the adsorbent bed where $r = r_o$ or $z = 0$ are open to the vapor flowing inside the vacuum chamber and therefore the vapor at these boundaries is at the condenser pressure:

$$P(t,r,z=0)=P(t,r=r_{bed},z)=P_c \tag{5.15}$$

Base parameters used in simulations are listed in Table 5.1.

Table 5.1 Base parameters used in simulations [2,101].

Parameter	Value	Unit
c_f	1930	J/kg K
$c_{p,l}$	4180	J/kg K
$c_{p,v}$	1880	J/kg K
c_s	837	J/kg K
c_t	385	J/kg K
D_o	5.8e-9	m^2/s
E_a	1e4	J/mol
h_c	100	W/m^2 K
k_f	0.115	W/m K
k_t	400	W/m K
P_c	4.247	kPa
R	8314	J/mol K
R_v	461.5	J/kg K
r_p	1e-3	M
T_{hot}	473	K
T_i	313	K
X_o	0.261	kg_w/kg_s
ΔH	3300	kj/kg
ε	0.635	
κ	3.4e-9	m^2
μ	1e-5	kg/m s
ρ_f	914	kg/m^3
ρ_s	1000	kg/m^3
ρ_t	8700	kg/m^3
b	0.001	m
L	0.5	m
r_t	0.013	m
d	0.01	m

5.4 Results And Discussion

The coupled heat and mass transfer analysis of the model has been made time dependently using Comsol Multiphysics. The governing equations are adapted to Comsol using three different modules. The heat transfer module for energy balances, the chemical engineering module for mass balances, and the PDE (partial differential equation) module for the LDF model are used. The geometry is meshed by using an extremely fine mesh property having 40,000-50,000 elements in simulations. The shape of the mesh is triangular. The solver parameter has a relative tolerance of 0.01 and an absolute tolerance 0.001 with a high accuracy and convergence.

The effects of adsorbent thermal conductivity, HTF velocity and adsorbent bed thickness on the dependent variables temperature, pressure and amount adsorbent are investigated for the desorption process of the thermal wave cycle. It should be noted that the thermal conductivity mentioned herein refers to effective thermal conductivity that includes the porosity effect. In reality the thermal conductivity of the adsorbent will vary during the process due to variations in temperature and amount adsorbed distributions. However, as a first approximation variations in the adsorbent's thermal conductivity are neglected and the adsorbent's thermal conductivity is assumed constant. Additionally, in reality the convective heat transfer coefficient will vary with HTF velocity, but as a first approximation the convective heat transfer coefficient is assumed constant in the investigation of the effect of HTF velocity.

5.4.1 The Effect of Thermal Conductivity of Adsorbent Material

Fig. 5.3 shows the effect of thermal conductivity of the adsorbent material on the temperature across the whole domain. Time increases rightward while thermal conductivity increases downward. Three values of the thermal conductivity, i.e. 0.2, 1 and 5 W/(mK), are examined. The HTF velocity and the bed thickness are taken as 0.001 m/s and 0.013 m, respectively. Time increases up to t=1000 s since the bed reaches a uniform temperature at the maximum cycle temperature (473 K) at or before that time. The right column of plots in Fig. 5.3 represents the temperature variation inside the bed at the instant when the HTF temperature reaches T=385 K at the tube outlet. The representation of the temperature distribution at this certain outlet temperature is useful for understanding how the heat coming from the HTF is transferred in radial and axial directions. For a thermal wave adsorption cooling cycle, the HTF outlet temperature is used to reverse the flow direction of HTF and it is desired to have a temperature as low/high as possible for regeneration between desorbing/adsorbing beds.

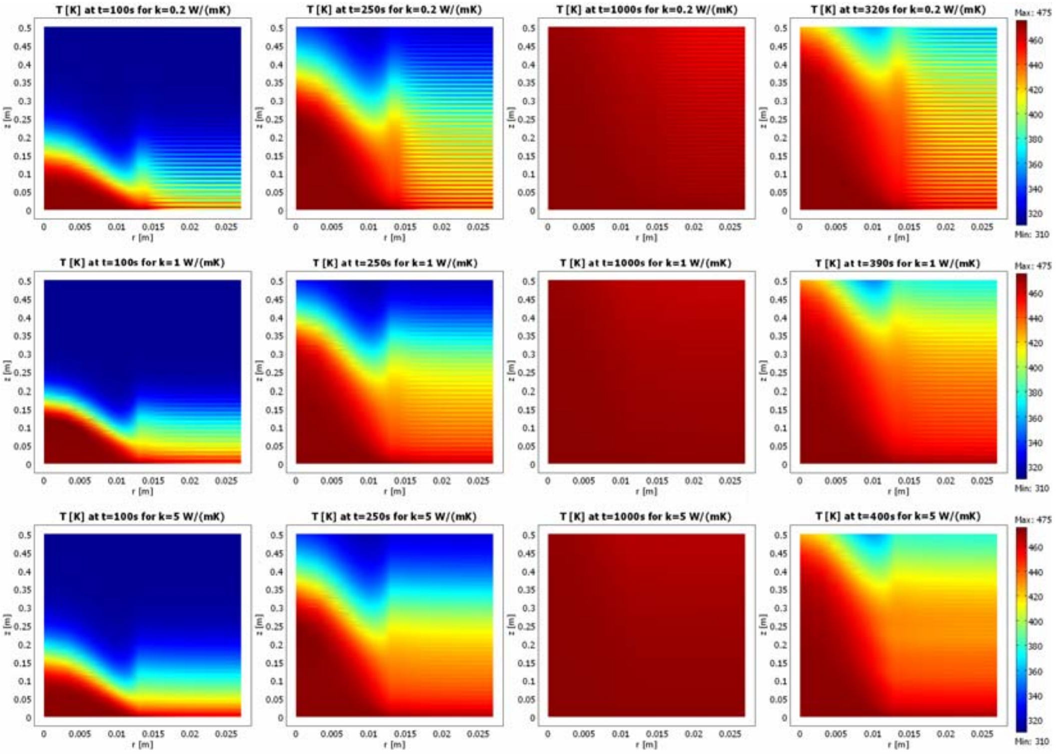

Fig. 5.3 The effects of time and thermal conductivity of the adsorbent material on temperature. $0 < z < 0.013$ m for HTF; $0.013 < z < 0.014$ m for tube; $z > 0.014$ m for absorbent and fins. Thermal conductivity increases for plots moving from top to bottom. Time increases for plots moving from left to right for the first 3 columns. The right column is the instant in time when the HTF temperature reaches T=385 K at the tube outlet.

An ideal thermal wave bed has no radial temperature gradients (radially isothermal) and very steep axial temperature gradients. The bed with the low thermal conductivity k = 0.2 W/(mK) has the worst heat transfer inside the adsorbent material as expected. Heat is primarily transferred to the tube and fins and the temperature front (or thermal wave) cannot progress rapidly in the axial direction. There is a larger temperature gradient in the radial direction than in the axial direction. On the other hand, for the moderate thermal conductivity k = 1 W/(mK), temperature gradients decrease in radial direction and the axial temperature front progresses more straightly. However, there is still a significant temperature difference between the fins and adsorbent material in the axial direction. The difference can obviously be seen by the horizontal hot lines formed on the fins. The appearance of these hot lines gradually decreases for the high thermal conductivity k = 5 W/(mK). The effect of variations in thermal conductivity is not significant for values higher than k = 5 W/(mK). It can be conluded that the thermal conductivity of the adsorbent material influences heat transfer significantly until the value 1 W/(mK). Low thermal conductivity of adsorbent materials is one of the major reasons for poor heat transfer inside the bed. Several studies have been made to increase the thermal conductivity of the adsorbent material, but a value over 15 W/(mK) could be rarely reached [84].

Pressure gradients are analyzed and the maximum pressure difference in the bed is 100 Pa (or approximately 2%) throughout the process. The pressure gradients are caused by the mass transfer resistances in the adsorbent bed. The gradient starts to increase with the sudden increase in the velocity of vapor desorbed from the bed. After peaking, the pressure gradient decreases and finally returns to the initial pressure P_c. Within the context of this work these pressure gradients are not significant and for brevity more detailed results for pressure distribution are not given.

Fig. 5.4 shows the effect of the thermal conductivity of adsorbent material on the amount adsorbed by the adsorbent. The amount adsorbed is a function of temperature, pressure and particle diameter of the adsorbent. Considering that the pressure is almost uniform, for a fixed particle diameter the variation of the amount adsorbed behaves in a manner parallel to temperature. This similarity can be seen by comparing Fig. 5.4 with Fig. 5.3. For the values of thermal conductivity 1 and 5 W/(mK), the waves of amount adsorbed which can also be defined as isochromatics are straighter relative to that for 0.2 W/(mK) thermal conductivity as in the case of the temperature fronts (isotherms) in Fig. 5.3.

The amount adsorbed varies between the maximum amount adsorbed, 0.261 kg_w/kg_s, and 0.036 kg_w/kg_s. The amount adsorbed decreases with time since the desorption process is simulated during which the adsorbate is desorbed and removed from the bed being heated. A uniform amount adsorbed distribution in the bed is obtained at or before t=1000

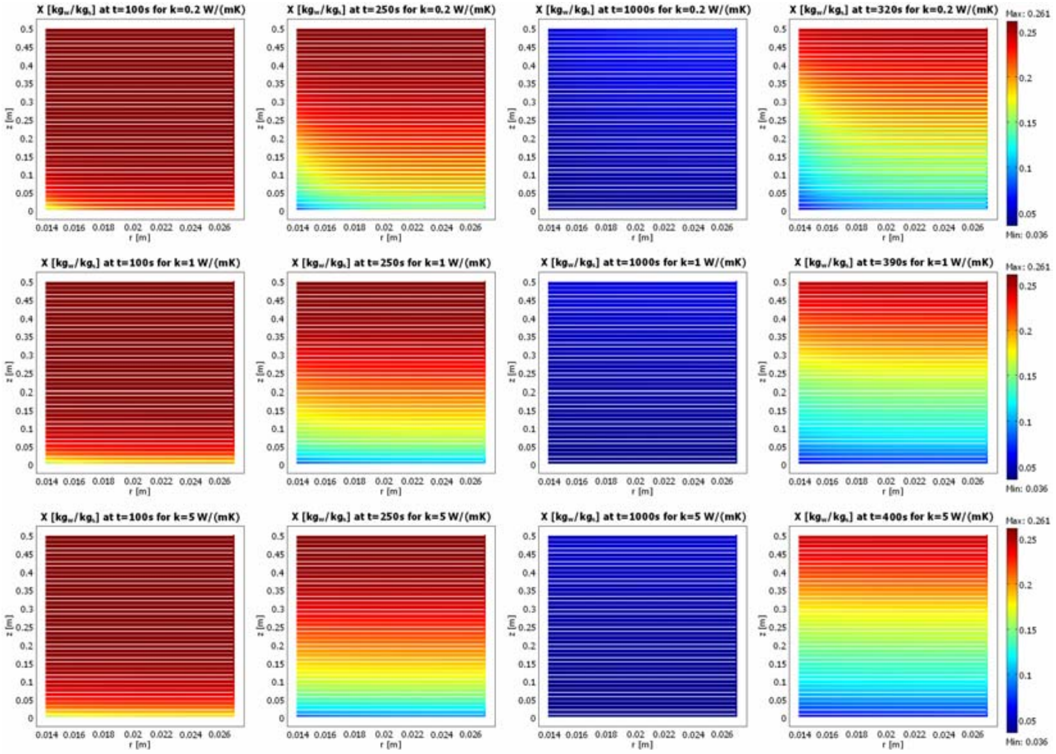

Fig. 5.4 The effect of time and thermal conductivity of the adsorbent material on amount adsorbed in the absorbent material subdomain ($z > 0.014$ m). Thermal conductivity increases for plots moving from top to bottom. Time increases for plots moving from left to right for the first 3 columns. The right column is the instant in time when the HTF temperature reaches T=385 K at the tube outlet.

s for the lowest thermal conductivity value. Cycle half-times can be considered less than 1000 s in this respect.

In Fig. 5.3 and Fig. 5.4, the right columns of plots show the distributions at the time when HTF exits the tube at the reversing temperature, 385 K. For low thermal conductivity, when the HTF reaches the reversing temperature relatively little heating of the bed and desorption has occurred. This causes lower heat regeneration between the beds of the thermal wave cycle resulting in lower performance. For higher thermal conductivities, it takes more time for the HTF to reach the reversing temperature since the HTF transfers more heat to the adsorbent, and thus the HTF is cooled while the adsorbent is heated. At the HTF reversing condition the amount desorbed for the high conductivity case is also more than that in the low conductivity case due to enhanced heat transfer. On the other hand, there are no significant differences in temperature and amount adsorbent distributions between thermal conductivities of 1 and 5 W/(mK). Therefore, it can be concluded that the temperature and amount adsorbent distributions are less sensitive to the thermal conductivity for values higher than 1 W/(mK) for the conditions explored.

5.4.2 The Effect of HTF Velocity

The velocity of the HTF is very critical for a two-bed thermal wave cycle regenerating the heat from one bed to the other bed. In fact, the strong dependence of dependent variables T and X on the velocity is confirmed after simulations. The simulations were performed assuming a thermal conductivity of the adsorbent and the adsorbent bed thickness as 5 W/(mK) and 0.013 m, respectively. The simulations indicate that for the geometry specified and for a thermal wave progressing at the same temperature as the HTF mean temperature, the HTF velocity should be extremely slow and in the range of 0.001-0.005 m/s. Otherwise, the outlet temperature of the HTF reaches the temperature at which the HTF enters the heat transfer tube before transferring significant heat to the adsorbent. In this case, more cooling energy is needed to decrease the HTF temperature to the cycle minimum temperature that is the temperature of the HTF entering the other bed being cooled. Consequently, the effectiveness of regeneration and hence the performance of thermal wave cycle decreases drastically.

For relatively high velocities of 0.01 and 0.05 m/s the failure in heat transfer can be seen in Fig. 5.5. The outlet temperature of the HTF reaches its inlet temperature of 385 K in times of just t = 36 s and t = 7 s for the velocities v=0.01 m/s and v=0.05 m/s respectively, but the temperature of the adsorbent and fins do not increase significantly. High velocities give rise to the adsorbent to be heated nearly uniformly by the HTF with a spatially uniform temperature like a reservoir. However, this is not the desired case for thermal regeneration that needs HTF outlet temperatures as low as possible for the adsorbent bed undergoing a desorption process. In the other bed undergoing an adsorption process, in a similar manner, temperatures as high as possible are needed at the outlet for reduced heating energy requirements. As a result, the velocity of the HTF is the most important parameter for the thermal wave behavior and should be low to achieve better heat transfer and performance, but this also increases cycle times and decreases specific cooling power.

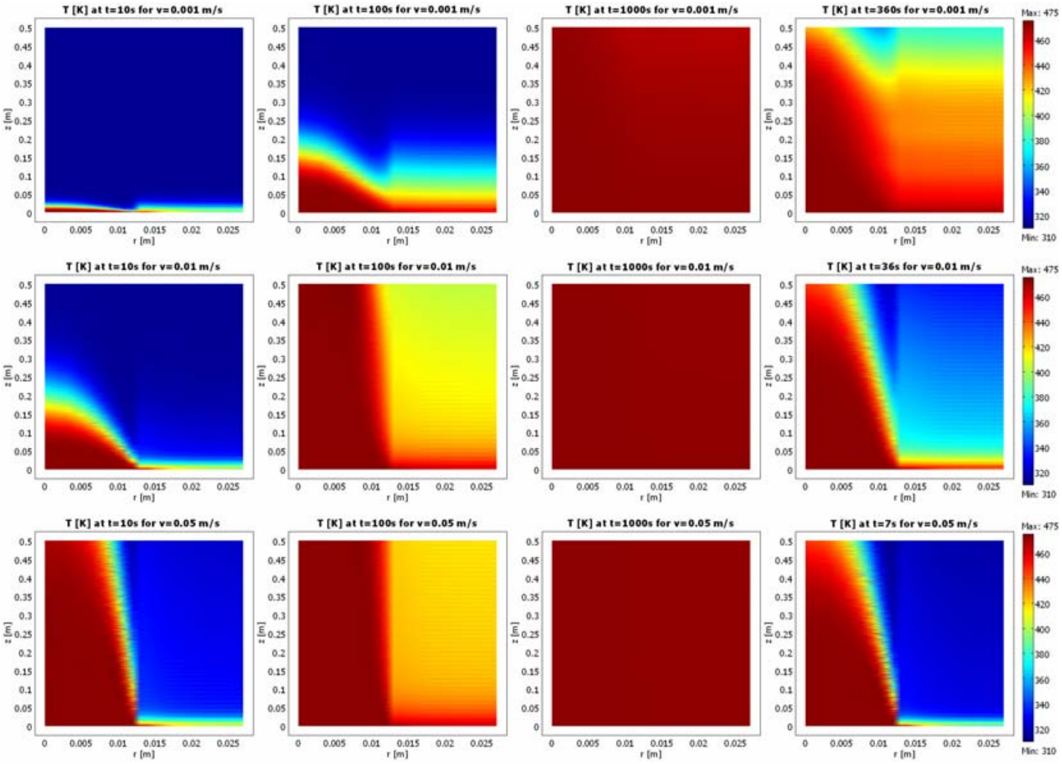

Fig. 5.5 The effects of time and HTF velocity on temperature. $0 < z < 0.013$ m for HTF; $0.013 < z < 0.014$ m for tube; $z > 0.014$ m for absorbent and fins. HTF velocity increases for plots moving from top to bottom. Time increases for plots moving from left to right for the first 3 columns. The right column is the instant in time when the HTF temperature reaches T=385 K at the tube outlet.

The variation of amount adsorbed with three different HTF velocities is shown in Fig. 5.6. The problems regarding the poor heat transfer and high HTF outlet temperature can be mentioned again for the amount adsorbed profile as in the temperature profile in Fig. 5.5. In the first column of plots in Fig. 5.6, no adsorbate is desorbed at time t=10 s for all three velocities. At that time, the HTF has not sufficiently progressed yet to heat the adsorbent for the low velocity v=0.001 m/s. For the other velocities 0.01 and 0.05 m/s, the HTF has quickly passed through the heat transfer tube without heating the adsorbent significantly. As time progresses, the adsorbate is desorbed uniformly in the whole domain by a uniform temperature distribution for these two velocities. On the other hand, significant desorption does not appear when the HTF outlet temperature reaches 385 K for the high velocities while desorption occurs gradually for the low velocity.

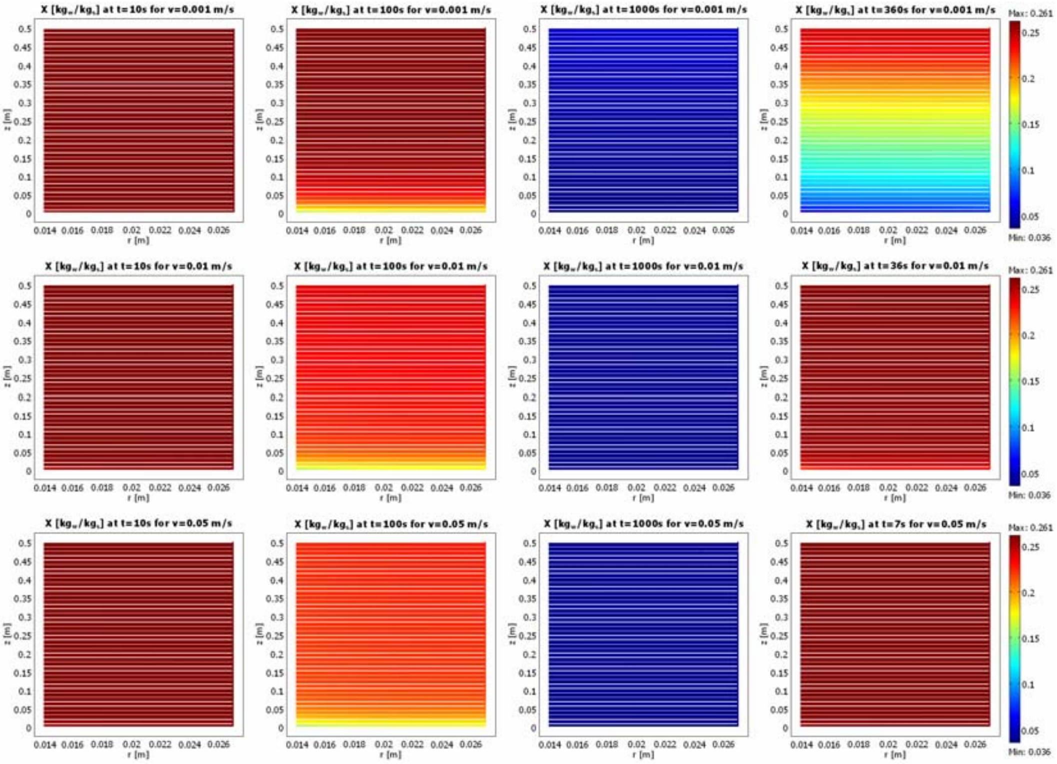

Fig. 5.6 The effects of time and HTF velocity on amount adsorbed in the absorbent material subdomain ($z > 0.014$ m). HTF velocity increases for plots moving from top to bottom. Time increases for plots moving from left to right for the first 3 columns. The right column is the instant in time when the HTF temperature reaches T=385 K at the tube outlet.

5.4.3 The Effect of Adsorbent Bed Thickness

The thickness of adsorbent bed is another important parameter that influences the dependent variables T and X. The thickness of adsorbent material and fin length are changed as the tube radius is kept constant. The thermal conductivity of the adsorbent is taken as 5 W/(mK). The effect of the adsorbent thickness on temperature is presented in Fig. 5.7. The thicknesses 0.0075, 0.013 and 0.02 m are examined. The thermal conductivity of the adsorbent and the HTF velocity are taken as 5 W/(mK) and 0.001 m/s, respectively. The distributions for both the temperature and amount adsorbed are shown from r = 0 to r = 0.027 m for comparison. Heat transfer is enhanced when the bed thickness decreases. This is due to the decrease in thermal resistances inside the adsorbent bed and the decrease in the volume to be heated (i.e. the heating load). Therefore, the extension of the adsorbent bed thickness is restricted by the requirement of enhanced heat transfer such that the temperature front in the porous media progresses along the axial direction at approximately the same temperature as the HTF. This condition is satisfied in the case that the adsorbent bed thickness is equal to at most the HTF tube radius, i.e. (r_{bed}-r_t) = r_t. Adsorbent bed thicknesses larger than the inner heat transfer fluid tube radius cause hysteresis in the temperature front progressing with the heat transfer fluid.

In Fig. 5.7, another interesting point is that the temperature distribution along the radial direction is nearly uniform even for the greatest thickness (r_{bed} - r_t) = 0.02 m. The temperature fronts, in other words the isotherms, are sufficiently straight for a thermal wave cycle. The times for the HTF to reach the reversing temperature at the outlet change expectedly for each bed thickness depending on the volumes to be heated.

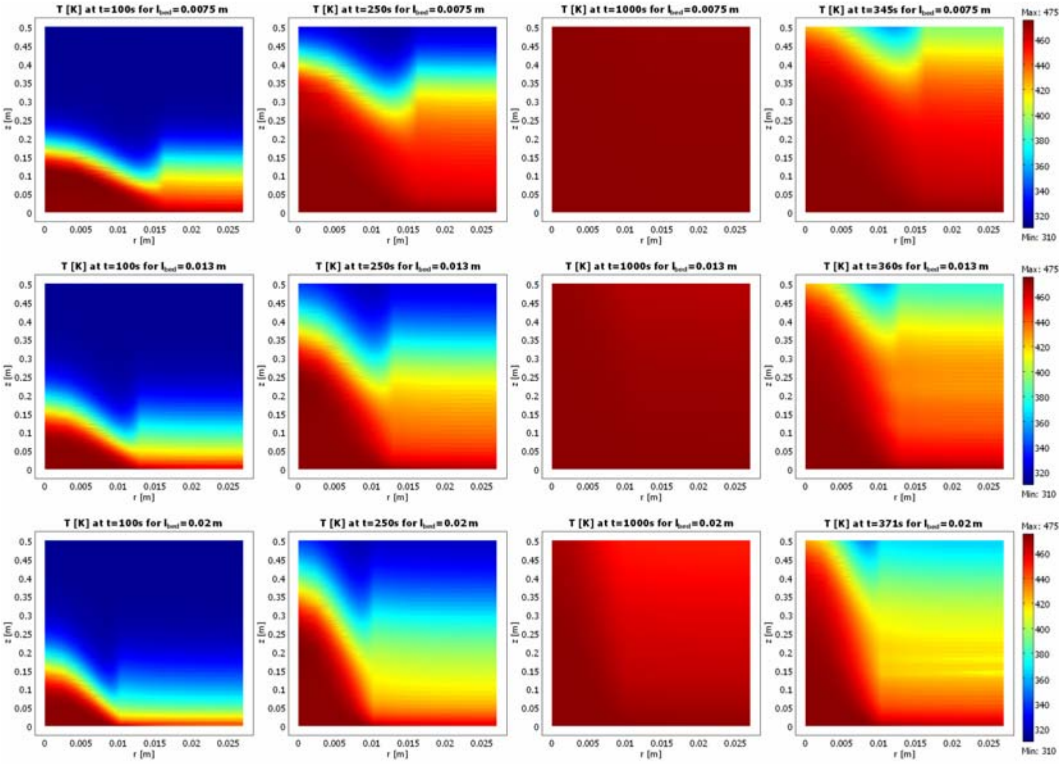

Fig. 5.7 The effects of time and adsorbent bed thickness on temperature. 0 < z < 0.013 m for HTF; 0.013 < z < 0.014 m for tube; z > 0.014 m for absorbent and fins. Adsorbent bed thickness increases for plots moving from top to bottom. Time increases for plots moving from left to right for the first 3 columns. The right column is the instant in time when the HTF temperature reaches T=385 K at the tube outlet.

A thin adsorbent layer with a large-diameter tube may be considered to be useful and effective in terms of heat transfer and cycle COP. However, acceptable cooling capacity or specific cooling power can only be obtained only if a sufficient amount of adsorbent material is used. The more adsorbent, the more adsorption and the more cooling can be obtained. On the other hand, the thickness limitation, (r_{bed} - r_t) = r_t, is valid for the HTF velocity selected. One can obtain a different relation between the bed thickness and tube radius when a different HTF velocity is used. The adsorbent bed thickness should be thinner as the HTF velocity increases and vice versa. The variation of amount adsorbed with time for different adsorbent bed thicknesses is shown in Fig. 5.8. As parallel to the temperature distribution, more desorption is generated for the thinner adsorbent bed. For the bed thickness 0.02 m, even after the time t=1000s the amount adsorbed has not completely decreased to the cycle minimum level of 0.036 kg_w/kg_s.

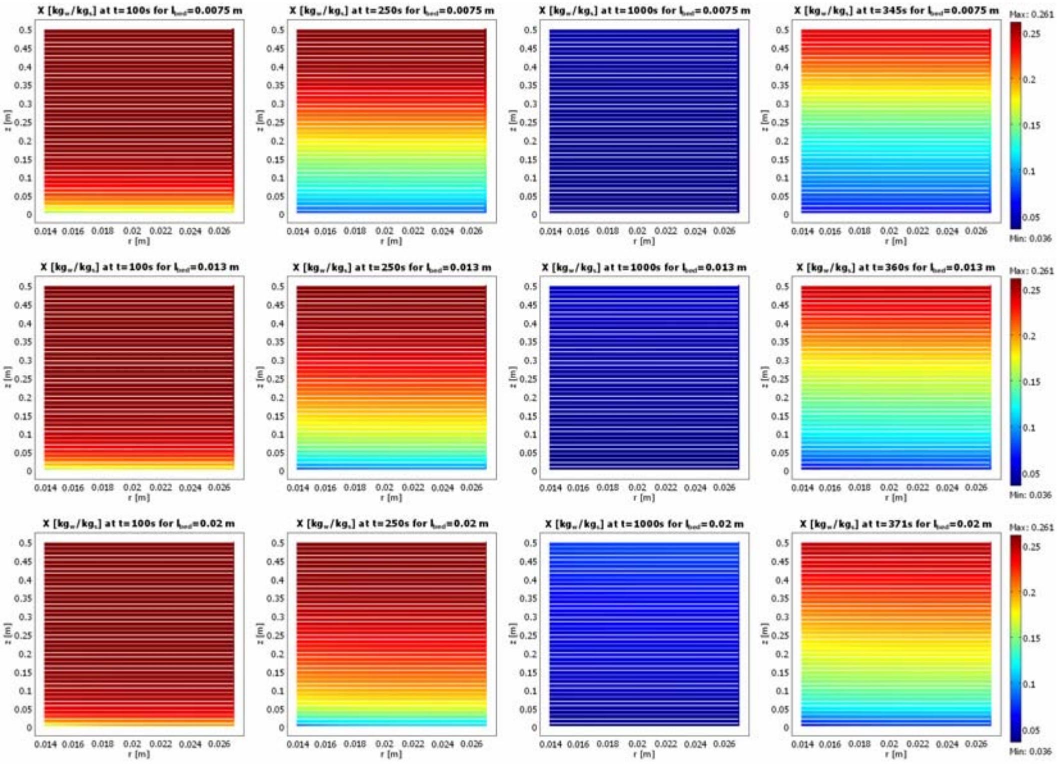

Fig. 5.8 The effects of time and adsorbent bed thickness on amount adsorbed in the absorbent material subdomain (z > 0.014 m). Adsorbent bed thickness increases for plots moving from top to bottom. Time increases for plots moving from left to right for the first 3 columns. The right column is the instant in time when the HTF temperature reaches T=385 K at the tube outlet.

CHAPTER 6

EXPERIMENTAL INVESTIGATION

In this chapter, the construction of the experimental setup and experiments are explained in detail. The experimental study covers the measurement of thermophysical properties of the adsorbent material, the explanation of the components of the experimental setup manufactured, the measurement devices used during the experiments, the experimental results and discussion.

6.1 Measurement of the Thermophysical Properties of the Adsorbent Material

Thermal analyses are made for determining the thermophysical properties. The thermal conductivity, specific heat capacity and density of the adsorbent material are measured in order to investigate the heat transfer inside the bed.

6.1.1 Thermal Conductivity Experiments

The thermal conductivity of adsorbent materials varies with the molecular structure, chemical compound, packed bed density and temperature of the material. Adsorbent materials have generally low thermal conductivity values. Heat transfer inside the bed is therefore poor. To overcome this problem in this study, the thermal conductivity of the adsorbent material is increased by adding copper chips or pieces into the adsorbent as well as designing a finned tube adsorbent bed to increase the heat transfer in the radial direction. The adsorbent material and copper chips are homogenously mixed in different proportions and the thermal conductivity of the mixture is measured experimentally for each mixture.

The thermal conductivity experiments were first planned to be made in METU Central Laboratory at the beginning of the experimental study. Unfortunately, the thermal conductivity of porous materials cannot be measured properly in this laboratory because of lack of experimental setup for this purpose. Therefore, an experimental setup has been established with the use of existing facilities in the Department of Mechanical Engineering in METU to measure the thermal conductivity of adsorbent materials to be used in the experiments. The picture of the experimental setup is given in Figure 6.1.

Figure 6.1 Transient hot-wire thermal conductivity measurement system.

The thermal conductivity of porous materials can be measured by two methods: steady state or transient methods. The steady state methods require measurements of temperature gradient and heat flux. On the other hand, the transient methods require a temperature change as a function of time at a known distance from the heat sink or heat source [150]. The measurement of thermal conductivity in steady state condition is relatively simple and easy to compute. However, the measurement time is quite lengthy due to the need to wait for steady state conditions. In transient analysis, the measurement time is relatively short although the computation of thermal conductivity is more complicated. The experimental setup presented in Figure 6.1 is a transient-method thermal conductivity measuring device and is especially established for measuring the thermal conductivity of porous materials and their mixtures with metallic pieces.

In the transient analysis, thermal diffusivity and specific heat of the adsorbent material as well as the thermal conductivity can be calculated. In the transient hot-wire measurement system, a resistance wire is horizontally placed in the middle of a Plexiglas container with inside dimensions of 14x14 cm by 30 cm in length. The container is filled with the adsorbent material. A low voltage is supplied to the resistance wire by a DC power source. Two thermocouples are placed in the porous media as parallel to the resistance wire at two different distances from the wire. Temperature gradient with time can be measured by these thermocouples. Variation of temperature with time is plotted on a semi logarithmic graph. The parabolic curve obtained from this plot is used for determining the coefficients of transient heat conduction equation applied to the system. The coefficients are function of the properties, thermal conductivity, thermal diffusivity and specific heat and hence these properties can be calculated by the coefficients.

A series of test are performed with the transient-method experimental setup described above in order to measure the thermal conductivity. However, results obtained showed that the experimental setup did not work properly. The thermal conductivity values obtained from the experiments were much larger than the values found in the literature. It was concluded that there were some faults in either the experimental setup or mathematical model of the transient analysis. Therefore, the measurement of the thermal conductivity with the steady state method is considered to give more reliable and stable results. For this reason, new experiments in steady state conditions were made using the steady state method experimental setup that was constructed in a previous TÜBİTAK Project (Project No: 105M244) [151]. A picture from this setup is given in Figure 6.2. In this setup, a 130 mm resistance rod in length is placed in the middle of a glass tube with outer diameter of 44 mm and inner diameter of 40.7 mm. The glass tube is insulated from both ends such that heat loss from both sides in axial direction can be neglected. Inside the glass tube is filled with the adsorbent material. Two thermocouples are placed at the following locations: one is placed on the resistance rod; the other one is placed on the middle point between the inner surface of the glass tube and the outer surface of the resistance rod.

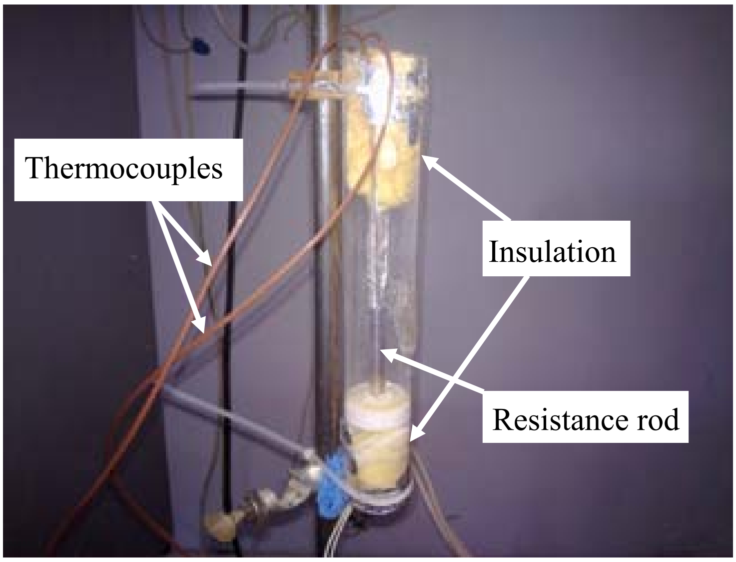

Figure 6.2 Steady state method thermal conductivity test facility.

A constant power is supplied to the resistance rod by using a variac and heat is transferred through the adsorbent material. It is considered that all the electrical power supplied to the rod is converted to heat. This amount of energy is adjusted by the variac in unit of Watt. Two voltmeters are also used to measure the voltage and current. The heat transfer can then be calculated as follows

$$Q = P = VI \tag{6.1}$$

Using the power and the temperatures measured by the thermocouples, the thermal conductivity can be calculated by Fourier's law of heat conduction as follows

$$Q = -kA\frac{dT}{dr} \tag{6.2}$$

In above equation, *q, k, T* and *r* represent the amount of heat transfer (W), thermal conductivity (W/(mK)), temperature (K) and radius (m), respectively.

After the construction of setup was completed, first the thermal conductivity of pure zeolite was measured. To increase the thermal conductivity of the zeolite, electrolytic pure copper rod that has the maximum thermal conductivity in the market was purchased. The copper rod was cut into small pieces to obtain a sufficient amount of copper chips. In two different proportions, 16.6% and 25.1%, copper chips were added to the zeolite and they were mixed homogenously. Effective thermal conductivity of the mixtures was then measured. Furthermore, thin copper wire with 0.5 mm diameter was bought from OSTİM industrial district and this wire was cut in short sizes such that the pieces can be placed in the glass tube in the radial direction. The pieces were placed in the tube with 1 cm distances in the axial direction. 7 pieces are placed at each step in the radial direction. The effective thermal conductivity of the mixture was measured and the effect of copper wires on the thermal conductivity was investigated. All these results obtained from the pure zeolite and the other three mixtures are given in Table 6.1.

Table 6.1 Data for thermal conductivity measurement of the adsorbent.

Material	Data number	T_{resist} (^oC)	T_{ads} (^oC)	I (A)	V (V)	P (W)	k (W/(mK))
Pure zeolite	1	47.4	36.9	0.08	10	0.8	0.137
	2	133	75.2	0.25	26.9	6.7	0.210
	3	172.4	95.7	0.3	32.5	9.8	0.229
	4	248.5	138.2	0.38	40.6	15.4	0.252
	5	340	176.1	0.47	50.4	23.7	0.260
16.6% Copper chips	1	57	46.3	0.13	13.8	1.8	0.302
	2	99.9	74	0.21	22.6	4.7	0.330
	3	167.6	115.6	0.31	32.9	10.2	0.354
	4	249.6	169.7	0.39	41.6	16.2	0.366
25.1% Copper chips	1	60	50.2	0.13	14.1	1.8	0.337
	2	105.2	79	0.22	23.5	5.2	0.356
	3	172.1	125.7	0.3	32.5	9.8	0.379
	4	245.3	170.3	0.39	41.3	16.1	0.387
Copper wires	1	57	43.2	0.13	13.9	1.8	0.236
	2	100.8	67.7	0.21	23.2	4.9	0.265
	3	173.3	108.7	0.31	33.8	10.5	0.292
	4	249.6	147.3	0.4	43.2	17.3	0.304

The variation of thermal conductivity with temperature is also shown in Figure 6.3 using the data given the table above. As seen from Figure 6.3, the mixture of 25.1% copper chips and 74.9% zeolite has the highest thermal conductivity among all samples. This result shows that copper chips have a significant effect on the enhancement of the thermal conduction inside the adsorbent bed which improves the bed performance. This composition is used as adsorbent material in the adsorption/desorption experiments due to its highest thermal conductivity.

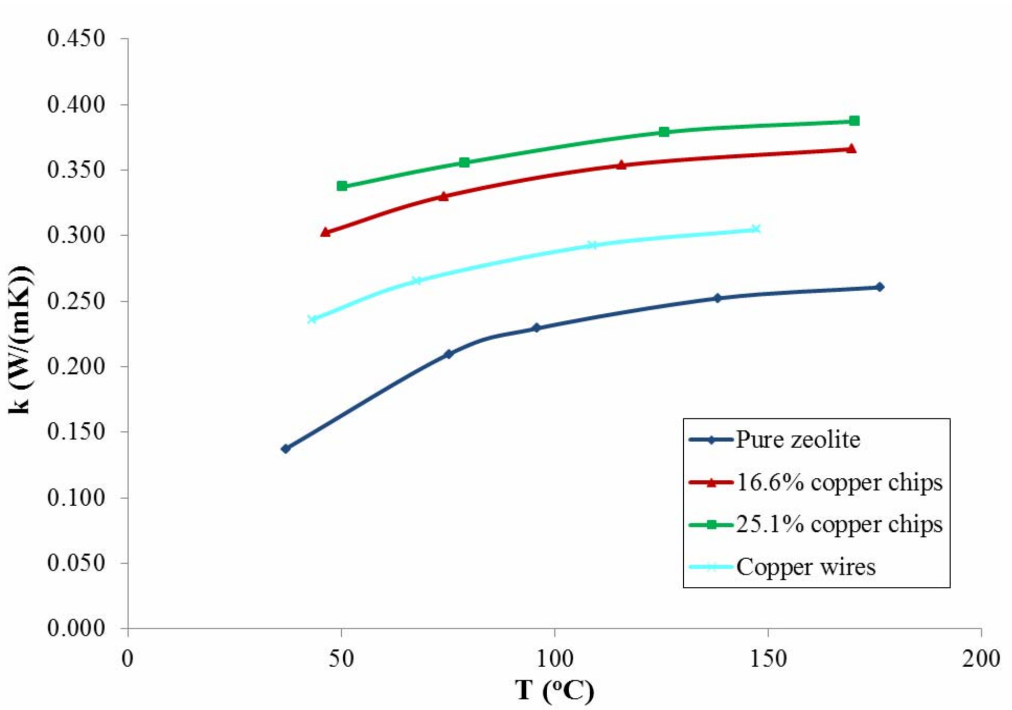

Figure 6.3 Variation of thermal conductivity of copper-zeolite mixtures with temperature.

6.1.2 Specific Heat Capacity Analysis

A heat capacity analysis is performed to measure the specific heat of the adsorbent material, zeolite. This thermal analysis was made in METU Central Laboratory due to the lack of test facility in the department of mechanical engineering for this purpose. Specific heat measurement tests were made by DSC (Differential Scanning Calorimetry) test method in the temperature range of 0-200 °C. The tests were performed for two samples:

pure zeolite and the mixture of 25.1% copper chips and 74.9% zeolite. Test results are presented in Figure 6.4. The results show that the specific heat capacity of the mixture of 25.1% copper chips and 74.9% zeolite is 774 J/(kg^{o}C) and the specific heat capacity of the pure zeolite is 1202 J/(kg^{o}C). The decrease in the specific heat of the mixture relative to that of the pure zeolite is due to lower heat capacity of copper (385 J/(kg^{o}C)).

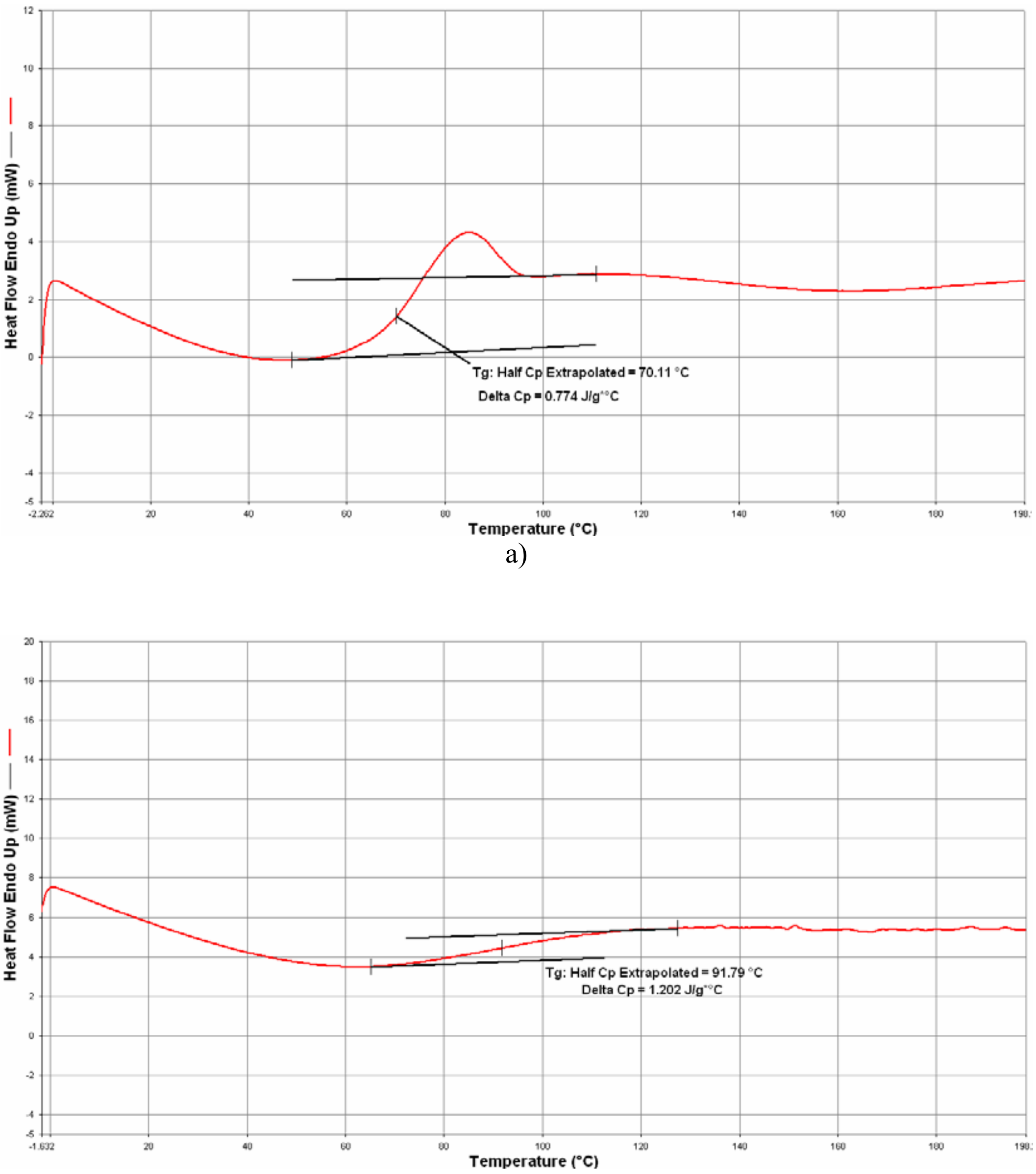

a)

b)

Figure 6.4 DSC heat capacity test results: a) 25.1% copper chips-74.9% zeolite mixture; b) pure zeolite.

6.1.3 Density Measurements

Before the density measurements, zeolite was washed with deionized water and dried first in the atmospheric conditions and then in an oven at a temperature of 200 ^{o}C. Dry zeolite was finally screened by a metallic sieve. The reason for this process is that the dry zeolite is packed in the adsorbent bed and used at the beginning of the experiments. After the washing, drying and screening processes, the density of pure zeolite and the mixture of copper chips-zeolite were measured by using a precision scale and a container with a known volume. The results show that the density of the pure zeolite and the mixture are 747 kg/m^3 and 1158 kg/m^3, respectively. The detailed information and data for the density measurements can be found in [151].

6.2 Experimental Setup and Components of the Thermal Wave Cycle

The experimental setup of the thermal wave adsorption cooling system consists of two main flow lines: refrigerant vapor line and oil line. The refrigerant vapor line operates under vacuum. There are four main components in the vacuum line. They can be listed as follows:

1. Condenser
2. Expansion valve and capillary tube
3. Evaporator
4. Adsorbent bed

On the other hand, main components used in the oil line are oil heater, oil cooler, hot and cold storage tanks and circulating pump. Each of these main components is described in detail below.

6.2.1 Adsorbent Bed

The most important part of the adsorption refrigeration systems is the adsorbent bed. Adsorption and desorption processes occur in the adsorbent bed. Adsorption and desorption processes take place sequentially and the cycle is repeated at intervals of cycle time. During the adsorption process, steam coming from the evaporator is adsorbed by the adsorbent material. The bed is initially hot and should be cooled by a fluid in the adsorption process. During the desorption process, the vapor desorbed from the adsorbent flows to the condenser and then the water liquefied is sent to the evaporator. At the beginning of the desorption process, the bed is cold and should be heated by hot fluid such as heat transfer oil. The adsorbent bed consists of two parts: one is the vacuum chamber made of stainless steel and the other is a finned tube through which the HTF passes.

6.2.1.1 Construction of the Vacuum Chamber

The vacuum chamber was designed by taking all the requirements into account and the manufacturing is made by Vaksis Company. It was professionally manufactured and tested for vacuum leaks by the company. Vacuum leaks became a big problem in the previous project and it took long time to solve the sealing problem. Vaksis firm is specialized and expert on manufacturing vacuum systems. The vacuum chamber is made of stainless steel material so that dust-free environment can be achieved at high temperature and hard operation conditions. The technical drawing of the vacuum chamber and views after construction are shown in Figures 6.5 and 6.6, respectively.

There are flanges on both sides of the vacuum chamber. The bottom flange was welded in order to reduce the risk of vacuum leaks. On the top flange, there are totally four ports: two ports for thermocouple feedthroughs and two for HTF tube inlet and exit. Viton o-ring was used for vacuum tightness between the top flange and main body. The top flange was connected to the main body with four clamps. At the bottom side of the vacuum chamber, there are two ports. One of these ports is used for vacuum line in which refrigerant vapor flows. A T-pipe is added to this port. One exit of the T-pipe is used to evacuate the system at the beginning of the experiments. The other port at the bottom side of the vacuum chamber is an auxiliary port.

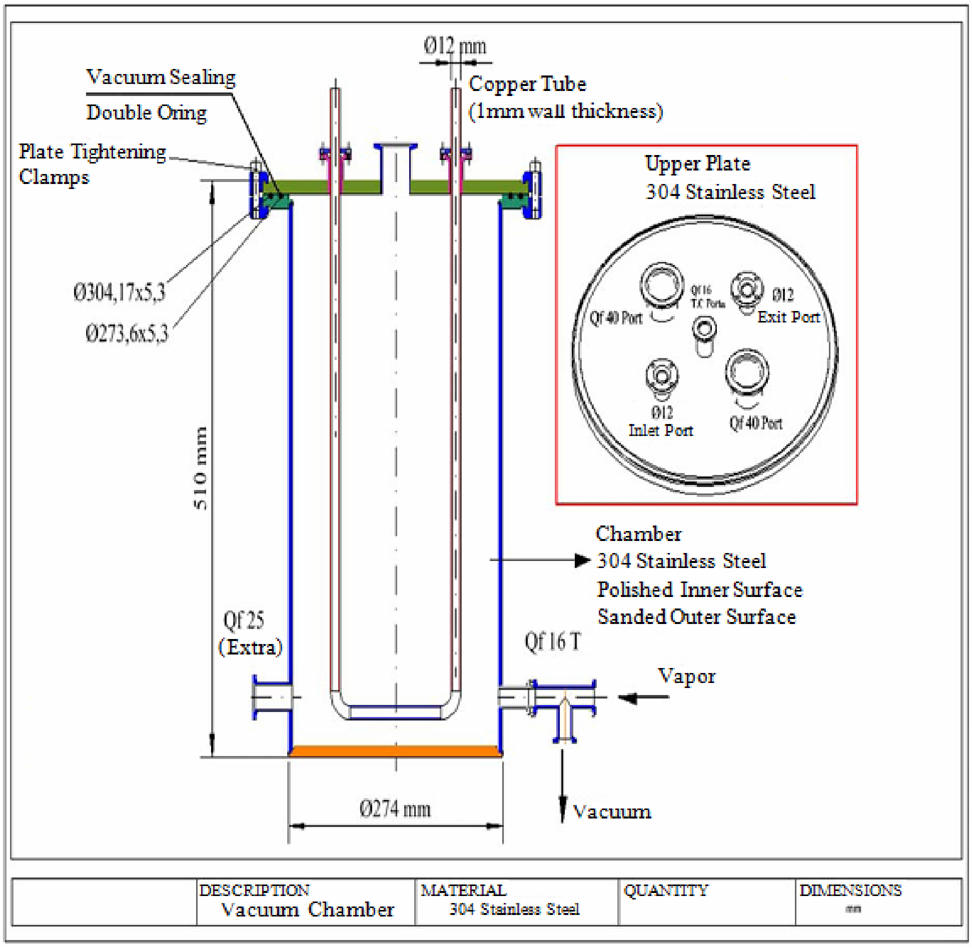

Figure 6.5 Technical drawing of the vacuum chamber.

Figure 6.6 Different views of the vacuum chamber.

6.2.1.2 Construction of the Finned Tube

A finned tube adsorbent bed was constructed and placed inside the vacuum chamber. The HTF passes inside the finned tube. Outside of the tube was filled with the adsorbent material and enclosed by a metallic net. The 3D drawing of the finned tube adsorbent bed drawn at the design stage is given in Figure 6.7. Views from the finned tube during the construction process are given in Figure 6.8.

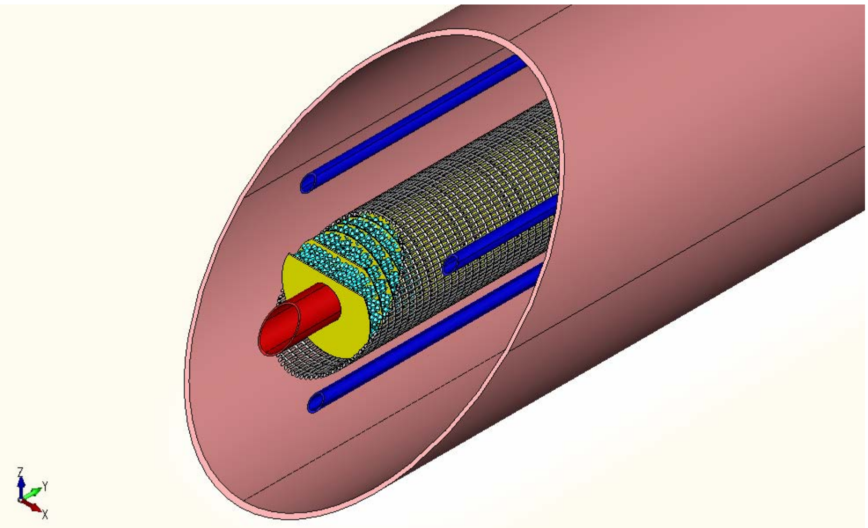

Figure 6.7 3D drawing of the finned tube adsorbent bed at the design stage.

Figure 6.8 Views of the the finned tube during construction.

The finned tube was made of copper for maximizing the heat transfer from the HTF (heat transfer fluid) to the adsorbent. Fins are used to increase the heat transfer in radial direction through the adsorbent and to obtain a more effective regeneration between the beds of the thermal wave cycle.

The finned tube has 25 mm outer diameter and 500 mm length. 25 fins were cut from 2 mm thick copper sheet so that fins had 50 mm outer diameter and 25 mm inner diameter. Fins were processed in guillotine, drilling and turning machines, respectively, in the machine shop of the Mechanical Engineering Department at METU. The fins were finally welded to the tube by oxygen welding.

The HTF tube exit as well as the tube inlet was taken out of the vacuum chamber from the top flange creating a U shape piping in the vacuum chamber. As seen in the last photo in Figure 6.8, one side of the U piping is the finned tube while the other side is a straight tube. The HTF always enters the adsorbent bed from the finned tube side and leaves the vacuum chamber from the straight tube side.

Heat transfer oil is used as HTF to cool and heat the adsorbent bed. The HTF is circulated in a closed loop passing through the oil-heater, adsorbent bed and oil-cooler, respectively. Detailed information about the HTF loop will be given in Section 6.2.5.

The adsorbent bed constructed replaces the adsorbent bed of the previous TÜBİTAK project 105M244 [151]. The adsorbent bed of the previous study was constructed for an intermittent basic adsorption cycle. Only the adsorbent bed was taken out of the previous system and the adsorbent bed newly designed and constructed for a thermal wave was mounted to the system. Other components of the system remain the same. The previous bed was not removed from the place where it was mounted, only the flexible vacuum pipes at the inlet and outlet of the bed were taken out and mounted to the new bed located on a different table near the setup. Thus, the integrity of the old system was not disrupted and the old bed can be used if required. The final appearance of the adsorbent bed mounted on the experimental setup can be seen in Figure 6.9.

It should be noted here that a single bed is used in this study although two beds at least are required in a thermal wave adsorption cooling cycle. In a thermal wave adsorption cycle with two adsorbent beds, one adsorbent bed performs adsorption process while the other bed performs desorption process. Therefore, a continuous cooling can be obtained.

Figure 6.9 View of the adsorbent bed mounted on the system.

Furthermore, heat regeneration between the beds can be made due to the nature of being a heat regenerative cycle and hence the performance of the cycle can be improved. In this study, the main purpose is to design and construct a new adsorbent bed for the thermal wave cycle and to investigate the enhancements of heat and mass transfer in this new adsorbent bed observing the distributions of temperature and amount adsorbed inside the bed. In other words, only one bed is constructed and used since one bed is sufficient to test and investigate the enhancements. The amount of heat regeneration between the beds can be calculated by using the data and results from one-bed system tests since temperature data for HTF at the inlet and outlet of the adsorbent bed is sufficient to calculate the heat regeneration.

6.2.2 Condenser

The condenser of the thermal wave cycle is used to condense the refrigerant vapor coming from the adsorbent bed during the desorption process. The liquid refrigerant water is sent to the evaporator after condensation. During the condensation, the condenser rejects heat to a temperature-controlled water storage tank which acts as a sink. The condenser is shown in Figure 6.10.

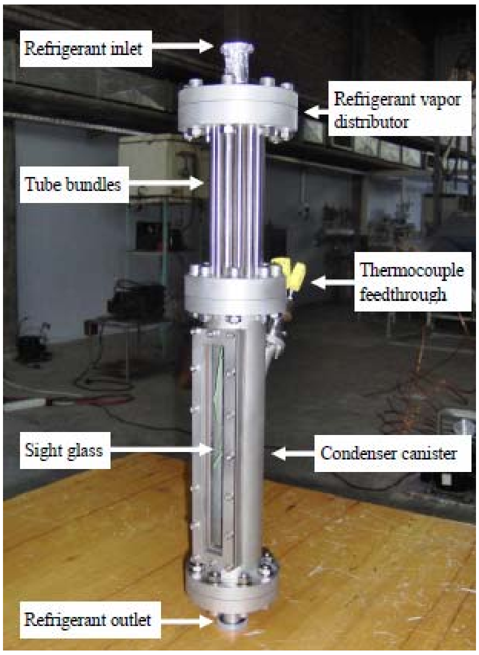

Figure 6.10 Photo of the condenser of the thermal wave cycle [133].

The condenser consists of two parts: a condenser canister and condenser tube bundle. The condenser canister (lower part of the condenser) is made of a stainless steel tube. The liquid water is accumulated in this part. A glass cover is placed on the front side of this tube in order to be able to see the change in the water level inside the condenser canister. Hence the amount of vapor desorbed by the adsorbent can be calculated during desorption. In a same manner, the amount of vapor adsorbed by the adsorbent during adsorption can be calculated. A ruler is placed near the glass cover and the volume and hence mass of the water can be determined by the level difference as well as the knowledge of tube diameter. The condenser tube bundle (upper part of the condenser) is made of a bunch of stainless steel tubes. The condensation process essentially takes place in this part. The condenser tube bundle is used to increase the heat transfer area. The condenser is placed into the water storage tank in such a way that both lower and upper parts of the condenser are submerged into the water.

As is understood from above, water is used as the condenser cooling medium instead of the surrounding air. The reason for that is to control the temperature of the cooling medium during the experiments. The temperature of the water storage tank can easily and quickly be controlled. This temperature is also known as condensation temperature. The condensation temperature is kept constant during an experiment. The experiments are performed at different condensation temperatures and the effect of the condensation temperature is hence investigated. To control the condensation temperature, a heater and cooler is mounted in the water tank. A thermocouple is also placed in the water tank. The thermocouple reads the temperature of the water and sends a signal to the digital channels of a datalogger. The digital channels turn on and off the heater and cooler receiving the signal from the temperature reading in order to keep the condenser temperature constant. When the condensation temperature is set as 'A' and if the water temperature in the tank is 'T', the heater starts to heat the water for the condition T<A and the cooler starts to cool the water for the condition T>A. Thus, the heater and cooler in order come into operation. Additionally, a circulation loop and pump are added to the water tank in order to obtain a uniform temperature distribution in the water tank. The pump is taken the water from the bottom side and pumps it to the top side of the water tank. The complete condenser system with the condenser, water tank, circulation loop, heater and cooler is shown in Figure 6.11.

Figure 6.11 Photo of the condenser unit and water tank.

6.2.3 Expansion Valve and Capillary Tube

Liquid water leaving the condenser passes through the throttle valve and capillary tubes. Thus, the pressure of the water is decreased to the evaporator pressure. The reason for using both the throttle valve and capillary tubes together is that the pressure could not be decreased to the desired pressure in case of using the throttle valve or capillary tube alone. Figure 6.12 shows the throttle valve and capillary tube mounted on the test system.

Figure 6.12 Photo of the throttle valve and capillary tube.

6.2.4 Evaporator

The evaporator is used to take heat from the space to be cooled. It enables the evaporation of liquid water with low pressure by transferring the heat taken from its surroundings to the refrigerant water inside it. The view of the evaporator is given in Figure 6.13.

The evaporator coil is a helical tube made of stainless steel. The reason for using a helical tube is to meet the cooling load of the media due to the large heat transfer area of the tube. The depressurized water enters the evaporator coil after leaving the throttle valve and capillary tube, respectively. A vacuum ball valve is added before the inlet of the evaporator in order to cut the flow when needed.

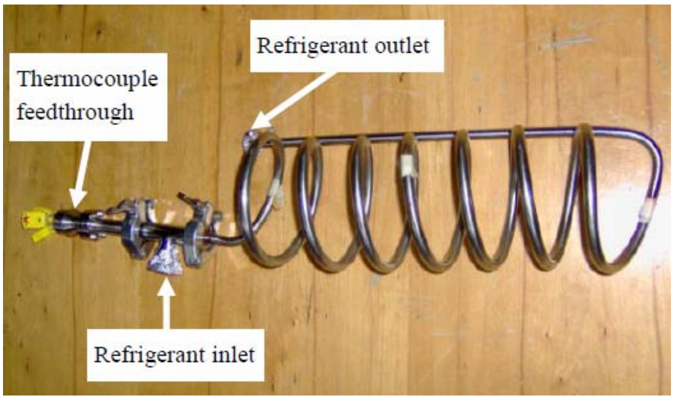

Figure 6.13 Photo of the evaporator [133].

The evaporator is placed in a tank filled with water as in the condenser. The media which is cooled is again water. But here, the amount of water in the tank and the temperature variation of water are very important to calculate the cooling power of the system. For this reason, a certain amount of water is filled into the tank and temperature variation is measured at three different points. Both condenser and evaporator tanks have been isolated from the external environment. The isolated water tank and the evaporator are shown in Figure 6.14.

Figure 6.14 Photo of the water tank and evaporator.

Further information for manufacturing details of the condenser, capillary tube and evaporator can be found in [151].

6.2.5 HTF Loop, HTF Heater and HTF Cooler

As mentioned before, during adsorption and desorption processes, the adsorbent bed is heated and cooled by the HTF passing through the HTF tube placed in the middle of the adsorbent bed. Heat transfer oil is used as the HTF. Heat transfer oil is heated by two electrical heaters and cooled by a cooling unit. According to the process taking place at that time, the heat transfer oil is circulated through one of two separate oil lines. The oil lines are different from the refrigerant vapor line. There are two separate oil storage tanks: one is for cold oil and the other is for hot oil. Two electrical heaters are placed in the hot oil tank. The temperature of the hot oil in this tank is controlled by a steady-state relay at the maximum cycle temperature that is also called the regeneration temperature. On the other hand, the evaporator of the cooling unit is placed in the cold oil tank. The temperature of the cold oil in this tank is controlled by another steady-state relay at the minimum cycle temperature. The hot and cold oil lines are joined with each other by a T-pipe before the pump of the HTF loop. The cold oil line is open during the adsorption process while the hot oil line is open during the desorption process. The hot and cold oil lines are opened and closed by using 4 valves. At the beginning of the experimental study, 4 solenoid valves were used for this purpose. However, afterwards 4 ball valves were used instead of the solenoid valves due to the limitation of number of digital channels of the datalogger that can control the devices. These ball valves were opened and closed manually according to the process performed in the cycle. The oil is circulated by the oil pump especially designed for high temperature resistance. The hot and cold oil tanks are shown in Figure 6.15.

a) Hot oil tank. b) Cold oil tank.

Figure 6.15 Photos of the heat transfer oil tanks.

6.2.6 Assembly and Final Shape of the Experimental Setup

The schematic of the experimental setup is represented in Figure 6.16. Blue line represents the vacuum line in which the refrigerant vapor flows while red line represents the heat transfer oil line. The complete view of the experimental setup is given in Figure 6.17 encompassing all elements of the system.

For the components of refrigerant vapor line that work under vacuum conditions, stainless steel vacuum pipes, vacuum ball valves and stainless steel flexible vacuum pipes are used. Connections in the vacuum line are made by Viton O-rings and clamps specially manufactured for vacuum conditions. Viton o-rings can resist high temperature (~200 ^{o}C). Sufficient numbers of ball valves are used between each component of the vacuum line in such a way that the components can be easily and independently removed from the system in the case of failure or change. Rigid vacuum pipes are used for stationary parts while flexible vacuum pipes are used for possible moving parts. Vacuum grease is applied to the Viton o-rings at the connections to obtain high vacuum sealing. Latex glove is used in the application of vacuum grease. The clamps are tightened to a certain extent.

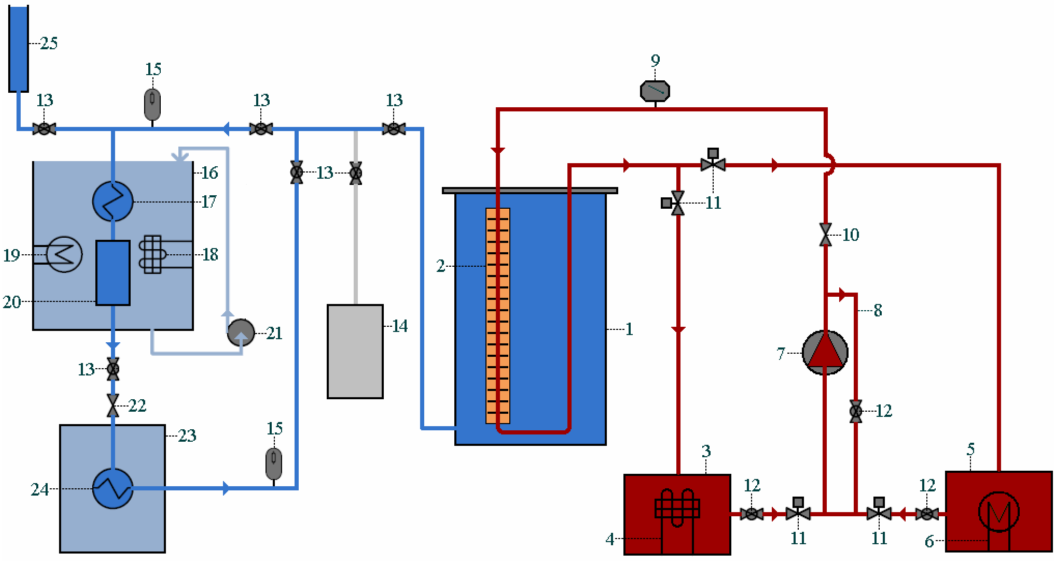

Figure 6.16 The schematic of the experimental setup (1 Vacuum chamber, 2 Adsorbent bed, 3 Cold oil tank, 4 Cooling unit (on oil line), 5 Hot oil tank, 6 Electrical heater (for oil), 7 Oil pump, 8 Bypass line, 9 Flowmeter, 10 Throttle valve (on oil line), 11 Solenoid valve, 12 Ball valve (on oil line), 13 Vacuum ball valve, 14 Vacuum pump, 15 Pressure transducer, 16 Condenser water tank, 17 Condenser, 18 Cooling unit (in condenser water tank), 19 Electrical heater (for water), 20 Water accumulation container (for water level reading), 21 Circulation pump, 22 Throttle valve (on vacuum line), 23 Evaporator water tank, 24 Evaporator, 25 Deionized water feeding tube.

The Viton o-rings and clamps are washed with alcohol before connections since rust and dirt on them cause connection failure and vacuum leaks. The system can be evacuated when the connections are properly completed. The evacuating process can be carried out by the vacuum pump shown in Figure 6.18.

After evacuating the system to a certain vacuum pressure (about 1-2 mbar), the vacuum pump is switched off and the system is observed and checked for vacuum leaks. If the vacuum pressure does not increase after a certain time (about three hours), it can be concluded that there is no vacuum leak on the system. Thus, the evacuating process is completed.

There exist additional equipments in the experimental setup in addition to the equipments mentioned above. One of these additional equipments is a large diameter (~20 cm) flexible pipe that is used for removing the oil vapor formed when the oil is heated to the

Figure 6.17 Photo of the experimental setup.

Figure 6.18 Photo of the vacuum pump.

maximum cycle temperature, i.e. 200 ^{o}C. The oil vapor has a foul odor and hazardous effect on the health and should therefore be removed from the test environment.

The second additional equipment is the glass tube that is used for taking the refrigerant of the thermal wave cycle, i.e. deionized water, into the vacuum line after evacuating process. The glass tube is mounted vertically near the experimental setup such that the glass tube remains above the level of the experimental setup. The glass tube is connected to the vacuum line from the bottom side by a flexible pipe adding a vacuum ball valve to control the flow. The glass tube is initially filled from the top side with the deionized water at a certain amount as the vacuum ball valve mounted here is closed. The top end of the glass tube is then closed by a paper or something else in order to prevent any dust to enter. A ruler is placed on the glass tube to measure how much water is taken into the system. The main idea behind the glass tube at the higher level than experimental setup is to provide a water flow by itself due to gravity. The third additional equipment in the setup is the fan that is used to cool the vacuum pump. It should be noted that the vacuum pump does not operate continuously. It works only during the evacuating process and this takes a few hours. However, the vacuum pump can overheat and needs to be cooled.

6.3 Measurement Devices

During the experiments, several measurement devices are used to measure temperature, pressure and flowrate. The measurement devices used are listed below:

a) Thermocouples
b) Pressure transducers
c) Flowmeter
d) Datalogger

Thermocouples are used to measure temperatures in the different components of the thermal wave cycle. In vacuum line, totally 16 K-type thermocouples are used: 10 thermocouples for measuring the temperature of the adsorbent material (zeolite) in the adsorbent bed, 3 thermocouples for measuring the water temperature in the condenser, and 3 thermocouples for measuring the water temperature in the evaporator. These 16 thermocouples are placed in the components not by drilling holes but using thermocouple feedthroughs especially designed for vacuum lines. The thermocouple feedthroughs are mounted on the components by a flange connection and hence prevent possible vacuum leaks. The arrangement of the 10 thermocouples placed in the adsorbent bed is given in Figure 6.19. The thermocouple feedthroughs used in the study are Kurt Lesker flanged type feedthroughs designed for K-type thermocouples. In addition to these 16 thermocouples, 11 more thermocouples are used outside the vacuum line. These thermocouples are T-type. 4 of them are used for measuring the temperature of the water inside the water tank in which the evaporator is placed. One of these 4 thermocouples is used for measuring the water temperature at the middle level of the tank and for controlling the evaporator temperature. The other 3 three thermocouples are placed on the evaporator coil by means of a metal strip mounted vertically on the evaporator coil to read the temperatures at the top, middle and bottom points of the evaporator coil. One thermocouple is used for measuring the ambient temperature and the other one is used for measuring and controlling the temperature of the tape heater wrapped on the vacuum line. The reason for using a tape heater on the vacuum line is to prevent the refrigerant vapor inside the vacuum line to condensate at the inner surface of the vacuum pipes. Therefore, the temperature of the pipe is kept above the condensation temperature of the water vapor at the corresponding vacuum pressure.

Two thermocouples are used to measure and control the temperatures of the oil in the hot and cold oil tanks. Two thermocouples are placed on the outer surface of the copper tubes at the inlet and outlet to the vacuum chamber in order to measure the inlet and outlet temperatures of the oil to the adsorbent bed. One more thermocouple is used to measure the temperature of the water in the water tank in which the condenser is placed. The heater and cooler in the condenser water tank can be controlled by using the signal taken from this thermocouple.

The pressure transducers are used to measure pressure in the vacuum line. The output signal of the pressure transducers is between 1-9 VDC (Volt). To convert Volt unit to Torr or mbar unit, the tables and equations supplied by the producer company or the datasheets downloaded from the website of the company are used. The output voltage values are read and saved by the datalogger. In the vacuum line, two pressure transducers are used: one is at the condenser inlet and the other is at the evaporator outlet. The pressure transducers used in this study are Kurt Lesker 910 series Piezo/Pirani type transducers. The photo of the pressure transducer is given in Figure 6.20.

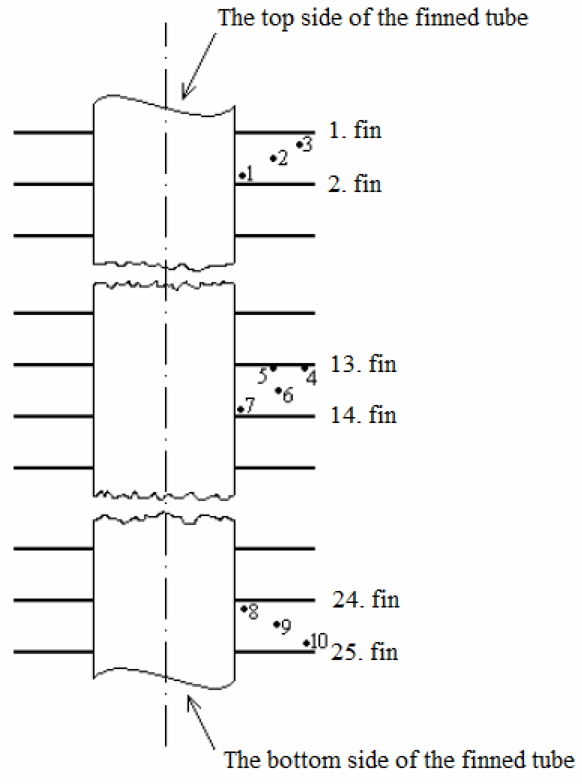

Figure 6.19 The arrangement of the thermocouples inside the adsorbent bed.

Figure 6.20 Photo of the pressure transducer.

The flowmeter is used to measure the volumetric flow rate of the oil in the HTF loop. The flow rate or velocity of the oil is required to calculate how much heat is transferred from the oil to the adsorbent bed or vice versa. For this purpose, a Krohne H250/M9 variable area type oil flowmeter is used. The flowmeter is a custom-made flowmeter for low oil flow rates and high temperatures. It can resist up to 250 °C. The flowmeter used is shown in Figure 6.21.

Figure 6.21 Photo of the oil flowmeter.

All the sensors mentioned above are connected to a datalogger. Datataker DT800 type datalogger is used in this study. The view of the datalogger is given in Figure 6.22. The datalogger can monitor, collect and save the data from the measurements. 27 thermocouples, 2 pressure tranducers and 1 flowmeter are connected the analog channels of the datalogger. 7 relays are connected to the digital channels of the datalogger to control the devices such as heater, cooler, etc. These devices can be turned on or off by receiving a signal from the temperature or pressure measurements and sending the signal to the digital channels. On the other hand, the datalogger is influenced significantly by the devices such as heater and frequency converter. Therefore, the datalogger was grounded to protect it from the negative effects for the reliability of measurements.

Figure 6.22 Photo of the datalogger.

6.4 Experimental Procedure

The experimental procedure used in conducting the experiments is listed below:

- The adsorbent material is dried in an electrical high-temperature oven and its adsorption level is reduced to about 0 kg_w/kg_s.

- The dry adsorbent material is filled between the fins of the finned tube heat exchanger and the finned tube is enclosed with a metallic net. The packed bed is obtained in this way.

- The packed adsorbent bed is placed into the vacuum chamber. The system is then evacuated. In evacuating process, a certain time (three hours) is waited to be sure that there is no vacuum leak. The evacuating process is completed when the increase in pressure ceases at a reasonable vacuum pressure.

- A certain amount of liquid refrigerant (water) is taken into the vacuum line from the glass tube refrigerant feeding line.

- After refrigerant feeding process, the refrigerant level inside the condenser canister is read using the ruler and recorded.

- Temperatures of condenser water, hot oil and cold oil are set to the desired temperatures by using the datalogger software program. Electricity power is supplied to the control panel. It is noted that the hot oil tank temperature should be set 30 ^{o}C above the desired temperature of the hot oil at adsorbent bed inlet. For instance, hot oil tank temperature is set to 150 ^{o}C if the hot oil temperature is required to be 120 ^{o}C. The main reason for that is the heat loss along the pipeline between the tank and adsorbent bed. Moreover, the velocity of the HTF is low and there is a temperature difference between HTF temperatures at the inner surface and center of the HTT. The HTF temperature reduces from the center toward the surface in the radial direction inside the HTT and it takes some time to reach a uniform temperature. For this reason, a bypass line is used to circulate the HTF and the HTF is waited to reach to the uniform temperature before it enters the adsorbent bed. The HTF temperature at the inlet and outlet of the adsorbent bed is measured on the outer surface of the HTT.

- The vacuum ball valves between the evaporator and adsorbent bed are opened to enable adsorbent material to adsorb the refrigerant water vapor. The oil pump is switched on to circulate the cold oil on the HTF line. The ball valves on the cold oil line are opened. The adsorption process is performed in this way.

- The increase in the adsorption level of the adsorbent material inside the adsorbent bed ceases when the adsorbent material has its maximum adsorption level. This cessation can be understood from the cessation of the decrease in the refrigerant water level inside the condenser canister. Thus, adsorption process is completed and desorption process is started.

- To desorb the adsorbent bed, the HTF is circulated through the hot oil line. The valves on the cold oil line are closed and the valves on the hot oil line are opened. The refrigerant water level in the condenser canister is read and recorded. The flowrate or velocity of the HTF is adjusted by the neddle valve on the oil line. Furthermore, the vacuum ball valves between the evaporator and adsorbent bed on the vacuum line are closed. The vacuum ball valves between the condenser and adsorbent bed are opened. The refrigerant adsorbed during the adsorption process is now desorbed. The pressure inside the adsorbent bed increases as the bed is heated and the refrigerant vapor is removed from the adsorbent bed when the pressure inside the bed exceeds the saturation pressure corresponding to the condenser water temperature. The water level in the condenser canister increases.

- The desorption process continues until the temperature of the adsorbent bed reaches to a certain temperature (usually regeneration temperature). The adsorption level of the adsorbent material packed in the bed decreases to a cetain value. The water level in the condenser is recorded at the end of the desorption process. Therefore, the amount of refrigerant water adsorbed by the adsorbent during the desorption process can be calculated by using the difference in the water level at the beginning and end of the process.

6.5 Experimental Results and Discussions

Two adsorbent/adsorbate pairs have been examined: zeolite-water and silica gel-water pairs. Clinoptilolite which is a natural zeolite found in Turkey is used as the type of zeolite. White silica gel and orange silica gel are used as the type of silica gel. White silica gel is tested in two different particle sizes with 2 mm and 4 mm diameters. The followings are the results obtained from the pairs used.

6.5.1 Results for Zeolite-Water Pair

The experiments are made at three different regeneration temperatures and three different HTF velocities. In the selection of regeneration temperature, high desorption temperatures of the zeolite is taken into account. Therefore, 150, 175 and 200 ^{o}C temperatures are selected as regeneration temperatures. The reason for the selection of at most 200 ^{o}C is that some components of the system can resist up to this temperature. Velocity is used for sizing the flow of HTF in order to compare the experimental results with the theoretical results. The volumetric flow rate measured by the oil flowmeter is converted to velocity by using the following equation

$$v = \frac{10^{-3}V}{60A} \tag{6.3}$$

where v is velocity in m/s, V is volumetric flow rate in l/m and A is cross-sectional area of the finned tube in m^2. 0.001, 0.005 and 0.025 m/s are selected as the HTF velocities. The reason for the selection of such low HTF velocity values is to investigate the enhancement of the heat transfer in the radial direction inside the adsorbent bed as the HTF passes through the bed with low velocity. At higher velocities than selected, the HTF exits the adsorbent bed at a temperature near to the temperature at which it enters the adsorbent bed with a poor heat transfer in the radial direction. Therefore, the thermal wave in the adsorbent bed cannot be formed at a desired shape. For this reason, the velocity of the HTF is kept in the interval mentioned above.

As a result of experiments carried out at the temperatures and velocities selected, temperature distributions in the adsorbent bed at the points whose arrangement are shown in Figure 6.19 are represented both experimentally and theoretically in this section. The theoretical results are obtained from Comsol Multiphysics simulations while the experimental results are the values collected and saved by the datalogger during the experiments. In the following figures, solid lines represent the theoretical results while the other plots represent the experimental results. Temperatures are plotted with 10 s time intervals as degrees Kelvin (K). The numbers at the right hand side of the figures are the numbers corresponding to the thermocouple points shown in Figure 6.19.

6.5.1.1 The Effect of HTF Velocity

Figure 6.23 shows the temperature distributions measured in the adsorbent bed at 10 points for 200 ^{o}C regeneration temperature and 0.001 m/s HTF velocity. From these 10 points, the points 4 and 5 represent the surface temperature of the middle fin while the other points represent zeolite temperature as seen in Figure 6.19.

In Figure 6.23, it can be seen that the temperatures at first three points (the points 1, 2 and 3) increase more quickly, and the temperatures at the middle points of the adsorbent bed (the points 4, 5, 6 and 7) increase more slowly, and the temperatures at the bottom points (the points 8, 9 and 10) increase very slowly. The reason for the delay in the increase in the temperatures at the bottom side of the finned tube is that the HTF passes through this part of the tube after a certain period of time due to its low velocity. When the finned tube is considered to be divided into three parts as the top, middle and bottom parts, the temperatures at the points on each part are seen to be close to each other and to have similar trends. However, temperature differences between the parts are very large and temperature distributions and hence thermal waves of each part show different trends. On the other hand, the difference in temperatures and in the shape of thermal waves decreases with increasing HTF velocity as can be seen in Figures 6.24 and 6.25.

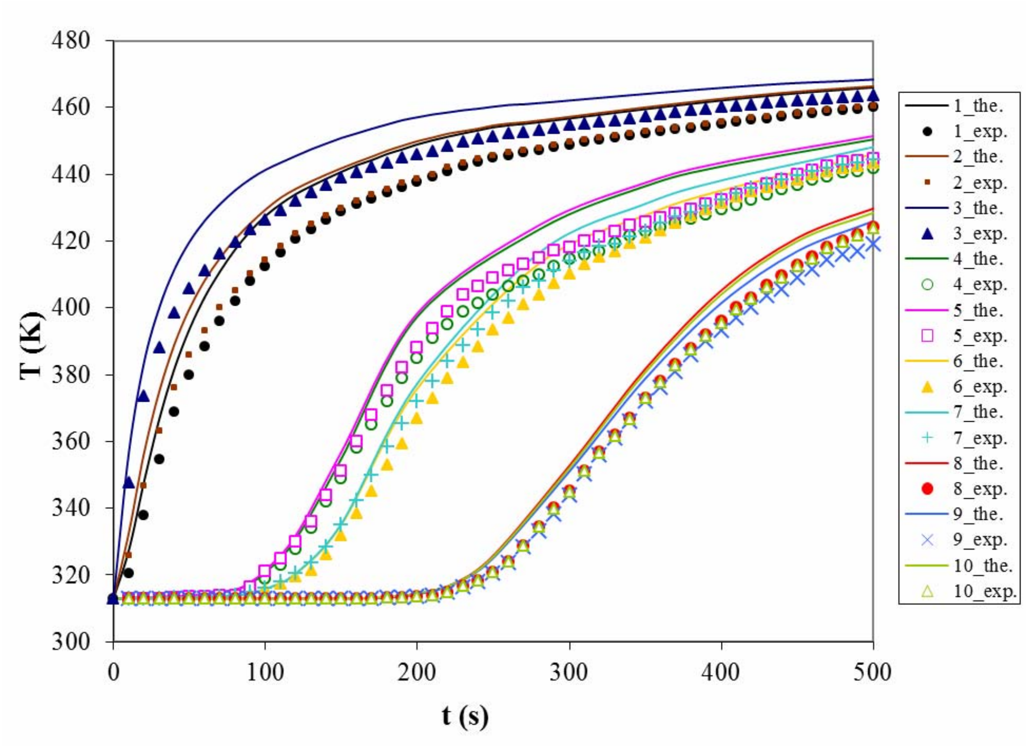

Figure 6.23 Temperature distributions in the adsorbent bed for 200 ^{o}C regeneration temperature and 0.001 m/s HTF velocity.

In Figures 6.24 and 6.25, the HTF velocity is increased while the regeneration temperature is kept constant at 200 ^{o}C. Figure 6.24 and 6.25 represents the temperature distributions in the adsorbent bed for HTF velocities 0.005 m/s and 0.025 m/s, respectively. As mentioned above, the temperatures at each three parts (the top, middle and bottom parts) of the finned tube are seen to get close to each other as the HTF velocity increases. It can be concluded that as the HTF velocity increases, the heat transfer in the radial direction inside the bed decreases whereas the heat transfer in the axial direction increases. Therefore, the temperatures in the whole bed get close to each other without forming a thermal wave or temperature front. The temperatures are closer for the HTF velocity 0.025 m/s that that for 0.005 m/s. The whole adsorbent bed has approximately uniform temperature after *t* = 500s for 0.025 m/s HTF velocity. The uniform temperature can be obtained for longer periods of time at low HTF velocities.

When the theoretical and experimental results are compared to each other, the experimental results are seen to be lower than the theoretical results by maximum 5% in Kelvin and 10% in ^{o}C at most. According to these results, it can be said that the experimental results are in good agreement with the theoretical results when the accuracy of the measurement devices and the experimental conditions are considered.

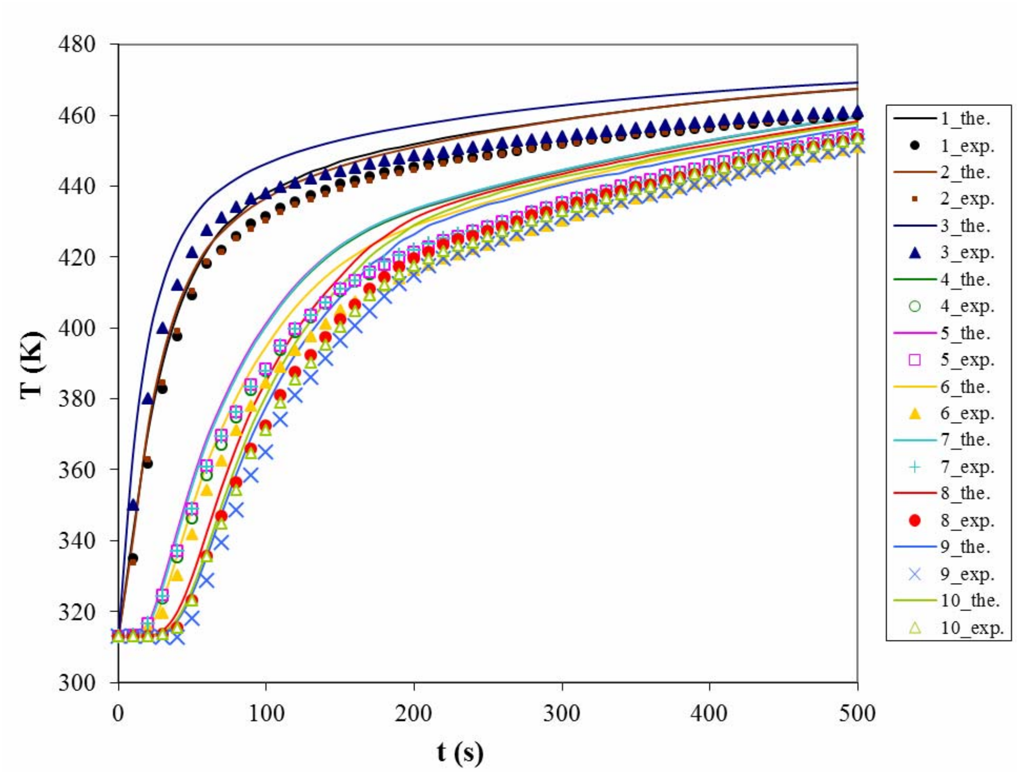

Figure 6.24 Temperature distributions in the adsorbent bed for 200 ^{o}C regeneration temperature and 0.005 m/s HTF velocity.

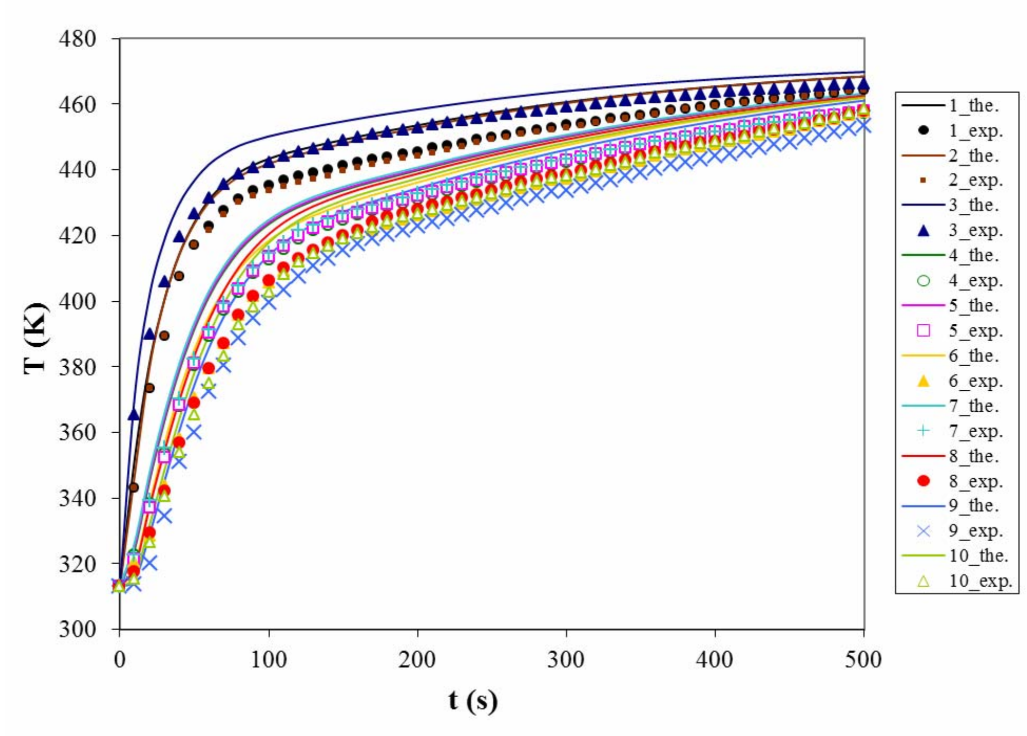

Figure 6.25 Temperature distributions in the adsorbent bed for 200 ^{o}C regeneration temperature and 0.025 m/s HTF velocity.

6.5.1.2 The Effect of Regeneration Temperature

The following two figures, Figures 6.26 and 6.27, show the temperature distributions with time in the adsorbent bed for different regeneration temperatures. The HTF velocity is kept constant at v = 0.005 m/s. The plots are given for 175 ^{o}C and 150 ^{o}C regeneration temperatures since the plot for 200 ^{o}C is given before in Figure 6.24. As seen from the three figures, i.e. Figures 6.24, 6.26 and 6.27, the trends in the temperature distributions do not change, but the maximum temperatures reached change. It can be concluded here that the regeneration temperature has an effect not on the heat transfer direction but heat transfer amount.

Finally, temperature distributions in the axial direction inside the adsorbent bed have been investigated. Only the measurement points 2, 6 and 9 are at the same level in the radial direction and at the same conditions (in the middle point of two fins) and can therefore be used for investigating the temperature distribution in the axial direction. Thus, the

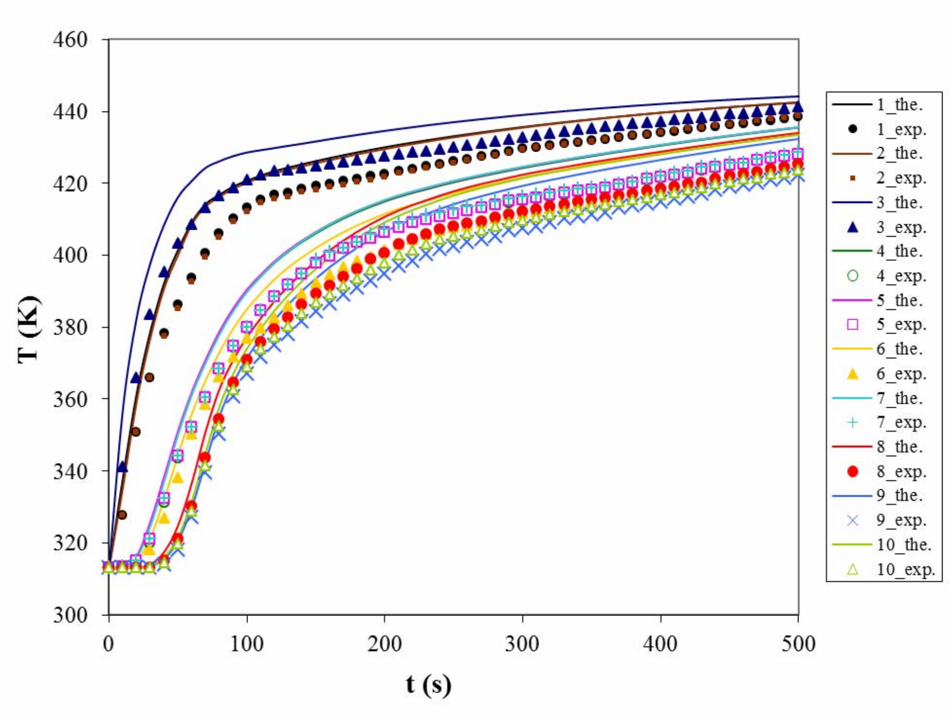

Figure 6.26 Temperature distributions in the adsorbent bed for 175 °C regeneration temperature and 0.005 m/s HTF velocity.

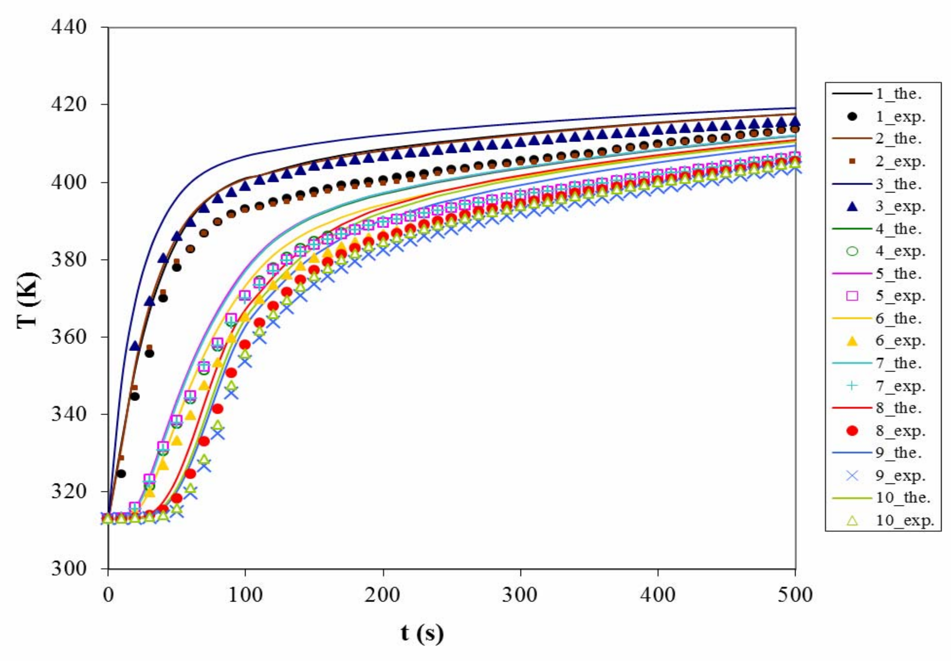

Figure 6.27 Temperature distributions in the adsorbent bed for 150 °C regeneration temperature and 0.005 m/s HTF velocity.

temperature distributions of the zeolite at the points 2, 6 and 9 are plotted and compared with the theoretical results obtained for these points. Figure 6.28 shows the temperature distributions in the axial direction (*z*) inside the adsorbent bed for three different HTF velocity values (0.001 m/s, 0.005 and 0.025 m/s) and five time values (0, 25, 100, 250 and 500 s). In Figure 6.28, the lines denote the theoretical results while the points denote the experimental results. As can be seen from the theoretical results in Figure 6.28, there is a temperature difference and oscillations between the fins and zeolite since the fins has higher temperatures due to their higher thermal conductivity.

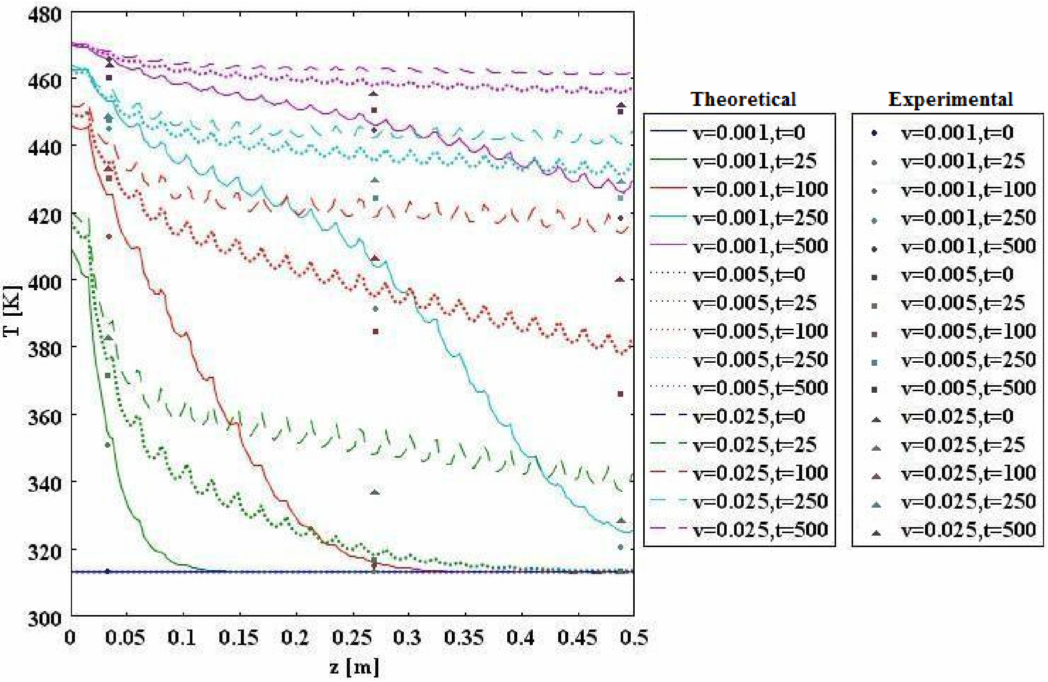

Figure 6.28 Temperature distributions in the axial direction in the adsorbent bed, solid lines for theoretical results, and points for experimental results.

It can be seen once again in Figure 6.28 that the heat transfer rate in the axial direction is higher at higher HTF velocities. At low velocities, heat transfer in the radial direction is improved. Good agreement between the theoretical and experimental results is seen in the above figure. When plotting this figure, the theoretical results are first plotted in Comsol Multiphysics, and then the experimental results for the points 2, 6 and 9 are added to this graph in Paint program. That is the reason for poor resolution in the figure.

The vapor pressures measured in the vacuum line during the experiments are shown in Table 6.2 in mbar. In the table, the condenser inlet pressure and adsorbent bed pressure are given for the selected values of the parameters investigated above, i.e. for three different HTF velocities and regeneration temperatures. Data for the pressure were collected every 5 seconds. The condenser inlet pressure is seen to remain constant during the process. Its value is also similar in all the experiments. The reason for this is that the condenser temperature is set at 35 ^{o}C in all experiments performed. The pressure listed below is about saturation pressure corresponding to this temperature. It is noted that the vacuum ball valve between the condenser and adsorbent bed is closed during the process.
Pressure transducers have 1-9 VDC output as mentioned before. Therefore pressures are recorded by the datalogger as volt. This voltage value can be converted to Torr unit by the following equation

$$P\ (\text{Torr}) = 10^{(V-6)} \tag{6.4}$$

Torr unit can be converted to mbar by the following equality

$$1\ \text{Torr} = 1.33322\ \text{mbar} \tag{6.5}$$

The pressure can also be calculated in Pa by the equality 1 mbar = 100 Pa.

Table 6.2 Measured vapor pressures in the vacuum line (mbar).

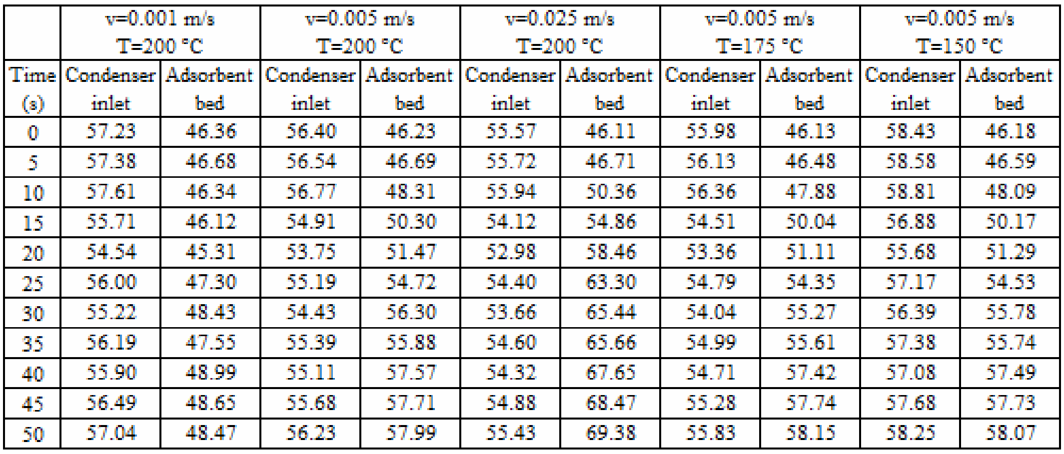

	v=0.001 m/s T=200 °C		v=0.005 m/s T=200 °C		v=0.025 m/s T=200 °C		v=0.005 m/s T=175 °C		v=0.005 m/s T=150 °C	
Time (s)	Condenser inlet	Adsorbent bed	Condenser inlet	Adsorbent bed	Condenser inlet	Adsorbent bed	Condenser inlet	Adsorbent bed	Condenser inlet	Adsorbent bed
0	57.23	46.36	56.40	46.23	55.57	46.11	55.98	46.13	58.43	46.18
5	57.38	46.68	56.54	46.69	55.72	46.71	56.13	46.48	58.58	46.59
10	57.61	46.34	56.77	48.31	55.94	50.36	56.36	47.88	58.81	48.09
15	55.71	46.12	54.91	50.30	54.12	54.86	54.51	50.04	56.88	50.17
20	54.54	45.31	53.75	51.47	52.98	58.46	53.36	51.11	55.68	51.29
25	56.00	47.30	55.19	54.72	54.40	63.30	54.79	54.35	57.17	54.53
30	55.22	48.43	54.43	56.30	53.66	65.44	54.04	55.27	56.39	55.78
35	56.19	47.55	55.39	55.88	54.60	65.66	54.99	55.61	57.38	55.74
40	55.90	48.99	55.11	57.57	54.32	67.65	54.71	57.42	57.08	57.49
45	56.49	48.65	55.68	57.71	54.88	68.47	55.28	57.74	57.68	57.73
50	57.04	48.47	56.23	57.99	55.43	69.38	55.83	58.15	58.25	58.07

Table 6.2 Continued

55	57.04	49.16	56.23	59.18	55.43	71.24	55.83	59.52	58.25	59.35
60	56.23	49.45	55.43	59.39	54.65	71.33	55.04	59.67	57.42	59.53
65	56.93	49.95	56.12	60.02	55.32	72.11	55.72	59.67	58.13	59.84
70	57.70	50.53	56.88	59.78	56.07	70.73	56.47	59.44	58.92	59.61
75	56.82	50.33	56.01	61.04	55.21	74.03	55.61	60.69	58.02	60.86
80	57.40	51.11	56.59	61.24	55.79	73.37	56.19	60.89	58.62	61.06
85	57.33	51.51	56.53	61.99	55.75	74.62	56.14	61.64	58.55	61.82
90	58.61	51.83	57.80	62.60	57.00	75.61	57.39	62.24	59.86	62.42
95	58.41	51.54	57.60	63.06	56.81	77.16	57.20	62.70	59.66	62.88
100	55.74	51.52	54.97	63.64	54.21	78.61	54.59	63.28	56.94	63.46
105	54.56	51.58	53.81	62.80	53.06	76.46	53.43	62.44	55.73	62.62
110	56.58	52.95	55.80	63.58	55.03	76.34	55.41	63.21	57.79	63.40
115	57.68	52.95	56.88	64.84	56.10	79.39	56.49	64.47	58.92	64.65
120	57.69	52.60	56.90	64.76	56.11	79.73	56.50	64.39	58.93	64.57
125	56.51	52.53	55.73	64.62	54.96	79.50	55.34	64.25	57.72	64.44
130	56.47	53.22	55.70	64.60	54.94	78.40	55.32	64.22	57.69	64.41
135	57.85	54.26	57.06	65.65	56.28	79.42	56.67	65.27	59.10	64.90
140	57.64	54.00	56.85	66.61	56.07	82.16	56.46	66.23	58.88	65.85
145	59.16	54.18	58.35	67.12	57.55	83.15	57.95	66.74	60.44	66.35
150	58.18	54.00	57.38	67.03	56.59	83.21	56.99	66.65	59.43	66.27
155	56.13	55.66	55.36	67.85	54.61	82.71	54.98	67.46	57.34	67.07
160	57.99	55.12	57.19	67.67	56.41	83.07	56.80	67.24	59.24	66.81
165	58.35	54.29	57.55	67.55	56.76	84.06	57.15	67.12	59.61	66.69
170	58.45	54.44	57.65	67.92	56.86	84.74	57.25	67.49	59.71	67.06
175	57.92	56.59	57.12	69.62	56.34	85.65	56.73	69.17	59.17	68.73
180	57.31	55.54	56.53	68.85	55.75	85.36	56.14	68.41	58.55	67.97
185	57.90	55.95	57.10	68.85	56.32	84.73	56.71	68.41	59.14	67.98
190	58.15	54.83	57.35	68.40	56.56	85.35	56.96	67.97	59.40	67.53
195	56.87	57.27	56.09	70.14	55.32	85.91	55.71	69.70	58.10	69.25
200	57.44	56.18	56.65	69.86	55.88	86.88	56.26	69.42	58.68	68.98
205	56.38	56.10	55.61	69.55	54.85	86.21	55.23	68.94	57.60	68.33
210	60.59	57.10	59.76	70.70	58.94	87.52	59.35	70.07	61.89	69.46
215	58.49	56.08	57.71	70.14	56.93	87.74	57.32	69.53	59.77	68.92
220	57.75	56.97	56.97	71.66	56.21	90.12	56.59	71.03	59.01	70.40
225	55.79	56.61	55.04	71.28	54.30	89.75	54.67	70.65	57.00	70.03
230	59.39	58.16	58.59	72.00	57.81	89.12	58.20	71.36	60.68	70.74
235	58.54	57.06	57.75	71.44	56.98	89.44	57.36	70.81	59.81	70.19
240	62.12	56.74	61.28	71.56	60.46	90.26	60.87	70.94	63.47	70.31
245	59.53	58.73	58.73	72.50	57.95	89.51	58.34	71.87	60.83	71.23
250	58.25	58.34	57.46	72.74	56.69	90.70	57.08	72.10	59.51	71.47
255	59.49	58.21	58.70	73.21	57.91	92.08	58.30	72.57	60.79	71.93
260	57.16	58.91	56.39	73.28	55.63	91.15	56.01	72.44	58.40	71.62
265	58.97	58.84	58.18	73.87	57.40	92.72	57.79	73.02	60.25	72.19
270	57.94	59.63	57.17	73.93	56.40	91.65	56.78	73.08	59.20	72.25
275	57.52	59.27	56.75	74.20	55.99	92.88	56.37	73.35	58.77	72.52
280	58.99	60.24	58.20	75.31	57.42	94.15	57.81	74.45	60.28	73.60
285	58.67	59.83	57.88	75.63	57.11	95.59	57.49	74.76	59.95	73.91
290	58.61	58.87	57.83	75.21	57.05	96.09	57.44	74.35	59.89	73.50
295	59.32	61.14	58.53	76.46	57.74	95.62	58.13	75.59	60.61	74.73
300	58.18	59.95	57.40	75.35	56.63	94.71	57.01	74.49	59.45	73.64
305	58.14	59.96	57.38	76.24	56.62	96.95	57.00	75.37	59.42	74.52
310	59.49	60.14	58.71	76.30	57.94	96.82	58.32	75.43	60.80	74.57
315	58.39	61.05	57.63	76.41	56.87	95.65	57.24	75.36	59.68	74.32

Table 6.2 Continued

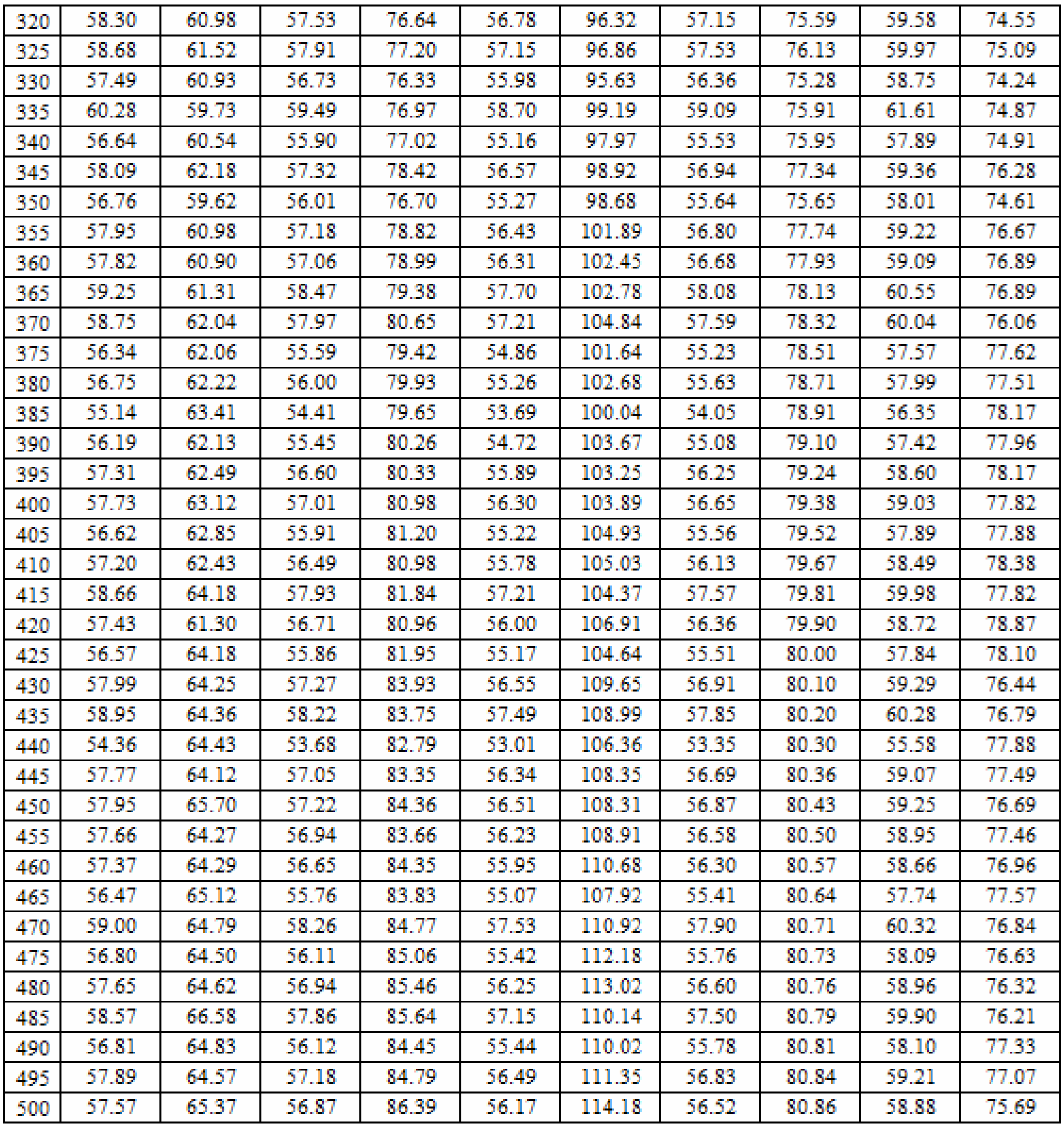

320	58.30	60.98	57.53	76.64	56.78	96.32	57.15	75.59	59.58	74.55
325	58.68	61.52	57.91	77.20	57.15	96.86	57.53	76.13	59.97	75.09
330	57.49	60.93	56.73	76.33	55.98	95.63	56.36	75.28	58.75	74.24
335	60.28	59.73	59.49	76.97	58.70	99.19	59.09	75.91	61.61	74.87
340	56.64	60.54	55.90	77.02	55.16	97.97	55.53	75.95	57.89	74.91
345	58.09	62.18	57.32	78.42	56.57	98.92	56.94	77.34	59.36	76.28
350	56.76	59.62	56.01	76.70	55.27	98.68	55.64	75.65	58.01	74.61
355	57.95	60.98	57.18	78.82	56.43	101.89	56.80	77.74	59.22	76.67
360	57.82	60.90	57.06	78.99	56.31	102.45	56.68	77.93	59.09	76.89
365	59.25	61.31	58.47	79.38	57.70	102.78	58.08	78.13	60.55	76.89
370	58.75	62.04	57.97	80.65	57.21	104.84	57.59	78.32	60.04	76.06
375	56.34	62.06	55.59	79.42	54.86	101.64	55.23	78.51	57.57	77.62
380	56.75	62.22	56.00	79.93	55.26	102.68	55.63	78.71	57.99	77.51
385	55.14	63.41	54.41	79.65	53.69	100.04	54.05	78.91	56.35	78.17
390	56.19	62.13	55.45	80.26	54.72	103.67	55.08	79.10	57.42	77.96
395	57.31	62.49	56.60	80.33	55.89	103.25	56.25	79.24	58.60	78.17
400	57.73	63.12	57.01	80.98	56.30	103.89	56.65	79.38	59.03	77.82
405	56.62	62.85	55.91	81.20	55.22	104.93	55.56	79.52	57.89	77.88
410	57.20	62.43	56.49	80.98	55.78	105.03	56.13	79.67	58.49	78.38
415	58.66	64.18	57.93	81.84	57.21	104.37	57.57	79.81	59.98	77.82
420	57.43	61.30	56.71	80.96	56.00	106.91	56.36	79.90	58.72	78.87
425	56.57	64.18	55.86	81.95	55.17	104.64	55.51	80.00	57.84	78.10
430	57.99	64.25	57.27	83.93	56.55	109.65	56.91	80.10	59.29	76.44
435	58.95	64.36	58.22	83.75	57.49	108.99	57.85	80.20	60.28	76.79
440	54.36	64.43	53.68	82.79	53.01	106.36	53.35	80.30	55.58	77.88
445	57.77	64.12	57.05	83.35	56.34	108.35	56.69	80.36	59.07	77.49
450	57.95	65.70	57.22	84.36	56.51	108.31	56.87	80.43	59.25	76.69
455	57.66	64.27	56.94	83.66	56.23	108.91	56.58	80.50	58.95	77.46
460	57.37	64.29	56.65	84.35	55.95	110.68	56.30	80.57	58.66	76.96
465	56.47	65.12	55.76	83.83	55.07	107.92	55.41	80.64	57.74	77.57
470	59.00	64.79	58.26	84.77	57.53	110.92	57.90	80.71	60.32	76.84
475	56.80	64.50	56.11	85.06	55.42	112.18	55.76	80.73	58.09	76.63
480	57.65	64.62	56.94	85.46	56.25	113.02	56.60	80.76	58.96	76.32
485	58.57	66.58	57.86	85.64	57.15	110.14	57.50	80.79	59.90	76.21
490	56.81	64.83	56.12	84.45	55.44	110.02	55.78	80.81	58.10	77.33
495	57.89	64.57	57.18	84.79	56.49	111.35	56.83	80.84	59.21	77.07
500	57.57	65.37	56.87	86.39	56.17	114.18	56.52	80.86	58.88	75.69

6.5.2 Results for Silica Gel-Water Pair

The experiments with silica gel-water pair are made with two types of silica gel: white and orange silica gels. Futhermore, two different size of white silica gel with 2 mm and 4 mm particle diameters is tested to see the effect of particle diameter on the temperature distribution inside the adsorbent bed. Three different HTF velocities for the white silica gel and two different HTF velocities for the orange silica gel are used in the experiments.

The effect of HTF velocity is therefore investigated. The pictures from the silica gels used are given in Figure 6.29.

A new finned-tube heat exchanger is constructed and used in the silica gel experiments. The shape of the finned tube is the same as the first one, but the diameters of the tube and fin are doubled. The diameters of the second tube and fin are 50 mm and 100 mm, respectively. Both tube and fin thicknesses are 2 mm. The tube is 420 mm in length. The number of fins used is 20. The distance between the fins is 20 mm. The main reason for the construction of the second finned-tube heat exchanger is to investigate the difference in temperature gradient and difference in thermal wave formation between the first adsorbent bed and the second adsorbent bed doubled in size. The second finned-tube heat exchanger is shown in Figure 6.30.

Figure 6.29 Silica gels used in the experiments.

Figure 6.30 Pictures from the second adsorbent bed.

The arrangement of thermocouples in the second adsorbent bed is shown in Figure 6.31. This arrangement is a little bit different from the arrangement used in the first bed. A more appropriate arrangement is made to see the temperature variation along *r* and *z* axes and between two fins. Totally 10 thermocouples are used. 4 of them are placed on the fins while the other 6 thermocouples are placed on the silica gel between the fins.

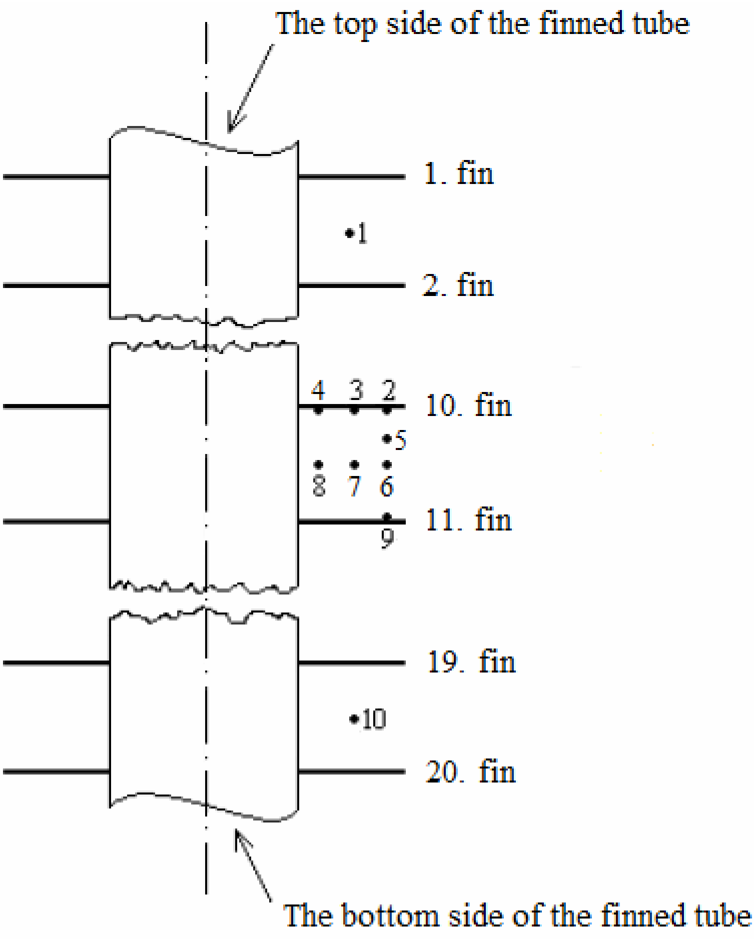

Figure 6.31 The arrangement of the thermocouples inside the second adsorbent bed.

Two dimensional theoretical temperature distribution of the adsorbent bed with white silica gel-water pair is shown in Figure 6.32. This temperature distribution is simulated for v = 0.0246 m/s HTF velocity and T = 120 ^{o}C regeneration temperature at time t = 1000 s. It can be seen from Figure 6.32 that silica gel between fins has not reached to the regeneration temperature yet whereas the fins have reached to temperatures about regeneration temperature. The temperature decreases towards the middle point between two fins. The reason for this poor heat transfer is the low thermal conductivity of the silica gel which is *k* = 0.175 W/(mK). Another reason is that the distance between the fins is 20 mm. This distance is a large distance for transferring heat from the fins to silica gel by conduction effectively and can be reduced for more effective heat transfer.

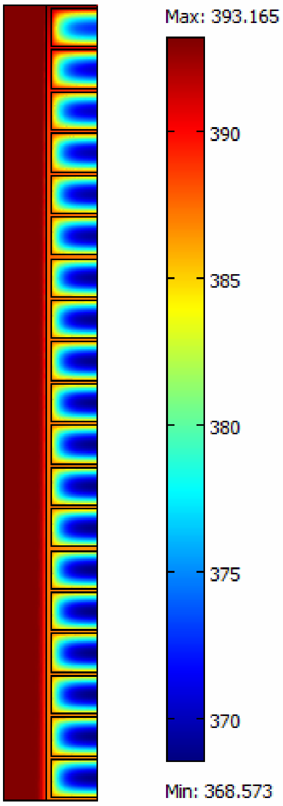

Figure 6.32 Two dimensional temperature distribution inside the the adsorbent bed for white silica gel-water pair after 1000 s.

Variation of temperature with time is also shown in Figures 6.33-6.40 to compare the theoretical results with the experimental results. First, the effect of HTF velocity on the temperature distribution inside the bed has been investigated for white silica gel-water pair. Temperature distributions for v = 0.0246 m/s, v = 0.0169 m/s and v = 0.0025 m/s HTF velocities are examined. The regeneration temperature is selected as T = 120 ^{o}C.

Secondly, the effect of condenser pressure has been investigated. 2.339 kPa, 4.247 kPa and 7.384 kPa condenser pressures which are the saturation pressures corresponding to condensation temperatures 20 ^{o}C, 30 ^{o}C and 40 ^{o}C, respectively, have been examined. The regeneration temperature is kept same as T = 120 ^{o}C. HTF velocity is taken as v = 0.0025 m/s in the investigation of the effect of varying condenser pressure. Thirdly, the effect of partical diameter of white silica gel has been investigated. White silica gels with 2 mm and 4 mm diameters have been tested. In the investigation of the effect of silica gel particle diameter, the HTF velocity and regeneration temperature are taken as v = 0.0025 m/s and T = 120 ^{o}C, respectively. Finally, orange silica gel-water pair has been tested for two different HTF velocities. The orange silica gel has a higher maximum amount adsorbed than the white silica gel. The effect of maximum amount adsorbed has been therefore investigated comparing the white and orange silica gels.

Temperature distributions of white silica gel for 0.0246 m/s, 0.0169 m/s and 0.0025 m/s HTF velocities are presented in Figure 6.33, 6.34 and 6.35, respectively, as the regeneration temperature is 120 ^{o}C and the condenser pressure is 4.247 kPa. For HTF velocities 0.0246 m/s and 0.0169 m/s, the temperature distributions are seen to be close to each other since both velocities values are very high so that the HTF leaves the bed very fast without heating the silica gel effectively due to its low thermal conductivity. There are certainly differences in the temperature distributions for both velocities, but it is difficult to see the small differences in the large temperature range 303-393 K in Figures 6.33 and 6.34. Temperature differences are a bit larger at the fin surfaces due to the high thermal conductivity copper material. Figure 6.35 shows the temperature distribution for 0.0025 m/s HTF velocity. As HTF velocity decreases to 0.0025 m/s, the delay in the increase in temperature can be clearly seen in Figure 6.35 when compared to Figures 6.33 and 6.34. Temperatures at low HTF velocity are lower than that at high HTF velocities at the same moment in time. On the other hand, after 1000 s, temperatures get closer to each other for low and high velocities. This is due to that heat is dominantly transferred in the radial direction at low velocities and bed temperatures reach to the same temperatures as in the case of high velocities after a certain time. It is emphasized in discussing the results of experiments with zeolite that the HTF velocity should be very low to obtain a thermal wave and heat transfer enhancement in the radial direction. The need for low velocity is once again proved from silica gel experiments.

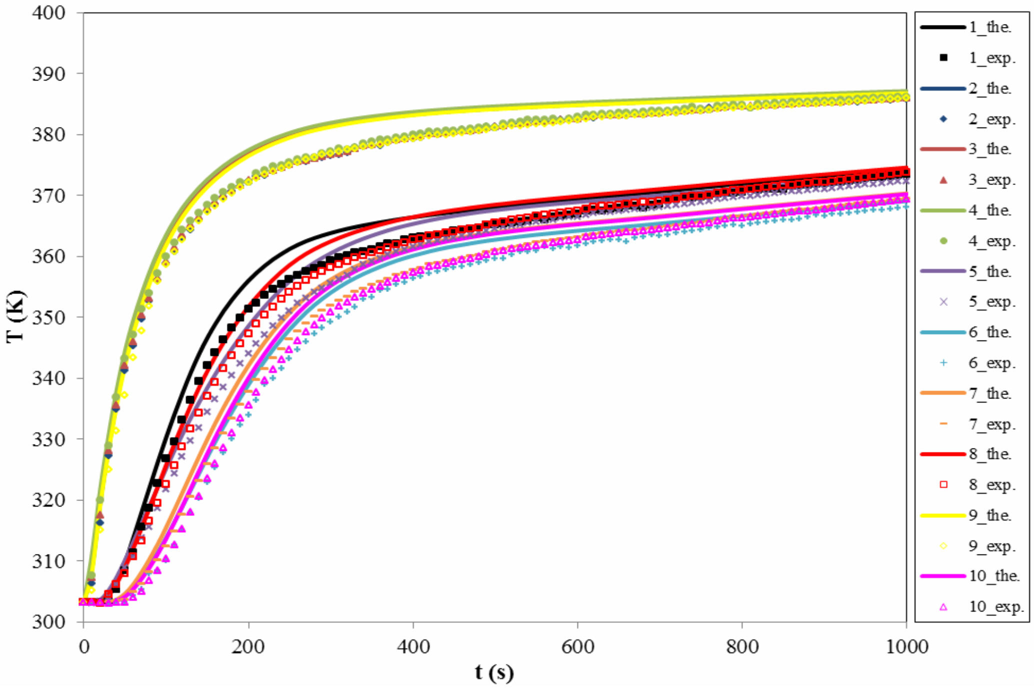

Figure 6.33 Temperature distributions in the adsorbent bed with white silica gel for 0.0246 m/s HTF velocity.

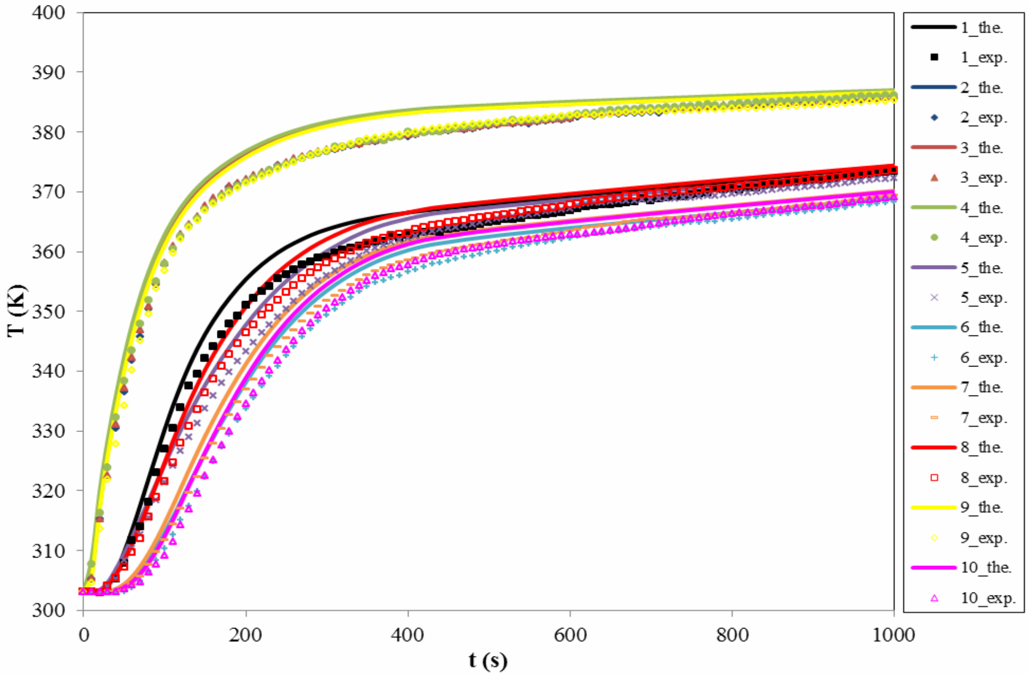

Figure 6.34 Temperature distributions in the adsorbent bed with white silica gel for 0.0169 m/s HTF velocity.

When the temperatures of fin and adsorbent material are compared in Figures 6.33-6.35, the points 2, 3, 4, and 9 that are located on the fins seem to be heated faster due to the high thermal conductivity of copper. When the points 6, 7 and 8 shown in Figure 6.31 compared to each other, temperature of point 8 is higher than temperatures of the other two points and temperature of point 7 is higher than that of point 6. This is due to that point 8 is the closest and point 6 is the remotest point to the HTF which is heat source. Furthermore, when point 5 is compared with these three points, it can be seen that the temperature of point 5 is higher than the temperatures of points 6 and 7, but lower than temperature of point 8 due to its closeness to fin. Among the points located on silica gel, point 1 has the highest temperature and point 10 has the lowest temperature as shown in Figures 6.33-6.35. The temperature differences between points 7 and 10 are clearly seen to be higher for low HTF velocity as seen in Figue 6.35.

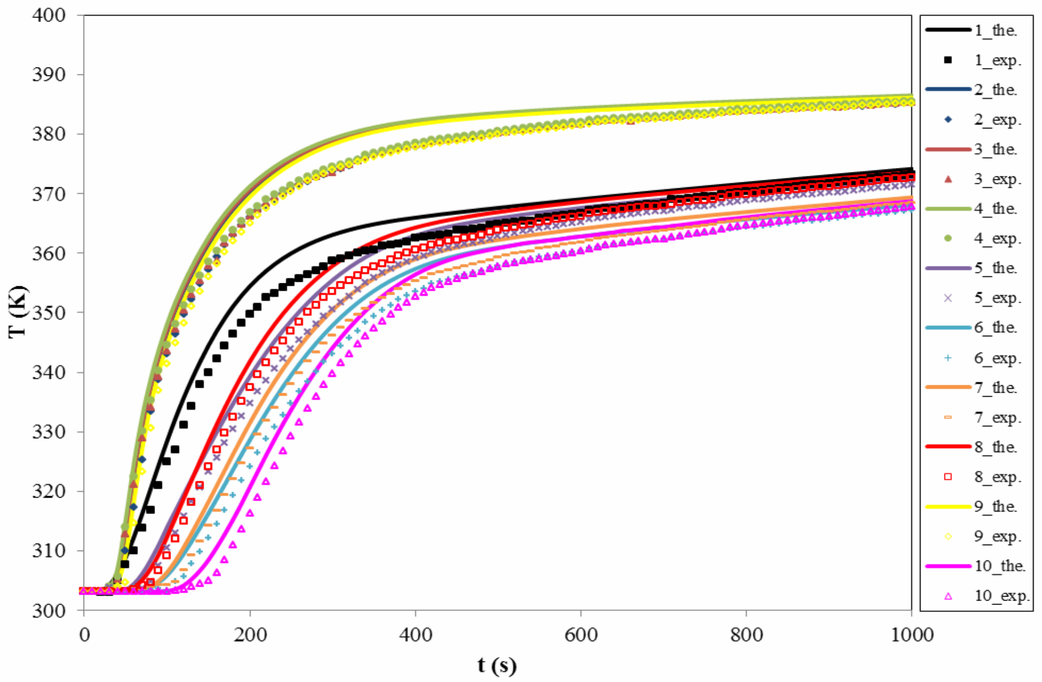

Figure 6.35 Temperature distributions in the adsorbent bed with white silica gel for 0.0025 m/s HTF velocity.

Good agreement can be seen when the theoretical and experimental results are compared in Figures 6.33-6.35. The maximum temperature difference between the theoretical and experimental study is observed as 5.81 ^{o}C. The experimental data is taken from the datalogger with 10 s time intervals. The temperature difference decreases at the end of the process when the bed temperature approaches to regeneration temperature.

Temperature distributions at different condenser pressures for 0.0025 m/s HTF velocity and 120 ^{o}C regeneration temperature are shown in Figures 6.36 and 6.37. The results for 2.339 kPa condenser pressure are presented in Figure 6.36 while the results for 7.384 kPa condenser pressure are presented in Figure 6.37. Furthermore, Figure 6.35 shows the results the moderate condenser pressure 4.247 kPa. The trends in temperature variation for three condenser pressures are almost the same but the temperature values are a little bit different from each other. The temperatures in the adsorbent bed increase with increasing condenser pressure. This is due to that desorption of refrigerant vapor occurs later at higher condenser pressures and less heat of desorption is rejected from the adsorbent bed. This situation causes the temperature of the bed to remain at higher values.

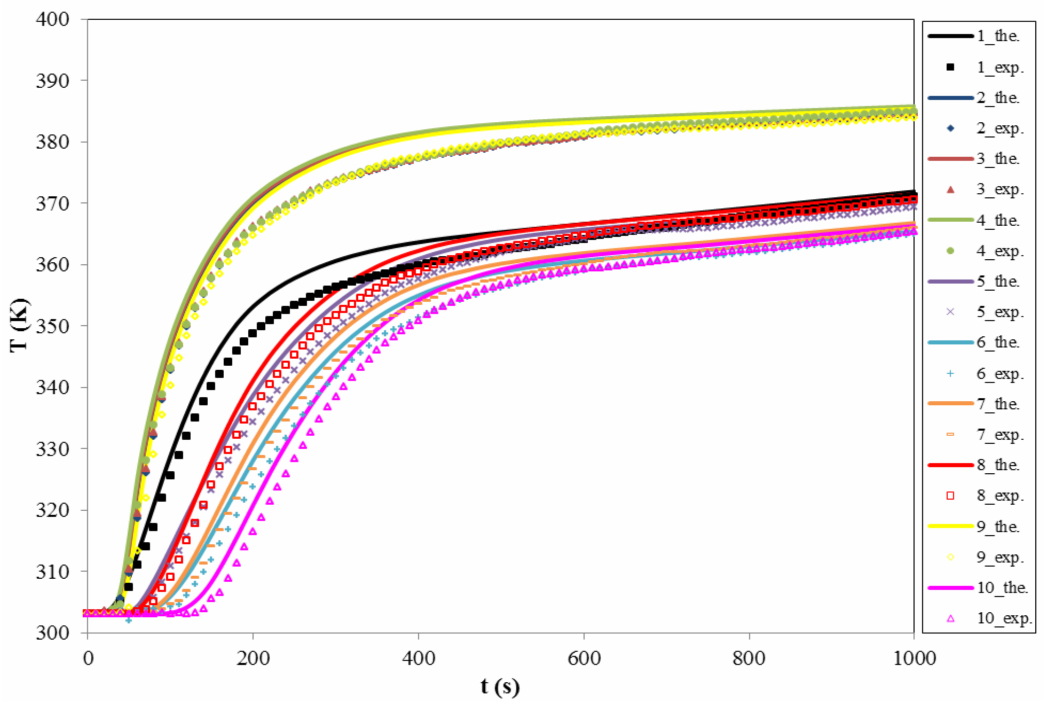

Figure 6.36 Temperature distributions in the adsorbent bed with white silica gel for 0.0025 m/s HTF velocity and 2.339 kPa condenser pressure.

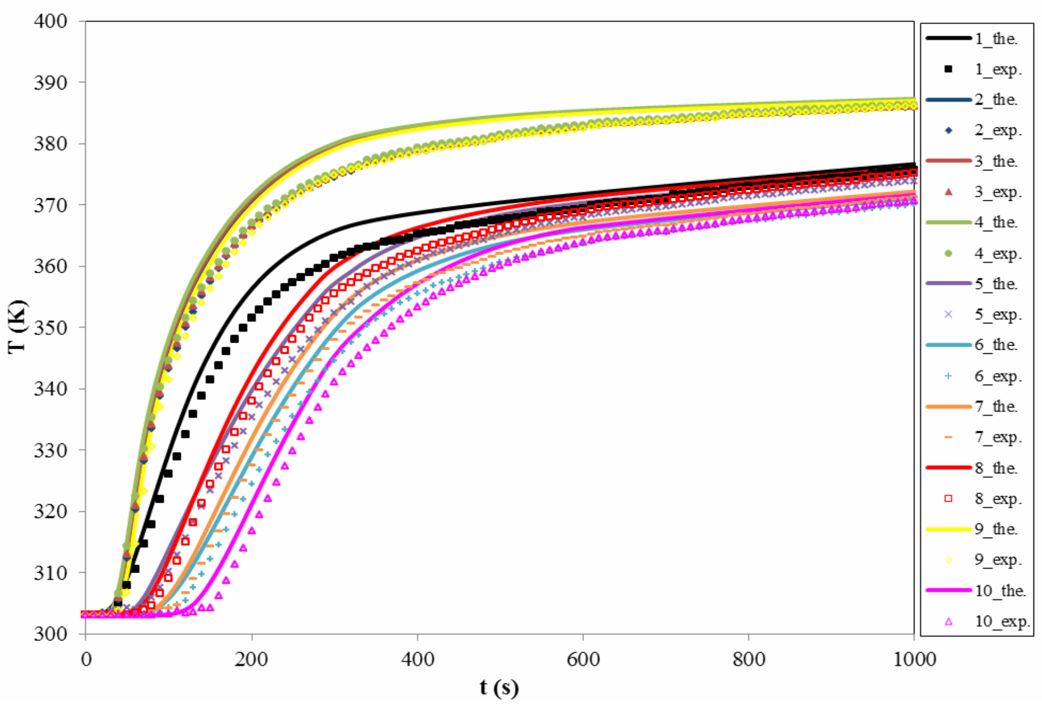

Figure 6.37 Temperature distributions in the adsorbent bed with white silica gel for 0.0025 m/s HTF velocity and 7.384 kPa condenser pressure.

The results for the experiments using orange silica gel are presented in Figures 6.38 and 6.39 for two different velocities: 0.0036 m/s and 0.0231 m/s, respectively. The regeneration temperature is set to 150 °C in both experiments. The condenser temperature is set to 30 °C, so the condenser pressure is 4.247 kPa. As in the case of white silica gel, the adsorbent bed starts to heat later at lower HTF velocity, but the temperatures get closer to the temperatures at higher velocity as time increases. The heat transfer in radial direction is larger for lower HTF velocity and a preferable thermal wave can be obtained in lower velocities. Furthermore, temperature differences between fins and silica gel can be clearly seen from the temperature variations of measurement points in Figures 6.38 and 6.39.

It should be noted that in both white and orange silica gel experiments, the effect of regeneration temperature has not been investigated since this effect has been already investigated at the zeolite experiments before. In that study, it was concluded that the regeneration temperature does not change the trend of the temperature variation, but only changes the temperature values. Therefore, such a study is not performed again.

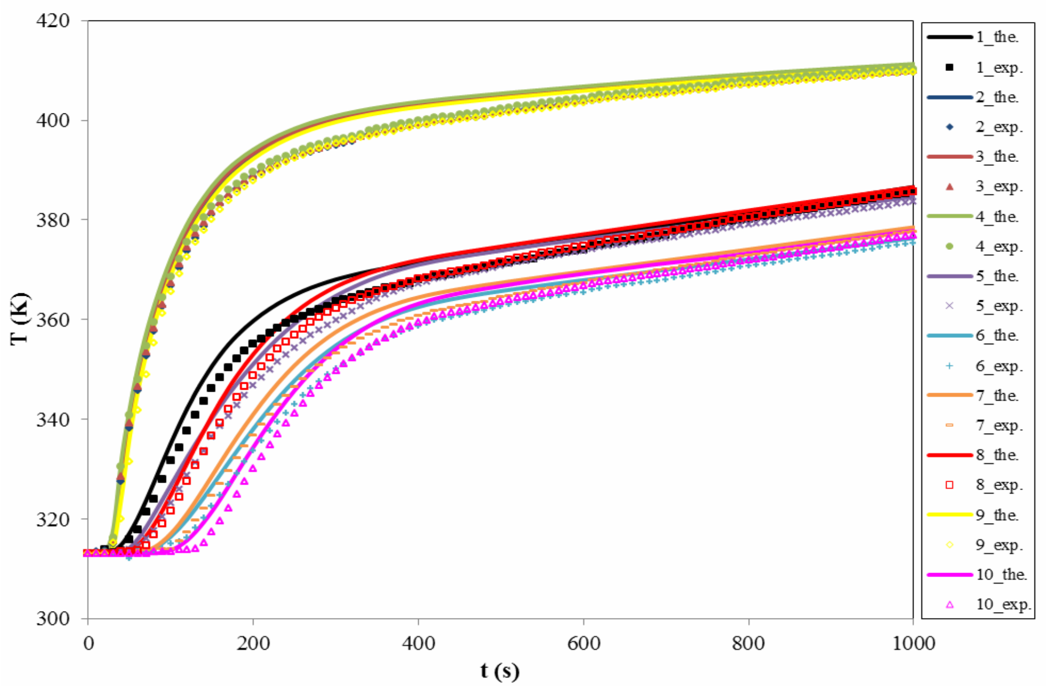

Figure 6.38 Temperature distributions in the adsorbent bed with orange silica gel for 0.0036 m/s HTF velocity.

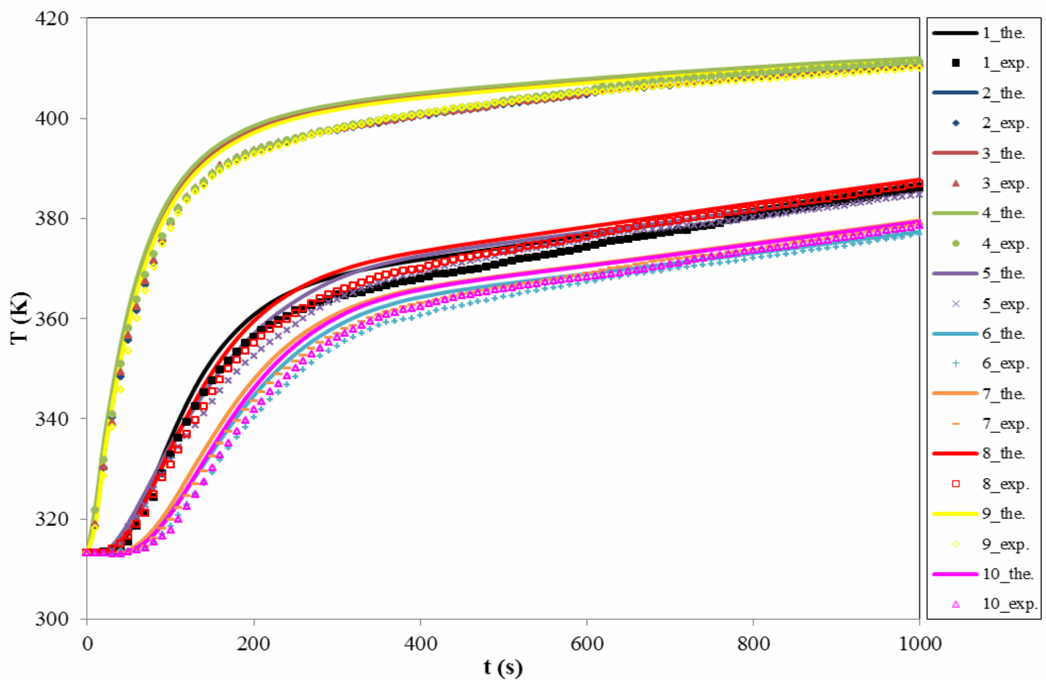

Figure 6.39 Temperature distributions in the adsorbent bed with orange silica gel for 0.0231 m/s HTF velocity.

Finally, the effect of the particle diameter of adsorbent material can be seen in Figure 6.40. Figure 6.40 presents temperature distribution for 2 mm diameter white silica gel while Figure 6.35 presents that for 4 mm white silica gel. The HTF velocity, regeneration temperature and condenser pressure are 0.0025 m/s, 120 ^{o}C and 4.247 kPa, respectively. When the two figures are compared, it can be seen that the diameter of the adsorbent particle has significant influence on the temperature distribution. As the particle diameter decreases, smaller particles have higher desorption response rates, which results in these particles having higher heat rates taken during the desorption process, and smaller temperature gradients.

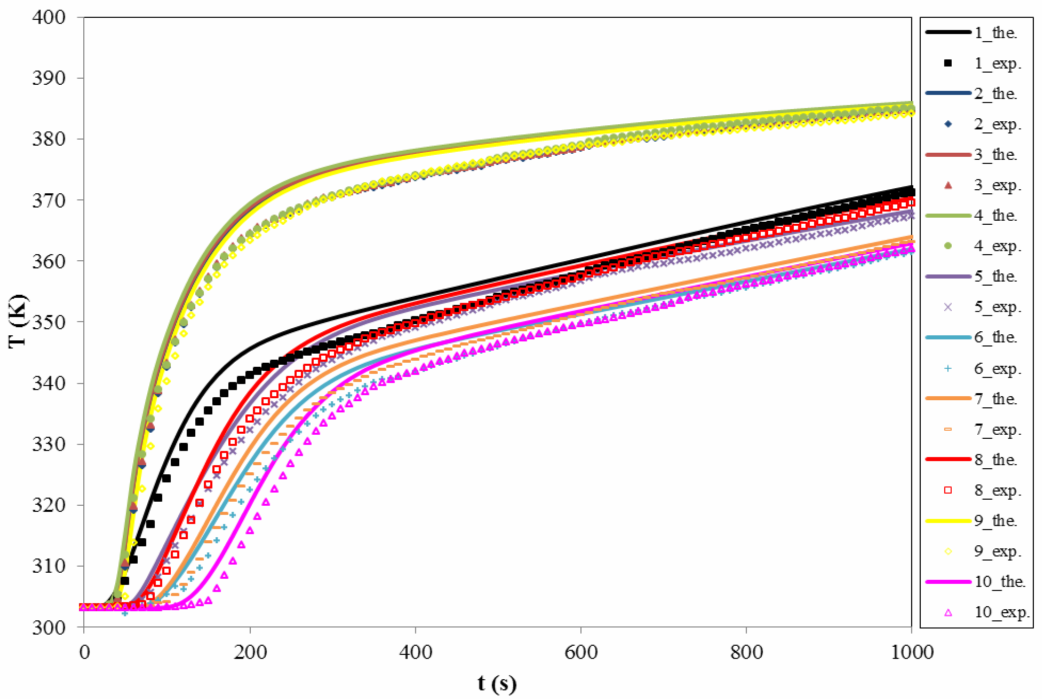

Figure 6.40 Temperature distributions in the adsorbent bed with white silica gel for 0.0025 m/s HTF velocity and 2 mm particle diameter.

CHAPTER 7

CONCLUSIONS AND RECOMMENDATIONS

In this thesis, three different studies have been performed. Firstly, a theoretical study has been performed for the solution of base-case coupled heat and mass transfer model developed for a thermal wave adsorption cooling cycle. Secondly, a theoretical parametric study has been performed for the investigation of the effects of several parameters on the heat and mass transfer inside the adsorbent bed of the thermal wave cycle. Finally, an experimental study has been performed to test a new design finned tube adsorbent bed in term of heat and mass transfer. The experimental results have been compared with the theoretical results. Conclusions and recommendations for each study are summarized below.

In the first theoretical study, i.e. the base-case model, a finless tube type adsorbent bed has been analyzed two dimensionally for the coupled heat and mass transfer based on a thermal wave adsorption cooling cycle. Zeolite-water pair has been used for simulations. Temperature and pressure distributions and variations of amount adsorbed, equilibrium adsorption capacity and mass transfer coefficient have been investigated. Pressure inside the bed varied between 4245-4545 Pa and may be assumed to be uniform throughout the process. Amount adsorbed varied between 0.261-0.0889 kg water per kg zeolite. The mass transfer coefficient varied between 0.00186-0.0052 1/s and has a similar wave with temperature due to its temperature dependence.

The results presented in this first study are valid for model parameters used. After this study was completed, a parametric study that investigates the effects of design and operation parameters on the distributions was recommended to improve the first model.

In this way, solutions for enhancing the heat transfer in the adsorbent bed and the performance of a thermal wave cycle might be developed.

In the second theoretical study, i.e. the parametric study, a finned tube adsorbent bed has been analyzed two dimensionally for the coupled heat and mass transfer based on a thermal wave adsorption cooling cycle. The effects of thermal conductivity of adsorbent material, HTF velocity and adsorbent bed thickness on the distributions of temperature, pressure and amount adsorbed have been investigated. Significant results obtained in this study for the conditions investigated can be summarized as follows:

(a) There are no significant pressure gradients inside the bed and therefore pressure can be assumed to be uniform.

(b) Heat transfer inside the bed is enhanced as thermal conductivity of adsorbent material increases. However for the values higher than 1 W/m K, there are no significant enhancements in the heat transfer and desorption rate.

(c) HTF velocity has a very significant effect on the formation of the thermal wave. A HTF with low velocity provides a straight thermal wave in the adsorbent progressing at a temperature close to HTF temperature. However, for higher velocities, a proper thermal wave is not formed and the HTF heats the bed uniformly.

(d) Heat transfer inside the bed deteriorates as the adsorbent bed thickness increases. Optimum bed thickness is dependent on HTF velocity. A thinner adsorbent bed is needed for high velocities.

In the experimental study, the problems encountered in the establishment of the experimental setup and in carrying out the experiments are summarized below. Several recommendations are given for the solution of these problems. Furthermore, necessary studies are recommended for the improvement of the system and for getting better results.

The minimum regeneration temperature of the thermal wave cycle is selected as 150 ^{o}C for the natural zeolite used (clinoptilolite) since the refrigerant adsorbed cannot be desorbed significantly under 150 ^{o}C. To obtain a significant desorption (regeneration) at lower temperatures, a suitable working pairs whose regeneration temperature is low such as silica gel-water, activated carbon-methanol or activated carbon-ammonia pairs should be used. Silica gel-water pair with both lower regeneration temperature (120 ^{o}C) and higher maximum amount adsorbed (0.35 kg_w/kg_s) has been examined as continuation of this study.

In TÜBİTAK project 105M244 [151] performed previously, big experiences were gained about the vacuum sealing. Therefore, no difficulty in the vacuum sealing has been encountered in this study. It can be said that only problem encountered in the vacuum line is the measurement method of the amount adsorbed/desorbed. In this method, the amount adsorbed or desorbed is calculated by measuring the water level difference via a ruler located on the water accumulation container (lower part) of the condenser. If the weight of the adsorbent material used in tests is very low (under 1 kg of adsorbent material), the water level changes very little and cannot be read well by the ruler. Thus, the amount adsorbed/desorbed cannot be calculated accurately. Furthermore, the ruler cannot be seen very well when the water in the condenser cooling water tank becomes dirty after a certain period of time. To solve these problems, either the use of a liquid levelmeter or the use of more adsorbent material is recommended. Thus the level and hence the amount adsorbed/desorbed can be measured accurately and easily. In this study, a torch has been used to for a better view of the ruler.

The most important issue to be considered in the heat transfer oil line is that all equipments in the oil line should be resistant to high temperature resistance, particularly to the maximum cycle temperature, i.e. regeneration temperature. At the beginning of the experiments, some problems regarding to this issue occurred. These problems were immediately solved and the deformed components were replaced with high temperature resistant materials. It is recommended to consider and select carefully the materials to be used in the hot oil line even at the beginning. A second important recommendation related to the oil line is that it will be better to add ball valves together with solenoid valves. The solenoid valves can fail and need to be replaced. Moreover, the solenoid valves could not be used due to the limitation of digital channels on the datalogger that can turn on/off the valves. For this reason, ball valves were added to the system. These valves are turned on/off manually. However, the valve is turned on or off only at the end of the process, so it remains open or close during the process.

The experimental study will continue with new adsorbent bed configurations and adsorbent/refrigerant pairs. A larger finned tube that can contain about 2 kg adsorbent material has already been constructed. Thus, both the amount adsorbed/desorbed can therefore be measured more accurately and the cooling capacity can be significantly increased. Silica gel-water working pairs with white and orange-colored silica gels have been tested in this new adsorbent bed. As a continuation of the experimental study, the tests for activated carbon-methanol pair, zeolite 13X-water pair with two different sizes of zeolite 13X are planned. Furthemore, the mixtures of adsorbent materials and different metal additives will be tested experimentally to investigate the enhancements in the effective thermal conductivity of the adsorbent bed.

It should be noted finally that the main parameter investigated in this study is the temperature distribution in the adsorbent bed of the thermal wave cycle. The temperatures can be directly measured by the thermocouples and do not require a significant computational work. If the performance of the system will be investigated, a set of calculations should be made by using the pressure and amount adsorbed data as well as the temperature data. One can have information about the performance of the system and cooling capacity in this way. However, the main purpose of this study is not to investigate how efficient the adsorption cycle is as mentioned before. The purpose of this study is to test the new model adsorbent bed and to examine whether an effective heat and mass transfer inside this bed can be reached. The study has focused on the development of a new adsorbent bed design that enables the HTF to exit the adsorbent bed at a temperature as low as possible. Thus, the heat regeneration between two beds of thermal wave cycle and hence the performance indirectly have been tried to increase. In summary, the temperature distribution in the adsorbent bed gives an idea about the performance of the system.

REFERENCES

[1] A. Dabrowski, Adsorption and its applications in industry and environmental protection, Vol. 2: applications in environmental protection, *Elsevier Science & Technology Books*, 1999.

[2] M.W. Ellis, W.J. Wepfer, Effects of adsorbent conductivity and permeability on the performance of a solid sorption heat pump, *ASME Journal of Energy Resources Technology,* 121 (1999) 51-59.

[3] D.E. Demirocak, Thermodynamic and economic analysis of a solar thermal powered adsorption cooling cycle, MSc. Thesis, *Middle East Technical University*, 2008.

[4] K.E. Herold, R. Radermacher, S.A. Klein, Absorption chillers and heat pumps, *CRC Press, Inc.*, 1996.

[5] R. Zarzycki, A. Chacuk, Absorption: fundamentals and applications, *Pergamon Press*, Oxford, 1993.

[6 F. Rouquerol, J. Rouquerol, K.S.W. Sing, Adsorption by powders and porous solids: principles, methodology and applications, *Academic Press*, 1999.

[7] H. Demir, M. Mobedi, S. Ülkü, A review on adsorption heat pump: problems and solutions, *Renewable and Sustainable Energy Reviews*, 12 (2008) 2381-2403.

[8] S.G. Wang, R.Z. Wang, X.R. Li, Research and development of consolidated adsorbent for adsorption systems, Technical note, *Renewable Energy*, 30 (2005) 1425-1441.

[9] L. Yong, R.Z. Wang, Adsorption refrigeration: a survey of novel technologies, *Recent Patents on Engineering*, 1 (2007) 1-21.

[10] B. Crittenden, W.J. Thomas, Adsorption technology and design, *Butterworth Heinemann*, 1998.

[11] J. Keller, R. Staudt, Gas Adsorption Equilibria: Experimental Methods and Adsorptive Isotherms, *Springer Science and Business Media, Inc.*, Boston, 2005.

[12] G. Barbero, L.R. Evangelista, Adsorption phenomena and anchoring energy in nematic liquid crystals, *CRC Press, Taylor & Francis Group*, 2006.

[13] A. Hajji, W.M. Worek, Thermodynamics of constant-pressure and constant-volume sorption processes in closed-cycle solid desiccant systems, *Chemical Engineering Communications,* 104 (1991) 21-40.

[14] T.F. Qu, R.Z. Wang, W. Wang, Study on heat and mass recovery in adsorption refrigeration cycles, *Applied Thermal Engineering*, 21 (2001) 439-452.

[15] H. Demir, M. Mobedi, S. Ülkü, Adsorpsiyonlu ısı pompaları, *VII. Ulusal Tesisat Mühendisliği Kongresi*, 535-545.

[16] S. Fischer, S. Labinov, Not-in-kind technologies for residential and commercial unitary equipment, *Oak Ridge National Laboratory*, Oak Ridge, Tennessee, 2000.

[17] K. Sumathy, K.H. Yeung, L. Yong, Technology development in the solar adsorption refrigeration systems, *Progress in Energy and Combustion Science*, 29 (2003) 301-327.

[18] X. Wang, H.T. Chua, A comparative evaluation of two different heat-recovery schemes as applied to a two-bed adsorption chiller, *International Journal of Heat and Mass Transfer,* 50 (2007) 433-443.

[19] B.B. Saha, S. Koyama, J.B. Lee, K. Kuwahara, K.C.A. Alam, Y. Hamamoto, A. Akisawa, T. Kashiwagi, Performance evaluation of a low-temperature waste heat driven multi-bed adsorption chiller, *International Journal of Multiphase Flow,* 29 (2003) 1249-1263.

[20] K. Thu, B.B. Saha, A. Chacraborty, W.G. Chun, K.C. Ng, Study on an advanced adsorption desalination cycle with evaporator-condenser heat recovery circuit, *International Journal of Heat and Mass Transfer,* 54 (2011) 43-51.

[21] T.X. Li, R.Z. Wang, L.W. Wang, Z.S. Lu, Experimental study on an innovative multifunction heat pipe type heat recovery two-stage sorption refrigeration system, *Energy Conversion and Management,* 49 (2008) 2505-2512.

[22] L. Yong, K. Sumathy, Performance analysis of a continuous multi-bed adsorption rotary cooling system, *Applied Thermal Engineering,* 25 (2005) 393-407.

[23] X. Wang, H.T. Chua, K.C. Ng, Experimental investigation of silica gel-water adsorption chillers with and without a passive heat recovery scheme, *International Journal of Refrigeration,* 28 (2005) 756-765.

[24] L. Yong, K. Sumathy, Modeling and simulation of a solar powered two bed adsorption air conditioning system, *Energy Conversion and Management,* 45 (2004) 2761-2775.

[25] R.Z. Wang, Performance improvement of adsorption cooling by heat and mass recovery operation, *International Journal of Refrigeration,* 24 (2001) 602-611.

[26] E. Voyiatzis, N. Stefanakis, J. Palyvos, A. Papadopoulos, Computational study of a novel continuous solar adsorption chiller: performance prediction and adsorbent selection, *International Journal of Energy Research,* 31/10 (2007) 931-946.

[27] R.Z. Wang, R.G. Oliveira, Adsorption refrigeration–An efficient way to make good use of waste heat and solar energy, *Progress in Energy and Combustion Science,* 32 (2006) 424-458.

[28] R.Z. Wang, L. Wang, Adsorption refrigeration–green cooling driven by low grade thermal energy, *Chinese Science Bulletin,* 50/3 (2005) 193-204.

[29] W. Wang, T.F. Qu, R.Z. Wang, Influence of degree of mass recovery and heat regeneration on adsorption refrigeration cycles, *Energy Conversion and Management,* 43 (2002) 733-741.

[30] K.C.A. Alam, A. Akahira, Y. Hamamoto, A. Akisawa, T. Kashiwagi, A four-bed mass recovery adsorption refrigeration cycle driven by low temperature waste/renewable heat source, *Renewable Energy,* 29 (2004) 1461-1475.

[31] D.C. Wang, Y.H. Li, D. Li, Y.Z. Xia, J.P. Zhang, A review on adsorption refrigeration technology and adsorption deterioration in physical adsorption systems, *Renewable and Sustainable Energy Reviews,* 14 (2010) 344-353.

[32] M.Z.I. Khan, K.C.A. Alam, B.B. Saha, A. Akisawa, T. Kashiwagi, Study on a re-heat two-stage adsorption chiller–The influence of thermal capacitance ratio, overall thermal conductance ratio and adsorbent mass on system performance, *Applied Thermal Engineering,* 27 (2007) 1677-1685.

[33] M.Z.I. Khan, K.C.A. Alam, B.B. Saha, Y. Hamamoto, A. Akisawa, T. Kashiwagi, Parametric study of a two-stage adsorption chiller using re-heat–The effect of overall thermal conductance and adsorbent mass on system performance, *International Journal of Thermal Sciences,* 45 (2006) 511-519.

[34] M.Z.I. Khan, S. Sultana, A. Akisawa, T. Kashiwagi, Numerical simulation of advanced adsorption refrigeration chiller with mass recovery, *Journal of Naval Architecture and Marine Engineering,* 3 (2006) 59-67.

[35] A. Akahira, K.C.A. Alam, Y. Hamamoto, A. Akisawa, T. Kashiwagi, Mass recovery four-bed adsorption refrigeration cycle with energy cascading, *Applied Thermal Engineering,* 25 (2005) 1764-1778.

[36] A. Akahira, K.C.A. Alam, Y. Hamamoto, A. Akisawa, T. Kashiwagi, Experimental investigation of mass recovery adsorption refrigeration cycle, *International Journal of Refrigeration,* 28 (2005) 565-572.

[37] A. Akahira, K.C.A. Alam, Y. Hamamoto, A. Akisawa, T. Kashiwagi, Mass recovery adsorption refrigeration cycle—improving cooling capacity, *International Journal of Refrigeration,* 27 (2004) 225-234.

[38] L.X. Gong, R.Z. Wang, Z.Z. Xia, C.J. Chen, Design and performance prediction of a new generation adsorption chiller using composite adsorbent, *Energy Conversion and Management,* 52 (2011) 2345-2350.

[39] S.L. Li, Z.Z. Xia, J.Y. Wu, J. Li, R.Z. Wang, L.W. Wang, Experimental study of a novel $CaCl_2$/expanded graphite-NH_3 adsorption refrigerator, *International Journal of Refrigeration,* 33 (2010) 61-69.

[40] H.L. Luo, Y.J. Dai, R.Z. Wang, J.Y. Wu, Y.X. Xu, J.M. Shen, Experimental investigation of a solar adsorption chiller used for grain depot cooling, *Applied Thermal Engineering,* 26 (2006) 1218-1225.

[41] R.G. Oliveira, V. Silveira Jr., R.Z. Wang, Experimental study of mass recovery adsorption cycles for ice making at low generation temperature, *Applied Thermal Engineering,* 26 (2006) 303-311.

[42] L.W. Wang, R.Z. Wang, Z.S. Lu, C.J. Chen, J.Y. Wu, Comparison of the adsorption performance of compound adsorbent in a refrigeration cycle with and without mass recovery, *Chemical Engineering Science,* 61 (2006) 3761-3770.

[43] L.W. Wang, R.Z. Wang, Z.S. Lu, C.J. Chen, K. Wang, J.Y. Wu, The performance of two adsorption ice making test units using activated carbon and a carbon composite as adsorbents, *Carbon,* 44 (2006) 2671-2680.

[44] R.Z. Wang, Adsorption refrigeration research in Shanghai Jiao Tong University, *Renewable and Sustainable Energy Reviews,* 5 (2001) 1-37.

[45] K.C. Leong, Y. Liu, System performance of a combined heat and mass recovery adsorption cooling cycle: A parametric study, *International Journal of Heat and Mass Transfer,* 49 (2006) 2703–2711.

[46] Z.S. Lu, R.Z. Wang, Z.Z. Xia, Q.B. Wu, Y.M. Sun, Z.Y. Chen, An analysis of the performance of a novel solar silica gel-water adsorption air conditioning, *Applied Thermal Engineering,* 31 (2011) 3636-3642.

[47] C.J. Chen, R.Z. Wang, Z.Z. Xia, J.K. Kiplagat, Z.S. Lu, Study on a compact silica gel–water adsorption chiller without vacuum valves: Design and experimental study, *Applied Energy,* 87 (2010) 2673-2681.

[48] A.S. Uyun, A. Akisawa, T. Miyazaki, Y. Ueda, T. Kashiwagi, Numerical analysis of an advanced three-bed mass recovery adsorption refrigeration cycle, *Applied Thermal Engineering,* 29 (2009) 2876-2884.

[49] Z. Xia, D. Wang, J. Zhang, Experimental study on improved two-bed silica gel-water adsorption chiller, *Energy Conversion and Management,* 49 (2008) 1469-1479.

[50] D.C. Wang, Z.Z. Xia, J.Y. Wu, R.Z. Wang, H. Zhai, W.D. Dou, Study of a novel silica gel-water adsorption chiller. Part I. Design and performance prediction, *International Journal of Refrigeration,* 28 (2005) 1073-1083.

[51] Qenawy, A.M. and Mohamad, A.A., Current technologies and future perspectives in solar powered adsorption systems, *Canadian Solar Buildings Conference*, Montreal, 2004.

[52] K.C. Leong, Y. Liu, Numerical study of a combined heat and mass recovery adsorption cooling cycle, *International Journal of Heat and Mass Transfer,* 47 (2004) 4761-4770.

[53] T.F. Qu, W. Wang, R.Z. Wang, Study of the effects of mass and heat recovery on the performances of activated carbon/ammonia adsorption refrigeration cycles, *Transactions of the ASME, Journal of Solar Energy Engineering,* 124 (2002) 283-290.

[54] R.Z. Wang, Z.Z. Xia, L.W. Wang, Z.S. Lu, S.L. Li, T.X. Li, J.Y. Wu, S. He, Heat transfer design in adsorption refrigeration systems for efficient use of low-grade thermal energy, *Energy,* 36 (2011) 5425-5439.

[55] Z.S. Lu, L.W. Wang, R.Z. Wang, Experimental analysis of an adsorption refrigerator with mass and heat-pipe heat recovery process, *Energy Conversion and Management,* 53 (2012) 291-297.

[56] X.Q. Zhai, R.Z. Wang, Experimental investigation and performance analysis on a solar adsorption cooling system with/without heat storage, *Applied Energy,* 87 (2010) 824-835.

[57] X.Q. Zhai, R.Z. Wang, Experimental investigation and theoretical analysis of the solar adsorption cooling system in a green building, *Applied Thermal Engineering,* 29 (2009) 17-27.

[58] R.Z. Wang, Efficient adsorption refrigerators integrated with heat pipes, *Applied Thermal Engineering,* 28 (2008) 317-326.

[59] D.C. Wang, Z.X. Shi, Q.R. Yang, X.L. Tian, J.C. Zhang, J.Y. Wu, Experimental research on novel adsorption chiller driven by low grade heat source, *Energy Conversion and Management,* 48 (2007) 2375-2381.

[60] T.X. Li, R.Z. Wang, L.W. Wang, Z.S. Lu, J.Y. Wu, Influence of mass recovery on the performance of a heat pipe type ammonia sorption refrigeration system using $CaCl_2$/activated carbon as compound adsorbent, *Applied Thermal Engineering,* 28 (2008) 1638-1646.

[61] T.X. Li, R.Z. Wang, L.W. Wang, Z.S. Lu, C.J. Chen, Performance study of a high efficient multifunction heat pipe type adsorption ice making system with novel mass and heat recovery processes, *International Journal of Thermal Sciences,* 46 (2007) 1267-1274.

[62] S.V. Shelton, Solid adsorbent heat pump system, *US Patent 4610148*, 1986.

[63] O. Taylan, Numerical modeling and performance analysis of solar-powered ideal adsorption cooling systems MSc Thesis, *Middle East Technical University*, 2010.

[64] Y. Liu, K.C. Leong, Numerical study of a novel cascading adsorption cycle, *International Journal of Refrigeration,* 29 (2006) 250-259.

[65] M. Li, R.Z. Wang, Heat and mass transfer in a flat plate solar solid adsorption refrigeration ice maker, *Renewable Energy,* 28 (2003) 613-622.

[66] R.Z. Wang, J.Y. Wu, Y.X. Xu, Y. Teng, W. Shi, Experiment on a continuous heat regenerative adsorption refrigerator using spiral plate heat exchanger as adsorbers, *Applied Thermal Engineering*, 18 (1998) 13-23.

[67] M. Linder, R. Mertz, E. Laurien, Experimental results of a compact thermally driven cooling system based on metal hydrides, *International Journal of Hydrogen Energy,* 35 (2010) 7623-7632.

[68] B.B. Saha, S. Koyama, I.I. El-Sharkawy, K. Kuwahara, K. Kariya, K.C. Ng, Experiments for measuring adsorption characteristics of an activated carbon fiber/ethanol pair using a plate-fin heat exchanger, *HVAC&R Research,* 12 (2006) 767-782.

[69] R.E. Critoph, Z.T. Telto, G.N.L. Davies, A prototype of a fast cycle adsorption refrigerator utilizing a novel carbon-aluminium laminate, Proceedings of the Institution of Mechanical Engineers, 214 (2000) 439-448.

[70] A. Bejan, S. Lorente, Design with constructal theory, *Jon Wiley & Sons, Inc.*, 2008.

[71] A. Bejan, Shape and structure, from engineering to nature, *Cambridge University Press,* 2000.

[72] L. Bonaccorsi, E. Proverbio, Synthesis of thick zeolite 4A coatings on stainless steel, *Microporous and Mesoporous Materials,* 74 (2004) 221-229.

[73] G. Restuccia, A. Freni, G. Maggio, A zeolite-coated bed for air conditioning adsorption systems: parametric study of heat and mass transfer by dynamic simulation, *Applied Thermal Engineering,* 22 (2002) 619-630.

[74] M. Tatlıer, A.E. Şenatalar, Effects of metal mass on the performance of adsorption heat pumps utilizing zeolite 4A coatings synthesized on heat exchanger tubes, *International Journal of Refrigeration,* 23 (2000) 260-268.

[75] D. Zhu, S. Wang, Experimental investigation of contact resistance in adsorber of solar adsorption refrigeration, *Solar Energy,* 73 (2002) 177-185.

[76] G. Restuccia, A. Freni, F. Russo, S. Vasta, Experimental investigation of a solid adsorption chiller based on a heat exchanger coated with hydrophobic zeolite, *Applied Thermal Engineering,* 25 (2005) 1419-1428.

[77] K.S. Chang, M.T. Chen, T.W. Chung, Effects of the thickness and particle size of silica gel on the heat and mass transfer performance of a silica gel-coated bed for air-conditioning adsorption systems, *Applied Thermal Engineering,* 25 (2005) 2330-2340.

[78] W. Mittelbach, T. Büttner, R. Herrmann, Compact adsorption chillers with coated adsorbent heat exchangers *International Sorption Heat pump Conference,* Seoul National University, Seoul, September 23-26, 2008.

[79] L.L. Vasiliev, Heat pipes in modern heat exchangers, *Applied Thermal Engineering*, 25 (2005) 1-19.

[80] L.W. Wang, R.Z. Wang, Z.S. Lu, C.J. Chen, Studies on split heat pipe type adsorption ice-making test unit for fishing boats: Choice of heat pipe medium and experiments under unsteady heating sources, *Energy Conversion and Management,* 47 (2006) 2081-2091.

[81] F. Meunier, Solid sorption heat powered cycles for cooling and heat pumping applications, *Applied Thermal Engineering,* 18 (1998) 715-729.

[82] R.E. Critoph, The use of thermosyphon heat pipes to improve the performance of a carbon-ammonia adsorption refrigerator, *International Journal of Environmentally Conscious Design & Manufacturing,* 9 (2000) 3-10.

[83] Z.Z. Xia, R.Z. Wang, J.Y. Wu, L.W. Wang, Compound alternate heat pipe reactor powered by waste heat, *China patent 200410018291.3,* 2004.

[84] R.E. Critoph, Y. Zhong, Review of trends in solid sorption refrigeration and heat pumping technology, *Proceedings of the Institution of Mechanical Engineers, Part E: Journal of Process Mechanical Engineering,* 219 (2005) 285-300.

[85] Z.T. Telto, R.E. Critoph, Monolithic carbon for sorption refrigeration and heat pump applications, *Applied Thermal Engineering,* 21 (2001) 37-52.

[86] G. Cacciola, G. Restuccia, G. van Benthem, Influence of the adsorber heat exchanger design on the performance of the heat pump system, *Applied Thermal Engineering,* 19 (1999) 255-269.

[87] A. Celzard, M. Krzesinska, D. Begin, J.F. Mareche, S. Puricelli, G. Furdin, Preparation, electrical and elastic properties of new anisotropic expanded graphite-based composites, *Carbon,* 40 (2002) 557-566.

[88] T. Dellero, D. Sarmeo, P. Touzain, A chemical heat pump using carbon fibers as additive. Part I: enhancement of thermal conduction, *Applied Thermal Engineering,* 19 (1999) 991-1000.

[89] H. Demir, M. Mobedi, S. Ülkü, The use of metal piece additives to enhance heat transfer rate through an unconsolidated adsorbent bed, *International Journal of Refrigeration*, 33 (2010) 714-720.

[90] C. Wu, S. Hsu, R. Chu, M. Chen, Enhancing the thermal conductivity of the heat exchanger in a non-compressive system as a means of energy efficiency improvement of the system, *International Journal of Green Energy,* 6 (2009) 490-507.

[91] M.A. Alghoul, M.Y. Sulaiman, B.Z. Azmi, M.A. Wahab, Advances on multi-purpose solar adsorption systems for domestic refrigeration and water heating, *Applied Thermal Engineering,* 27 (2007) 813-822.

[92] S. Mauran, P. Prades, F. L'Haridon, Heat and mass transfer in consolidated reacting beds for thermochemical systems, *Heat Recovery Systems and CHP,* 13 (1993) 315-319.

[93] X. Py, E. Daguerre, D. Menard, Composites of expanded natural graphite and in situ prepared activated carbons, *Carbon*, 40 (2002) 1255-1265.

[94] J.H. Han, K.H. Lee, H. Kim, Effective thermal conductivity of graphite-metallic salt complex for chemical heat pumps, *Journal of Thermophysics and Heat Transfer,* 13 (1999) 481-488.

[95] T.H. Eun, H.K. Song, J.H. Han, K.H. Lee, J.N. Kim, Enhancement of heat and mass transfer in silica-expanded graphite composite blocks for adsorption heat pumps: Part I. Characterization of the composite blocks, *International Journal of Refrigeration,* 23 (2000) 64-73.

[96] J.J. Guilleminot, A. Choisier, J.B. Chalfen, S. Nicolas, J.L. Reymoney, Heat transfer intensification in fixed bed adsorbers, *Heat Recovery Systems & CHP*, 13 (1993) 297-300.

[97] LL. Bonaccorsi, E. Proverbio, A. Freni, G. Restuccia, In situ growth of zeolites on metal foamed supports for adsorption heat pumps, *Journal of Chemical Engineering of Japan*, 40 (2007) 1307-1312.

[98] A.O. Dieng, R.Z. Wang, Literature review on solar adsorption technologies for ice-making and air-conditioning purposes and recent developments in solar technology, *Renewable and Sustainable Energy Reviews,* 5 (2001) 313-342.

[99] R.Z. Wang, Q.B. Wang, Adsorption mechanism and improvements of the adsorption equation for adsorption refrigeration pairs, *International Journal of Energy Research,* 23 (1999) 887-898.

[100] A. Ertan, CO_2, N_2 and Ar adsorption on zeolites, MSc. Thesis, *İzmir Institute of Technology*, 2004.

[101] L.W. Wang, R.Z. Wang, R.G. Oliveira, A review on adsorption working pairs for refrigeration, *Renewable and Sustainable Energy Reviews,* 13 (2009) 518-534.

[102] H. Yüncü, E. Paykoç, Y. Yener, Solar energy utilization, NATO Scientific Affairs Division, *Martinus Nijhoff Publishers*, Dordrecht, 1987.

[103] Q. Cui, G. Tao, H. Chen, X. Guo, H. Yao, Environmentally benign working pairs for adsorption refrigeration, *Energy,* 30 (2005) 261-271.

[104] D.K. Baker, Thermodynamic limits to thermal regeneration in adsorption cooling cycles, *International Journal of Refrigeration*, 31 (2008) 55-64.

[105] D.K. Baker, B. Kaftanoğlu, Limits to the thermodynamic performance of a thermal wave adsorption cooling cycle, *5th International Conference on Heat Transfer, Fluid Mechanics and Thermodynamics*, Sun City, South Africa, 2007.

[106] L.M. Sun, N.B. Amar, F. Meunier, Numerical study on coupled heat and mass transfers in an adsorber with external fluid heating, *Heat Recovery Systems & CHP*, 15/1 (1995) 19-29.

[107] S.V. Shelton, W.J. Wepfer, D.J. Miles, Square wave analysis of the solid-vapor adsorption heat pump, *Heat Recovery Systems & CHP*, 9/3 (1989) 233-247.

[108] S.V. Shelton, W.J. Wepfer, D.J. Miles, Ramp wave analysis of the solid/vapor heat pump, *Journal of Energy Resources Technology*, 112 (1990) 69-78.

[109] L.M. Sun, Y. Feng, M. Pons, Numerical investigation of adsorptive heat pump systems with thermal wave heat regeneration under uniform-pressure conditions, *Int. J. Heat Mass Transfer*, 40/2 (1997) 281-293.

[110] T.A. Fuller, W.J. Wepfer, S.V. Shelton, M.W. Ellis, A two-temperature model of the regenerative solid-vapor heat pump, *Journal of Energy Resources Technology*, 116 (1994) 297-304.

[111] N.B. Amar, L.M. Sun, F. Meunier, Numerical analysis of adsorptive temperature wave regenerative heat pump, *Applied Thermal Engineering*, 16/5 (1996) 405-418.

[112] B.K. Sward, M.G. LeVan, F. Meunier, Adsorption heat pump modeling: the thermal wave process with local equilibrium, *Applied Thermal Engineering*, 20 (2000) 759-780.

[113] M. Pons, Analysis of the adsorption cycles with thermal regeneration based on the entropic mean temperatures, *Applied Thermal Engineering*, 17/7 (1997) 615-627.

[114] M. Pons, Y. Feng, Characteristic parameters of adsorptive refrigeration cycles with thermal regeneration, *Applied Thermal Engineering,* 17/3 (1997) 289-298.

[115] M. Pons, Global analysis of refrigerative adsorption cycles with thermal regeneration (non-uniform temperature), *International Journal of Refrigeration*, 20/6 (1997) 411-420.

[116] S. Waszkiewicz, S. Jenkins, H. Saidani-Scott, M. Tierney, Analysis of a finned heat exchanger working in an adsorption refrigeration system using zeolite and methanol, *Heat Transfer Engineering,* 24/6 (2003) 71-78.

[117] W. Zheng, W.M. Worek, G. Nowakowski, Effect of operating conditions on the performance of two-bed closed-cycle solid-sorption heat pump systems, *Journal of Solar Energy Engineering,* 117 (1995) 181-186.

[118] D.J. Miles, S.V. Shelton, Design and testing of a solid-sorption heat-pump system, *Applied Thermal Engineering,* 16/5 (1996) 389-394.

[119] J.A. Jones, Sorption refrigeration research at JPL/NASA, *Heat Recovery Systems & CHP,* 13/4 (1993) 363-371.

[120] F. Meunier, F. Poyelle, M.D. LeVan, Second-law analysis of adsorptive refrigeration cycles: the role of thermal coupling entropy production, *Applied Thermal Engineering,* 17/1 (1997) 43-55.

[121] S. Szarzynski, Y. Feng, M. Pons, Study of different internal vapour transports for adsorption cycles with heat regeneration, *International Journal of Refrigeration,* 20/6 (1997) 390-401.

[122] D. Zejli, R. Benchrifa, A. Bennouna, O.K. Bouhelal, A solar adsorption desalination device: first simulation results, *Desalination,* 168 (2004) 127-135.

[123] M.H. Chahbani, J. Labidi, J. Paris, Modeling of adsorption heat pumps with heat regeneration, *Applied Thermal Engineering,* 24 (2004) 431-447.

[124] R.E. Critoph, Modular regenerative adsorption cycles with fixed beds, applied to trigeneration, *Proceedings of the Institution of Mechanical Engineers, Part E: Journal of Process Mechanical Engineering,* 219 (2005) 197-204.

[125] M.A. Lambert, Design of solar powered adsorption heat pump with ice storage, *Applied Thermal Engineering,* 27 (2007) 1612-1628.

[126] O. Taylan, D.K. Baker, B. Kaftanoğlu, COP trends for ideal thermal wave adsorption cooling cycles with enhancements, *International Journal of Refrigeration,* 35 (2012) 562-570.

[127] S.J. Metcalf, R.E. Critoph, Z. Tamainot-Telto, Optimal cycle selection in carbon-ammonia adsorption cycles, *International Journal of Refrigeration,* 35 (2012) 571-580.

[128] R.E. Critoph, Forced convection adsorption cycles, *Applied Thermal Engineering*, 18 (1998) 799-807.

[129] R.E. Critoph, Forced convection adsorption cycle with packed bed heat regeneration, *International Journal of Refrigeration,* 22 (1999) 38-46.

[130] H.-M. Lai, An enhanced adsorption cycle operated by periodic reversal forced convection, *Applied Thermal Engineering,* 20 (2000) 595-617.

[131] H.-M. Lai, C.-Y. Li, Application of periodic reversal flow reactors to chemical heat pump systems based on solid/vapor non-catalytic reaction, *Chemical Engineering Science,* 51/11 (1996) 2971-2976.

[132] M.J. Tierney, Feasibility of driving convective thermal wave chillers with low-grade heat, *Renewable Energy,* 33 (2008) 2097-2108.

[133] İ. Solmuş, D.A.S. Rees, C. Yamalı, D. Baker, B. Kaftanoğlu, Numerical investigation of coupled heat and mass transfer inside the adsorbent bed of an adsorption cooling unit, *International Journal of Refrigeration,* 35 (2012) 652-662.

[134] P.C. Wankat, Large-scale adsorption and chromatography, Volume I, *CRC Press, Inc.,* 1986.

[135] P.C. Wankat, Rate-controlled separations, *Chapman & Hall,* 1994.

[136] A. Mhimid, Theoretical study of heat and mass transfer in a zeolite bed during water desorption: validity of local thermal equilibrium assumption, *International Journal of Heat and Mass Transfer,* 41 (1998) 2967-2977.

[137] L. Tschaepe, A.E. Ruggles, J.D. Freels, R.T. Primm, Evaluation of HFIR LEU fuel using the comsol multiphysics platform, *Oak Ridge National Laboratory,* Oar Ridge, Tennessee, March 2009.

[138] F.P. Incropera, D.P. DeWitt, T.L. Bergman, A.S. Lavine, Fundamentals of heat and mass transfer, 6th edition, *Wiley,* 2006.

[139] J.H. Lienhard IV, J.H. Lienhard V, A heat transfer textbook, 3th edition, *Phlogiston Press,* Cambridge, Massachusetts, USA, 2004.

[140] D.M. Ruthven, Principles of adsorption and adsorption processes, *John Wiley & Sons, Inc.,* 1984.

[141] M. Suzuki, Adsorption engineering, *Kodansha Ltd.,* Japan, 1990.

[142] D.A. Nield, A. Bejan, Convection in porous media, Third edition, *Springer Science+Business Media, Inc.,* 2006.

[143] D.B. Ingham, I. Pop, Transport phenomena in porous media III, *Elsevier Ltd.,* 2005.

[144] E.A. Moreira, M.D.M. Innocentini, J.R. Coury, Permeability of ceramic foams to compressible and incompressible flow, *Journal of the European Ceramic Society,* 24 (2004) 3209-3218.

[145] L. Yong, K. Sumathy, Review of mathematical investigation on the closed adsorption heat pump and cooling systems, *Renewable and Sustainable Energy Review,* 6 (2002) 305-337.

[146] İ. Solmuş, C. Yamalı, B. Kaftanoğlu, D. Baker, A. Çağlar, Adsorption properties of a natural zeolite-water pair for use in adsorption cooling cycles, *Applied Energy,* 87 (2010) 2062-2067.

[147] Comsol Multiphysics User's Guide, Version 3.5a, *COMSOL AB.,* 2008

[148] R. W. Pryor, Multiphysics Modeling Using Comsol: A First Principles Approach, *Jones and Bartlett Publishers,* 2010.

[149] İ. Solmuş, D.A.S. Rees, C. Yamalı, D. Baker, B. Kaftanoğlu, Numerical investigation of coupled heat and mass transfer inside the adsorbent bed of an adsorption cooling unit, *International Journal of Refrigeration,* 35 (2012) 652-662.

[150] Y. Deng, C. Fedler, J. Gregory, Predictions of thermal characteristics for mixed porous media, *Journal of Materials in Civil Engineering,* 4 (1992) 185-195.

[151] B. Kaftanoğlu, C. Yamalı, D.K. Baker, İ. Solmuş, A. Çağlar, O. Taylan, Güneş enerjisi destekli zeolit iklimlendirme sistemi, *TÜBİTAK Projesi Sonuç Raporu,* Proje No:105M244, 2009.

APPENDIX A

ADAPTATION OF THE GOVERNING EQUATIONS TO COMSOL MULTIPHYSICS

The HTF (heat transfer fluid) has energy transport by conduction and convection and the governing equation for the HTF can be written as following:

$$\rho_f c_f \frac{\partial T_f}{\partial t} - k_f \nabla^2 T_f + \rho_f c_f v_f \nabla T_f + \frac{2}{r_t} h_i (T_f - T_t) = 0 \tag{A.1}$$

Eqn. (A.1) can be adapted to Comsol Multiphysics by using convection and conduction physics modes and its *Graphical User Interface* (GUI) is shown in Figure A.1.

There are several options to implement convection and conduction physics modes in Comsol. One can use one of four different modules: General Comsol Multiphysics module, Chemical Engineering Model, Earth Science Module or Heat Transfer Module. The equations supplied by each module can be a little different, but it is always possible to adapt current equations to the equations of any Comsol module. Chemical Engineering Module has been used for the adaptation of energy equation for the HTF in this study.

In Fig. A.1, k_f, rho_f and cp_f are the thermal conductivity, density and specific heat of the fluid. They are assumed to be constant and are defined in constants window in Comsol. All constants can be entered in the contants window and then can be used anywhere symbolically. The vel_f is the velocity of the HTF and is written in y direction since the HTF flows vertically.

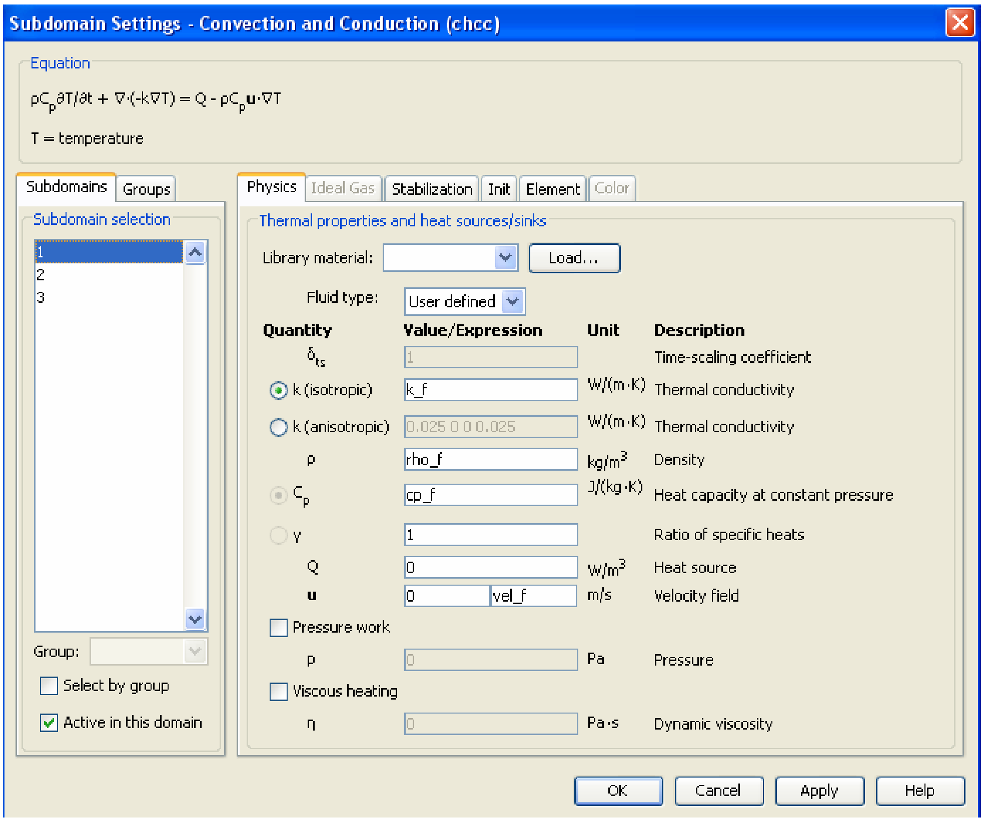

Subdomain Settings - Convection and Conduction (chcc)

Equation

$\rho C_p \partial T/\partial t + \nabla\cdot(-k\nabla T) = Q - \rho C_p \mathbf{u}\cdot\nabla T$

T = temperature

Subdomain selection: 1, 2, 3

Group:

☐ Select by group

☑ Active in this domain

Thermal properties and heat sources/sinks

Library material:

Fluid type: User defined

Quantity	Value/Expression	Unit	Description
δ_{ts}	1		Time-scaling coefficient
● k (isotropic)	k_f	W/(m·K)	Thermal conductivity
○ k (anisotropic)	0.025 0 0 0.025	W/(m·K)	Thermal conductivity
ρ	rho_f	kg/m^3	Density
● C_p	cp_f	J/(kg·K)	Heat capacity at constant pressure
○ γ	1		Ratio of specific heats
Q	0	W/m^3	Heat source
u	0 vel_f	m/s	Velocity field
☐ Pressure work			
p	0	Pa	Pressure
☐ Viscous heating			
η	0	Pa·s	Dynamic viscosity

Fig. A.1 A picture from GUI of Comsol Multiphysics for the adaptation of HTF energy equation.

The HTF is assumed to have a parabolic velocity profile in the HTT (heat transfer tube). The fluid dynamics were also computed by Incompressible Navier-Stokes application mode in Comsol. The results showed that the parabolic velocity profile is almost the same with the velocity profile obtained by the application of Incompressible Navier-Stokes mode. The parabolic velocity profile which is a function of average HTF velocity and radius is defined in the global expressions window in Comsol. All expressions can be entered in the global expressions dialog box if they are not a differential form. PDE forms or weak forms can only be used for differential equations.

It is noted that the equation given in Fig. A.1 does not include the last term of the left hand side of Eqn. (A.1). This term comes from convective boundary condition and Comsol takes this boundary as “continuity boundary” automatically in its boundary settings.

The energy equation for the HTT can be given as:

$$\rho_t c_t \frac{\partial T_t}{\partial t} - k_t \nabla^2 T_t + \frac{h_i}{b}(T_t - T_f) + \frac{h_o}{b}(T_t - T_s) = 0 \qquad \text{(A.2)}$$

The GUI of Comsol for HTT energy equation is shown in Fig. A.2.

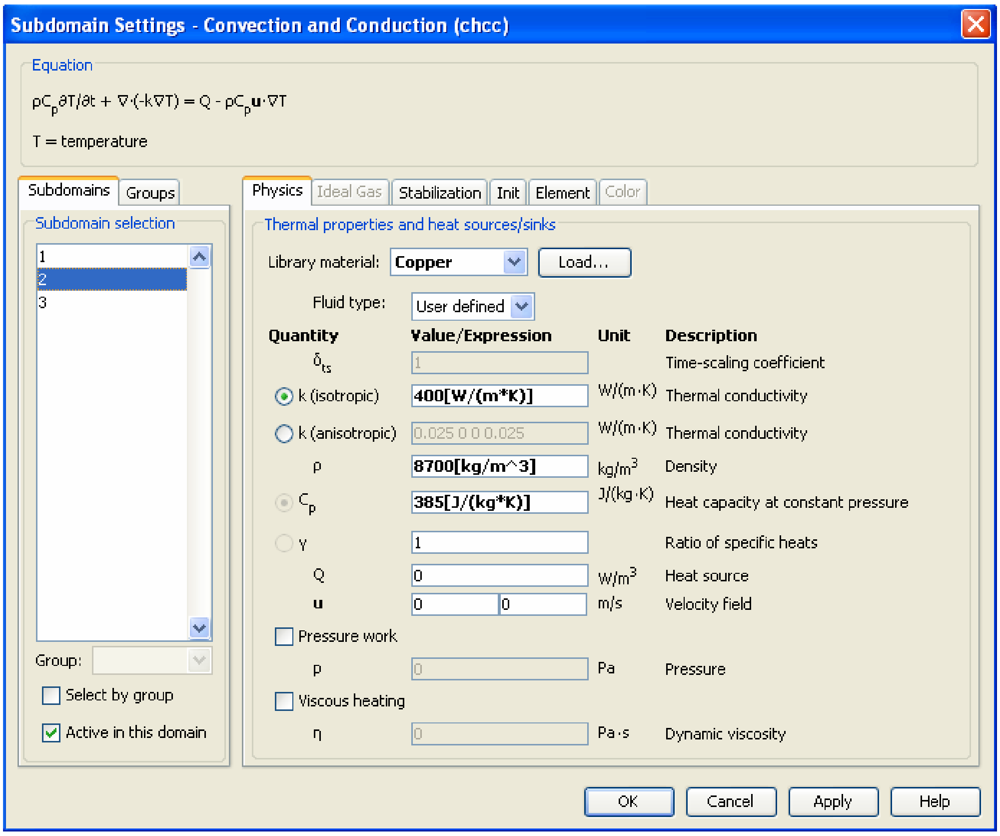

$\rho C_p \partial T/\partial t + \nabla\cdot(-k\nabla T) = Q - \rho C_p \mathbf{u}\cdot\nabla T$

T = temperature

Subdomain selection: 1, 2, 3

Group:

☐ Select by group

☑ Active in this domain

Library material: Copper

Fluid type: User defined

Quantity	Value/Expression	Unit	Description
δ_{ts}	1		Time-scaling coefficient
● k (isotropic)	400[W/(m*K)]	W/(m·K)	Thermal conductivity
○ k (anisotropic)	0.025 0 0 0.025	W/(m·K)	Thermal conductivity
ρ	8700[kg/m^3]	kg/m^3	Density
● C_p	385[J/(kg*K)]	J/(kg·K)	Heat capacity at constant pressure
○ γ	1		Ratio of specific heats
Q	0	W/m^3	Heat source
u	0 0	m/s	Velocity field
☐ Pressure work			
p	0	Pa	Pressure
☐ Viscous heating			
η	0	Pa·s	Dynamic viscosity

Fig. A.2 A picture from GUI of Comsol Multiphysics for the adaptation of HTT energy equation.

Copper is the predefined material for the tube and the thermal properties of copper are taken from Material Library of Comsol. There are many materials whose properties are given in Material Library of Comsol. Any material and its properties can be added to this library if the libray has no information about that material.

Only conduction occurs in the HTT. The second and third terms in Eqn. (A.2) are canceled in Comsol since these two terms are related to heat transfers at the boundaries and Comsol performs these equations as “continuity boundary” in boundary settings part. Fig. A.3 shows a picture from the boundary settings box for convection and conduction mode in Comsol.

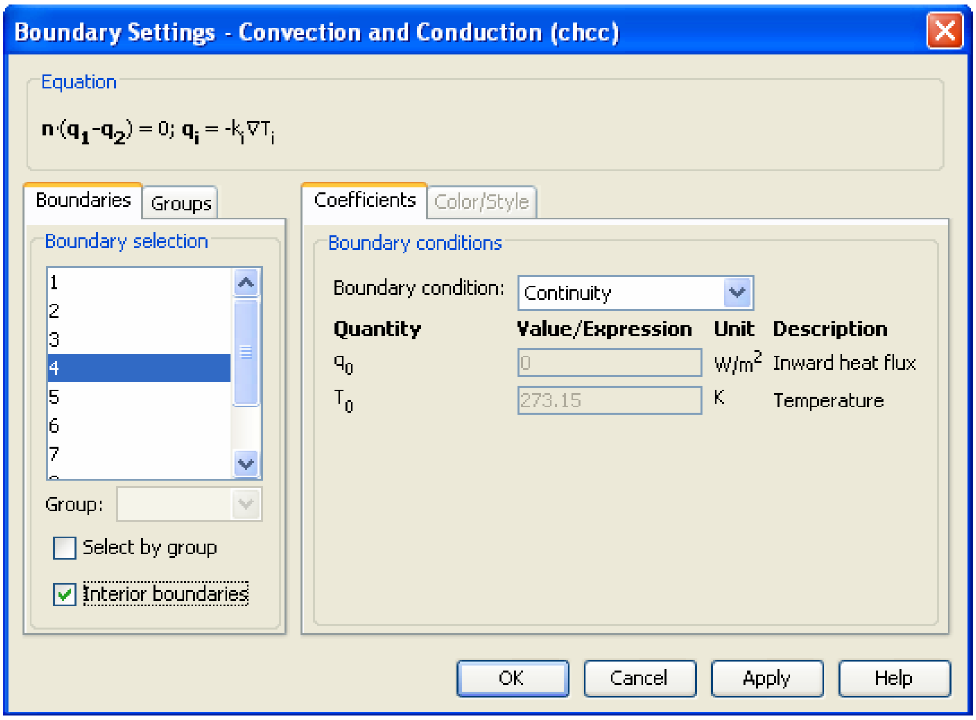

Boundary Settings - Convection and Conduction (chcc)

Equation

$\mathbf{n}\cdot(\mathbf{q}_1-\mathbf{q}_2) = 0;\ \mathbf{q}_i = -k_i\nabla T_i$

Boundary selection: 4

☐ Select by group

☑ Interior boundaries

Boundary conditions

Boundary condition: Continuity

Quantity	Value/Expression	Unit	Description
q_0	0	W/m^2	Inward heat flux
T_0	273.15	K	Temperature

Fig. A.3 A picture from Comsol Multiphysics for the boundary settings of HTT domain.

The energy equation for the porous media is given as follows:

$$\begin{aligned}&(1-\varepsilon)\rho_s c_s \frac{\partial T_s}{\partial t} + \varepsilon\rho_v c_{p,v}\frac{\partial T_s}{\partial t} + (1-\varepsilon)\rho_s X c_{p,l}\frac{\partial T_s}{\partial t} - (1-\varepsilon)\rho_s \left|H\right| \frac{\partial X}{\partial t}\\ &-k_s\nabla^2 T_s + \rho_v c_{p,v}\mathbf{u}\nabla T_s + \frac{h_o}{b}(T_s - T_t) = 0\end{aligned} \tag{A.3}$$

The adaptation of energy equation for the porous media to Comsol is shown in Fig. A.4. The last term in Fig. A.4, that is convective term for the adsorbent material, is zero because the sorbent does not move in the bed. Time rate of change of the sorbent temperature and conduction terms can be seen in Comsol’s energy equation as given in Eqn. (A.3). All other terms in Eqn (A.3), on the other hand, are written into the source term as Q in Comsol. The source term Q is introduced in “global expressions” box.

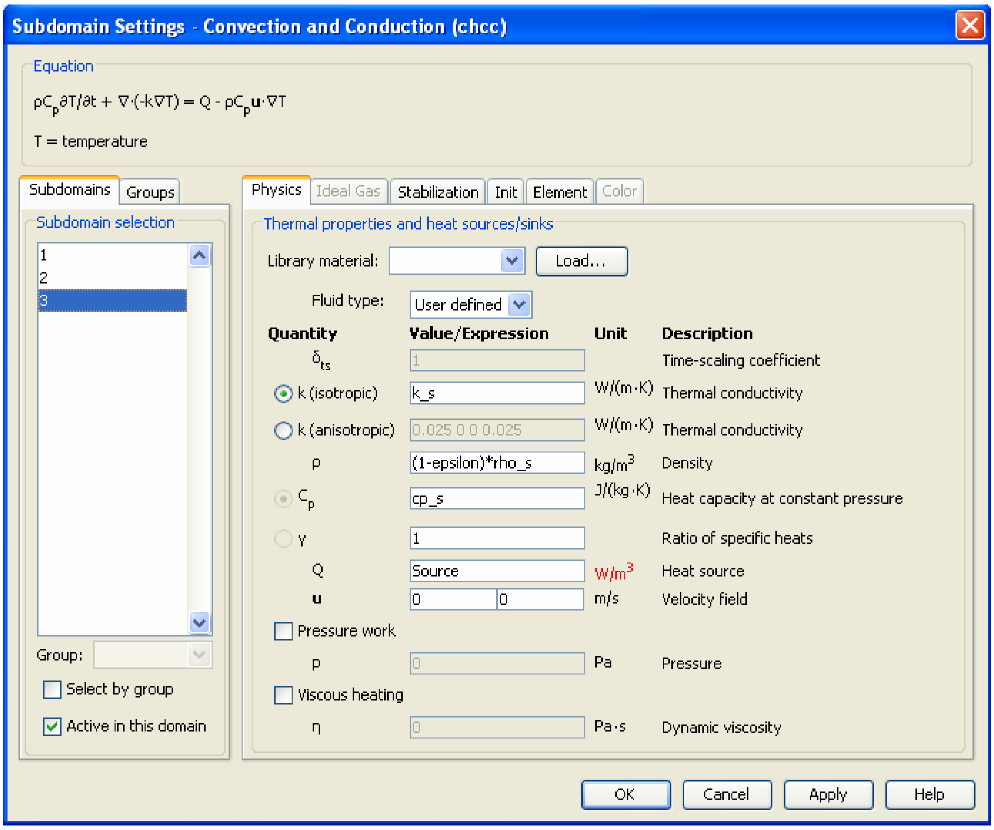

Equation

$\rho C_p \partial T/\partial t + \nabla\cdot(-k\nabla T) = Q - \rho C_p \mathbf{u}\cdot\nabla T$

T = temperature

Subdomain selection: 1, 2, 3 (3 selected)

Group:

☐ Select by group

☑ Active in this domain

Thermal properties and heat sources/sinks

Library material:

Fluid type: User defined

Quantity	Value/Expression	Unit	Description
δ_{ts}	1		Time-scaling coefficient
● k (isotropic)	k_s	W/(m·K)	Thermal conductivity
○ k (anisotropic)	0.025 0 0 0.025	W/(m·K)	Thermal conductivity
ρ	(1-epsilon)*rho_s	kg/m^3	Density
● C_p	cp_s	J/(kg·K)	Heat capacity at constant pressure
○ γ	1		Ratio of specific heats
Q	Source	W/m^3	Heat source
u	0 | 0	m/s	Velocity field
☐ Pressure work			
p	0	Pa	Pressure
☐ Viscous heating			
η	0	Pa·s	Dynamic viscosity

Fig. A.4 A picture from GUI of Comsol Multiphysics for the adaptation of the energy equation for the porous media.

The density of the vapor can be found by ideal gas relation since the water vapor behaves as an ideal gas in low pressure conditions. The equation of state of ideal gas can be written as follows:

$$P = \rho_v R_v T_s \tag{A.4}$$

and this relation is introduced to Comsol in global expressions tool box.

The mass balance equation can be written as follows for the porous media:

$$\varepsilon\frac{\partial\rho_v}{\partial t}+(1-\varepsilon)\rho_s\frac{\partial X}{\partial t}-D_m\nabla^2\rho_v+\nabla(\mathbf{u}\rho_v)=0 \qquad \text{(A.5)}$$

The second term at LHS of Eqn. (A.5) defines the rate of desorption/adsorption. The mass balance equation is adapted to Comsol the convection and diffusion physics under the Chemical Enginnering Module. The default equation is set in the non-conservative form, i.e. the velocity vector in the last term at LHS of Eqn. (A.5) is taken out of gradient operator, and thus it is converted to the conservative form by using *Properties* tool in Comsol. The third term in Eqn. (A.5) defines the diffusive mass transfer and is usually neglected. This study takes this term into account assuming that D_m is constant. A picture from GUI for the convection and diffusion mode of Comsol is given in Fig. A.5.

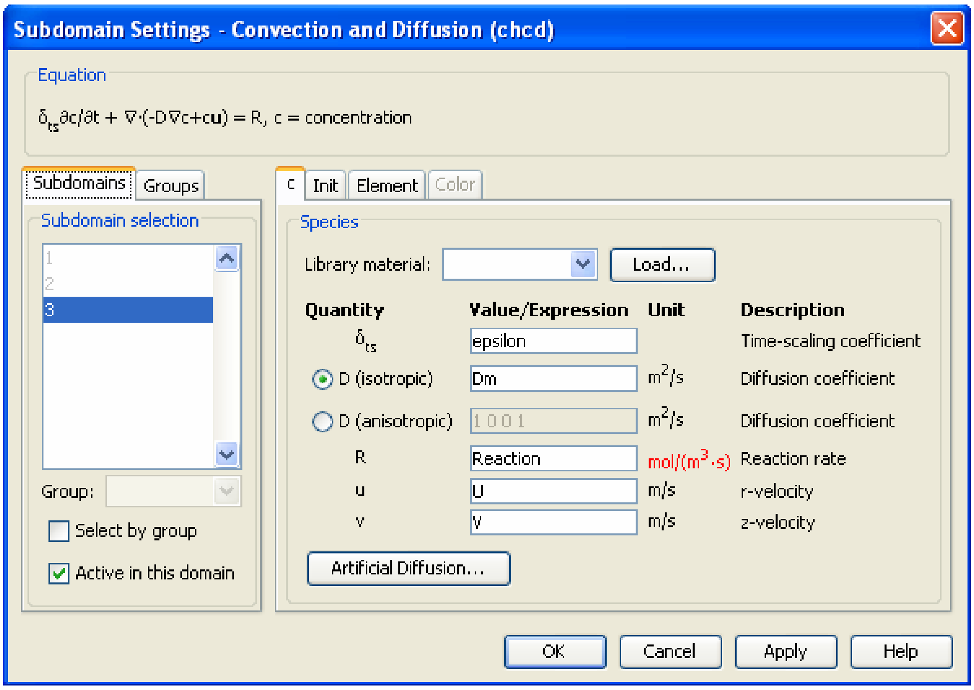

Subdomain Settings - Convection and Diffusion (chcd)

Equation

$\delta_{ts}\partial c/\partial t + \nabla\cdot(-D\nabla c+cu) = R$, c = concentration

Subdomain selection: 3

Library material:

Quantity	Value/Expression	Unit	Description
δ_{ts}	epsilon		Time-scaling coefficient
● D (isotropic)	Dm	m^2/s	Diffusion coefficient
○ D (anisotropic)	1 0 0 1	m^2/s	Diffusion coefficient
R	Reaction	$mol/(m^3\cdot s)$	Reaction rate
u	U	m/s	r-velocity
v	V	m/s	z-velocity

☐ Select by group

☑ Active in this domain

Fig. A.5 A picture from GUI of Comsol Multiphysics for the adaptation of mass balance equation for the porous media.

As seen in Fig. A.5, the convection and diffusion equation is deactivated for subdomains 1 and 2, i.e. HTF and HTT domains, since the conservation of mass is written for only the porous media. The equation given by Comsol includes the time rate of change of the concentration (not the density) of vapor, diffusive, convective and reaction terms, respectively. The reaction term is introduced in the global expressions. The convection and diffusion equation in Comsol is in molar basis. In other words, the concentration of vapor is used instead of density. Therefore, the density can be introduced to Comsol by entering the following equation in the global expressions:

$$\rho = cM_w \tag{A.6}$$

Eqn. (A.5) is, therefore, adapted to the equation given in Fig. (A.5). Comsol solves the concentration using reaction term and then Eqn.(A.6) converts it to the density and this density is used in the whole model when necessary.

The velocity of refrigerant vapor is given in vectorial form in Equations (A.3) and (A.5). r and z components of the velocity of refrigerant vapor can be found from the momentum equation which is defined by Darcy flow. Therefore, the momentum equation can be expressed in an open form calculating r and z velocities seperately as follows:

$$\begin{aligned} u &= -\frac{\kappa}{\mu}\frac{\partial P}{\partial r} \\ v &= -\frac{\kappa}{\mu}\frac{\partial P}{\partial z} \end{aligned} \tag{A.7}$$

The velocities are introduced into Comsol in the global expressions.

Both the reaction term in the mass balance equation and the source term in the energy equation for the porous media have X (the amounted adsorbed) and derivatives of X. Linear Driving Force (LDF) model can be used for solving X applying the following expression:

$$\frac{\partial X}{\partial t} = k_m (X_e - X) \tag{A.8}$$

Eqn. (A.8) has a differential form and can be introduced to Comsol by using a PDE form under Comsol Multiphysics module. A PDE can be introduced to Comsol Multiphysics by creating a PDE coefficient form, general form or weak form. PDE coefficient form is used in this model. The picture of GUI of the PDE coefficient form created is given Fig. A.6.

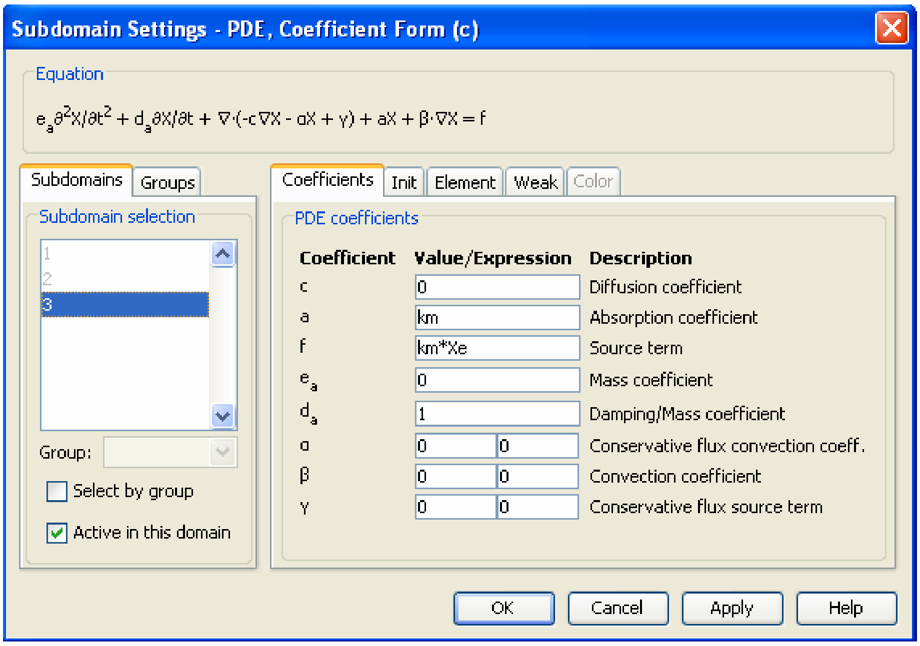

Equation

$e_a \partial^2 X/\partial t^2 + d_a \partial X/\partial t + \nabla\cdot(-c\nabla X - \alpha X + \gamma) + aX + \beta\cdot\nabla X = f$

Subdomain selection

1
2
3

Group:

☐ Select by group

☑ Active in this domain

PDE coefficients

Coefficient	Value/Expression		Description
c	0		Diffusion coefficient
a	km		Absorption coefficient
f	km*Xe		Source term
e_a	0		Mass coefficient
d_a	1		Damping/Mass coefficient
α	0	0	Conservative flux convection coeff.
β	0	0	Convection coefficient
γ	0	0	Conservative flux source term

Fig. A.6 A picture from GUI of the PDE coefficient form created for the adaptation of LDF model.

The internal mass transfer coefficient, k_m, can be found by the expression:

$$k_m = \frac{15}{r_p^{\,2}} D_o \exp\left(-\frac{E_a}{RT_s}\right) \qquad (A.9)$$

The equilibrium adsorption capacity, X_e, can be found by the expression:

$$X_e = X_o \exp\left[-A\left(\frac{T_s}{T_{sat}} - 1\right)^n\right] \qquad (A.10)$$

T_{sat} in Eqn (A.10) is the saturation temperature of water vapor corresponding to the pressure inside the sorbent bed and can be calculated as follows:

$$T_{sat} = 39.724 + \frac{1730.63}{8.07131 - \log 10(7.500638 \cdot 10^{-3} \cdot P)} \qquad \text{(A.11)}$$

Equations (A.9), (A.10) and (A.11) are introduced to Comsol in the global expressions and all the equations introduced in the global expressions tool box can be seen in Fig. A.7.

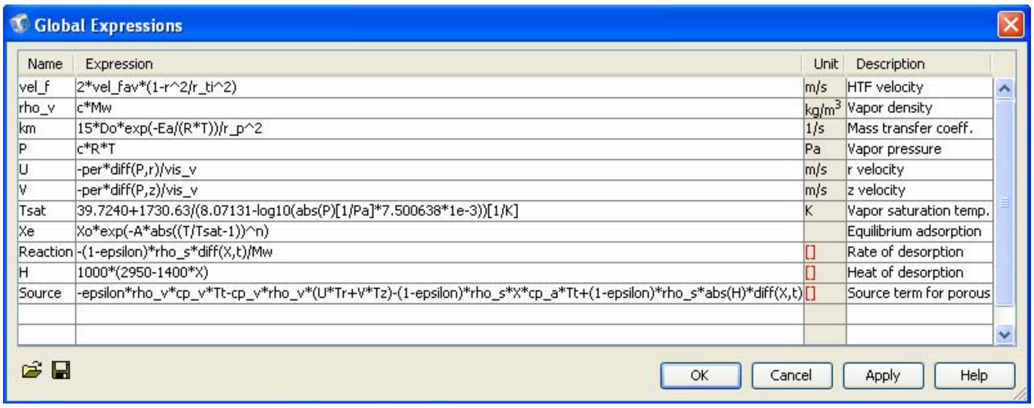

Name	Expression	Unit	Description
vel_f	2*vel_fav*(1-r^2/r_ti^2)	m/s	HTF velocity
rho_v	c*Mw	kg/m^3	Vapor density
km	15*Do*exp(-Ea/(R*T))/r_p^2	1/s	Mass transfer coeff.
P	c*R*T	Pa	Vapor pressure
U	-per*diff(P,r)/vis_v	m/s	r velocity
V	-per*diff(P,z)/vis_v	m/s	z velocity
Tsat	39.7240+1730.63/(8.07131-log10(abs(P)[1/Pa]*7.500638*1e-3))[1/K]	K	Vapor saturation temp.
Xe	Xo*exp(-A*abs((T/Tsat-1))^n)		Equilibrium adsorption
Reaction	-(1-epsilon)*rho_s*diff(X,t)/Mw	[]	Rate of desorption
H	1000*(2950-1400*X)	[]	Heat of desorption
Source	-epsilon*rho_v*cp_v*Tt-cp_v*rho_v*(U*Tr+V*Tz)-(1-epsilon)*rho_s*X*cp_a*Tt+(1-epsilon)*rho_s*abs(H)*diff(X,t)	[]	Source term for porous

Fig. A.7 Global expressions used in the model.

Consequently, three physics, i.e. the convection and conduction, the convection and diffusion, and the rate of desorption/adsorption in PDE form, run interactively and are solved simultaneously using the constants and global expressions shown in Fig. A.7.

Adaptation of Boundary Conditions to Comsol Multiphysics

Boundary conditions (BCs) for the heat transfer physics can be adapted to Comsol as follows:

BC 1: Axial symmetry

BC 2: Temperature boundary, set to T_{hot}

BC 3: Convective flux boundary (see Fig. A.9)

BC 4,7: Continuity, default expression by Comsol at the interfaces,

BC 5,6,8,9,10: Thermal insulation

Boundary numbers can be seen in Fig. A.8. A sample picture from Comsol boundary settings dialog box is given in Fig. A.9.

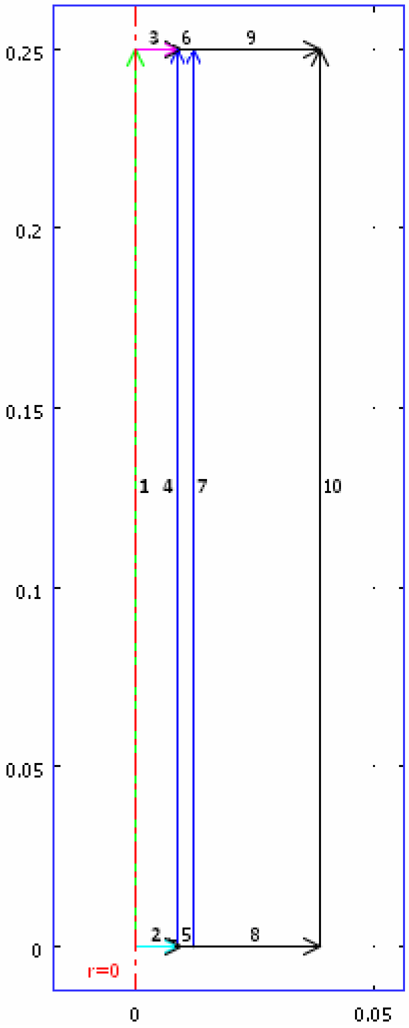

Fig. A.8. The assigned numbers of the boundaries.

BCs for the mass transfer physics can be adapted to Comsol as follows:

BC 7: Flux boundary, set to $c*D_m*Tr/T$; This BC comes from the adaptation of pressure BC to concentration BC using ideal gas relation. There is no information about concentration, but the pressure on this boundary is known. The pressure gradient is zero for this boundary since the velocity is zero by no slip condition at the solid surface. Darcy equation can be checked for the validation. Note that Tr means temperature gradient in r direction, i.e. $\partial T/\partial r$, in Comsol.

BC 8,10: Concentration boundary, set to $P_c/(R*T)$; Pressure is constant for these boundaries and using the ideal gas relation again, the adapted BC can be obtained. These boundaries are open to vapor region and thus the pressure can be taken as constant.

BC 9: Flux boundary, set to $c*D_m*Tz/T$; Pressure gradient is zero on this boundary since the boundary is the solid surface and the velocity is zero at this surface. This pressure BC is adapted to concentration BC. Note that Tz means temperature gradient in z direction, i.e. $\partial T/\partial z$.

The other boundaries are automatically deactivated by Comsol since there is no mass transfer on those boundaries.

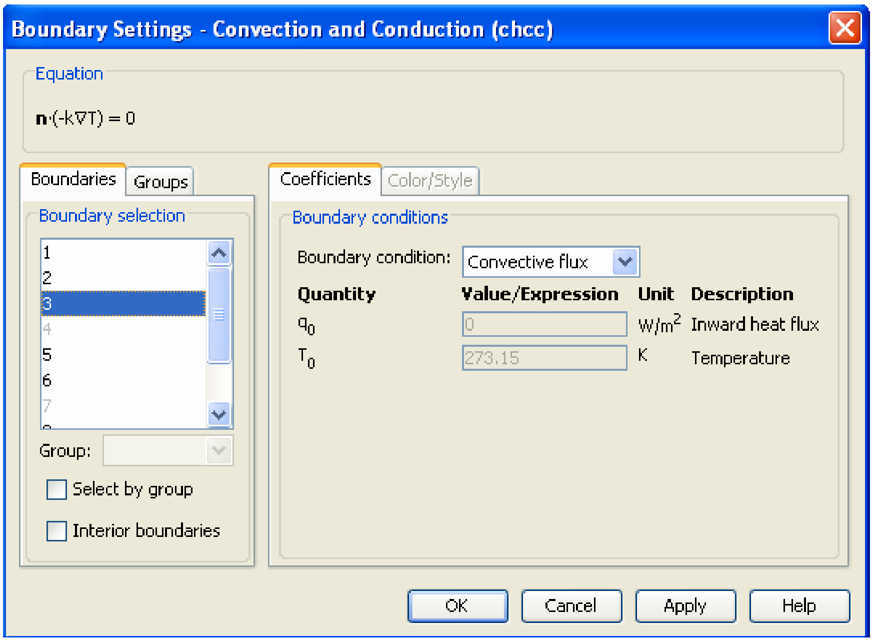

Boundary Settings - Convection and Conduction (chcc)

Equation

$\mathbf{n}\cdot(-k\nabla T) = 0$

Boundary condition: Convective flux

Quantity	Value/Expression	Unit	Description
q_0	0	W/m^2	Inward heat flux
T_0	273.15	K	Temperature

Fig. A.9 A picture from Comsol boundary settings for the heat transfer.

Note that the initial conditions (ICs) of all subdomains are set to T_i for the heat transfer. IC of the concentration is set to $P_c/(R.T_i)$ taking from the ideal gas relation for the mass transfer. P_c, i.e. the condenser pressure, is taken initially since the model simulates the desorption process.

APPENDIX B

COMSOL MODEL REPORT

The following is a sample model report generated by Comsol Multiphysics.

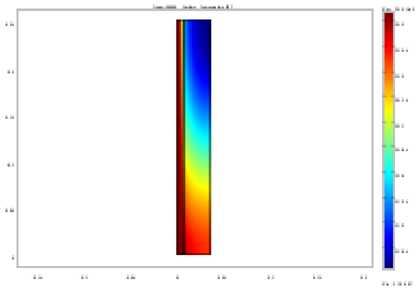

2.1. Table of Contents

- Title - COMSOL Model Report
- Table of Contents
- Model Properties
- Constants
- Global Expressions
- Geometry
- Geom1
- Materials/Coefficients Library
- Solver Settings
- Postprocessing

2.2. Model Properties

Property	**Value**
Model name	
Author	
Company	
Department	
Reference	
URL	
Saved date	Jan 17, 2011 12:24:37 AM

Creation date	Jan 15, 2011 12:04:38 PM
COMSOL version	COMSOL 3.5.0.494

File name: C:\Documents and Settings\Administrator\My Documents\Adsorption.mph

Application modes and modules used in this model:

- Geom1 (Axial symmetry (2D))
  - Convection and Conduction (Chemical Engineering Module)
  - Convection and Diffusion (Chemical Engineering Module)
  - PDE, Coefficient Form

2.3. Constants

Name	Expression	Value	Description
r_ti	0.00635[m]		Tube inner radius
b_t	0.001[m]		Tube thickness
r_to	r_ti+b_t		Tube outer radius
l_t	1[m]		Tube length
r_fin	0.03[m]		Fin radius
b_fin	0.5[mm]		Fin thickness
k_f	0.115[W/(m*K)]		HTF thermal conductivity
rho_f	914[kg/m^3]		HTF density
cp_f	1930[J/(kg*K)]		HTF specific heat
k_t	400[W/(m*K)]		Tube thermal conductivity
rho_t	8700[kg/m^3]		Tube density
cp_t	385[J/(kg*K)]		Tube specific heat
k_s	1[W/(m*K)]		Sorbent thermal conductivity
rho_s	572[kg/m^3]		Sorbent density
cp_s	837[J/(kg*K)]		Sorbent specific heat
vis_v	1e-5[kg/m/s]		Vapor dynamic viscosity
epsilon	0.4		Void fraction
per	1e-12[m^2]		Permability
fs	1		
Xo	0.346		Max. adsorption level
A	5.6		Adsorption equilibrium constant
P_c	4.247[kPa]		Condenser pressure
n	1.6		Adsorption equilibrium constant
Mw	18.015[kg/kmol]		Water molecular weight
R_v	0.4615[kJ/(kg*K)]		Ideal gas constant for vapor
Do	2.54e-4[m^2/s]		Reference diffusivity
Ea	4.2e4[J/mol]		Activation energy
R	8.314[kJ/(kmol*K)]		Universal gas constant
d_p	3.2e-3[m]		Sorbent particle diameter
r_p	d_p/2		Sorbent particle radius
vel_fav	0.005 [m/s]		HTF inlet average velocity
cp_v	1.88[kJ/(kg*K)]		Specific heat of vapor water
cp_a	4.18[kJ/(kg*K)]		Specific heat of liquid water

Ti	40[degC]		Initial temperature
Thot	150[degC]		Hot fluid inlet temperature
Dm	9e-5[m^2/s]		Mass diffusivity of vapor
Tsati	30[degC]		
Hi	3000[kJ/kg]		

2.4. Global Expressions

Name	Expression	Unit	Description
vel_f	2*vel_fav*(1-r^2/r_ti^2)	m/s	HTF velocity
rho_v	c*Mw	kg/m^3	Vapor density
km	15*Do*exp(-Ea/(R*T))/r_p^2	1/s	Mass transfer coeff.
P	c*R*T	Pa	Vapor pressure
U	-per*diff(P,r)/vis_v	m/s	r velocity
V	-per*diff(P,z)/vis_v	m/s	z velocity
Tsat	39.7240+1730.63/(8.07131-log10(abs(P)[1/Pa]*7.500638*1e-3))[1/K]	K	Vapor saturation temp.
Xe	Xo*exp(-A*abs((T/Tsat-1))^n)		Equilibrium adsorption
Reaction	-(1-epsilon)*rho_s*diff(X,t)/Mw		Rate of desorption
H	1000*(2950-1400*X)		Heat of desorption
Source	-epsilon*rho_v*cp_v*Tt-cp_v*rho_v*(U*Tr+V*Tz)-(1-epsilon)*rho_s*X*cp_a*Tt+(1-epsilon)*rho_s*abs(H)*diff(X,t)		Source term for porous media

2.5. Geometry

Number of geometries: 1

2.6. Geom1

Space dimensions: Axial symmetry (2D)

Independent variables: r, phi, z

2.6.1. Mesh

2.6.1.1. Mesh Statistics

Number of degrees of freedom	28488
Number of mesh points	2971
Number of elements	5703
Triangular	5703
Quadrilateral	0
Number of boundary elements	599
Number of vertex elements	8
Minimum element quality	0.8088
Element area ratio	0.052

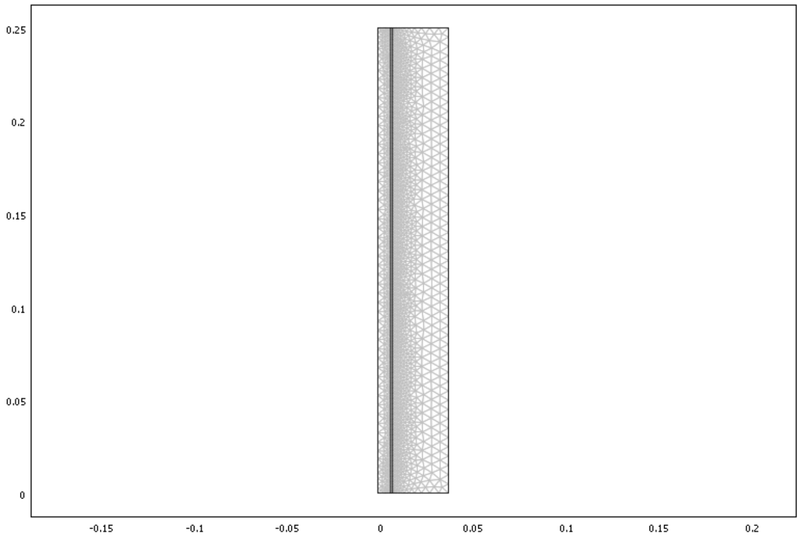

2.6.2. Application Mode: Convection and Conduction (chcc)

Application mode type: Convection and Conduction (Chemical Engineering Module)

Application mode name: chcc

2.6.2.1. Scalar Variables

Name	Variable	Value	Unit	Description
Rg	Rg_chcc	8.31451	J/(mol*K)	Universal gas constant

2.6.2.2. Application Mode Properties

Property	**Value**
Default element type	Lagrange - Quadratic
Analysis type	Transient
Species diffusion	Inactive
Turbulence model	None
Predefined multiphysics application	Off
Frame	Frame (ref)
Weak constraints	Off
Constraint type	Ideal

2.6.2.3. Variables

Dependent variables: T

Shape functions: shlag(2,'T')

Interior boundaries not active

2.6.2.4. Boundary Settings

Boundary		5-6, 8-10	1	2
Type		Thermal insulation	Axial symmetry	Temperature
Temperature (T0)	K	273.15	273.15	**Thot**

Boundary		3
Type		Convective flux
Temperature (T0)	K	273.15

2.6.2.5. Subdomain Settings

Subdomain		1	2	3
Thermal conductivity (k)	W/(m·K)	**k_f**	**400[W/(m*K)] (Copper)**	**k_s**
Density (rho)	kg/m^3	**rho_f**	**8700[kg/m^3] (Copper)**	**(1-epsilon)*rho_s**
Heat capacity at constant pressure (C)	J/(kg·K)	**cp_f**	**385[J/(kg*K)] (Copper)**	**cp_s**
Heat source (Q)	W/m^3	0	0	**Source**
z-velocity (v)	m/s	**vel_f**	0	0

Subdomain initial value		1	2	3
Temperature (T)	K	Ti	Ti	Ti

2.6.3. Application Mode: Convection and Diffusion (chcd)

Application mode type: Convection and Diffusion (Chemical Engineering Module)

Application mode name: chcd

2.6.3.1. Application Mode Properties

Property	**Value**
Default element type	Lagrange - Quadratic
Analysis type	Transient
Equation form	Conservative
Equilibrium assumption	Off
Frame	Frame (ref)
Weak constraints	Off
Constraint type	Ideal

2.6.3.2. Variables

Dependent variables: c

Shape functions: shlag(2,'c')

Interior boundaries not active

2.6.3.3. Boundary Settings

Boundary		9	7	8, 10
Type		Flux	Flux	Concentration

Inward flux (N)	mol/(m^2·s)	**c*Dm/T*Tz**	**c*Dm/T*Tr**	0
Concentration (c0)	mol/m^3	0	0	**P_c/(R*T)**

2.6.3.4. Subdomain Settings

Subdomain		3
Diffusion coefficient (D)	m^2/s	**Dm**
Reaction rate (R)	mol/(m^3·s)	**Reaction**
Time-scaling coefficient (Dts)	1	**epsilon**
r-velocity (u)	m/s	**U**
z-velocity (v)	m/s	**V**

Subdomain initial value		3
Concentration, c (c)	mol/m^3	P_c/(R*Ti)

2.6.4. Application Mode: PDE, Coefficient Form (c)

Application mode type: PDE, Coefficient Form

Application mode name: c

2.6.4.1. Application Mode Properties

Property	**Value**
Default element type	Lagrange - Quadratic
Wave extension	Off
Frame	Frame (ref)
Weak constraints	Off

2.6.4.2. Variables

Dependent variables: X, X_t

Shape functions: shlag(2,'X')

Interior boundaries not active

2.6.4.3. Boundary Settings

Boundary		7-10
Type		Neumann boundary condition

2.6.4.4. Subdomain Settings

Subdomain		3
Diffusion coefficient (c)		**0**
Absorption coefficient (a)		**km**
Source term (f)		**km*Xe**

Subdomain initial value		3
X		Xo

2.7. Materials/Coefficients Library

2.7.1. Copper

Parameter	**Value**
Heat capacity at constant pressure (C)	385[J/(kg*K)]
Young's modulus (E)	110e9[Pa]
Reference temperature (T0)	298[K]
Thermal expansion coeff. (alpha)	17e-6[1/K]
Temperature coefficient (alphares)	0.0039[1/K]
Relative permittivity (epsilonr)	1
Thermal conductivity (k)	400[W/(m*K)]
Relative permeability (mur)	1
Poisson's ratio (nu)	0.35
Resistivity at reference temperature (res0)	1.72e-8[ohm*m]
Density (rho)	8700[kg/m^3]
Electric conductivity (sigma)	5.998e7[S/m]

2.8. Solver Settings

Solve using a script: off

Analysis type	Transient
Auto select solver	On
Solver	Time dependent
Solution form	Automatic
Symmetric	auto
Adaptive mesh refinement	Off
Optimization/Sensitivity	Off
Plot while solving	Off

2.8.1. Direct (UMFPACK)

Solver type: Linear system solver

Parameter	**Value**
Pivot threshold	0.1
Memory allocation factor	0.7

2.8.2. Time Stepping

Parameter	**Value**
Times	0:10:20000
Relative tolerance	0.01
Absolute tolerance	0.0010
Times to store in output	Specified times
Time steps taken by solver	Free
Maximum BDF order	5
Singular mass matrix	Maybe

Consistent initialization of DAE systems	Backward Euler
Error estimation strategy	Include algebraic
Allow complex numbers	Off

2.8.3. Advanced

Parameter	**Value**
Constraint handling method	Elimination
Null-space function	Automatic
Automatic assembly block size	On
Assembly block size	1000
Use Hermitian transpose of constraint matrix and in symmetry detection	Off
Use complex functions with real input	Off
Stop if error due to undefined operation	On
Store solution on file	Off
Type of scaling	Automatic
Manual scaling	
Row equilibration	On
Manual control of reassembly	Off
Load constant	On
Constraint constant	On
Mass constant	On
Damping (mass) constant	On
Jacobian constant	On
Constraint Jacobian constant	On

2.9. Postprocessing

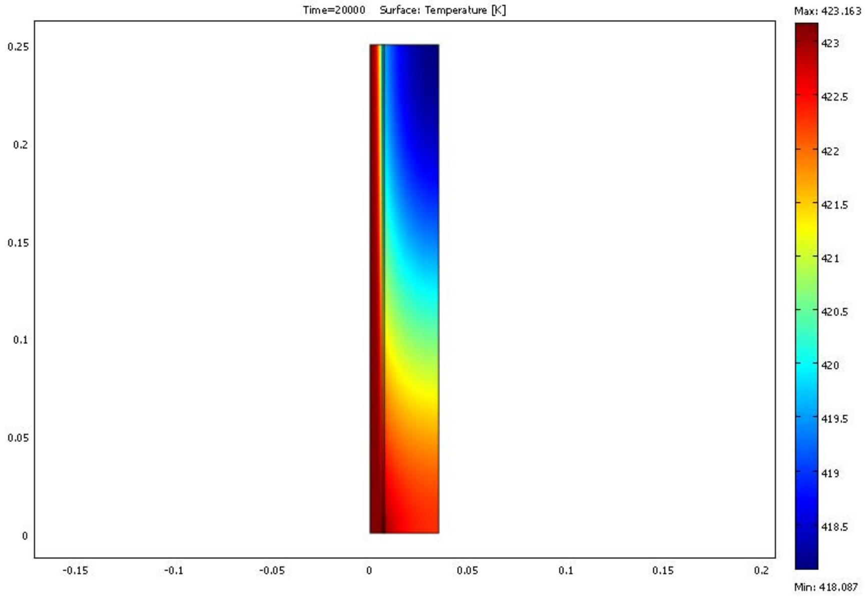

APPENDIX C

UNCERTAINTY ANALYSIS

The experimental uncertainties in volumetric flowrate, temperature and pressure measurements were calculated by using the Gauss' error propagation law. According to this law, if a result R is to be calculated by a function $R=f(x_1, x_2, x_3 \ldots x_n)$ from a single set of values of the input data x_n, then uncertainty in R is expressed by:

$$w_R = \left[\left(\frac{\partial R}{\partial x_1} w_1 \right)^2 + \left(\frac{\partial R}{\partial x_2} w_2 \right)^2 + \ldots\ldots + \left(\frac{\partial R}{\partial x_n} w_n \right)^2 \right]^{1/2} \tag{C.1}$$

where, w_n represents the uncertainty in the nth independent variable.

Uncertainty in Volumetric Flowrate Measurements

The volumetric flowrate of the heat transfer oil was calculated as a function of measured volume and measured time as follows:

$$\dot{V} = \frac{V}{t} \tag{C.2}$$

The mean values and experimental uncertainties in measuring the volume and time are V=2 ± 0.05 l, and t=71 ± 0.5 s. The partial derivatives of the volumetric flowrate with respect to the volume and time can be written as follows:

$$\frac{\partial \dot{V}}{\partial V} = \frac{1}{t} = 0.014 \quad \text{and} \quad \frac{\partial \dot{V}}{\partial t} = -\frac{V}{t^2} = -0.000397 \tag{C.3}$$

Using Equation (C.1), the uncertainty for the volumetric flowrate can be calculated as follows:

$$w_{\dot{V}} = \left[\left(\frac{\partial \dot{V}}{\partial V} w_V \right)^2 + \left(\frac{\partial \dot{V}}{\partial t} w_t \right)^2 \right]^{1/2} = \left[(0.014 \cdot 0.05)^2 + (-0.000397 \cdot 0.5)^2 \right]^{1/2}$$
$$w_{\dot{V}} = 0.000728 \ \frac{\text{l}}{\text{s}} \ = 0.0437 \ \frac{\text{l}}{\text{min}} \tag{C.4}$$

$$\text{Percent uncertainty (\%)} = \frac{w_{\dot{V}}}{\dot{V}} = \frac{0.0437}{\frac{2}{71} 60} = 0.0258 \cong 2.6\% \tag{C.5}$$

Uncertainties in Temperature and Pressure Measurements

The factors that cause errors in the temperature and pressure measurements are as follows:

(e1) Accuracy of the thermocouple: ±0.5 ^{o}C

(e2) Accuracy of the presssure transducer: ±1%, or ±0.8 mbar for the experimental mean value of pressure 79.6 mbar

(e3) Accuracy of the datalogger: ±0.02 ^{o}C for temperature and ±0.15 mbar for pressure

(e4) Errors due to connections: ±0.1 ^{o}C for temperature and ±0.1 mbar for pressure

Total uncertainties for the temperature and mean pressure measurements caused by these factors can be determined as follows, respectively:

$$w_T = \left[(\text{e1})^2 + (\text{e3})^2 + (\text{e4})^2 \right]^{1/2} = \left[(0.5)^2 + (0.02)^2 + (0.1)^2 \right]^{1/2}$$
$$w_T = \pm 0.51 \ ^{o}\text{C} \qquad \text{uncertainty for temperature}$$
$$w_P = \left[(\text{e2})^2 + (\text{e3})^2 + (\text{e4})^2 \right]^{1/2} = \left[(0.8)^2 + (0.15)^2 + (0.1)^2 \right]^{1/2}$$
$$w_P = \pm 0.82 \ \text{mbar} \quad \text{uncertainty for pressure} \tag{C.6}$$

CURRICULUM VITAE

PERSONAL INFORMATION

Surname, Name: Çağlar, Ahmet
Nationality: Turkish (TC)
Date and Place of Birth: 29 June 1980, Tokat
Marital Status: Married with one son
Phone:+90 505 656 72 01 (GSM)
Fax: +90 312 210 25 36
email: acaglar@metu.edu.tr, ahcaglar@hotmail.com

EDUCATION

Degree	Institution	Year of Graduation
MS	METU Mechanical Engineering	2006
BS	Kocaeli University Mechanical Engineering	2001
High School	Mehmet Akif Ersoy High School, İstanbul	1997

WORK EXPERIENCE

Year	Place	Enrollment
2002-Present	METU Department of Mechanical Engineering	Research Assistant

FOREIGN LANGUAGES

Advanced English

PUBLICATIONS

1. Çağlar A., Yamalı C. "Analysis of Heat and Mass Transfer in the Adsorbent Bed of a Thermal Wave Adsorption Cooling Cycle", 9th International Conference on Heat Transfer, Fluid Mechanics and Thermodynamics HEFAT2012, 16-18 July 2012, Malta

2. Çağlar A., Yamalı C., Baker D., Kaftanoğlu B. "Measurement of Solar Radiation in Ankara, Turkey", Journal of Thermal Science and Technology, *accepted on July 2012*

3. Çağlar A., Yamalı C. "Performance Analysis of a Solar-Assisted Heat Pump with an Evacuated Tubular Collector for Domestic Heating", Energy and Buildings, *accepted on 3 August 2012*

4. Solmuş İ., Yamalı C., Kaftanoğlu B., Baker D., Çağlar A., "Adsorption Properties of a Natural Zeolite-Water Pair for Use in Adsorption Cooling Cycles", Applied Energy, 87, 2062-2067 (2010)

5. Çağlar A., Yamalı C., Baker D., Kaftanoğlu B. "Testing the Thermal Performances of Solar Collectors", 7th International Conference on Heat Transfer, Fluid Mechanics and Thermodynamics HEFAT2010, 19-21 July 2010, Turkey

6. Çağlar A., Yamalı C. "Vakum Borulu Toplayıcı Kullanılarak Güneş Enerjisi Destekli Bir Isı Pompası Performansının Analizi, IV. Ege Energy Sempozyumu, 21-23 Mayıs 2008, İzmir

REVIEWER

1. Enegy and Buildings
2. International Journal of Thermodynamics
3. HEFAT

PROJECTS PARTICIPATED

1. Yamalı C., Çağlar A. "The Design and Construction of the Adsorbent Bed of a Thermal Wave Adsorption Cooling Cycle", TÜBİTAK Project 110M378, 2011

2. Kaftanoğlu B., Yamalı C., Baker D., Solmuş İ., Çağlar A., Taylan O. "Solar Powered Adsorption Cooling System Using Zeolite/Water Pair", TÜBİTAK Project 105M244, 2009

3. Nisan Elektromekanik Enerji San. Tic. A.Ş. in collaboration with METU, "Parabolik Güneş Kollektörleri Kullanılarak Güneş Enerjisinden Elektrik Üretiminde Kullanılabilecek Özellikte Buhar Üretimi ve Soğutma Uygulaması", TÜBİTAK TEYDEP Project 3090199, 2009

4. Yamalı C., Çağlar A. "Theoretical and Experimental Performance Analysis of a Solar Assisted Heat Pump, METU BAP Project (2003-2006).

COMPUTER SKILLS

1. Comsol Multiphsics
2. Key Creator
3. Mathcad
4. Mathematica
5. LaTex
6. AutoCAD
7. Matlab

HOBBIES

Reading, Books, Table Tennis, Football, Movies, Fishing, Cooking, Travelling